Continuous Multi-Modal Monitoring of Cerebrovascular Reactivity in Adult Traumatic Brain Injury

Frederick A. Zeiler BSc MD FRCSC (Neurosurgery)

Queens' College

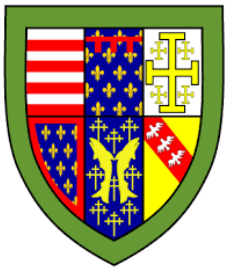

University of Cambridge

Date of Submission: January 5th, 2019

This dissertation is submitted for the degree of Doctor of Philosophy

This dissertation is the result of my own work and includes nothing which is the outcome of work done in collaboration except where specifically indicated in the text.

It is not substantially the same as any that I have submitted, or, is being concurrently submitted for a degree or diploma or other qualification at the University of Cambridge or any other University or similar institution except as declared in the Preface and specified in the text. I further state that no substantial part of my dissertation has already been submitted, or, is being concurrently submitted for any such degree, diploma or other qualification at the University of Cambridge or any other University or similar institution except as declared in the Preface and specified in the text.

This dissertation does not exceed the word limit of 60,000 words.

TABLE OF CONTENTS

SUMMARY

Impaired cerebral autoregulation following traumatic brain injury (TBI) in adults has been linked to worse global outcome. Continuously updating indices of cerebrovascular reactivity provide a convenient and continuous metric regarding an individual patients' autoregulatory status. To date, the vast majority of the literature has focused on pressure reactivity index (PRx), which has emerged as the "gold standard" for continuous monitoring of cerebrovascular reactivity in adult TBI, but many questions concerning its clinical utility remain unanswered. The focus of this thesis was to address some of these previously unanswered questions, using data from experimental models and from multi-modality monitoring (MMM) in adult TBI patients.

Specific questions addressed in this thesis include: [A] Do other ICP-derived indices to assess cerebrovascular reactivity exist? [B] Do ICP-derived indices actually measure autoregulation? [C] What are the inter-index relationships between various MMM techniques? [D] Can one estimate/predict the "gold standard" invasive PRx using non-invasive means? [E] What are the critical thresholds associated with outcome for ICP derived indices? [F] Are any specific ICP derived index/indices superior for outcome prediction? and [G] What role do intra-cranial (IC) and extra-cranial (EC) injury burden play in driving autoregulatory function in TBI?

These studies evaluated a newly described index derived from pulse amplitude of ICP and cerebral perfusion pressure (CPP), RAC, which provides information regarding both cerebrovascular reactivity and compensatory reserve. Using experimental models of arterial hypotension and IC hypertension, it was demonstrated that the three ICP derived indices (including RAC) of cerebrovascular reactivity measure the lower limit of autoregulation (LLA), providing some of the first evidence to validate these indices as measures of autoregulation. It still remains unclear as to whether these indices can measure the upper limit of autoregulation (ULA).

Indices derived from MMM display reproducible inter-index relationships between various populations of adult TBI patients. Transcranial Doppler (TCD) based systolic flow index is most closely associated with ICP indices, while cortical autoregulation (measured using laser Doppler) is more closely linked to mean flow index. Given these relationships and the potential for non-invasive measurement of systolic flow index, attempts at modelling the "gold standard" PRx were made. From this, it is possible to both estimate and predict PRx using non-invasive systolic flow index, employing complex time-series techniques.

Outcome analysis showed that RAC provides superior outcome prediction, with more stable critical thresholds, compared to all other ICP derived indices. Furthermore, IC injury markers (subarachnoid hemorrhage thickness, diffuse axonal injury, and presence of subdural hematoma) were associated with impaired cerebral autoregulation as measured by ICP derived indices, implicating diffuse cerebral injury as a driver of impaired reactivity. The data also suggest that EC injury burden may play a role in impairment of cerebrovascular reactivity.

ACKNOWLEDGMENTS

First, I would like to thank all of the adult TBI patients for providing the data and opportunity to shed light on cerebral autoregulation. We are indebted for your sacrifice.

Second, I would like to thank Prof David Menon for his patience and immense support through my PhD studies. I am indebted for the life changing experience to work with you. Without your advice and direction, this would have not been possible. I look forward to ongoing mentorship and collaboration.

Third, I would like to thank Prof Marek Czosnyka for his support and teaching around cerebrovascular physiology. It was a truly humbling experience to be able to work with the world expert in cerebral autoregulation. Without your previous work and advice, writing this thesis would not have been possible.

Fourth, thank you to Dr. Ari Ercole and Dr. Peter Smielewski for your support and interest in my work. It was an honor to work with you. Your advice regarding signal analysis techniques and the complex modelling techniques within my thesis were invaluable.

Fifth, thank you to Dr. Jennifer Lee (John's Hopkins) and Dr. Ken Brady (Baylor) for allowing me to use their experimental data to investigate the ability of these indices to measure autoregulation. I look forward to ongoing collaborative efforts.

Sixth, thank you to the Brain Physics Laboratory group, past and present, at the University of Cambridge for sharing the wealth of raw physiologic data collected over numerous decades. Also, thank you for all of the support and teaching around using ICM+ software. Specifically thank you to: Prof Marek Czosnyka, Dr. Peter Smielewski, Dr. Zofia Czosnyka, Dr. Joseph Donnelly and Dr. Danilo Cardim.

Seventh, this work was made possible through salary support through the Cambridge Commonwealth Trust Scholarship, the Royal College of Surgeons of Canada – Harry S. Morton Travelling Fellowship in Surgery, the University of Manitoba Clinician Investigator Program, R. Samuel McLaughlin Research and Education Award, the Manitoba Medical Service Foundation, and the University of Manitoba Faculty of Medicine Dean's Fellowship Fund.

Finally, and most importantly. Thank you to my wife, Kaitlin. I am eternally indebted for your patience and support throughout all of these years of neurosurgery residency, neurocritical care fellowship and PhD studies. I truly am the luckiest man alive.

LIST OF PUBLICATIONS

Primary Original Works Publications based both on retrospective and prospective data (Published and Accepted)

1. **Zeiler FA**, Czosnyka M, Smielewski P. Optimal Cerebral Perfusion Pressure via Transcranial Doppler in TBI: Application of Robotic Technology. Acta Neurochir (Wien). Accepted, Sept 14th 2018.

2. **Zeiler FA**, Smielewski P. Application of Robotic Transcranial Doppler for Extended Duration Recording in Moderate/Severe Traumatic Brain Injury: First Experiences. Crit Ultrasound J. 2018; 10(1):16. doi: 10.1186/s13089-018-0097-0.

3. **Zeiler FA**, Smielewski P, Stevens A, Czosnyka M, Menon DK, Ercole A. Non-Invasive Pressure Reactivity Index Using Doppler Systolic Flow Parameters: A Pilot Analysis. J Neurotrauma. August 2018, In Press.

4. **Zeiler FA**, Donnelly J, Calviello L, Lee JK, Smielewski P, Brady K, Kim DJ, Czosnyka M. Validation of pressure reactivity and pulse amplitude indices against the lower limit of autoregulation, Part I: experimental intra-cranial hypertension. J Neurotrauma. June 2018, In Press.

5. **Zeiler FA**, Lee JK, Smielewski P, Czosnyka M, Brady K. Validation of ICP derived cerebrovascular reactivity indices against the lower limit of autoregulation, Part II: experimental model of arterial hypotension. J Neurotrauma. May 2018, In Press.

6. **Zeiler FA**, Donnelly J, Thelin EP, Smielewski P, Czosnyka M, Ercole A, Menon DK. Intra- and Extra-Cranial Injury Burden as Drivers of Impaired Cerebrovascular Reactivity in Traumatic Brain Injury. J Neurotrauma. Feb 2018, In Press.

7. **Zeiler FA**, Smielewski P, Donnelly J, Czosnyka M, Menon DK, Ercole A. Estimating pressure reactivity index using non-invasive Doppler based systolic flow index. J Neurotrauma. Jan 2018, In Press.

8. **Zeiler FA,** Donnelly J, Smielewski P, Menon DK, Hutchinson PJA, Czosnyka M. Critical Thresholds of ICP Derived Continuous Cerebrovascular Reactivity Indices for outcome prediction in Non-Craniectomized TBI Patients: PRx, PAx and RAC. J Neurotrauma. 2017, Dec 6, In Press.

9. **Zeiler FA,** Donnelly J, Menon DK, Smielewski P, Hutchinson PJ, Czosnyka M. A Description of a New Continuous Physiologic Index in TBI using the Correlation Between Pulse Amplitude of ICP and Cerebral Perfusion Pressure. J Neurotrauma. Nov 2017, In Press.

10. **Zeiler FA**, Cardim D, Donnelly J, Menon DK, Czosnyka M, Smielewski P. Transcranial Doppler Systolic Flow Index and ICP Derived Cerebrovascular Reactivity Indices in TBI. J Neurotrauma. Sept 2017, In Press. doi: 10.1089/neu.2017.5364.

11. **Zeiler FA**, Donnelly J, Cardim D, Menon DK, Smielewski P, Czosnyka M. ICP versus Laser Doppler Cerebrovascular Reactivity Indices to Assess Brain Autoregulatory Capacity. Neurocrit Care. Sept 2017, In Press. doi: 10.1007/s12028-017-0472-x.

12. **Zeiler FA**, Donnelly J, Smielewski P, Menon DK, Zweifel C, Brady K, Czosnyka M. Continuous Autoregulatory Indices Derived from Multi-modal Monitoring: Each One is Not Like the Other. J Neurotrauma. 2017; 34(22):3070-3080. doi: 10.1089/neu.2017.5129.

Primary Literature Reviews

1. **Zeiler FA**, Thelin EP, Donnelly J, Stevens A, Smielewski P, Czosnyka M, Hutchinson PJ, Menon DK. Genetic drivers of cerebral blood flow dysfunction in traumatic brain injury: a speculative synthesis. Nat Rev Neurol. Accepted, August 21st 2018.

2. **Zeiler FA**. Traumatic Brain Injury (TBI) in NCCU: Usefulness and Experience of Robotic TCD in: NeuroSonology in Critical Care (NESCC) - Monitoring the Neurologic Impact of the Critical Pathology – 1st Ed. Springer, USA, 2018: In Press.

3. **Zeiler FA**, McFayden C, NewCombe V, Synnot A, Donoghue E, Ripatti S, Steyerberg E, Gruen R, Rosand J, Palotie A, Maas A, Menon DK. Genetic Influences on Patient Oriented Outcomes in TBI: A Living Systematic Review of Non-APOE Single Nucleotide Polymorphisms. J Neurotrauma. Apr 2018, In Press.

4. **Zeiler FA**, Menon DK. Response: Microdialysis as a useful tool to detect cerebral metabolic crises. Acta Neurochir (Wien). Jan 2018, In Press.

5. **Zeiler FA,** Czosnyka M. Monitoring in Cerebral Neurotrauma in Prabhakar H: Essentials of Anesthesia for Neurotrauma – 1st Ed. Taylor and Francis – CRC Press, USA, 2018: In Press.

6. **Zeiler FA**, Thelin E, Helmy A, Czosnyka M, Hutchinson PJ, Menon DK. A Systematic Review of Cerebral Microdialysis and Outcomes in TBI: Relationships to Patient Functional Outcome, Neurophysiologic Measures and Tissue Outcome. Acta Neurochir (Wien). 2017; 159(12):2245-2273. doi: 10.1007/s00701-017-3338-2.

7. **Zeiler FA**, Thelin E, Czosnyka M, Hutchinson PJ, Menon DK, Helmy A. Cerebrospinal Fluid and Microdialysis Cytokines in Aneurysmal SAH: A Scoping Systematic Review. Front Neurol. 2017; 8:379. doi: 10.3389/fneur.2017.00379.

8. **Zeiler FA**, Thelin E, Czosnyka M, Hutchinson PJ, Menon DK, Helmy A. Cerebrospinal Fluid and Microdialysis Cytokines in Severe TBI: A Scoping Systematic Review. Front Neurol. 2017; 8:331. doi: 10.3389/fneur.2017.00331.

9. **Zeiler FA**, Donnelly J, Calviello L, Smielewski P, Menon DK, Czosnyka M. Pressure Autoregulation Measurement Techniques in Adult TBI, Part II: A Scoping Review of Continuous Methods. J Neurotrauma. June 2017, In Press. doi: 10.1089/neu.2017.5086.

10. **Zeiler FA**, Donnelly J, Calviello L, Smielewski P, Menon DK, Czosnyka M. Pressure Autoregulation Measurement Techniques in Adult TBI, Part I: A Scoping Review of Intermittent Methods. J Neurotrauma. June 2017, In Press. doi: 10.1089/neu.2017.5085.

Meeting Proceeding Publications

1. **Zeiler FA**, Smielewski P. Application of Robotic TCD in Critically Ill TBI Patients: First Experiences. J Neurotrauma. 2018 August; 35(16):PS1.04.11.

2. **Zeiler FA**, Donnelly J, Calviello L, Lee JK, Smielewski P, Brady K, Kim DJ, Czosnyka M. Validation of PRx and PAx Indices Against the Lower Limit of Autoregulation in Intra-Cranial Hypertension. J Neurotrauma. 2018 August; 35(16):PS2.04.01.

3. **Zeiler FA**, Kim DJ, Cabeleira M, Calviello L, Smielewski P, Czosnyka M. Impaired Cerebral Compensatory Reserve is Associated with Diffuse Insult in Traumatic Brain Injury. J Neurotrauma. 2018 August; 35(16):PS2.04.04.

"Other"/Collaborative Publications (Published/Accepted)

1. Hasen M, Almojuela A, **Zeiler FA**. Autonomic Dysfunction and Associations with Functional and Neurophysiologic Outcome in Moderate/Severe Traumatic Brain Injury: A Scoping Review. J Neurotrauma. Accepted Oct 17th 2018.

2. **Zeiler FA**. A Promising New Non-Invasive Measure of Cerebrovascular Reactivity - Not Yet Cerebral Autoregulation. Neurocrit Care. July 2018, In Press.

3. **Zeiler FA**. Cerebral Perfusion Pressure Targets in Traumatic Brain Injury – The "Fuzzy" Spots Above Optimal Cerebral Perfusion Pressure. Can J Neurol Sci. July 2018, In Press.

4. **Zeiler FA**, Kim DJ, Cabeleira M, Calviello L, Smielewski P, Czosnyka M. Impaired Cerebral Compensatory Reserve is Associated with Admission Imaging Characteristics of Diffuse Insult in Traumatic Brain Injury. Acta Neurochir (Wein). July 2018, In Press.

5. Donnelly, J, Czosnyka M, Adams H, Cardim D, Kolias A, **Zeiler FA**, Lavinio A, Aries M, Robba C, Smielewski P, Hutchinson PJA, Menon DK, Pickard JD, Budohoski KP. 25 Years of Intracranial Pressure Monitoring After Severe Traumatic Brain Injury: A Retrospective, Single Center Analysis. Neurosurgery. Submitted as Original Article. April 2018.

6. Nourallah B, **Zeiler FA**, Czosnyka M, Menon DK. Critical thresholds for intracranial pressure vary over time in non-craniectomized traumatic brain injury patients. Acta Neurochir (Wien). Apr 2018, In Press.

7. Nourallah B, Menon DK, **Zeiler FA**. Midline Shift is Unrelated to Pupillary Reactivity in Moderate and Severe Traumatic Brain Injury. Neurocrit Care. Mar 2018, In Press.

8. Calviello L, Donnelly J, Cardim D, Robba C, **Zeiler FA**, Smielewski P, Czosnyka M. Compensatory-reserve-weighted intracranial pressure and its association with outcome after traumatic brain injury. Neurocrit Care. Oct 2017, In Press. doi: 10.1007/s12028-017-0475-7.

9. Thelin EP, Tajsic T, **Zeiler FA**, Hutchinson PJA, Menon DK, Carpenter KLH, Morganti-Kossmann MC, Helmy A. Monitoring the neuroinflammatory response following acute brain injury. Front Neurol. 2017; 8:351. doi: 10.3389/fneur.2017.00351.

10. Thelin EP, **Zeiler FA**, Ercole A, Mondello S, Buki A, Helmy A, Menon DK, Nelson DW. Monitoring brain injury by assessing protein biomarkers in serum – a systematic review of serial sampling in humans. Front Neurol. 2017; 8:300. doi: 10.3389/fneur.2017.00351.

11. Calviello L, Nicolás de Riva, Donnelly J, Czosnyka M, Smielewski P, Menon DK, **Zeiler FA**. Relationship Between Brain pulsatility and cerebral perfusion pressure: replicated validation using different drivers of CPP change. Neurocrit Care. 2017; 27(3):392-400. doi: 10.1007/s12028-017-0404-9.

12. Calviello LA, Donnelly J, **Zeiler FA**, Thelin E, Czosnyka M. Cerebral autoregulation in acute brain injury: what's the evidence? Minerva Anestesiol. 2017; 83(8):844-857. doi: 10.23736/S0375-9393.17.12043-2.

DISTINCTIONS/AWARDS

1. Royal College of Surgeons of Canada – Harry S. Morton Travelling Fellow in Surgery (2017 – 2018)
2. Royal College of Surgeons of Canada – Harry S. Morton Travelling Fellow in Surgery (2016 – 2017)
3. Cambridge Trust Scholar, University of Cambridge, Cambridge, UK (2016 – 2019)
4. R. Samuel McLaughlin Fellow, Rady Faculty of Health Sciences, University of Manitoba, Winnipeg, Canada (2016 – 2017)
5. Manitoba Medical Services Foundation Research Fellow, Rady Faculty of Health Sciences, University fo Manitoba, Winnipeg, Canada (2016-2017)
6. Dean's Fellow, Rady Faculty of Health Sciences, University of Manitoba, Winnipeg, Canada (2016 – 2017)

LIST OF FIGURES

LIST OF TABLES

Table 9.3: Univariate Logistic Regression of Admission Demographics and Scores with ICP Index – Grand Mean Data

LIST OF FORMULAE

1. *Formula for calculating CPP:*

$$CPP = MAP - ICP \qquad (3.1)$$

Where: CPP = cerebral perfusion pressure (in mm Hg), ICP = intra-cranial pressure (in mm Hg), and MAP = mean arterial pressure (in mm Hg)

2. *Fisher Logarithmic Transformation:*

$$z = \tfrac{1}{2}(\ln(1+x)-\ln(1-x)) \qquad (6.1)$$

Where: z = Fisher transformed variable, x = variable

3. *Basic Box-Jenkins Autoregressive Moving Average (ARMA) Process model for PRx:*

$$PRx_t = c + \varepsilon_t + \sum_{i=1}^{p} \varphi PRx_{t-i} + \sum_{i=1}^{q} \theta \varepsilon_{t-i} \qquad (7.1)$$

Where: c= constant, t = time "t", i = integer, p = autoregressive order, PRx = pressure reactivity index, q = moving average order, φ = autoregressive coefficient "i", θ = moving average coefficient "i", ε = error term.

LIST OF ABBREVIATIONS

ABP – arterial blood pressure
ABPd – diastolic arterial blood pressure
ABPs – systolic arterial blood pressure
ACE – angiotensin converting enzyme
AHC – agglomerative hierarchal clustering
AMP – pulse amplitude of ICP
APO - apolipoprotein
ARI – autoregulatory index
$AVDO_2$ – arterial – venous difference in oxygen
AUC – area under the curve
a.u. – arbitrary units
BNDF – brain derived neurotrophic factor
CA – cerebral autoregulation
CBF – cerebral blood flow
CBFV – cerebral blood flow velocity
CBV – cerebral blood volume
CPP – cerebral perfusion pressure
CSF – cerebrospinal fluid
CSV – coma separate variable
cm - centimeter
CMD – cerebral microdialysis
CNN – convolutional neural network
CT – computed tomography
CTP – CT perfusion
DC – decompressive craniectomy
Dx – diastolic flow index
Dx_a – diastolic flow index based on MAP
FV – flow velocity
FVd – diastolic flow velocity
FVm – mean flow velocity
FVs – systolic flow velocity
GRADE - Grading of Recommendation Assessment Development and Education
GCS – Glasgow Come Scale
GOS – Glasgow Outcome Score
Hb – total hemoglobin concentration
HHb – deoxygenated hemoglobin
HbO – oxygenated hemoglobin
Hz - Hertz
ICM+ - intensive care monitoring “plus” software
ICP – intracranial pressure
ICU – intensive care unit
IL – interleukin
ISS – injury severity score
KMCA – k-means cluster analysis
LDF – laser Doppler flowmetry
LPR – lactate:pyruvate ratio
Lx – LDF CBF index
Lx_a – LDF CBF index derived from MAP
MAP – mean arterial pressure
MCA – middle cerebral artery
MLR – muli-variate logistic regression
mm Hg – millimeter of Mercury
MMM – multi-modal monitoring
MRI – magnetic resonance imaging
Mx – mean flow index
Mx_a – mean flow index based on MAP
mW – milli-Watts
NCCU – neuroscience critical care unit
NICU – neuro-intensive care unit
NIRS – near infrared spectroscopy
nm – nanometers
NOS – nitric oxide synthase
NT - neurotransmitter
OHT - orthostatic hypotension test
PAx – pulse amplitude index
$PbtO_2$ – brain tissue oxygen
PCA – principal component analysis
PET – positron emission tomography
PRISMA - Preferred Reporting Items for Systematic Reviews and Meta-Analyses
PRx – pressure reactivity index
RAC – correlation between AMP and CPP
RAP – correlation between AMP and ICP
ROC – receiver operative curve
sec - seconds
SNP – single nucleotide polymorphism
SR – systematic review
Sx – systolic flow index
Sx_a – systolic flow index based on MAP
TBI – traumatic brain injury
TCD – transcranial Doppler
TCDT - thigh cuff deflation technique
TD – thermal diffusion
TF-ARI – transfer function ARI
THI – total hemoglobin index
THRT - transient hyperemic response test
TOI – total oxygenation index
TOx – total oxygen index
TOx_a – TOx based on MAP
THx – correlation between THI and CPP
THx_a – THx based on MAP
TNF – tumor necrosis factor
ULR – univariate logistic regression
Xe-CT – Xenon CT

CHAPTER 1: INTRODUCTION

Cerebral autoregulation (CA) is defined as the innate ability of the cerebrovascular system to maintain relatively constant cerebral blood flow (CBF) despite changes in systemic mean arterial pressure (MAP) or cerebral perfusion pressure (CPP).[1] Our current understanding of normal CA capacity stems from the work of Fog[2] and Lassen,[1] who identified that autoregulation was preserved in normal humans between approximately 50 mm Hg (referred to as the lower limit of autoregulation - LLA) and 150 mm Hg (referred to as the upper limit of autoregulation - ULA) of MAP. Systemic MAP, or CPP, below the LLA may lead to impaired CBF, hypoperfusion, metabolic failure, cytotoxic edema and potentially ischemia or infarction, while CPP or MAP above the ULA could result in hyperaemia, vasogenic oedema and haemorrhage.[1,3,4]

It is well understood that various neuropathologic states impact CA capacity, potentially leading to deleterious outcomes.[3,5–7] Traumatic brain injury (TBI) is one pathologic state in which CA capacity has been thoroughly studied and linked to morbidity and mortality in the adult population.[3,4,8,9] Various methods have been designed to measure CA in adult TBI, including both intermittent and continuous techniques,[4,10] and patients displaying "impaired" autoregulatory capacity have been shown to be at higher risk of secondary neurological insult and increased morbidity/mortality.

The most commonly employed methods of CA monitoring in TBI within the neuro-intensive care unit (NICU) involve continuously updating indices of autoregulation, which have received support through international consensus statements and recently published multi-modal monitoring guidelines in TBI.[11,12] These indices are derived on the premise that the correlation between slow-wave fluctuations in surrogate measures of pulsatile cerebral arterial blood volume (CBV), such as intracranial pressure (ICP), and slow-wave fluctuations in a driving pressure for CBF, such as MAP or CPP, providing insight into the autoregulatory function in any given patient.[3,13] Based on this concept, various indices of CA have been developed based on signals derived from multi-modal monitoring (MMM) devices.[4,10]

However, despite many options for continuous monitoring of autoregulatory capacity in adult TBI, and literature supporting an association with patient global outcome, there are some important questions which remain unanswered:

1. Are there any relationships between commonly measured physiologic variables which may better approximate autoregulation/cerebrovascular reactivity in TBI patients?

2. Do these indices actually measure cerebral autoregulation?
3. What are the inter-index relationships between these continuous CA indices derived from various multi-modal monitoring metrics? Are all indices the same or related to one another?
4. Can one estimate indices of cerebrovascular reactivity using non-invasive surrogates, which correlate with more classical measures derived from invasive measures?
5. How well do ICP derived indices predict outcome in adult TBI? Is one superior? Are there critical thresholds?
6. Does injury burden drive impaired cerebrovascular reactivity in adult TBI?

Having answers to these questions is of great importance to: the validity in clinical monitoring of CA in TBI, detection of failed CA and prediction of CA impairment. Answers to these questions would also provide a validated and robust platform for future investigation of biologic drivers of impaired reactivity, understanding the long-term tissue consequences to impaired CA post-TBI, and potentially leading to therapeutic targets for the avoidance/treatment of CA dysfunction. Thus, the goal of this dissertation is to shed light on these above defined questions.

1.1 Aims and Hypothesis

1.1.1 Defining a New Continuous Index

Current continuous monitoring of cerebrovascular reactivity/autoregulation in adult TBI focus mainly on the use of the pressure reactivity index (PRx).[4,11,12] This index is the defined as the moving Pearson correlation coefficient between slow-wave fluctuations in ICP and MAP. PRx has emerged as the "gold standard" for continuous monitoring of vascular reactivity, with strong links to 6-month outcome and defined critical thresholds in adult TBI.[3,9] Furthermore, this index has been validated as a measure of the LLA in an experimental model of arterial hypotension.[14] Despite this, there exists a potential for other continuous indices to be derived from ICP and MAP monitoring.[15] The first step within this thesis was to explore a new index of cerebrovascular reactivity in adult TBI, RAC: the correlation between pulse amplitude of ICP (AMP) and CPP. RAC stands for: R = Pearson correlation coefficient, A = pulse amplitude of ICP, C = cerebral perfusion pressure.

<u>Hypothesis I:</u> The moving correlation coefficient between slow-wave fluctuations in AMP and CPP, defined as RAC, will provide information regarding cerebrovascular reactivity, and may be used in place of existing ICP based reactivity indices in adult TBI patients.

1.1.2 Experimental Validation of ICP Derived Indices

Within the current literature on continuous indices of cerebrovascular reactivity measurement, very few indices have been validated experimentally to measure autoregulation.[14] The baseline assumption surrounding all MMM based continuous indices of vascular reactivity is based on the concept that the relationship between slow-wave fluctuations in a driving pressure (ie. MAP or CPP) and a surrogate measure of pulsatile CBV or CBF, is a measure of autoregulation.[13] Unfortunately, only three indices to date have been validated experimentally to measure the LLA. These include PRx and two near infrared spectroscopy (NIRS) derived indices.[14] Furthermore, validation against the ULA has not been clearly demonstrated within the literature. Finally, the current validation studies focused on a model of arterial hypotension for assessing the LLA, with no literature to support that the assessed indices (ie. PRx) measure the LLA during intra-cranial (IC) hypertension. This is an important aspect in TBI, given many patients suffer from ICP control issues during their acute phase of care. Such preliminary validation with respect to the LLA would require: A. demonstration of cerebrovascular reactivity indices to trend towards progressively more positive values at CPP levels below the LLA, and B. statistically significant logistic regression analysis for each cerebrovascular reactivity index in the prediction of having CPP values above or below the cohort defined LLA; similar to the previous existing experimental work.[14] Simiarly, preliminary validation work into the ULA would require: A. demonstration of cerebrovascular reactivity indices to trend towards progressively more positive values at CPP levels above the ULA, and B. logistic regression analysis confirming statistically significant ability of cerebrovascular reactivity indices to predict CPP being above or below the ULA. Therefore, the second step of this thesis was to explore the LLA and ULA in data that were available in various pre-clinical experimental models, in order to provide validation for all ICP derived indices of cerebrovascular reactivity: PRx, PAx (correlation between AMP and MAP), and RAC.

<u>Hypothesis II:</u> PRx, PAx and RAC will measure the LLA in an experimental piglet model of arterial hypotension, displaying trends towards progressively more positive values below the LLA and logistic regression techniques demonstrating the ability to accurately predict CPP values about this threshold.

<u>Hypothesis III:</u> PRx, PAx and RAC will measure the LLA in an experimental rabbit model of sustained intracranial hypertension, displaying trends towards progressively more positive values below the LLA and logistic regression techniques demonstrating the ability to accurately predict CPP values about this threshold.

<u>Hypothesis IV:</u> PRx, PAx and RAC will measure the ULA in an experimental piglet model of arterial hypertension, displaying trends towards progressively more positive values above the ULA and logistic regression techniques demonstrating the ability to accurately predict CPP values about this threshold.

1.1.3 Multi-Model Index Relationships

Various continuous indices of cerebrovascular reactivity exist in adult TBI.[4] These measures are based on various invasive and non-invasive MMM devices commonly employed within the intensive care unit (ICU) in the treatment of TBI patients. Such monitoring includes: ICP,[3,15] brain tissue oxygen ($PbtO_2$),[16–18] transcranial Doppler (TCD)[8] and NIRS.[19,20] Numerous small studies exist providing some basic statistical links between individual indices. However, one question remains: Are all of these indices the same? To date, there has not been an in-depth exploration of the inter-index relationships between multiple MMM devices simultaneously. This approach could potentially shed light on which indices closely co-vary and which may be used as a surrogate measure for the other. The third step of this thesis involves exploring the inter-index relationships of MMM derived continuous indices of cerebrovascular reactivity across multiple adult TBI populations.

<u>Hypothesis V:</u> Continuous indices derived from MMM are not all the same, and display specific covariance structure between monitoring devices used, which is reproducible across populations.

1.1.4 Non-Invasive Modelling of Pressure Reactivity

The literature supports a strong association between PRx and 6-month outcome in adult TBI. Further, as aluded to above, PRx has emerged as the "gold standard" for continuous monitoring of cerebrovascular

reactivity in adult TBI. The main limitation to PRx is that is requires invasive ICP monitoring. Given this limitation, some important questions arise: Is it possible to model PRx using non-invasive surrogates? Can PRx be accurately estimated non-invasively? Can we forecast (ie. predict) PRx via non-invasive means? The fourth part of this thesis attempts to answer these questions.

Hypothesis VI: ***PRx can be accurately estimated via non-invasive TCD alternatives, systolic flow index (Sx_a) and mean flow index (Mx_a).***

Hypothesis VII: ***PRx can be predicted via the non-invasive TCD based alternative Sx_a.***

1.1.5 Critical Thresholds Associated with Outcome

Thresholds associated with 6-month outcome in adult TBI have been defined for PRx[9] and the TCD based Mx (correlation between mean flow velocity (FVm) and CPP).[8] These thresholds have been defined for two dichotomized 6-month outcomes: A. mortality and B. favourable/unfavourable functional status (as per Glasgow Outcome Score (GOS)). Aside from these two indices, critical thresholds for other indices are unknown.

Importantly, PRx isn't the only ICP derived index, with PAx and RAC potentially providing similar (or superior) outcome prediction capacity.[15,21] Furthermore, the previous study which defined PRx thresholds in adult TBI was based on grand mean PRx values from a large heterogeneous patient population, including those with decompressive craniectomy (DC) and those without.[9] It is known that craniectomy in TBI impacts both ICP and PRx,[22] leading to uncertainty in the assessment of cerebrovascular reactivity using PRx during the post-craniectomy phase of care. Thus, the current defined thresholds for PRx[9] are difficult to apply to all TBI patients, with thresholds for non-DC patients (ie. the majority of critically ill TBI patients) currently unknown. Determining which ICP index is superior for outcome prediction, and what the critical thresholds for these indices are in non-DC patients, would prove valuable for continued application of this monitoring within the ICU. The fifth part of the thesis addresses this.

Hypothesis VIII: ***Outcome prediction with ICP indices are not equal, with RAC providing superior predictive capabilities for 6-month patient outcomes.***

<u>Hypothesis IX:</u> Critical thresholds for 6-month outcome in adult TBI for ICP derived reactivity indices are not all the same, with some indices displaying more "stable" thresholds over time.

Aside from invasive ICP derived indices for monitoring cerebrovascular reactivity, TCD provides a convenient and potentially completely non-invasive means of measuring CA. To date, Mx (correlation between TCD mean flow velocity (FVm) and CPP) and Mx_a (correlation between FVm and MAP) are the only TCD indices with defined critical thresholds in adult TBI.[8] Given strong associations between ICP derived indices and those from TCD, particularly with Sx/Sx_a, determining the critical thresholds for other TCD indices may prove valuable for future work in the non-invasive assessment of cerebrovascular reactivity. This is also addressed within the fifth part of this thesis.

<u>Hypothesis X:</u> Both Sx and Sx_a have well defined critical thresholds associated with 6-month outcome in adult TBI.

1.1.6 Injury Burden as a Driver of Impaired Reactivity

Finally, despite being able to monitor cerebrovascular reactivity in adult TBI with confidence, which would be provided through the previously mentioned aims/hypothesis of this thesis, understanding what drives impaired reactivity is also crucial. Specifically, does injury pattern/burden play a role in developing impaired cerebrovascular reactivity? What role does IC injury burden play? What about extra-cranial (EC) injury burden? Currently, these questions remain unanswered in the literature. The sixth part of this thesis addresses and answers these questions.

<u>Hypothesis XI:</u> Specific patterns of IC injury are associated with impaired cerebrovascular reactivity in TBI.

<u>Hypothesis XII:</u> EC injury burden will be associated with cerebral vascular reactivity in polytrauma patients.

1.2 Overview of Thesis

Chapter 2 provides an extensive review of the pertinent literature surrounding continuous monitoring of cerebrovascular reactivity in adult TBI. This review includes both narrative and systematically conducted components. The chapter will overview the concept of cerebral autoregulation and theorized mechanisms of control. Subsequent sub-sections will highlight systematic reviews of the literature conducted as part of the review of literature for this thesis,[4,10] including overviewing monitoring techniques for autoregulation and any existing literature documenting the association between autoregulation monitoring and injury burden.

Chapter 3 provides an overview of general methodology for the studies conducted within the subsequent chapters. This chapter covers the experimental models used, including experimental procedures. It also reviews the adult TBI patient populations studied and general treatment received while within the ICU. General signal acquisition, processing, ethical considerations and statistics are also covered.

Chapters 4 through 9 report the results from the studies performed in this thesis. Chapter 4 presents results from the description of a "new" physiologic index of cerebrovascular reactivity, RAC, in an adult TBI population (addressing hypothesis I). Chapter 5 presents the results of experimental validation of ICP derived indices for measuring the LLA and ULA (addressing hypotheses II, III and IV). Chapter 6 presents the results of the assessment of inter-index relationships between MMM derived continuous measures of cerebrovascular reactivity, across various adult TBI populations (addressing hypothesis V). Chapter 7 presents the results of non-invasive modelling of PRx using TCD based surrogates (addressing hypotheses VI and VII). Chapter 8 presents the results of the studies exploring of outcome prediction of ICP and TCD derived indices of cerebrovascular reactivity, with the assessment of critical thresholds (addressing hypotheses VIII, IX, and X). Finally, Chapter 9 presents the results of the analysis of injury burden and its association with impaired cerebrovascular reactivity in adult TBI (addressing hypotheses XI and XII).

Chapter 10 summarizes the results of this thesis, providing an overall conclusion. Chapter 11 overviews potential future directions of research regarding continuous cerebrovascular reactivity monitoring in adult TBI.

CHAPTER 2: REVIEW OF LITERATURE

2.1 Cerebral Autoregulation

2.1.1 Concept

Cerebral autoregulation (CA) is defined as the cerebral vessel's innate ability to regulate and maintain constant CBF across a wide range of MAP or CPP.[1] First defined by Lassen, and outlined in his seminal work in 1959, CA in humans is characterized by the relationship between MAP and CBF seen in Figure 2.1. Lassen's original description of this phenomenon consisted of a small heterogenous group of patients, in which measures of cerebral blood flow were conducted during manipulations in MAP and partial pressure of carbon dioxide (pCO_2).[1] Similar relationships between MAP and CBF were observed in Lassen's observations, regardless of the physiologic manipulation undertaken.

Figure 2.1: Classical Representation of Cerebral Autoregulatory Curve in Humans

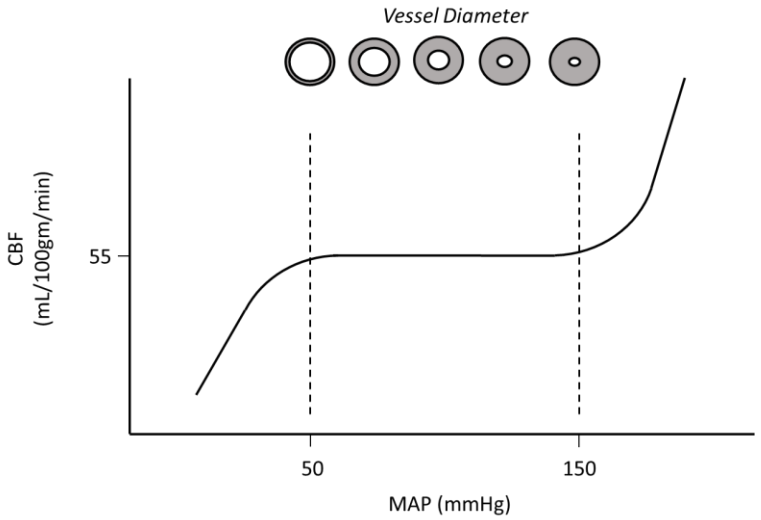

CBF = cerebral blood flow, gm = gram, MAP = mean arterial pressure, min = minute, mL = milliliter, mmHg = millimetres of Mercury. Vertical dashed black lines represent the lower limit of autoregulation (ie. ~50 mm Hg) and the upper limit of autoregulation (ie. ~150 mm Hg) seen within healthy subjects. Vessel diameter changes can be seen along the top of the graph, indicating that at lower MAP values the vessel dilates allowing maintained CBF, while at high MAP the vessel constricts. Beyond the lower and upper limits, CBF becomes pressure passive as the cerebral vessels are unable to regulate constant flow. Since its first appearance, the general understanding of autoregulation has been modified. First, x-axis has been scaled in cerebral perfusion pressure (CPP), acknowledging that not only variations in MAP may modify CBF outside limits of autoregulation, but variations of ICP may also contribute. Second, not only an inner diameter of flow regulating arteries changes, but outer diameter changes as well, with inner diameter (ie. luminal) changes leading to modulation of arterial cerebral blood volume.

This description, which has been validated in animal models and human studies, describes a range of "normal" cerebral autoregulation across MAP ranges of 50 to 150 mm Hg (ie. the "lower" and "upper" limits of autoregulation), allowing for a relatively constant CBF, near or around ~55 mL/100gm/min.[1,3] MAP outside of this range, exceeds the ability of cerebral vessels to regulate CBF, leading to deleterious consequences. Below the LLA, MAP is low, and CBF cannot be maintained, leading to hypoperfusion, ischemia, and potentially infarction. Above the ULA, the cerebral vessels are unable to regulate flow, leading to a hyperperfusion state.[23] This quickly overwhelms the capillary bed, via elevated capillary filling pressures, leading to cerebral edema, impaired nutrient transport, and potentially intra-cerebral hemorrhage.

The mechanism involved in cerebral autoregulation is believed to be related to variations in the cerebral vessel caliber in response to the driving pressure seen.[23] While the caliber of vessels involved in this cerebral autoregulatory process is debated, pre-capillary arterioles, measuring up to a few hundred microns in diameter, remain the most likely candidates.[24–26] The response of the cerebral vessels to changes in MAP are believed to occur in the frequency range of 0.005 to 0.05 Hertz (Hz), implicating "slow-wave" responses of these vessels to alterations in MAP.[13,27]

2.1.2 Theorized Regulatory Mechanisms

The exact mechanisms involved cerebral autoregulation and the innate ability of cerebral vessels to regulate CBF through changes in tone and caliber are not clear. Current theories include: myogenic, metabolic, neurotransmitter and endothelial based concepts.[23,28] The myogenic theory focuses on the direct mechanical reflex of vascular smooth muscle in response to variations in cerebral perfusion pressure mediated via vascular stretch experienced by the cerebral vessels. As perfusion pressure increases, there is an increase in stretch experienced by the tunica media, leading to a reflex vasoconstriction, ensuring constant CBF. Conversely, low cerebral perfusion pressure leads to relaxation of the cerebral vessels consequent to decreased stretch of the tunica media. This theory, however, fails to explain biochemically driven cerebrovascular responses seen in vitro. The metabolic theory states that byproducts of cerebral metabolism can impact or dictate cerebral vessel caliber. For example, in states of hypoperfusion, cerebral metabolism quickly shifts to anaerobic metabolism, generating lactate, amongst other metabolic products. It is believed these products may impact vessel caliber, in an attempt to restore adequate CBF. The downside to this theory is that it fails to explain the relatively

rapid temporal response of cerebral vessels, as it takes time to produce metabolic byproducts in significant concentrations such that the cerebral vasoreactivity would be impacted. The neurotransmitter theory implies that all cerebrovascular reactivity is driven via direct neural input to the smooth muscle. This theory would account for the rapidity of cerebral vascular response, but does not fully explain other biochemical or endothelial responses. Finally, the endothelial response implies that changes in perfusion pressure drive direct endothelial responses which regulate vessel caliber. Such endothelial based mediators include nitric oxide (NO) produced by by nitric oxide synthase (NOS), eicosanoid release, and endothelin production.

Aside from these mechanisms which apply in health, aspects of the injury response may modulate cerebrovascular reactivity in disease. For example, the inflammatory response appears to play a role in outcome within TBI[29] and SAH.[30,31] The potential exists that the inflammatory response to both the primary and secondary injury may drive autoregulatory dysfunction. Autonomic response via catecholamine action on cerebral vasculature, may directly modulate vascular tone and regulate autoregulatory capacity post-TBI.[32] Other evidence suggests a role for abnormal cerebral electrophysiologic responses to injury. Spreading cortical depression (SCD) has recently emerged as potential player in cerebrovascular reactivity in animal models.[33–36] The presence, or increased frequency, of such electrophysiologic patterns may also drive autoregulatory dysfunction post injury.[37] Furthermore, recent literature in humans supports an association CBF dysfunction and vascular reactivity dysfunction in adult TBI.[38,39] Such SCD episodes have been demonstrated to occur frequently in moderate and severe TBI patients.[38,39] In corollary, dynamic temporal links between SCD and impaired CBF has been demonstrated in small cohorts of adult TBI patients.[38] Similarly, data suggests the temporal link between SCD and both excitotoxicity and metabolic crisis, as defined by elevated cerebral microdialysis glutamate and lactate:pyruvate ratio.[40] Finally, disruption of solute/nutrient transport across the blood brain barrier (BBB) may play a role in the potentiation of autoregulatory dysfunction.

2.2 Review of Literature on Cerebrovascular Reactivity in Adult TBI

In order to gain a comprehensive understanding of the available literature on: intermittent/semi-intermittent autoregulation measurement techniques,[10] continuous methods of autoregulation measures in adult TBI,[4] and association between injury burden and vascular reactivity, various systematic reviews (SR's) were conducted.

All SR's were conducted independently for the review of literature component of this thesis, with the involvement of a second literature filterer only for the purpose of abiding by standard SR guidelines as outlined by the Cochrane Handbook of Systematic Reviews.[41] For the SR's presented in the sections to follow, Dr. Eric P. Thelin (Karolinska Institute) was the second reviewer. The summation of results, analysis and presentation were all conducted independently by the author of this thesis.

The systematic reviews were conducted to outline the literature body in the following areas:

A. Intermittent/semi-intermitent techniques for cerebrovascular reactivity measurement in adult TBI, evaluating the link between these measures and both: other cerebral physiology measures and patient global outcome. The following intermittent/semi-intermitent techniques were evaluated: computed tomographic perfusion (CTP)/Xenon-CT (Xe-CT), positron emission tomography (PET), magnetic resonance imaging (MRI), arterio-venous difference in oxygen (AVDO2) technique, thigh cuff deflation technique (TCDT), transient hyperemic response test (THRT), orthostatic hypotension test (OHT), mean flow index (Mx) and transfer function autoregulation index (TF-ARI).

B. Continuous techniques for cerebrovascular reactivity measurement in adult TBI, evaluating the link between these measures and both: other cerebral physiologic measures and global patient outcome. The following continuous techniques were evaluated: PRx, laser Doppler flowmetry (LDF), NIRS techniques, PbtO2, and thermal diffusion (TD) techniques.

C. Evaluation of any link between systemic or intra-cranial injury burden and impaired cerebrovascular reactivity in adult TBI patients.

Each systematic review was conducted in a robust format, adhering to standard methodological processes for SR's. All methodological principles employed for the SR, including: search strategies, inclusion/exclusion criteria, article filtering processes, data curation and summary techniques can be found in the individual published manuscripts. The results of these SR's conducted for this thesis, detailed in the subsections to follow, can be found in the various separate publications.[4,10,29,31,42]

2.2.1 Methods of Measurement and Associations with Outcome

2.2.1.1 Intermittent/Semi-Intermittent Methods

A systematic, scoping review of commonly described intermittent/semi-intermittent autoregulation measurement techniques in adult TBI was performed. Techniques were defined as intermittent if they produced a single point measure of autoregulatory capacity. Further, some TCD based techniques were defined as semi-intermittent, given the labor-intensive nature of TCD and limited duration of recordings obtainable in clinical practice, mostly due to unstable fixation of ultrasound probes. A detailed account of the results can be seen in the publication Zeiler et al.[10]

Nine separate systematic searches were conducted for each intermittent technique: CTP/Xe-CT, PET, MRI, $AVDO_2$ technique, TCDT, THRT, OHT, Mx and TF-ARI. MEDLINE, BIOSIS, EMBASE, Global Health, Scopus, Cochrane Library (inception to December 2016) and reference lists of relevant articles were searched.

The total number of articles utilizing each of the 9 searched techniques for intermittent/semi-intermittent autoregulation techniques in adult TBI were: CTP/Xe-CT (10),[43–52] PET (6),[53–58] MRI (0), $AVDO_2$ (10),[55,59–67] autoregulation index (ARI) based TCDT (9),[47,68–75] THRT (6),[62,76–80] OHT (3),[79,81,82] Mx (17)[3,8,54,83–96] and TF-ARI (6).[94,97–101] Studies focusing on Mx were limited to those with 50 or more patients, assessing the association to patient outcome. The premise behind all of the intermittent techniques is manipulation of systemic blood pressure/blood volume via either chemical (such as vasopressors) or mechanical (such as thigh cuffs or carotid compression) means. Exceptionally, Mx[97] and TF-ARI[94] are based on spontaneous fluctuations of CPP or MAP. The method for assessing the cerebral circulation during these manipulations varies, with both imaging-based techniques and TCD utilized.

Despite the limited literature for intermittent/semi-intermittent techniques in adult TBI (apart from Mx), it is important to acknowledge the availability of such tests. They have provided fundamental insight into human autoregulatory capacity, leading to the development of continuous and more commonly applied techniques in the ICU. Numerous methods of intermittent/semi-intermittent pressure autoregulation assessment in adult TBI exist, including: CTP/Xe-CT, PET, AVDO2 technique, TCDT based ARI, THRT, OHT, Mx and TF-ARI. MRI based techniques in adult TBI are yet to be described, with the main focus of MRI techniques on metabolic based vascular reactivity and not pressure-based autoregulation. A complete and detailed assessment of each intermittent/semi-intermittent measurement technique in adult TBI can be found in the Zeiler et al article.[10]

Semi-intermittent measures deserve further mention, as they include TCD-derived continuously updating indices (such as Mx), and have been utilized in the studies conducted within this thesis. Mx is derived from a moving Pearson correlation coefficient between two continuously measured signals, mean cerebral blood flow velocity (FVm) and CPP.[97] In this context, cerebral blood flow velocity (CBFV) is obtained through TCD insonation of the middle cerebral artery (MCA). Given the need for continuous TCD monitoring to calculate this updating index, the duration of recording is typically limited to 60 minutes or less. Thus, this technique is referred to as a "semi-intermittent" autoregulatory measurement technique.

The concept of this autoregulatory measure is that the slow wave responses in FVm to slow waves in CPP are believed to be governed by autoregulatory capacity. TCD ultrasound is used to capture the MCA velocity. As with all the other TCD based measures the signal can be acquired either unilaterally or bilaterally, thus providing insight into the symmetry of cerebral autoregulation. In addition, continuous recording of MAP (via either invasive arterial line or continuous non-invasive techniques) and ICP are required for determination of CPP (based on: CPP = MAP – ICP). The signals are recorded and stored, with the option of both off-line and real-time calculation of Mx. Both FVm and CPP are processed via a 10-second moving average filter and sampling frequency decimated to 0.1 Hz (in other words replacing original FVm and CPP by times series composed of their non-overlapping 10s averages). The correlation coefficient is then calculated based on 30 consecutive 10-second mean values (ie. 5 minutes), with the coefficient updated every 10 or 60 seconds. This produces an Mx time series with the similar sampling rate as mean FVm/CPP. Variations in the correlation window length have been described, though the above-mentioned parameters are the most commonly cited, particularly in more recently. Similar to

pressure reactivity index (PRx – derived from invasive ICP and MAP), Mx in routine autoregulation monitoring should be averaged for a minimum period of 30 minutes to reduce its inherent variance.

Some variations in the technique have been described. The use of MAP instead of CPP has been explored (termed Mx_a) as this renders the technique potentially non-invasive.[84] However, by using MAP and not CPP, the impact of ICP on FVm is not considered during the calculation of the correlation coefficient. Literature comparing standard Mx to Mx_a has demonstrated that Mx is superior in terms of outcome prediction in TBI, hence Mx_a is limited to these cases when ICP is not directly monitored.[84] Similarly, instead of using FVm in the correlation, there has been investigation into utilizing either only systolic or diastolic flow velocities (FVs or FVd), creating two alternate indices (Sx and Dx, respectively; and their "non-invasive" versions Sx_a and Dx_a).[84] Again, as with Mx_a, Sx/Sx_a and Dx/Dx_a have not been found to be grossly superior to Mx. Thus, Mx is most commonly quoted.[10]

The metric generated by calculating these TCD indices ranges from -1 to +1, as it is a correlation coefficient. A value that is highly positive indicates potentially "impaired" autoregulation, as it signifies a passive, linear relationship between CPP and FVm/FVs/FVd. Similarly, a zero or negative index value indicates that fluctuations in CPP are heavily attenuated and phase shifted in recorded FV (FVm, FVs, or FVd), thus suggesting "intact" autoregulation. The exact index value at which autoregulation is "impaired" and pathologic is not clear. Sorrentino et al evaluated thresholds of Mx as they related to mortality and GOS at 6 months post-TBI.[8] A double peaked threshold was found for Mx with threshold of +0.3 and +0.05 discriminating between both life versus death, and good versus poor outcome. Both thresholds are utilized within the literature to denote "impaired" autoregulation.

The search of the adult TBI literature yielded 17 studies, with 50 or more subjects, describing the association between Mx and patient outcome. [3,8,54,83–96] The patients suffered from moderate to severe TBI, with an average of 212 patients per study. Of note, all of these papers originated from Addenbrooke's hospital in Cambridge, as part of either retrospective reviews of a prospectively maintained database on TCD in TBI, or as prospective cohort studies. Thus, the actual number of unique patients overall across all of the studies is much lower, since there is overlap in patient inclusion across the multiple studies. Despite this, across these 17 papers, Mx is noted to be strongly associated with patient outcome. Furthermore, given the ability to obtain MCA velocities bilateral, asymmetry in autoregulatory capacity has been documented, with the greater right-left difference in Mx being associated with worse outcome. The incidence of "impaired" autoregulation, as defined by Mx, was not clear in most of the included studies, as the search for TCD based Mx studies focused on those

documenting an association to patient functional outcome. In addition, "impaired" autoregulation detection using Mx is difficult, given the lack of an exact threshold for this physiologic event, and only thresholds for morbidity and mortality that have been well defined.

2.2.1.2 Continuous Methods

A systematic scoping review of the literature on commonly described continuous autoregulation measurement techniques in adult TBI was conducted. The goal was to provide an overview of methodology for each technique. This review is detailed in Zeiler et al.[4]

Five separate systematic reviews were conducted for each of the continuous techniques: PRx, LDF, NIRS techniques, $PbtO_2$, and TD techniques. Articles from MEDLINE, BIOSIS, EMBASE, Global Health, Scopus, Cochrane Library (inception to December 2016) and reference lists of relevant articles were searched. The literature base identified from the individual searches was limited, except for PRx.

The total number of articles utilizing each of the 5 searched techniques for continuous autoregulation in adult TBI were: PRx (28),[3,9,15,27,58,83,85,91,102–121] LDF (4),[122–125] NIRS (9),[20,126–133] $PbtO_2$ (10),[116,127,128,130,134–139] and TD (8).[38,64,128,135,140–143] Studies focusing on PRx were limited to those assessing the association to patient outcome. All continuous techniques described in adult TBI are based on moving correlation coefficients. The premise behind the calculation of these moving correlation coefficients focuses on the impact of slow fluctuations in either MAP or CPP on some indirect measure of CBF or CBV, such as: ICP, LDF, NIRS signals, $PbtO_2$ or TD CBF. The conceptual basis for such measures is that the correlation between a hemodynamic driving factor (such as MAP or CPP), and a surrogate for CBF or CBV, sheds insight on the state of cerebral autoregulation. Both PRx and NIRS indices were validated experimentally against the 'gold standard' static autoregulatory curve at least around the lower threshold of autoregulation.[14] PRx has the largest literature base supporting the association with patient outcome.

Various methods of continuous autoregulation assessment are described within the adult TBI literature. Many studies exist on these various indices, and suggest an association between their values and patient morbidity/mortality. Given these multi-modal monitoring (MMM) derived techniques are the main focus of this thesis, further details on each continuous technique can be found below:

1. *Pressure Reactivity Index (PRx)*

The use of continuously updating PRx monitoring was first described in the mid to late 1990's, and this technique is currently one of the most common methods for continuous assessment of autoregulation employed within the ICU.[3] Furthermore, this index is one of the only continuous cerebrovascular reactivity indices that has been experimentally validated to measure the LLA.[14] The concept behind this index of autoregulatory capacity is that the continuous relationship between slow-wave (ie. 0.005 to 0.05 Hz) vasogenic fluctuations in ICP and MAP are an indirect measure of the cerebrovascular response. The correlation between slow-wave changes in a surrogate measure of fluctuating CBV (ie. ICP) and MAP provides information regarding signal phase-shift and autoregulatory status. In order to obtain this value, a moving correlation coefficient is calculated between slow-waves ICP and MAP. First, continuous, full waveform quality, signals of MAP (typically from a radial artery line) and ICP (typically from any invasive ICP monitoring device) are recorded. Processing these signals to determine PRx may be conducted off-line or in real-time. Next, a 10 second moving average is calculated for both ICP and MAP and decimated to 0.1Hz, using 10 second non-overlapping data windows averages (to remove the influence of cardiac cycle and respiration). The Pearson correlation coefficient is then calculated using 30 consecutive average ICP and MAP values, spanning 5 minutes of data. This calculation is then repeated every 60 seconds (thus introducing 80% overlap, 4 min), producing a minute-by-minute update to the PRx value. The concept behind PRx is that changes in ICP within the 5-minute window in this calculation represent a surrogate for changes in intracerebral blood volume which in turn represent most likely arteriolar vasodilation or constriction. Thus, PRx can be considered a measure of vascular reactivity. A single value of PRx is difficult to interpret. Averaging over a minimal period of 30 minutes is suggested, unless transient responses of PRx to deep and sudden events are being explored (such as a change in ICP during plateau waves, response to change in $PaCO_2$, etc). Other calculation window lengths have been described.

PRx values produced from the above described calculation range from -1 to +1, given that they are correlation coefficients. A positive value indicates a strong positive correlation between MAP and ICP such that any increase in MAP leads to an increase in ICP (ie. no phase shift between the ICP and MAP waveforms), and thus represents "impaired" autoregulation. Conversely, a negative PRx indicates a negative correlation between MAP and ICP, indicating "intact" autoregulation. The model which assumes MAP slow variations are an input to which responses in ICP can be observed, is not always relevant. For example, when ICP is already high, MAP responds in-phase to changes in ICP as a Cushing's

response, which makes PRx continuously close to +1. While the physiological significance of these extreme PRx values are self-evident, the threshold value of PRx that represents a transition from functioning autoregulation to "impaired" autoregulation is, as yet, not clear. Various thresholds of PRx have been identified within the literature.[9] The most commonly quoted are those by Sorrentino et al.[9] Within this study, various thresholds of PRx (mean value over the entire monitoring period) were assessed by their association with mortality and good vs. poor functional outcome as assessed by the Glasgow Outcome Scale (GOS) at 6 months post-TBI. Two thresholds were identified: 1. PRx of 0 or lower was associated with better 6-month GOS, 2. PRx >0.25 was associated with mortality. [9] Thus, to date, the threshold of 0.25 for PRx is the value many clinicians use to identify those patients with "impaired" autoregulation. When PRx is negative, autoregulation is good. The "intermediate" range of 0 to 0.25 for PRx, based on the two thresholds identified by Sorrentino, may provide warning of imperfect autoregulation or impending autoregulatory dysfunction, or may signify the rare state that power of slow waves of ICP and AMP is too low, to contain any useful information about cerebral pressure reactivity.

The use of PRx has led to the development of patient tailored therapy for CPP targets. By plotting PRx versus CPP, one can identify the CPP with the lowest PRx values (ie. "best" autoregulatory state). A recent systematic review of CPP optimum, as derived from PRx, displayed trends to improved outcomes when CPP was within the "optimum range".[144] This has sparked some interest in a trial of CPP optimum guided therapy, versus conventional CPP targets in TBI, which is now being conducted in three European centres.

The search strategy identified 28 papers which described the association of PRx to patient outcome in adult TBI. [3,9,15,27,58,83,85,91,102–121] Eighteen of these studies had 50 or more patients, with an average of 243 patients per study. The remaining 10 studies had less than 50 patients per study. The patients studied had moderate – severe TBI, with almost all patients within the included studies being of adult age. A small number of pediatric patients (age <18 years) were embedded within the large data sets, making it impossible to extract the pediatric information. Thus, the number of pediatric patients is quite small. The majority of the studies report strong associations between PRx and outcomes at various time points, regardless of study size. PRx is also noted to correlate with the individual TCD based intermittently monitored indices of autoregulation. Furthermore, correlation with individual NIRS based indices has also been confirmed.

2. LDF Based Techniques

The use of LDF monitoring in TBI has ceased in the clinical setting, with only a few studies documenting its use. [122–125] This technique was included in order to be thorough and describe a technique based on the assessment of cortical small arteriolar/microvasculature.

The LDF probe is placed in the subdural space, overlying the cortical surface of the brain. A low power solid-state laser diode emits infrared light onto the cortical surface. The reflected photons are Doppler shifted in frequency, with the shift being a function of the velocity of moving blood in the area. The reflected infrared signal is detected by the probe, with CBF reported in arbitrary units and recorded as a continuous signal. To derive an index of autoregulatory capacity, the similar technique of calculation of moving a Pearson correlation coefficient (as with PRx) can be used. 10 second mean values for CBF and CPP (updated every 10 seconds), with the correlation coefficient based on 30 consecutive values from a moving window are computed. This autoregulatory index based on LDF is called Lx. The premise here is that the impact of slow changes in CPP on LDF derived CBF are an indirect measure of autoregulatory capacity.

Given the small literature base on LDF in TBI, the exact values of Lx which denote "intact" versus "impaired" autoregulatory capacity are unclear. Values above a Lx of 0 likely indicated some degree of impairment of autoregulatory capacity, while those less than 0 likely indicated intact autoregulation.

The search of the adult TBI literature produced only 4 studies on the use of LDF for autoregulatory assessment. [122–125] The populations studied were moderate to severe TBI patients. Conclusions regarding the technique are limited given small patient numbers. However, persistently positive Lx values were associated with poor GOS at 6 months.

3. NIRS Techniques

The use of NIRS has generated numerous new indices of cerebral autoregulatory capacity. NIRS involves placing optodes on the patient's scalp (typically with a bifrontal distribution, since optodes requires placement on a hairless area). The NIRS device, depending on the manufacturer, uses two or more wavelengths of infrared light via typically a single emitter, with 2-4 detector photodiodes placed in line with the emitter at the distance of min 2.5 cm.[20] Based on the diffusion characteristics of infrared light, various measures can be mathematically derived from the signal using the modified Beer Lambert law.

Typically indices measured include uncalibrated changes in oxyhemoglobin (HbO or Co_2Hb), deoxyhemoglobin (HHb or CHb) and total hemoglobin concentration (HbT = HbO + Hb), hemoglobin difference (Hbdiff = HbO – HHb). Different indices (total hemoglobin – THI or HVI and and total oxygenation index - TOI, sometimes branded CO or rSO_2, nomencleature depending on manufacturer) are derived from the spatially resolved spectroscopy, a technique designed to overcome the problem of calibration due to unknown scattering coefficient, absorption path length and partition coefficient, and at the same time attempt to minimize the influence of scalp blood flow on NIRS based measures. Hb and HbO are believed to represent venous and predominantly arterial compartments respectively. Indices derived from both the oxygenated and deoxygenated NIRS measures are believed to represent blood transit from arterial to venous systems. In addition to the NIRS monitoring, continuous MAP or CPP are required for continuous autoregulatory assessment. The change in NIRS based measures with respect to CPP is believed to represent autoregulatory function.

Autoregulatory assessment with NIRS applied in TBI patients is all based on moving Pearson correlation coefficients between the various NIRS measures (HbO, HHb, HbT, TOI, THI and Hbdiff) and CPP or MAP. The method of calculation is the same as that for PRx or Mx. The indices introduced in the literature include, TOx (or COx), based on TOI (or rSO_2) and THx (also known as HVx), based on THI, or HbT respectively. Thresholds for autoregulatory "impairment" have not been determined, given a small number of studies available in adult TBI, evaluating a small number of patients. Similar to PRx, positive index values may represent "impaired' autoregulation, while negative values may denote "intact" status.

The literature search identified 9 manuscripts describing NIRS bases autoregulatory indices in adult TBI.[20,126–133] A total of 187 TBI patients were described across the 9 studies, with an average of 21 patients per study. Within these studies various NIRS based autoregulatory indices were compared to existing indices (such as PRx and Mx) and patient outcomes. THx and TOx were found to be correlated to PRx and Mx.

4. Brain Tissue Oxygen Monitoring ($PbtO_2$) based ORx

Brain tissue oxygen monitoring ($PbtO_2$) can be utilized to derive a continuous index of autoregulation (ORx). The $PbtO_2$ probe is typically a Clark electrode situated within the brain parenchyma, where diffusible oxygen is measured by the catheter tip continuously. This generates a value for the partial pressure of brain tissue oxygen ($PbtO_2$). With continuous MAP and ICP recording, one can calculate a

moving Pearson correlation coefficient between CPP and $PbtO_2$. The thought is that the slow wave correlation between CPP and $PbtO_2$ provides an indirect measure of autoregulatory function. However, caution is needed in interpreting results, given that $PbtO_2$ levels can fluctuate in response to many local and systemic factors. The Pearson correlation coefficient is calculated in a similar manner to PRx, but over much longer windows (over 30 or 60 minutes in duration). However, ORx has also been described using 5-minute moving windows as well.

As with the less common indices (ie. Lx and NIRS), threshold-based studies do not exist for ORx. Thus, the exact point where autoregulation becomes "impaired" is unclear currently. However, positive ORx values are believed to represent an impairment of the autoregulatory capacity, while negative ORx values are believed to represent an "intact" state. Although this point is controversial. Some authors think that positive ORx signifies that $PbtO_2$ can be improved by rising CPP, and zero ORx informs that the range of PbtO2 regulation has been exhausted.

The search of the adult TBI literature produced 10 studies on ORx.[14,125,126,128,132–137] A total of 159 patients were described across these studies, with an average of 17 patients per study. The main purpose of the individual studies was quite variable, with some reporting correlations with other indices (such as NIRS or PRx), while other were reporting CPP optimal based targets derived from ORx. ORx displayed some correlation to NIRS based HHbx and PRx. Furthermore, some agreement between CPP optimum derived from ORx and that from PRx has been noted. To date, this index is not routinely utilized for autoregulatory assessment, given the $PbtO_2$ signals propensity to be influence by various factors unrelated to the central nervous system.

5. Thermal Diffusion (TD) Technique

The use of thermal diffusion (TD) probes affords the ability to estimate regional cerebral blood flow and perfusion. This device consists of a dual thermistor probe which is inserted directly into the brain parenchyma. The distal thermistor generates heat at ~2 degrees Celsius above tissue temperature, while the proximal thermosensor (5 mm proximal) records the brain temperature outside of the distal thermistor's heat field.[134] Thus, the relative changes in brain temperature related to blood transit regionally can be measured and correlated with CBF. The device regularly re-calibrates, interrupting continuity of the data stream, and the values it generates can be influenced by systemic factors, such as pyrexia,[141] with a reduction in the reliability of CBF measurement using the device.

Regardless of limitations of the device, autoregulation measurement has been conducted with the TD catheter. Two methods have been described. The first is intermittent and will be mentioned only in passing. It involves the measurement of CBF via the catheter during active manipulation of the MAP using vasopressor agents. Only, 2 studies to date have described this approach in adult TBI, and are included here for completeness on TD based autoregulation.[64,142]

The second technique of autoregulation measurement is continuously updating, assuming an uninterrupted TD based CBF signal. This technique is again based on a moving Pearson correlation coefficient between CBF and CPP, called CBFx. The method of calculation is similar to PRx, Mx and Lx. The premise behind its association with autoregulation is similar to the concept for LDF based Lx measurement. As with the other less utilized indices, there are no guidelines as to thresholds for CBFx during particular states of autoregulatory capacity. Thus, positive CBFx values are believed to denote impairment of autoregulation, while negative CBFx values are believe to represent intact states.

The search of the adult TBI literature yielded 8 papers on TD based autoregulatory assessment. [38,64,128,135,140–143] As mentioned, 2 studies were intermittent, and only mentioned here for completeness. [64,142] These were not included within the intermittent part of this manuscript series, as they it is not a "commonly" described technique of intermittent autoregulation assessment. The remaining 6 studies, focused on CBFx calculation in adult TBI. Various physiologic outcomes were described in relation to CBFx. Optimal CPP was derived from CBFx in one study.[128] Very small patient numbers were found in these studies, so the conclusions drawn are limited.

2.2.2 Potential Drivers of Impairment

2.2.2.1 Injury Burden

To date, the available literature linking IC and EC injury burden to the development of impaired cerebrovascular reactivity in adult TBI is scarce. Only one study by Hiler et al attempted to evaluate this association.[107] This study focused on a heterogeneous group of 126 adult TBI patients, both with and without DC. They evaluated whether the Marshall computed tomography (CT) grade on admission was associated with impaired cerebrovascular reactivity during the ICU stay, as defined by a grand mean PRx value greater than zero. The results failed to demonstrate a strong link between IC injury burden and vascular reactivity post-TBI. A few limitations existed, mainly: including both DC and non-DC patients,

taking a grand mean over the entire recording period, and using a basic CT grading system (ie. Marshall CT grade). Furthermore, no attempts to date have been made to assess the link between EC injury burden and host response, as they both relate to cerebrovascular reactivity post-TBI.

2.2.3 Concepts Lacking Literature Support

Considering the aims and hypotheses of this thesis, outlined in Chapter 1, it is important to highlight the areas where literature is lacking on cerebrovascular reactivity in TBI, all of which were identified by the results of the above outlined systematic review of literature. First, currently the majority of literature on cerebrovascular reactivity monitoring in TBI focuses on PRx, as previously mentioned. It is unclear as to whether a different correlation index would provide similar information, superior outcome prediction and more temporally stable critical thresholds. Second, only PRx, TOx and HVx have been validated to measure the LLA in an experimental study of arterial hypotension.[14] It is currently unclear as to whether PRx measures the LLA during IC hypertension. Furthermore, it is unclear as to whether other ICP derived continuous indices measure the LLA during both arterial hypotension and IC hypertension. Finally, for all continuous indices, it is unclear whether they can measure the ULA. Third, the majority of studies evaluating indices derived from different MMM devices only investigated individual associations, failing to assess multi-variate co-variance structures. Thus, the true inter-index associations are currently poorly understood. Fourth, given difficulties with complex time-series analysis, there are currently a lack of robust attempts at modelling PRx using non-invasive surrogates. Finally, as highlighted in 2.3.2.1, the literature on IC injury burden and cerebrovascular reactivity is limited. The only available preliminary study failed to document an association using basic neuroimaging measures.[107] EC injury burden and its links to cerebrovascular reactivity post-TBI has yet to be explored.

Thus, based on the above-mentioned lack of literature, there exists the need to explore the hypotheses listed in Chapter 1. The chapters to follow will outline the methodology and results of various studies conducted to address these hypotheses.

CHAPTER 3: GENERAL METHODS

The experiments and results that comprise this thesis were, in some instances, conceptually complex, and the data required integrated analyses and a complex data-analysis approach. Consequently, some of the initial concepts, methods and experiments are provided in several contexts. This aim to provide relevant information close to sites where data and interpretation are being described has inevitably led to some repetition, but this has been retained to improve readability without having to move between chapters or sections of chapters.

The methods outlined below provide a general overview of the analyzed populations described within the various studies conducted as a part of this thesis, both experimental models and human adult TBI. In addition, information regarding physiologic signal acquisition and processing is provided. The statistics section provides a brief overview of methodology, however is not a detailed account of the techniques applied in individual studies. Given the complexity of the statistical techniques employed as a part of this thesis, each subsequent chapter will contain the detailed explanation of the applied statistical methodologies.

3.1 Experimental Model Management

*Note: Raw data from experimental studies was collected previously and retrospectively analyzed for the purpose of this thesis. The data from New Zealand rabbits for evaluation of the LLA during IC hypertension was collected in the 1990's at the University of Cambridge, with the raw data made available for this thesis by Prof Marek Czosnyka. Similarly, raw data from an animal model (piglet model), collected in the late 2000's, were provided graciously by Dr. Jennifer Lee (John's Hopkins) and Dr. Ken Brady (Baylor) for analysis of the LLA and ULA, using paradigms of arterial hypotension and arterial hypertension respectively. None of the previous results reported using these experimental models have been included within this thesis.[14,145–148] All analysis and results from these models reported in this thesis were conducted independently, addressing different questions from those posed in other publications from the above-mentioned investigators. Table 3.1 summarizes the experimental models that were retrospectively analyzed for this thesis.

Table 3.1 - Experimental Models

Population	Source (lead investigator and institution)	Number of Subjects	Years Raw Physiologic Data Collected	Chapters
Piglets	Jennifer Lee (Hopkins) and Ken Brady (Baylor)	22 *Model of pure arterial hypotension using IVC balloon inflation.	2006 - 2011	5.1
Piglets	Jennifer Lee (Hopkins) and Ken Brady (Baylor)	6 *Model of pure arterial hypertension using aortic balloon inflation and vasopressors.	2006 - 2011	5.3
New Zealand White Rabbits	Marek Czosnyka (Cambridge)	12 *Model of sustained IC hypertension using CSF infusion.	1995 - 1996	5.2

CSF = cerebrospinal fluid, IC = intra-cranial, IVC = inferior vena cava.

3.1.1 New Zealand Rabbits

Data from New Zealand (NZ) white rabbits were utilized for the study validating the ICP derived indices against the LLA during IC hypertension, Chapter 5.2. The animals described within this study have in part been described in previous studies related the physiologic response to intra-cranial hypertension.[145,146] Archived data from a subset of 12 animals from these previous studies was utilized for the analysis in this thesis. The initial experiments were conducted between 1995 and 1996, in accordance with the standards of the UK Animals Scientific Procedures act of 1986, under a UK home office license and with permission form the institutional animal care and use committee at the University of Cambridge.

Twenty-eight white New Zealand (NZ) rabbits (7 female, 21 male; weight 2.7 – 3.7 kg) were subjected to cerebrospinal fluid (CSF) infusions. No adverse events were recorded within this animal cohort. As with

previous publications on this animal cohort, experiments are reported in compliance with the ARRIVE guidelines for the reporting of animal experiments.[149]

Animals were placed under general anesthetic via alphalaxone/alphadalone induction, with 1-3% halothane in 3:1 nitrous oxide/oxygen maintenance. Each animal subsequently had ligation of the common carotid arteries, leaving the brain entirely basilar artery dependent and allowing for TCD assessment of global blood flow. Once 2 weeks had passed, the animals were placed under general anesthestic again, with cannulation of the jugular vein and placement of a tracheostomy. Arterial blood pressure (ABP) was measured through in the dorsal aorta after catheter insertion in the femoral artery (GaelTec, Dunvegan, UK). Cerebral blood flow velocity was measured using an 8MHz Doppler ultrasound probe (PCDop 842, SciMed, Bristol, UK) positioned over the basilar artery (accessed through a 7 mm burr-hole at the bregma). ICP was monitored using an intraparenchymal microsensor (Codman and Shurtleff, Raynham, MA, USA) inserted through a right frontal burr-hole, and an LDF probe was placed subdurally through a further right frontal burr-hole (Moor Instruments, Axbridge, Devon, UK).

A lumbar laminectomy was performed to allow the positioning of a permanent catheter (sealed with cyanoacrylate after introduction) into the lumbar subarachnoid space. This facilitated the controlled infusion of artificial cerebrospinal fluid during the experimental protocol. Rectal temperature was monitored and the animals were placed on a padded warming blanket. The rabbits were given an intravenous infusion of pancuronium (pavulon, 0.5 mg/kg/h) and ventilation was controlled according to arterial pCO_2 via periodic arterial blood gas analyses. The animals were supported in the Sphinx position using a purpose-built head frame with three-point skull fixation. All experiments were performed in an animal laboratory at the same time of day.

The protocol for CSF infusion is identical to that previously reported. After completion of the lumbar laminectomy, the animals were allowed to rest for 20 minutes, with 5 minutes of baseline data recorded. Subsequently, the animals were subjected to raised ICP secondary to CSF infusion with Hartmanns solution into the lumbar cistern. Infusion rates were initially 0.1 mL/min, allowing ICP increase to reach a plateau of around 40 mm Hg after approximately 10 min. Thereafter the infusion rate was increased to rates between 0.2 and 2 mL/min to produce severe intracranial hypertension. ICP was increased until the point where diastolic flow velocity approached zero, which corresponded to an ICP of between 60 and 100 mm Hg (mean 75 mm Hg) at the termination of the experiment. Rabbits were euthanized with thiopental at the conclusion of the test. No pCO_2 manipulations occurred during

this experiment. Further details can be found in the previous studies reporting these experiments. ICP, ABP, LDF-CBF and TCD CBFV (from basilar artery) were recorded during this experiment.

3.1.2 Piglets

To explore the LLA during arterial hypotension and the ULA during arterial hypertension, a piglet model was utilized. The raw physiologic signal data were retrospectively analyzed for the purpose of this thesis. The neonatal piglet data described within this thesis were retrospectively amalgamated from 3 separate experiments.[14,147,148] Inclusion criteria for the current study were normothermic, sham control piglets that had complete and time synchronized data for arterial blood pressure, laser Doppler flowmetry, and ICP from previously published studies. Twenty-two piglets met the inclusion criteria for the arterial hypotension LLA study:

A. control animals from a study on LLA (n=8; age 5 to 10 days; weight 2.2 – 3.9 kg).

B. sham controls for a model of cardiac arrest (n=7; age 3 to 5 days; weight 1 – 2.5 kg), and

C. sham normothermic controls for a model of cardiac arrest with hypothermic therapy (n=7; age 3 to 5 days; weight 1 – 2.5 kg).

For the arterial hypertension ULA study, only 6 sham animals were included (n=6; age 5 to 10 days). All animals were male in both the LLA and ULA studies. All procedures were approved by the Animal Care and Use Committee at Johns Hopkins University and complied with the United States Public Health Service Policy on Human Care and Use of Laboratory Animals and the Guide for the Care and Use of Laboratory Animals. Furthermore, animal care was in accord with National Institutes of Health Guidelines and ensured the animals' comfort.

Of note, a few limitations regarding these piglet models deserve mentioning. These piglet models and experiments were designed for investigation into cerebrovascular physiology with potential translation to neonatal care. They were not intended to be translatable to adult cerebrovascular physiology. As such, the prematurity of the cerebral vasculature in these models may have impacted the LLA and ULA values determined, and the behaviour of the derived cerebrovascular reactivity indices across the LLA and ULA with subsequent manipulation in CPP in the respective experiments. Further to this, the skulls of these piglets were unfused given the neonatal age of the models employed. As such, in the absence

of a fixed cranial vault, the measurement of ICP and derived vascular reactivity indices may have been impacted by this.

LLA – Arterial Hypotension

The male piglets were intubated and mechanically ventilated to maintain normocapnea. General anesthesia was provided with isoflurane in a 50%/50% nitrous oxide/oxygen mixture, fentanyl infusion and as needed boluses, and pancuronium or vecuronium infusions. Fentanyl and neuromuscular blockade were given through a femoral venous catheter. The isoflurane dose was held constant for the duration of the experiment. Arterial blood pressure was continuously monitored by an indwelling femoral artery catheter. A 5F esophageal balloon catheter (Cooper Surgical, Trundall Conn) was placed into the contralateral femoral vein and advanced into the inferior vena cava for later induction of hypotension. A ventricular ICP monitor and a cortical LDF probe (Moor Instruments, Devon, UK; model DRT4; 60Hz) to measure CBF were placed through small cranial burr holes. ICP and LDF were monitored in the same cerebral hemisphere. ICP, ABP and cortical LDF-CBF were recorded during the experiment.

The balloon catheter was slowly inflated in the inferior vena cava using a saline syringe pump. Hypotension was induced from baseline to near-zero blood pressure over 2 to 3 hours. This slow induction of hypotension permitted capture of slow wave intracranial pressure fluctuations for analysis of cerebrovascular reactivity.

ULA – Arterial Hypertension

The male piglets underwent a similar anesthetic as those for the LLA arterial hypotension study. The only major variation is that the esophageal balloon catheter was placed in the femoral artery, and advanced towards the distal aorta. This catheter was used to slowly increase systemic blood pressure to death of the animal. In addition, phenylephrine infusions were administered in attempt to push the MAP to maximal values. ICP, ABP and cortical LDF-CBF were recorded during the experiment.

3.2 Adult TBI Management

Throughout the analysis presented in this thesis (Chapter 4, Chapters 6 through 9), various different populations of adult TBI patients were studied. Table 3.2 provides a summary of those different populations.

Table 3.2 - Adult TBI Populations

Population	**Number of Subjects**	**Years Raw Physiologic Data Collected**	**Chapters**
Adult TBI with all MMM	37 *TBI with ICP, $PbtO_2$, NIRS and TCD monitoring.	2008 - 2009	6.1
Adult TBI with LDF	40 *TBI with LDF, ICP and TCD monitoring.	1994 - 1998	6.2
Adult TBI with TCD	347 *TBI with ICP and TCD monitoring.	1992 - 2011	6.3, 7.1, 8.2
Adult TBI with Long TCD	20 *Prospectively collected with new robotic TCD for extended duration monitoring. ICP and NIRS signals also collected.	2017 – 2018	7.2, 7.3
Adult TBI without DC	358 *TBI without DC and available admission neuroimaging.	2005 – 2016	4, 8.1, 9

DC = decompressive craniectomy, ICP = intra-cranial pressure, LDF = laser Doppler flowmetry, MMM = multi-modal monitoring, NIRS = near infrared spectroscopy, $PbtO_2$ = brain tissue oxygen monitoring, TBI = traumatic brain injury, TCD = transcranial Doppler.

The management received by these patients within the NCCU at Addenbrooke's Hospital (Cambridge University Hospitals NHS Foundation Trust (CUH)) was similar across all patient populations. Patients were predominantly moderate or severe TBI patients, with moderate defined as a GCS of 9 to 12, and severe defined as a GCS or 8 or less. These patients were admitted to the NCCU for purposes of critical care during the acute phase of their illness. All patients had invasive ICP monitoring conducted as per Brain Trauma Foundation (BTF) guidelines.[150] Some mild TBI patients, defined as GCS 13 to 15, subsequently deteriorated clinically after admission to hospital, warranting transfer to the NCCU for invasive monitoring and therapy. Other monitoring modalities, such as $PbtO_2$, NIRS and TCD are conducted as part of standard monitoring practices within the NCCU at Addenbrooke's Hospital. All patients had ABP monitored during their NCCU stay. ABP was zeroed at the level of the right atrium for all patients in the NCCU prior to 2015.[151] Both ICP and ABP were zero referenced at the level of the tragus for all patients from 2015 onwards.[151]

One important limitation of the information available in the retrospective database of TBI patients is related to this concept of arterial line zeroing. Given data was not available on each and every patient as to where the arterial line was zero referenced, for the purpose of the analysis using this data set (ie. for Chapters 4, 6, 7, 8, and 9) it was assumed that most would have had the arterial line zeroed at the level of the tragus.[151] This zero reference for the arterial line does not impact the sign or magnitude of derived cerebrovascular reactivity indices, given these indices are correlation coefficients, dependent on the co-variation in the correlated signals, not the magnitude of the raw physiological readings. As such, regardless of the level of arterial line zero reference, the calculated cerebrovascular reactivity indices are unimpacted.[21,151,152]

General ICP and CPP directed therapy was provided to the patients as per the BTF guidelines,[150] with an ICP goal of less than 20 mm Hg and CPP goal of 60 to 70 mm Hg. ICP was controlled with various positioning techniques, mild hyperventilation (to ~33 mm Hg), bolus osmotic therapies (using mannitol or hypertonic saline), continuous sedation (typically with propofol and/or fentanyl) and CSF venting (when ventricular drain present for ICP monitoring). Therapeutic hypothermia (to a lowest of 33 degrees Celsius), neuromuscular blockade, barbiturate coma and decompressive craniectomy were used for refractory cases. CPP was maintained using intra-venous vasopressor agents to maintain goal values. Seizures, electrolyte imbalances and blood glucose were treated as standard management in the NCCU.

All physiologic signals were recorded and anonymized. Data on age, injury severity, and clinical status at hospital discharge were recorded at the time of monitoring in this database, and no attempt was made

to re-access clinical records for additional information. Since all data was extracted from the hospital records and fully anonymized, no data on patient identifiers were available, and formal patient or proxy consent was not required. Section 3.6 overviews the ethical considerations for access and use of such human clinical data.

3.3 Monitoring

3.3.1 Invasive Cerebral Monitoring

3.3.1.1 Intra-cranial Pressure (ICP)

ICP was acquired via an intra-parenchymal strain gauge probe (Codman ICP MicroSensor; Codman & Shurtleff Inc., Raynham, MA). This was conducted in both the experimental models and human adult TBI populations.

3.3.1.2 Brain Tissue Oxygen ($PbtO_2$)

$PbtO_2$ monitoring occurred via invasive parenchymal monitoring (Licox probe; Integra, Licox Brain Oxygen Monitoring System, Plainboro, NJ), typically placed in the right frontal lobe via a triple lumen bolt (Technicam Ltd).

3.3.1.3 Cortical Laser Doppler Flowmetry (LDF)

This invasive monitoring modality for adult TBI patients was only in place for a short period within the NCCU in the mid 1990's. LDF based CBF was obtained via placement of a MBF3D dual channel laser LDF (Moor Instrument Ltd, Devon UK) in the subdural space, ipsilateral to the ICP monitor. The LDF probe employed a low energy laser (0.5 to 1.5 mW) with light generated in the near infrared spectrum (780 to 820 nm). LDF signals were recorded at a frequency of 14.6 kHz. All probes were pre-calibrated prior to insertion. Details on the insertion technique and calibration method can be found in the 1994 study by

Kirkpatrick et al.[122] A similar probe, from the same manufacturer, was utilized within the experimental studies described within this thesis.

3.3.2 Non-Invasive Cerebral Monitoring

3.3.2.1 Transcranial Doppler (TCD)

Various different TCD devices were employed over the decades for measuring CBFV from the MCA. TCD assessment was conducted via Doppler Box (DWL Compumedics, Singen, Germany) or Neuroguard (Medasonic, Fremont, CA, USA), for the patient populations described in Chapters 6, 7.1 and 8.2. Finally, a new robotic TCD unit was employed for the purpose of this thesis, the Delica EMS 9D (Delica EMS 9D System, Shenzen Delica Medical Equipment Co. Ltd., China; http://www.delicasz/com). This newer robotic system will be described in detail in Chapters 7.2 and 7.3.

3.3.2.2 Near Infrared Spectroscopy (NIRS)

NIRS signals were recorded bilaterally over the frontal lobes utilizing the NIRO-200 or NIRO-200NX monitoring (Hamamatsu Photonics, Hamamatsu City, Shizuoka, Japan, www.hamamatsu.com). The following NIRS signals were recorded: oxygenated hemoglobin (HbO), deoxygenated hemoglobin (HHb), total oxygenation index (TOI), total hemoglobin index (THI) and total hemoglobin concentration (Hb).

3.3.3 Systemic Monitoring

3.3.3.1 Arterial Blood Pressure (ABP)

ABP was obtained through either radial or femoral arterial lines connected to pressure transducers (Baxter Healthcare Corp. CardioVascular Group, Irvine, CA).

3.4 Signal Capture and Processing

3.4.1 Signal Capture

All physiologic signals from the various MMM devices (ie. ICP, ABP, $PbtO_2$, NIRS, TCD and LDF) in both the experimental and human adult TBI studies were recorded in high frequency waveform (50 Hz or higher) using ICM+ software (Cambridge Enterprise Ltd, Cambridge, UK, http://icmplus.neurosurg.cam.ac.uk). Digital signals were directly recorded by ICM+. While analogue signals were digitized via analogue to digital converters (ADC) (DT300 for experimental studies, DT9801 or DT9803 for human studies; Data Translation, Marlboro, MA). All signals were linked in time-series automatically by ICM+.

3.4.2 Signal Processing

Post-acquisition processing of the above signals was conducted using ICM+. Signal artifact was cleared through a combination of manual and automated techniques. Pulse amplitude of ICP (AMP) was determined by calculating the fundamental Fourier amplitude of the ICP pulse waveforms over a 10 second window, updated every 10 seconds. For TCD CBFV, further processing was conducted to produce FVm, FVs and FVd. Systolic flow velocity (FVs) was determined by calculating the maximum flow velocity (FV) over a 1.5 second window, updated every second. Diastolic flow velocity (FVd) was calculated using the minimum FV over a 1.5 second window, updated every second. Mean flow velocity (FVm) was calculated using average FV over a 10 second window, updated every 10 seconds (ie. without data overlap).

A ten second moving average filter (updated every 10 seconds to avoid data overlap) was applied to all recorded signals: ICP, ABP (which produced MAP), AMP, CPP, $PbtO_2$, TCD CBFV, NIRS signals, and LDF-CBF. This decimated the signal frequency to ~0.1Hz, focusing on slow-waves of the various MMM variables: ICP, CPP, ABP, AMP, FVm, FVs, FVd, TOI, THI, $PbtO_2$, and LDF-CBF. Details regarding derived variables (ie. CPP and continuous indices of cerebrovascular reactivity) will be covered in the section to follow.

All variables, including derived entities, were output into comma separated variable (CSV) files for future statistical analysis. The update frequency for the time-series data that was output into the CSV files was minute-by-minute averages for all variables. The only exceptions to this were the data from Chapters 5.2 and 6.2, where the data was output in 10-second-by-10-second averages, due to short duration of these recordings.

3.4.3 Derived Physiologic Measures

3.4.3.1 Cerebral Perfusion Pressure (CPP)

CPP was derived via the difference between MAP and ICP signals:

$$CPP = MAP - ICP \qquad (3.1)$$

Where CPP, MAP and ICP are measured in mm Hg.

3.4.3.2 Continuous Indices of Cerebrovascular Reactivity

All continuous indices of cerebrovascular reactivity were calculated via a similar moving Pearson correlation coefficient method, correlating slow wave fluctuations in a surrogate marker for pulsatile CBV (ie. ICP, AMP, TOI, THI, $PbtO_2$) or CBF (ie. FVm, FVs, FVd, LDF-CBF) with that of a driving pressure (ie. MAP or CPP). The following example is for PRx, with identical calculation methods utilized for the other indices. PRx is calculated as the moving correlation coefficient between slow wave fluctuations of ICP and MAP. This is calculated using 30 consecutive 10 second windows of ICP and MAP (ie. five minutes of data), with the PRx index updated every minute (ie. having 80% data overlap between each PRx measure), unless otherwise specified in the individual Chapters. Table 3.3 displays all of the calculated continuous indices of cerebrovascular reactivity. These indices were calculated identically in both the experimental and human adult studies.

Table 3.3 – Continuous Indices of Cerebrovascular Reactivity Calculated

Index	Signals Correlated	Signal Averaging (sec)	Pearson Correlation Coefficient Calculation Window (min)	Index Calculation Update Frequency (sec)*
PRx	ICP and MAP	10	5	60
PAx	AMP and MAP	10	5	60
RAC	AMP and CPP	10	5	60
Mx	FVm and CPP	10	5	60
Mx_a	FVm and MAP	10	5	60
Sx	FVs and CPP	10	5	60
Sx_a	FVs and MAP	10	5	60
Dx	FVd and CPP	10	5	60
Dx_a	FVd and MAP	10	5	60
TOx	TOI and CPP	10	5	60
TOx_a	TOI and MAP	10	5	60
THx	THI and CPP	10	5	60
THx_a	THI and MAP	10	5	60
ORx-5	$PbtO_2$ and CPP	30	5	60
ORx-30	$PbtO_2$ and CPP	30	30	60
ORx-60	$PbtO_2$ and CPP	30	60	60
Lx	LDF-CBF and CPP	10	5	60
Lx_a	LDF-CBF and MAP	10	5	60

*CPP = cerebral perfusion pressure, FVd = diastolic flow velocity, FVm = mean flow velocity, FVs = systolic flow velocity, ICP = intracranial pressure, LDF-CBF = laser Doppler flowmetry cerebral blood flow, MAP = mean arterial pressure, min = minute, $PbtO_2$ = brain tissue oxygenation, sec = second, THI = total hemoglobin index, TOI = total oxygenated hemoglobin index. *Note: update frequency of the indices varied within the studies presented in this thesis, as a consequence of recording duration. Each subsequent chapter will mention the update frequency within the respective Methods sections.*

3.5 Neuroimaging

3.5.1 Computed Tomography (CT)

Chapter 9 deals with the study of IC injury burden as it relates to cerebrovascular reactivity in adult TBI. For this, all admission CT scans of the brain were manually collected from the electronic imaging repository at Addenbrooke's Hospital for adult TBI patients with archived ICM+ raw physiologic data. Each of these scans were downloaded and stored anonymously in DICOM format for future injury pattern or burden analysis. Only patients from March 2005 to December 2016 had their imaging collected, given digital imaging was not available prior to March 2005.

Each CT scan had a detailed assessment of IC injury, as measured by standard CT scoring systems (Marshall,[153] Rotterdam,[154] Helsinki[155] and Stockholm[156]). The CT scoring systems consist of the following:

1. Marshall CT Score[153]
    a. A categorical/ordinal scoring system (range: 1 to 6)
        i. I = no visible injury on CT
        ii. II = diffuse injury; <5 milimeters (mm) midline shift (MLS); basal cisterns visible; no lesion >25 mililiters (mL)
        iii. III = diffuse injury; <5 mm MLS; basal cisterns compressed or absent; no lesion >25 mL
        iv. IV = MLS >5 mm; basal cisterns compressed or absent; no lesion >25 mL
        v. V = any MLS; any basal cistern status; mass lesion >25 mL that is surgically evacuated
        vi. VI = any mass lesions >25 mL that is NOT surgically evacuated

2. Rotterdam CT Score[154]
    a. A summative scoring system consisting of the following point-based sytem (range:1 to 6)
        i. Basal Cisterns
            1. 0 = normal
            2. 1 = compressed
            3. 2 = absent
        ii. MLS
            1. 0 = no shift or <=5 mm
            2. 1 = Shift >5 mm
        iii. Epidural Mass Lesion
            1. 0 = present
            2. 1 = absent
        iv. Intraventricular Blood or Traumatic Subarachnoid Hemorrahge (tSAH)
            1. 0 = absent
            2. 1 = present
        v. Then total sum + 1 for final score

3. Helsinki CT Score[155]
    a. A summative scoring system consisting of the following point-based system (range: -3 to 14)
        i. Mass Lesion Type
            1. 2 = Subdural Hematoma (SDH)
            2. 2 = Intracerebral Hemorrhage
            3. -3 = Epidural Hematoma (EDH)
        ii. Mass Lesion Size
            1. 2 = > 25 mL
        iii. Intraventricular Hemorrhage (IVH)
            1. 3 = Yes
        iv. Suprasellar Cisterns
            1. 0 = normal
            2. 1 = compressed
            3. 5 = obliterated

4. Stockholm CT Score[156]
    a. A formula-based calculated scoring system based on the following formula:
        i. Score = (MLS/10) + (tSAH-IVH subscore/2) – 1(if EDH present) + 1 (if DAI present) + 1 (if dual-sided SDH present) + 1
        ii. Where:
            1. MLS is in mm
            2. tSAH-IVH subscore is a summed score:
                a. subscore = convexity tSAH score + basal cistern tSAH score + (IVH score*2)
                b. Where:
                    i. Convexity tSAH
                        1. 0 = none
                        2. 1 = vivisble in gyri
                        3. 2 = extensive bilateral (ie. >90% filled convexity)
                    ii. Basal cistern tSAH

1. 0 = none
2. 1 = visible blood
3. 2 = filled cisterns

iii. IVH

1. 0 = none
2. 1 = visible blood

The Stockholm score was also assessed as an ordinal score using the following system: 0 to 1 = 1; 1.1 to 2 = 2; 2.1 to 3 = 3; 3.1 to 4 = 4; 4.1 to 5 = 5; 5.1 to 6 = 6, which displayed a strong correlation with the continuous Stockholm CT score (r=0.947).

Next, a comprehensive CT lesion/characteristic database was constructed for each admission CT scan. This IC injury database consisted of:

1. Continuous variables: MLS – in mm, largest lesion volume – in mL, number of contusions, number of diffuse axonal injury (DAI) lesions, total contusion volume – in mL.

   MLS was measured on the admission CT using the distance of the septum pellucidum from bony midline (derived from the line connecting the crista gallae to the inion), at the level of the foramen of Monro. Volumes were calculated using the AxBxC/2 method for contusions and extra-axial hemotomas from the admission CT scans, where: A = maximal antero-posterior length in centimeters (cm), B = maximal thickness in cm, and C = # of 1 cm CT slices (where slices with ≥75% Area of Hemorrhage: Counts as 1 slice; slices with 25-75% Area of Hemorrhage: Counts as 0.5 slices; slices with <25% Area of Hemorrhage: Counts as 0 slices).[157] Volumes for each contusion were calculated individually.

2. Ordinal characteristics: A. basal cistern compression (none, compressed, complete), B. lateral ventricle compression (none, compressed, complete), C. convexity gyral compression (none, compressed, complete), D. 4th ventricle compression (none, compression, complete), E. convexity tSAH extent (none, visible in gyri, >90% of bilateral hemispheric coverage), F.

convexity tSAH maximal thickness (none, 1-5 mm, >5 mm), G. cisternal tSAH extent (none, visible, completely filled).

3. Binary characteristics:

A. basal cistern compression (none, any compression amount)

B. extreme basal cistern compression (none, complete effacement)

C. lateral ventricle compression (none, any compression)

D. extreme lateral ventricle compression (none, complete effacement)

E. 4th ventricle compression (none, any compression)

F. extreme 4th ventricle compression (none, complete effacement)

G. convexity gyri compression (none, any compression)

H. extreme convexity gyri compression (none, complete effacement)

I. tonsillar decent (no, yes), J. any lesion >25 mL (no, yes)

K. evacuated mass lesion (no, yes)

L. non-evacuated mass >25 mL (no, yes)

M. convexity subdural hematoma (SDH) (no, yes)

N. tentorial SDH (no, yes)

O. falcine SDH (no, yes)

P. bilateral convexity SDH (no, yes)

Q. convexity EDH (no, yes)

R. bilateral convexity EDH (no, yes)

S. contusion present (no, yes)

T. bilateral contusions (no, yes)

U. IVH (no, yes)

V. convexity tSAH (no, yes)

W. convexity tSAH >90% of hemispheres (no, yes)

Y. convexity tSAH >5mm thick (no, yes)

Z. cisternal tSAH (no, yes)

AA. cisternal tSAH completely filled (no, yes)

AB. DAI – subcortical (SC) (no, yes)

AC. DAI – corpus callosum (CC) (no, yes)

AD. DAI – basal ganglia (BG) (no, yes)

AE. DAI – brainstem (BS) (no, yes)

AF. Post-fossa SDH (no, yes)

AG. Post-fossa (EDH) (no, yes)

AH. Post-fossa contusion (no, yes)

3.6 Human Ethical Considerations

For Chapters 4, 6, 7, 8 and 9, all studies on human data were conducted as a retrospective analysis of a prospectively maintained database cohort, in which high frequency clinical neuromonitoring data had been archived. Monitoring of brain modalities was conducted as a part of standard NCCU patient care using an anonymized database of physiological monitoring variables in neurocritical care. Data on age, injury severity, and clinical status at hospital discharge were recorded at the time of monitoring on this database, and no attempt was made to re-access clinical records for additional information. Since all data was extracted from the hospital records and fully anonymized, no data on patient identifiers were available, and need for formal patient or proxy consent was waived. Within this institution, patient data may be collected with waiver of formal consent, as long as it remains fully anonymized, with no method of tracing this back to an individual patient. Patient physiologic, demographic and outcome data was collected by the clinicians involved with patient care, and subsequently recorded in an anonymous format. This anonymous data is then provided for future research purposes. Such data curation remains within compliance for research integrity as outlined in the UK Department of Health - Governance Arrangements for Research Ethics Committees (GAfREC), September 2011 guidelines, section 6.0.[158]

3.7 Statistical Analysis

The statistical analysis utilized for the studies in this thesis varied significantly from study to study, and were complex. Thus, a detailed account of each statistical method used is beyond the scope of this general section. Detailed account of the statistical methods utilized in each study can be found in the respective chapter methodology sections for each individual study. All statistics were performed with either XLSTAT (Addinsoft, New York, United States; https://www.xlstat.com/en/) add-on package to Microsoft Excel (Microsoft Office 15, Version 16.0.7369.1323) or R statistical software (R Core Team (2016). R: A language and environment for statistical computing. R Foundation for Statistical Computing, Vienna, Austria. URL https://www.R-project.org/).[159] For all statistical tests described, alpha was set at 0.05 for significance. In general, no correction for multiple comparisons was undertaken, unless explicitly

stated in the specific chapter and section of this thesis. Given the majority of the work presented is exploratory in nature, avoiding correction for multiple comparisons was acceptable.

In general, continuous variables were described using means and standard deviations, with ordinal data described via median and inter-quartile range (IQR). Normality was confirmed in continuous variables using Shapiro-Wilks test. Various x-y plots were produced within the studies, employing simple linear models and error bar plots.

Comparison between parametric variables employed t-tests and analysis of variance (ANOVA), while non-parametric data was compared via Mann-Whitney-U test, Kruskal-Wallis test, Friedman test and Jonckheere-Terpstra test. Correlation between variables was assessed via Pearson and Spearman ranked correlation coefficient, depending on the individual study.

Multi-variate assessment of inter-index co-variance occurred via principal component analysis (PCA),[159–161] agglomerative hierarchal clustering (AHC)[159,162] and k-means cluster analysis (KMCA).[159,160] AHC results were quantified using Cophenetic correlation coefficients,[162] while KMCA clustering was validated via the "elbow method".[159]

Linear modelling employed in the estimation and forecasting of PRx using non-invasive surrogates (Chapter 7.1, 7.2) utilized complex time-series techniques in R.[159,163–166] Autoregressive integrative moving average (ARIMA) time-series models were used to model PRx over time, and subsequently embedded in linear mixed effects (LME) models in order to build models that accurately estimated PRx using non-invasive TCD surrogate. Models were compared via autocorrelation function (ACF) plots, partial autocorrelation function (PACF) plots, Akaike Information Criterion (AIC), Bayesian Information Criterion (BIC), log likelihood (LL) and ANOVA. Further details can be found in Chapter 7.

Logistic regression models, both univariate and multi-variable, were built under the principal of parsimony for the assessment of relationships to binary outcomes. Models were compared via area under the receiver operating curve (AUC), chi-square testing, and Delong's test.

CHAPTER 4: DEFINING A "NEW" CONTINUOUS INDEX OF CEREBROVASCULAR REACTIVITY IN ADULT TBI - RAC

*The results of this study are also detailed in the publication: Zeiler et al., *J Neurotrauma*. 2017; Dec 6. doi: 10.1089/neu.2017.5241. [Epub ahead of print].[21]

4.1 Introduction

Continuous indices of autoregulatory capacity have been implemented within ICU's as a means of monitoring the pressure reactivity of the cerebrovascular system. The TBI patient population has provided the substrate for most publications on the use of these indices,[11,12] with data supporting an association between "poor" autoregulatory status, as assessed by these indices, with outcome.[8,9] Such use of autoregulatory monitoring has been supported by recent authoritative statements on multi-modal monitoring in TBI.[12]

These continuous indices are typically derived as moving Pearson correlation coefficients between slow wave fluctuations in: surrogates of pulsatile CBV (e.g. ICP or AMP) and the driving pressure for CBF (ie. MAP or CPP).[3] Two ICP derived indices of autoregulation have been described: PRx (correlation between ICP and MAP)[3] and PAx (correlation between AMP and MAP).[15]

The majority of literature has focused on PRx and its association with outcome, and PRx values above +0.25 have been associated with mortality at 6 months.[9] PRx has also been validated experimentally: CPP reduction below the LLA, defined using the gold standard of reductions in cerebral blood flow, is associated with an increase in PRx from negative to positive values.[14] PRx has been utilized clinically to determine the individual optimal CPP in TBI, and is likely to be the basis for planned studies that assess the benefit of CPP targets that are associated with best autoregulation – optimum CPP (CPPopt).[144] In contrast to this substantial literature on PRx, PAx is a relatively newly described autoregulatory index. However, preliminary data indicating potential superiority of PAx over PRx in outcome prediction in those with normal or low ICP.[15]

Despite this substantial literature supporting the use of these ICP derived autoregulation indices, there still exists room for the exploration of new indices of physiologic measure. In this chapter, a new

continuous index of cerebral physiology in a population of adult TBI patients without DC is defined.[21] This index is derived as the moving Pearson correlation between AMP and CPP, which is abbreviated as RAC (R for correlation coefficient, A for AMP and C for CPP). Given the potential added predictive capacity of the AMP-based index PAx over PRx in adult TBI,[15] the fact that all current ICP-derived indices were based on MAP as the driver for CBF,[3,15] and that the majority of non-ICP derived cerebrovascular reactivity indices (ie. TCD, NIRS, TD and $PbtO_2$ based indices) are based on the correlation with CPP as the driver for pulsatile changes in CBV or CBF, it was only natural to explore the correlation between AMP and CPP as a potential metric of cerebrovascular reactivity. RAC is potentially related to the general shape of the relationship between AMP and CPP observed clinically and also experimentally.[145] Given the correlation between CPP and AMP, it is possible that RAC combines information regarding cerebral compensatory reserve, similar to RAP (correlation coefficient between AMP and ICP), and cerebrovascular responsiveness, similar to PRx or PAx.

4.2 Methods

Patient Population

Extreme Physiology Examples

Time trends of ICP, CPP, AMP, RAP, PRx, PAx and RAC in 2 individual patient examples of "extreme" physiology in adult TBI are described. One patient displayed an episode of sustained intra-cranial hypertension (ICP >50 mm Hg for at least 1 hour), without return to baseline - Figure 4.1. The second patient displays systemic arterial hypotension in the presence of relatively normal ICP's - Figure 4.2. Both of these patients were chosen as examples in order to provide a large range of ICP and CPP variation during the recordings, allowing to display the AMP and RAC response in time over these ranges.

Non-DC Adult TBI Cohort

In order to display the relationships between AMP/RAP/PRx/PAx and RAC with ICP and CPP in a wider population of patients, all non-DC adult TBI patients (n=358) were utilized. None of the patients, at any point during their hospital stay, underwent DC, even for refractory ICP. Those with mass lesions

identified upon admission, had subsequent evacuation immediately upon admission. For those with mass lesion evacuation, all follow-up CT scans were assessed to confirm that the bone flap was replaced post-operatively and that all follow-up scans confirmed that the bone flap was not removed at any point during their hospital stay. Any patient undergoing mass lesion evacuation without replacement of the bone flap were excluded. All patients were admitted to the NCCU at Addenbrooke's Hospital, Cambridge, during the period of March 2005 to December 2016. In addition, only patients with at least 6 hours of recorded signals were included in this study. All patients suffered mild to severe TBI (defined as GCS of 8 or less). Those small number of patients with mild TBI (defined as GCS 13 or higher on admission) had subsequent clinical deterioration requiring admission to the NCCU and invasive monitoring. Treatment received during the recording periods included standard ICP-directed therapy, with an ICP goal of less than 20 mm Hg and CPP goal of greater than 60 mm Hg.

Only patients without DC were selected in order to prevent the introduction of confounding ICP measurements post removal of the bone flap.[22] It is known, that post-DC, PRx values are impacted. This stems from the fact that PRx is dependent on CBV-driven changes in ICP, and these are are severely attenuated in the highly compliant intracranial cavity post-DC. Thus, in order to prevent any impact from DC in assessing the relationship between all of the physiologic variables (ie. ICP, AMP, CPP) and the ICP derived indices (ie. RAC, PRx, PAx, RAP) these patients were excluded.

Signal Acquisition and Processing

Both ICP and ABP were recorded in all patients described within the manuscript. ABP was obtained through either radial or femoral arterial lines connected to pressure transducers (Baxter Healthcare Corp. CardioVascular Group, Irvine, CA), zeroed at the right atrium, or tragus, depending on when the patient was admitted to hospital. ICP was acquired via an intra-parenchymal strain gauge probe (Codman ICP MicroSensor; Codman & Shurtleff Inc., Raynham, MA). Mathematically, such variance in ABP zero level does not impact the derived correlation values, sign or magnitude, between slow-wave changes in ICP, ABP, AMP or CPP.

All signal acquisition and processing occurred as described with in Chapter 3.3 and 3.4. Minute-by-minute data for ICP, MAP, AMP, PRx, PAx and RAC were derived using ICM+, and utilized in further statistical analysis. RAP, the correlation coefficient between AMP and ICP (a measure of cerebral

compensatory reserve)[167–169] was also derived for comparison with the indices of cerebrovascular reactivity (PRx, PAx, and RAC).

Statistics

Statistics were performed utilizing XLSTAT (Addinsoft, New York, United States; https://www.xlstat.com/en/) add-on package to Microsoft Excel (Microsoft Office 15, Version 16.0.7369.1323) and R statistical software (R Core Team (2016). R: A language and environment for statistical computing. R Foundation for Statistical Computing, Vienna, Austria. URL https://www.R-project.org/).

As the purpose of this study was to define a new physiologic index and provide a time series description of RAC, PRx, PAx, RAP and AMP in a large, non-DC, cohort of adult TBI, very limited inferential statistical results are presented. A variety of plots were produced:

1. Plots of ICP, MAP, CPP, AMP, RAP, PRx, PAx and RAC over time for the 2 patient examples of extreme physiology.

2. Plots of the number of minute-by-minute observations per 5 mm Hg bins of ICP and CPP for the entire non-DC cohort.

3. Plots of AMP vs. ICP, AMP vs. CPP, RAP vs. ICP, RAP vs. CPP, PRx vs. ICP, PRx vs. CPP, PAx vs. ICP, PAx vs. CPP, RAC vs. ICP, and RAC vs. CPP for the entire non-DC cohort. Plots utilizing 5 mm Hg bins of ICP or CPP against the mean AMP, RAP, PRx, PAx or RAC for observations within those bins were produced.

4. CPPopt plots of PRx vs. CPP, PAx vs. CPP, and RAC vs. CPP (using 5 mm Hg CPP bins and mean PRx, PAx or RAC for observations in those bins) for the entire non-DC population.

Plots were created using R statistical software. Plots described in #3 and #4 above, display mean values for AMP, RAP, PRx, PAx and RAC per 5 mm Hg bin of ICP or CPP, with standard error bars. Values for CPP below 35 mm Hg were collated into 1 bin, given the small number of observations in a small number of patients. Thus, the mean values and standard error bars for values in this CPP range must be interpreted with caution. Similarly, for ICP values above 90 mm Hg, all of these observations were collated into one bin, called ">90 mm Hg", given the small number of patients and observations within this ICP range. Thus, the mean values and standard error bars in this ICP range must be interpreted with caution

Finally, the inter-index Pearson correlation coefficients between RAC and PRx, PAx and RAP, using grand mean data for the patient population (ie. one mean value per patient) were assessed. Linear regression analysis between RAC vs PRx, RAC vs. PAx and RAC vs. RAP was also performed.

4.2 Results

AMP and RAC During "Extremes" of ICP and CPP

Figure 4.1 displays one patient with sustained intra-cranial hypertension. Of note, there is substantial sustained increase in ICP, with subsequent decrease in CPP. Furthermore, it is noted that AMP gradually increases with ICP increase until at break point at ~60 mm Hg of ICP. This has been described previously as a probable effect caused by a collapse of cerebral arterial bed.[91,145,170] RAP remains elevated, near +1.0 as AMP progressively increases to its break-point, after which is decreases to negative numbers. The RAP response indicates severely impaired cerebral compensatory reserve with values decreasing to negative range in the last 2 hours of recording. Finally, RAC gradually becomes more positive (ie. increasing positive correlation between AMP and CPP) as ICP continues to increase, and as CPP decreases. This increase in RAC was initially gradual, but then appeared to sharply increase around the ICP range for the break point of AMP, with CPP falling below ~50 mm Hg. This increase in RAC may reflect progressive decrease in cerebral compensatory reserve in line with steady increase in both PRx and PAx, indicating autoregulatory dysfunction.

Figure 4.2 displays a patient with progressive arterial hypotension, in the setting of low ICP (<20 mm Hg). As MAP decreases, both ICP and CPP decrease. Of note, AMP increases with MAP less than 80 mm Hg. RAP starts close to zero, indicating relatively good cerebrospinal compensatory reserve, followed by a

subsequent decrease with progressive decrease in MAP. PRx, PAx and RAC progressively become more positive with decreases in MAP, potentially indicating impaired autoregulation with profound systemic hypotension.

Figure 4.1: Sustained Intra-Cranial Hypertension Patient Example – ICP, MAP, CPP, AMP, RAP, PRx and RAC Over Time

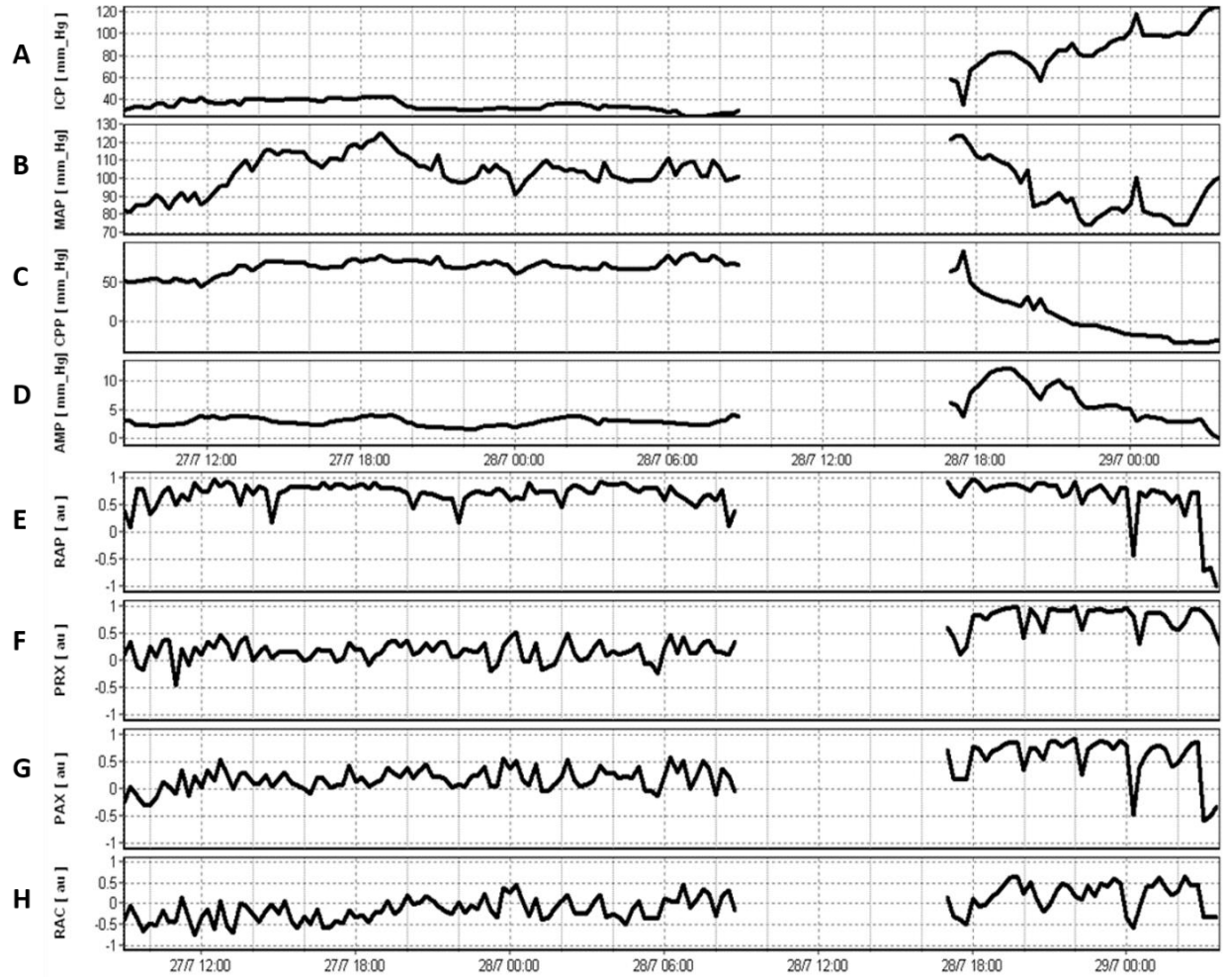

AMP = pulse amplitude of ICP, a.u. = arbitrary units, CPP = cerebral perfusion pressure, ICP = intra-cranial pressure, mm Hg = millimeters of Mercury, abp = MAP = mean arterial pressure, PAx = pulse amplitude index (correlation between AMP and MAP), PRx = pressure reactivity index (correlation between ICP and MAP), RAC = correlation coefficient between AMP and CPP, RAP = correlation coefficient between AMP and ICP. Panel A: ICP over time, Panel B: MAP over time, Panel C: CPP over time, Panel D: AMP over time, Panel E: RAP over time, Panel F: PRx over time, Panel G: PAx over time, Panel H: RAC over time.

Figure 4.2: Arterial Hypotension Patient Example – ICP, MAP, CPP, AMP, RAP, PRx and RAC Over Time

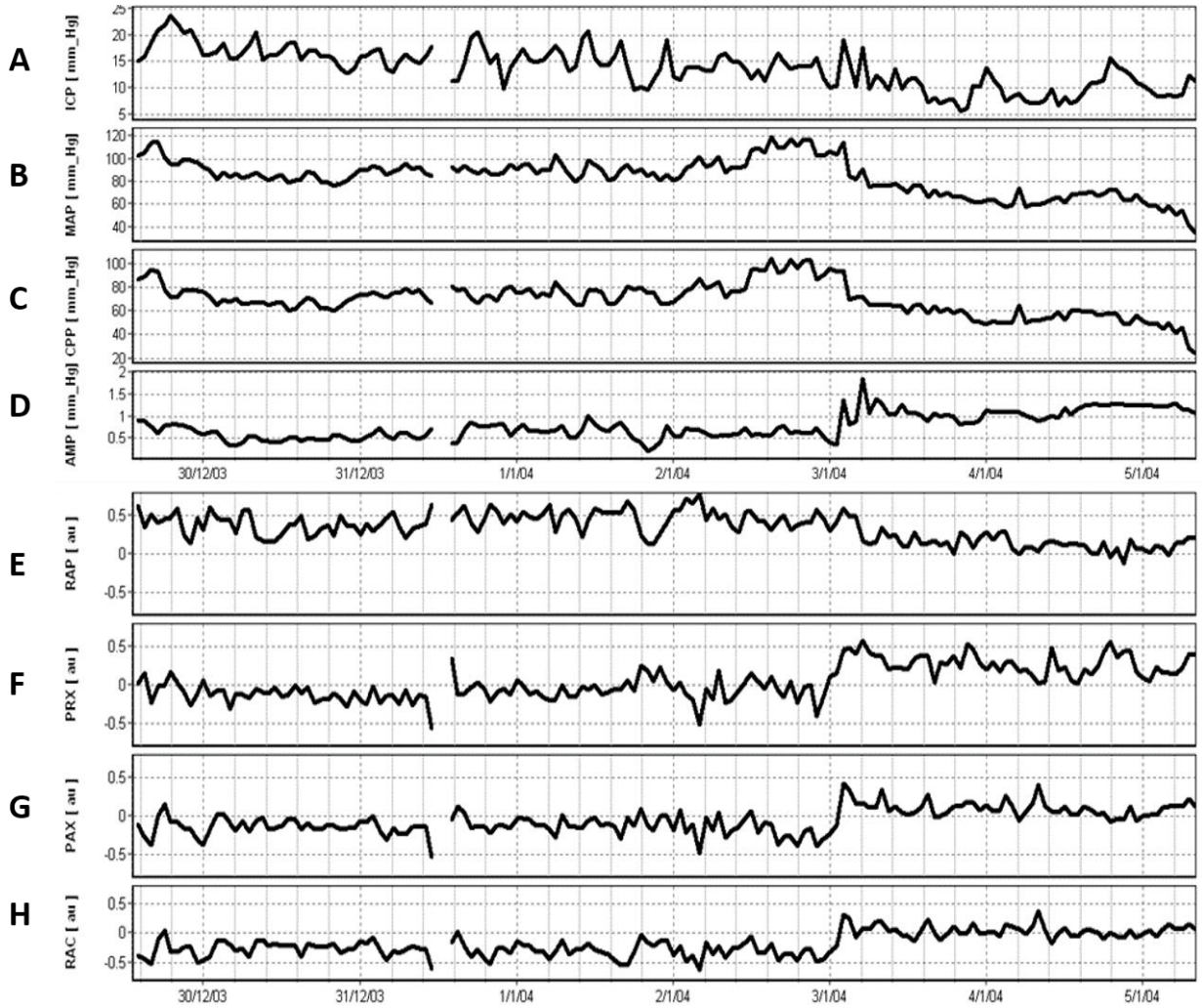

AMP = pulse amplitude of ICP, a.u. = arbitrary units, CPP = cerebral perfusion pressure, ICP = intra-cranial pressure, mm Hg = millimeters of Mercury, abp = MAP = mean arterial pressure, PAx = pulse amplitude index (correlation between AMP and MAP), PRx = pressure reactivity index (correlation between ICP and MAP), RAC = correlation coefficient between AMP and CPP, RAP = correlation coefficient between AMP and ICP. Panel A: ICP over time, Panel B: MAP over time, Panel C: CPP over time, Panel D: AMP over time, Panel E: RAP over time, Panel F: PRx over time, Panel G: PAx over time, Panel H: RAC over time.

AMP, RAP, PRx, PAx and RAC versus ICP and CPP in the Non-DC Cohort

Non-DC Cohort Patient Demographics

In total, there were 358 patients included for analysis. All patients suffered moderate to severe TBI, or mild TBI with secondary deterioration requiring sedation and mechanical ventilation for intracranial hypertension. In addition, all patients had at least 6 hours of high frequency signals recorded. The mean age was 40.6 +/-17.2 years (range: 16 to 89), with a median (range) Glasgow Coma Scale score of 7 (3 to 13). There were 272 males (76.0%), and the mean length of signal recording was 189.1 +/-151.1 hours (range: 8.5 to 1033.0 hours; median = 152.7 hours). The mean ICP, MAP, CPP, AMP, RAP, PRx, PAx and RAC were: 14.057 +/-7.6 mm Hg, 91.3 +/- 7.9 mm Hg, 77.5 +/- 8.5 mm Hg, 2.3 +/- 1.4 mm Hg, 0.638 +/- 0.208, 0.046 +/-0.173, -0.057 +/- 0.195, and -0.350 +/- 0.254; respectively.

Number of Data Points

In total, there were 2,780,930 minute-by-minute observations for each physiologic variable and index (RAP, PRx, PAx and RAC) across the 358 non-DC TBI patients included for analysis. Overall, 99.9% of the data points fell between ICP values of 0 and 65 mm Hg, and CPP values of 40 to 140 mm Hg.

Relationship Between AMP vs. ICP and AMP vs. CPP

Using 5 mm Hg bins for ICP and CPP, the mean AMP, RAP, PRx, PAx and RAC values for those bins were calculated and a range of plots were produced. Figure 4.3 displays the following relationships: CPP vs. ICP, (Figure 4.3A), AMP vs. ICP (Figure 4.3B), RAP vs. ICP (Figure 4.3C), PRx vs. ICP (Figure 4.3D), PAx vs. ICP (Figure 4.3E) and RAC vs. ICP (Figure 4.3F). Figure 4.4 displays: ICP vs. CPP (Figure 4.4A), AMP vs. CPP (Figure 4.4B), RAP vs. CPP (Figure 4.4C), PRx vs. CPP (Figure 4.4D), PAx vs. CPP (Figure 4.4E) and RAC vs. CPP (Figure 4.4F). Of note is the increase in AMP, as ICP increases, to a peak at an ICP of ~50-60 (Figure 4.3B), followed by sharp decline in AMP with increasing ICP value.

Similarly, as CPP decrease towards 50 mm Hg, AMP gradually increases and peaks at a CPP of ~40 mm Hg. This is followed by a sharp decrease in AMP with progressive decrease in CPP below 40 mm Hg

(Figure 4.4B). These two relations have both been previously described,[145] with the current data supporting the previous literature.

Relationship Between RAP vs. ICP and RAP vs. CPP

At low ICP, RAP starts at small positive values, indicating little correlation between AMP and ICP, thought to signify "good" cerebral compensatory reserve. RAP subsequently trends towards +1.0 as ICP increases towards the "break-point" in AMP (ie. ICP of 50 to 60 mm Hg – Can be seen in Figure 4.3B). This signifies a direct positive correlation between ICP and AMP, thus low cerebral compensatory reserve. Once ICP increases beyond 50-60 mm Hg (ie. the averaged AMP "break-point"), RAP rapidly declines towards zero. This is believed to reflect exhaustion of cerebrovascular reserve and vascular transmural pressure approaching the critical closing pressure of the cerebral vessels. All of this can be seen in Figure 4.3C.

Similarly, as CPP declines towards the LLA, we see a steep increase in RAP towards more positive values, implying poor cerebral compensatory reserve (Figure 4.4C). As CPP increases, RAP decreases towards zero, with relative stability in RAP (ie. become more positive) with CPP values above the ULA (Figure 4.4B). However, it must be acknowledged that the number of data points above a CPP of 130-140 mm Hg is much less, as seen by the error bar plots in this range.

Relationship Between PRx vs. ICP and PRx vs. CPP

PRx versus ICP plots display a consistent trend, with low PRx values during episodes of low ICP, and progressively more positive PRx values (ie. more impaired autoregulation) as ICP increases above 20 mm Hg (Figure 4.3D). The PRx versus CPP plots displays the classic parabolic distribution, with low PRx values (ie. intact autoregulation) within the CPP range of ~50 mm Hg to 130 mm Hg. Outside of these two limits of CPP, PRx subsequently trends toward positive values (indicating potentially impaired autoregulation) (Figure 4.4D).

Relationship Between PAx vs. ICP and PAx vs. CPP

Similar to PRx, PAx versus ICP plots display a consistent trend, with low PAx values during episodes of low ICP, and progressively more positive PAx values (ie. more impaired autoregulation) as ICP increases above 20 mm Hg (Figure 4.3E). The PAx versus CPP plots displays the classic parabolic distribution, with low PAx values (ie. intact autoregulation) within the CPP range of ~50 mm Hg to 130 mm Hg. Outside of these two limits of CPP, PAx subsequently trends toward positive values (indicating potentially impaired autoregulation) (Figure 4.4E).

Relationship Between RAC vs. ICP and RAC vs. CPP

Finally, interesting relationships were observed between RAC and both ICP and CPP. As ICP increases, RAC becomes progressively more positive (Figure 4.3F). This is similar to what was seen in the PRx vs. CPP plot (Figure 4.3D) and the PAx vs. CPP plot (Figure 4.3E). Thus, RAC may carry similar information regarding the cerebrovascular system as PRx and/or PAx. However, given the nature of the RAC coefficient, this may also represent physiologic processes related closely to alterations in cerebral compensatory reserve:

A. At low ICP (less than 20 mm Hg), RAC displays negative values, indicating a negative correlation between CPP and AMP (Figure 4.3F). This potentially represents states of good cerebral compensatory reserve (as seen with RAP values closer to zero; Figure 4.3C) and preserved autoregulation (as seen with PRx and PAx at low values; Figure 4.3D and 4.3E), in which changes in MAP do not lead to direct changes in ICP, nor AMP. Thus, the phase of slow wave fluctuations in both AMP and MAP (or CPP – since CPP is predominantly composed of MAP contribution at low ICP) are close to completely opposite in nature, hence the negative correlation coefficient generated by RAC. Furthermore, it may also be reflected in the decrease in AMP (Figure 4.3B) and increasing CPP (Figure 4.3A), as ICP decreases.

B. As ICP increases, above 20 mm Hg towards 60 mm Hg, we see a gradual increase in RAC towards zero (Figure 4.3F). During this ICP increase, cerebral compensatory reserve worsens, as seen with RAP approaching +1.0 (Figure 4.3B) and the increase in AMP (Figure 4.3B). However, this occurs during a progressive decrease in CPP, secondary to an increase in ICP (Figure 4.3A). This CPP decrease leads to a

decreased amplitude of slow wave fluctuations in CPP, and thus little to no correlation between slow wave phase of CPP and AMP (generating RAC values close to zero).

C. Finally, at further extreme levels of ICP (ie. above ~60 mm Hg), we see a gradual increase in RAC towards positive values (Figure 4.3F). At this point, cerebral compensatory reserve is believed to be at its worst. This is reflected in the "break-point" in the ICP versus AMP relationship (Figure 4.3A), and the progressive decrease in RAP towards zero (Figure 4.3C). CPP continues to trend low (Figure 4.3A), however given severely impaired compensatory reserve and pressure reactivity (highly positive PRx and PAx), any slow wave fluctuations in MAP are potentially amplified in ICP (and thus AMP, but this time with negative relationship, Fig 4.4B) leading to slow waves of CPP and AMP becoming progressively more "in phase" and thus producing the positive RAC value observed in this ICP range. Furthermore, AMP continues to decrease after this "break-point", while CPP drops secondary to extreme ICP values, also reflected in the positive index value for RAC. (Figure 4.3D, 4.3E and 4.3F).

The RAC vs. CPP plots also mimicked the PRx vs. CPP and PAx vs. CPP plots, displaying a parabolic relationship, with a minimum in the curve at a CPP of approximately 65 to 70 mm Hg for all three relationships. This minimum corresponded to the "most negative" value for each index: PRx, PAx and RAC. Thus, again, RAC may carry similar information regarding the cerebrovascular system as PRx and/or PAx. However, again, given the nature of the RAC index, it may carry some additional information about cerebral compensatory reserve during changes in CPP:

A. As CPP approaches the LLA (ie. ~50 mm Hg), RAC begins to gradually increase, with sharp increases towards more positive values as CPP continues to decrease below 50 mm Hg (Figure 4.4F). This corresponds to a steep increase in RAP towards +1.0, indicating progressing deterioration in cerebral compensatory reserve (Figure 4.4C) as it is associated with increases in ICP (Figure 4.4A). Thus, given impaired compensatory reserve, any slow wave fluctuations in MAP (and thus CPP) may be directly transmitted to ICP (and thus AMP), implying they become progressively more "in phase", producing the positive RAC coefficient.

Of more interest, is what happens as CPP progressively decreases below ~50 to 60 mm Hg. RAC continues toward more positive values, similar to PRx. However, RAP reaches its peak and subsequently decreases towards zero, reflective of the "break-point" in AMP and what is believed to be severely

impaired cerebral compensatory reserve. This may represent the point where cerebrovascular transmural pressure approaches critical closing pressure of the vessels, though this hasn't been proven. Thus, RAC values below this point in CPP may strictly carry cerebrovascular physiologic information, and not both: cerebrovascular and compensatory reserve information, as seen during CPP ranges above this critical point. However, it must be acknowledged that the majority the observations (ie. millions of data points) were in CPP ranges of 50 to 100 mm Hg, so interpretation of the relationships with CPP below 50 mm Hg must be interpreted with caution.

B. RAC reaches a minimum around CPP values of 65 to 70 mm Hg, similar to PRx. Outside of this CPP range, both RAC and CPP increase towards positive values. During this CPP range, there is a negative correlation between CPP and AMP. Thus, the phase of slow wave fluctuations in AMP and MAP (or CPP – since CPP is predominantly composed of MAP contribution at the low ICP values seen in this range for CPP; Figure 4.4A) may be closer to completely opposite in nature, hence the negative correlation coefficient generated by RAC.

C. Similarly, as CPP increases towards the ULA (ie. ~150 mm Hg), RAC gradually becomes more positive as well (Figure 4.4F), as seen with PRx (Figure 4.4D). This is in states with low ICP (Figure 4.4A). Cerebral compensatory reserve improves with CPP values up to ~130 to 140 mm Hg, as indicated by the decrease in RAP towards zero (Figure 4.4C) and AMP progressively decreasing (Figure 4.4B). With CPP values above ~140 mm Hg, RAP appears to remain low (Figure 4.4C), though we have a relatively low number of data points in this range (as previously mentioned), so this much be interpreted with caution given the error bar range. RAC continues to increase towards zero as CPP increases up to and beyond the ULA (Figure 4.4F), despite decreasing AMP during this process (Figure 4.4B). Thus, in this state of "good compensatory reserve", and deceasing AMP with increasing CPP, the trend towards more positive RAC values may represent a purely cerebrovascular phenomenon, similar to PRx and PAx in this CPP range. This could represent autoregulatory dysfunction at and beyond the ULA, as seen with both the PRx vs. CPP and PAx vs. CPP plots (Figure 4.4D and 4.4E), though this requires much further validation and again should be interpreted with caution given the limited data points beyond CPP values of ~130 to 140 mm Hg.

Figure 4.3: Non-DC Cohort – CPP vs. ICP, AMP vs. ICP, RAP vs. ICP, PRx vs. ICP, PAx vs. ICP and RAC vs. ICP Plots

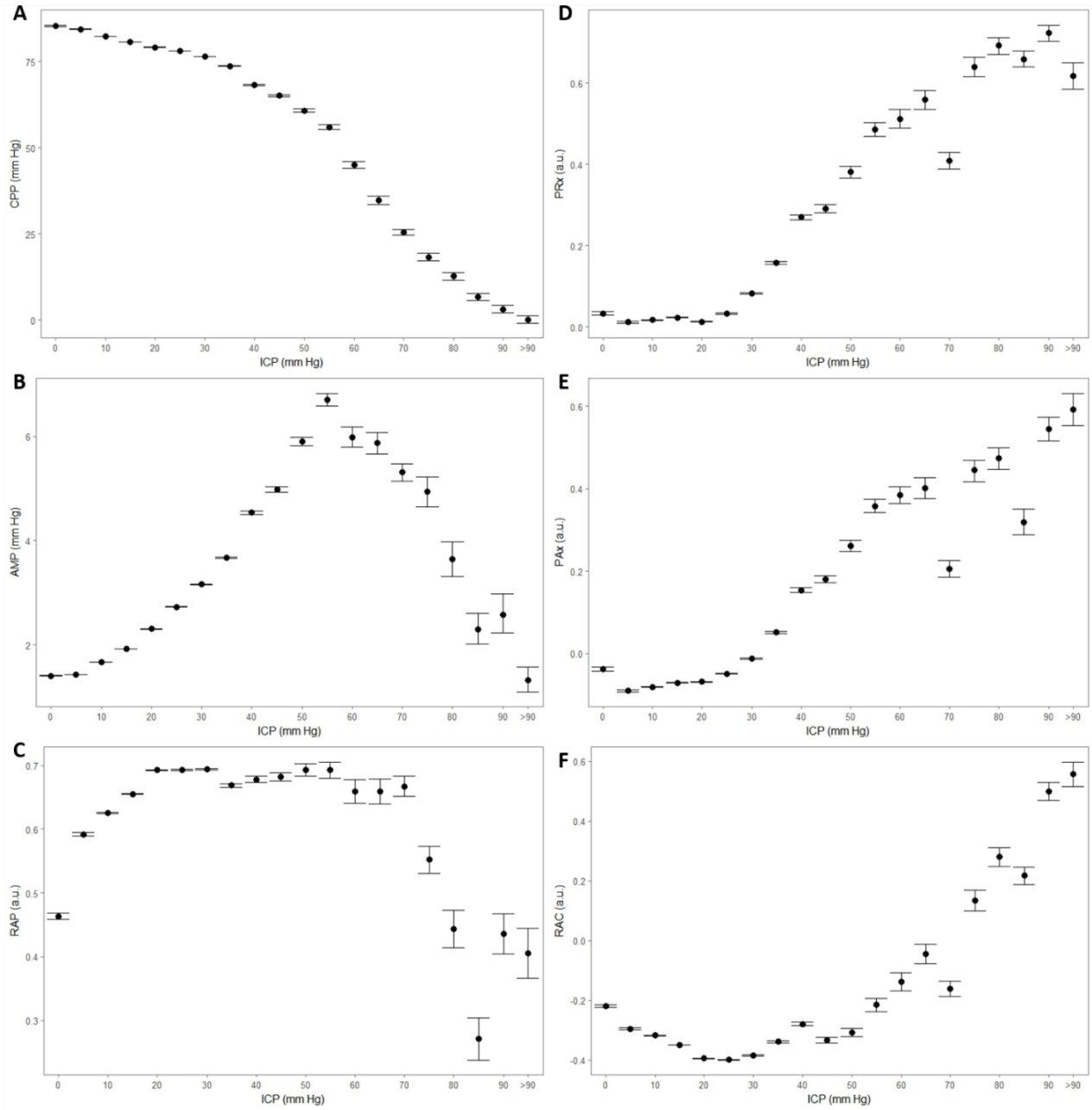

AMP = pulse amplitude of ICP, a.u. = arbitrary units, CPP = cerebral perfusion pressure, ICP = intra-cranial pressure, mm Hg = millimeters of Mercury, PAx = pulse amplitude index (correlation between AMP and MAP), PRx = pressure reactivity index, RAC = correlation coefficient between AMP and CPP, RAP = correlation coefficient between AMP and ICP. Panel A: CPP vs. ICP plot, Panel B: AMP vs. ICP plot, Panel C: RAP vs. ICP plot, Panel D: PRx vs. ICP plot, Panel E: PAx vs. ICP plot, Panel F: RAC vs. ICP plot.

Figure 4.4: Non-DC Cohort – ICP vs. CPP, AMP vs. CPP, RAP vs. CPP, PRx vs. CPP, PAx vs. CPP, and RAC vs CPP Plots

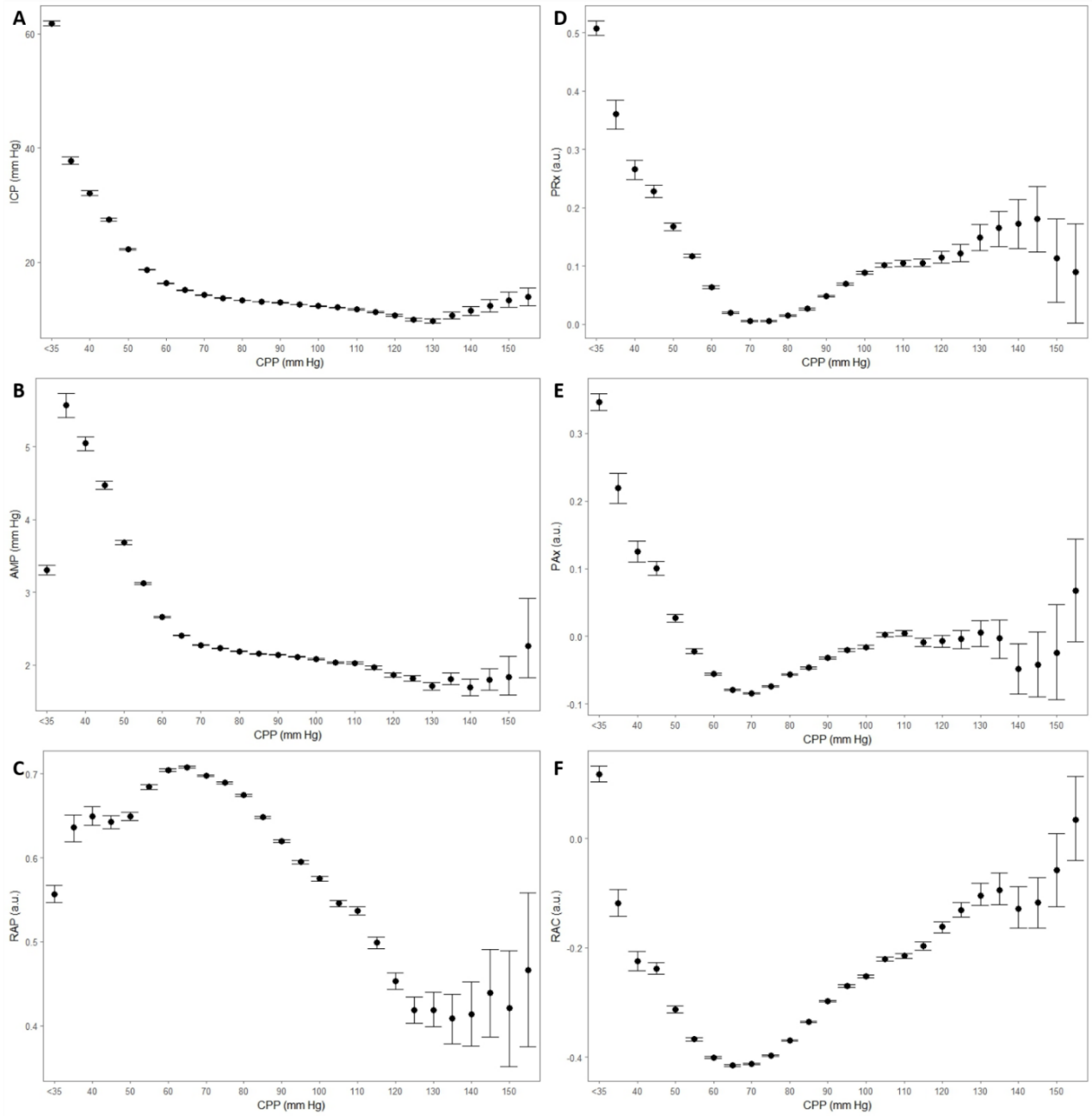

AMP = pulse amplitude of ICP, a.u. = arbitrary units, CPP = cerebral perfusion pressure, ICP = intra-cranial pressure, mm Hg = millimeters of Mercury, PAx = pulse amplitude index (correlation between AMP and MAP), PRx = pressure reactivity index, RAC = correlation coefficient between AMP and CPP, RAP = correlation coefficient between AMP and ICP. Panel A: CPP vs. ICP plot, Panel B: AMP vs. ICP plot, Panel C: RAP vs. ICP plot, Panel D: PRx vs. ICP plot, Panel E: PAx vs. ICP plot, Panel F: RAC vs. ICP plot

RAC and RAP/PRx/PAx – Inter-index Correlation

Using grand mean data for the non-DC cohort of patients (ie. one data point per variable, per patient) we calculated the Pearson correlation coefficients to be: 0.718 for RAC and PRx ($p<0.0001$), with a linear relationship (Figure 4.5A). The correlation between RAC and PAx was 0.816 ($p<0.0001$), with a linear relationship (Figure 4.5B). Finally, the correlation between RAC and RAP was -0.594 ($p<0.0001$), with a negative linear relationship (Figure 4.5C).

"Optimal CPP" Curves

Given the interest in optimal CPP (CPPopt), and the application of PRx for this purpose, we plotted both: RAC vs. CPP (Figure 4.4F), PRx vs. CPP (Figure 4.4D) and PAx vs. CPP (Figure 4.4E); using 5 mm Hg bins of CPP and mean values for RAC and PRx for observations within those bins, using the minute-by-minute data for the entire non-DC cohort. The optimal CPP is subsequently determined by finding the CPP values with the corresponding lowest PRx, PAx or RAC value (ie. the minimum of the parabola). The CPP optimum values from each of: PRx vs. CPP, PAx vs. CPP and RAC vs. CPP, are similar (ie. ~65 to 70 mm Hg). In addition, of interest is the improved parabolic shape of the RAC vs. CPP curve, compared to both the PRx vs. CPP and PAx vs. CPP curves. This is increasingly true for high values of CPP, where the PRx vs. CPP and PAx vs. CPP parabola appear to degenerate in shape, with this relationship appearing more preserved in the RAC vs. CPP curve. Thus, for CPP optimum determination, RAC may prove to be applicable in this instance. Further analysis of CPP optimum employing RAC is required.

Figure 4.5: Non-DC Cohort – RAC vs. PRx Plot, RAC vs. PAx Plot, and RAC vs. RAP Plot

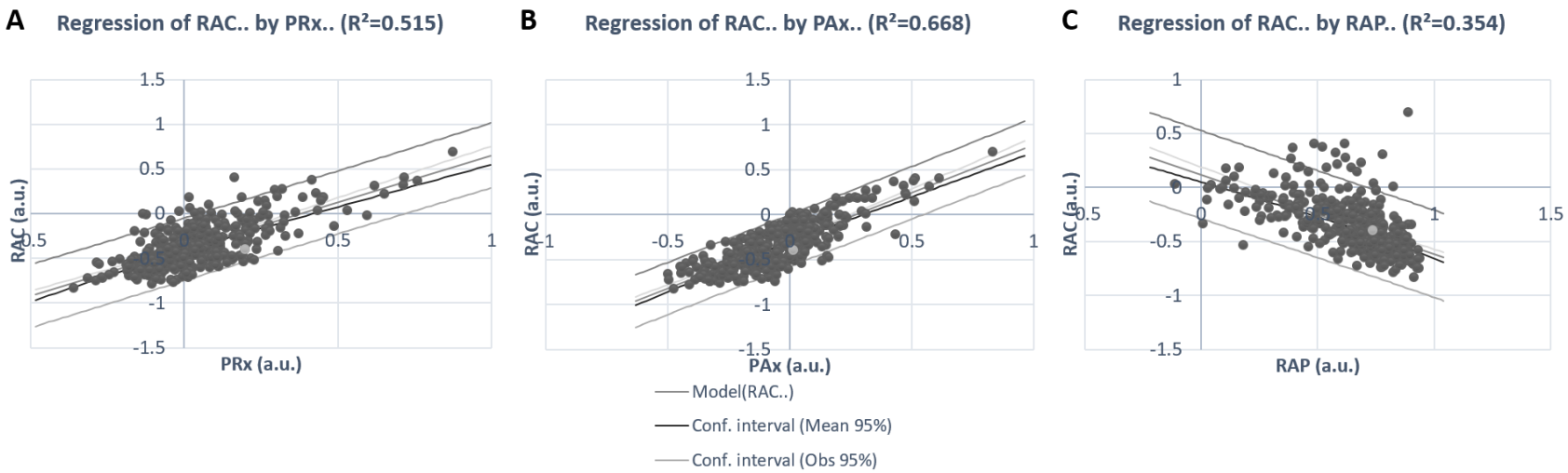

AMP = pulse amplitude of ICP, a.u. = arbitrary units, CPP = cerebral perfusion pressure, mm Hg = millimeters of Mercury, PAx = pulse amplitude index (correlation between AMP and MAP), PRx = pressure reactivity index (correlation between ICP and MAP), RAC = correlation coefficient between AMP and CPP, RAP = correlation between AMP and ICP.

4.4 Discussion

Through the analysis of both the individual examples and the large non-DC TBI cohort, some interesting features have been identified regarding a new physiologic RAC index that describes the relationship between cerebral perfusion pressure and ICP pulse amplitude. Several issues merit discussion.

First, being derived from the correlation between CPP and AMP, RAC appears to represent physiologic information pertaining to both: the cerebrovascular system (similar to PRx and PAx) and cerebral compensatory reserve (similar to RAP). This makes this index potentially unique and of importance. It is unlike other indices in that it carries information regarding multiple aspects of cerebral physiology. This aspect of RAC contributes to its potential usefulness clinically. However, it also contributes to the complexity of its interpretation. As outlined in the results section, the interpretation of RAC requires the assessment of not just RAC, but AMP, RAP and PRx/PAx. Only through this comprehensive analysis of multiple aspects of cerebral physiology can RAC be properly interpreted, allowing for an assessment of both cerebrovascular responsiveness and cerebral compensatory reserve. RAC requires much further investigation regarding its relation to cerebral compensatory reserve and autoregulation. It is too early to know the exact relationship between RAC with both cerebral autoregulation and cerebral compensatory reserve.

Second, based on the examples of extreme physiology (Figures 4.1, and 4.2), RAC appears to be temporally responsive to changes in both ICP and CPP, as seen in data obtained from patients experiencing varied insults: sustained intra-cranial hypertension and arterial hypotension. As ICP increase (or CPP decreases), there is a gradual increase in RAC to more positive values. An example of this is within the intracranial hypertension patients (Figure 4.1), where increased ICP and AMP (with corresponding decreases in CPP), results in increased RAC. This indicates an increasing direct positive correlation between AMP and CPP. Furthermore, in the patient with sustained intra-cranial hypertension (Figure 4.1), as ICP progressively increased towards ~60 mm Hg, AMP reaches a peak and subsequent break point, which has been previously described and is believed to potentially represent "exhaustion of cerebrovascular reserve" associated hypothetically with collapse of arterial bed.[91,145] After this break point in AMP is reached, and ICP remains elevated, RAC dramatically increases to values above +0.50, even approaching +1.0 in one example (Figure 4.1). Thus, it appears that the dramatic change in the rate of increase of RAC may denote this area of "exhaustion of cerebrovascular reserve". These changes occurred in concert with impaired cerebral compensatory reserve, as represented by RAP

values near +1.0. RAP responded with a rapid decrease towards negative values after the break-point in AMP, indicating severely impaired cerebral compensatory reserve. We must acknowledge that these observations are based on only case examples, and thus need further validation. However, both of these examples display RAC's ability to display information regarding cerebral compensatory reserve. Finally, the arterial hypotension case (Figure 4.2) displayed a progressive increase in PRx, PAx and RAC, during low ICP and "good" compensatory reserve (as per RAP). This supports the concept that RAC may carry some similar information to PRx or PAx, regarding cerebrovascular responsiveness.

Third, based on the non-DC TBI cohort, there is an increase in AMP, as ICP increases, to a peak at an ICP of ~50-60 (Figure 4.3B). Similarly, as CPP decreases towards 50 mm Hg, AMP gradually increases and peaks at a CPP of ~40 mm Hg. This is followed by a sharp decrease in AMP with further decreases in CPP (Figure 4.4B). These two relations have both been previously described,[145] with the current data supporting the previous literature. However, of interest is the RAC response at these two points. As ICP reaches ~50 to 60 mm Hg, and AMP peaks (Figure 4.3B), RAC begins to dramatically increase towards more positive values with further increases in ICP (Figure 4.3F). Similarly, as CPP decreases towards 40 mm Hg, RAC also increases dramatically towards more positive values (Figure 4.4F). However, these inferences are limited given the limited data for ICP above 50 mm Hg, and CPP below 40 mm Hg, compared the large volume of data for ICP and CPP values within the "normal" range. Within the results section the preliminary interpretation of these changes in RAC, with respect to AMP, RAP, PRx and PAx have been outlined. It is likely that RAC represents both aspects of changing cerebral compensatory reserve and cerebrovascular responsiveness, yielding uniqueness and complexity in this new index. Interpretation of RAC requires the evaluation of AMP, RAP and PRx/PAx.

Fourth, within the large non-DC TBI cohort, RAC appeared to respect the classic limits of the Lassen curve, with a trend to more positive RAC values when CPP was both below the LLA and above the ULA. As displayed in Figure 4.4F, RAC remains negative within the CPP range of ~50 to 140 mm Hg, with a trend to more positive RAC values as CPP approaches both thresholds (and in the case of the LLA, drops below it). This relationship is based on the ~2.7 million data points from the non-DC TBI cohort of 358 patients. However, it must be acknowledged that the number of data points for CPP values less than 50 mm Hg and close to/above the ULA were much less (ie. 1000's), compared to CPP values between 50 to 100 mm Hg (ie. 100,000's). Thus, strong conclusions on RAC's ability to delineate the LLA and ULA cannot be made at this time. It is unknown if RAC represents autoregulation at this time, though it appears to carry some similar information to PRx or PAx. Ideally this would be confirmed in a well-

controlled animal model, similar to PRx. As with extremes in ICP, RAC interpretation in relation to CPP changes requires evaluating response in AMP, RAP and PRx/PAx; given it seems to carry information regarding compensatory reserve and cerebrovascular responsiveness.

Fifth, based on a Pearson correlation coefficient:

A. RAC and PRx are strongly correlated ($r=0.718$, $p<0.0001$) with a linear relationship,

B. RAC and PAx are strongly correlated ($r=0.817$, $p<0.0001$) with a linear relationship.

In addition, comparing the mean RAC and PRx values across the entire non-DC TBI cohort, RAC is on average ~0.30 to 0.40 lower than PRx. This is also seen in Figure 4.4. It is clear that RAC carries similar information to both PRx and PAx (Figure 4.3D, 4.3E and 4.3F; Figure 4.4D, 4.4E and 4.4F), though we cannot confirm that the information regarding autoregulation in PRx or PAx is equally represented in RAC. This requires further investigation. It appears that RAC represents both cerebral compensatory reserve and cerebrovascular responsiveness.

Finally, when comparing the RAC vs. CPP (Figure 4.4F), PRx vs. CPP (Figure 4.4D) and PAx vs. CPP (Figure 4.4E) curves, using 5 mm Hg bins of CPP, some important features were seen. The RAC vs. CPP plot appeared to display a similar parabolic relationship to both the PRx vs. CPP and PAx vs. CPP curves, with the minimum at ~65 to 70 mm Hg in all instances. However, comparing the shape of the parabolic distributions, the RAC vs. CPP plot appears to retain the parabolic shape better at high CPP values, where both the PRx vs. CPP and PAx vs. CPP plots appear to degenerate. Thus, given these observations, RAC could potentially be utilized for CPP optimum determination. Furthermore, given the stronger parabolic relation displayed by CPP vs. RAC, RAC may prove superior for CPP optimum determination. However, substantial additional investigation of these issues is required before the RAC can be used to determine CPPopt.

Limitations

Despite the interesting results, there are some significant limitations which should be mentioned.

The patient examples of extreme physiology and the non-DC cohort are retrospective patient populations. Thus, within this population of patients, there is potential for significant heterogeneity in injury burden/pattern, co-morbidity and treatment. Furthermore, all of these patients were admitted to

the NCCU at Addenbrooke's Hospital, receiving therapies directed at maintaining ICP below 20 mm Hg and CPP greater than 60 mm Hg. Thus, strong conclusions from this data set must be cautioned, given the constant manipulation of ICP and CPP during the recording of this data. In addition, the impact of various vasopressor agents on the cerebrovascular pressure autoregulatory response is not well understood, and could potentially further impact the results seen.

All of the relationships and conclusions regarding RAC and its response to changes in ICP and CPP are preliminary, requiring much further work and investigation. As previously alluded to, the strength of conclusions related to RAC at CPP levels both below the LLA and above the ULAR must be tempered by the fact that the majority of data points are within the "normal" CPP range secondary to continuous CPP manipulation within the NCCU. Similarly, inferences regarding the response of RAC to ICP values above 30 mm Hg need to be cautious, given the relatively small number of data points for ICP's above this threshold. This is likely a consequence of ICP directed therapies within the NCCU, which may also account for the relative "discontinuity" in the RAC vs. CPP, PRx vs. CPP and PAx vs. CPP curves at CPP values below 30 mm Hg. With this said, the "small" number of data points outside of the normal CPP and ICP range, number in the thousands. Thus, despite hundreds of thousands of data points within the normal range for CPP and ICP, inferences drawn from thousands of data points recorded during extreme CPP and ICP values provide useful data regarding interesting trends in RAC, and allow to set hypotheses that can be tested in larger datasets.

Finally, even though the results described above for RAC are promising, they do not clearly demarcate the potential role, if any, for RAC monitoring within moderate and severe TBI patients. This important aspect has yet to be shown. Future plans exist to analyze the potential clinical relevance of RAC, compared to the existing indices PRx and PAx. Further to this, none of the patients included within this study underwent DC at any point during their hospital course, even for refractory ICP issues. Thus, no comments can be made on the temporal changes in RAC, or other indices, as a result of the DC procedure in TBI patients. Subsequent analysis of the value of monitoring RAC, among other physiologic indices, in patients undergoing DC is required. Future plans exist to pursue such analysis. In addition, the current population is unable to provide any information regarding the utility of RAC in predicting the need for subsequent craniotomy due to lesion progression, or new lesion development. This also requires further investigation.

4.1 Conclusions

A new continuous index of physiologic assessment in TBI is described, RAC, based on the moving Pearson correlation coefficient between AMP and CPP. Based on both examples of extreme physiology, and in a large non-DC cohort, RAC appears to be responsive to changes in ICP and CPP, at the expected limits of normal autoregulation. RAC appears to carry information regarding both: cerebral compensatory reserve and cerebrovascular responsiveness. This contributes RAC's uniqueness and complexity of interpretation. Validation of RAC as a means of potential autoregulation assessment is required. Further analysis of RAC in outcome prediction and CPP optimum estimation in TBI are required.

CHAPTER 5: EXPERIMENTAL VALIDATION OF ICP DERIVED INDICES OF VASCULAR REACTIVITY

*The studies described in Chapter 5.1 and 5.2 can also be found detailed in the following respective publications:

1. Zeiler et al., *J Neurotrauma.* 2018; 35(23):2812-2819. doi: 10.1089/neu.2017.5604.[171]

2. Zeiler et al., *J Neurotrauma.* 2018; 35(23):2803-2811. doi: 10.1089/neu.2017.5603.[172]

5.1 Lower Limit of Autoregulation in Piglet Model of Arterial Hypotension

5.1.1 Introduction

To date, numerous indices of cerebrovascular reactivity have been derived.[4] Given ICP monitoring is common in critically ill neurological patients, ICP-derived indices have received the most attention. PRx is the most widely cited index, and is the correlation between slow waves recorded in ICP and MAP.[3] Numerous studies link PRx to patient outcome in TBI, with critical thresholds associated with morbidity and mortality defined within the literature.[9] Furthermore, PRx has been validated in a piglet model against the LLA during arterial hypotension, one of only three indices to be validated in this type of model (the other being NIRS derived COx and HVx).[14]

Aside from PRx, two other ICP-derived indices of cerebrovascular reactivity exist. PAx, the correlation between AMP and MAP, has been demonstrated to be comparable to PRx in outcome prediction for TBI patients.[15] In cases with low ICP (like for example after decompressive craniectomy) PAx is probably more useful than PRx. However, limited literature exists in the application of PAx clinically. Similarly, RAC, the correlation (R) between AMP (A) and CPP (C), has been recently described within the TBI population and was highlighted in Chapter 4 of this thesis.[21] It remains currently unknown whether PAx or RAC measure the LLA.

This study was conducted to determine if PAx and RAC discriminate the LLA during arterial hypotension, as well as to provide validation for the previous PRx study[14] in a larger cohort of animals.

5.1.2 Methods

Animal Model

The data from studies in neonatal piglets described here were retrospectively amalgamated from 3 separate experiments. [14,147,148] Details regarding these models, including experimental treatment, has been outline in the general methodology section in Chapter 3.1. In brief, this cohort consisted of 3 separate sham animal populations, totaling 22 piglets, where no cerebral insult had occurred (ie. ICP elevations, cardiac arrest or hypothermia). All of these animals underwent similar anesthetic (see Chapter 3.1), and subsequently had an esophageal balloon within the IVC inflated to induce arterial hypotension over the course of 2 to 3 hours. ICP, ABP and LDF-CBF were recorded continuously throughout the experiment using ICM+.

Signal Acquisition and Processing

All signals from the combined monitoring modalities described above were recorded and archived for subsequent retrospective use. All recorded signals were digitized via an A/D converter (DT9804, Data Translation, Marlboro, MA), sampled at frequency of 50 Hertz (Hz) or higher, using ICM+ software (Cambridge Enterprise Ltd, Cambridge, UK, http://icmplus.neurosurg.cam.ac.uk). Signal artifacts, such as transducer adjustments, were removed prior to further processing or analysis using tools available in ICM+.

CPP was determined as: MAP – ICP. AMP was determined by calculating the fundamental Fourier amplitude of the ICP signal over a 10 second window, updated every 10 seconds. This was done over the range consistent with the normal range for piglet heart rate (ie. 100 – 350 bpm). Finally, 10 second moving averages (without data overlap) were calculated for all recorded signals: ICP, AMP, ABP (ie. producing MAP), CPP, and LDF-CBF. The piglets' archived signals were retrospectively interrogated and analyzed.

The following continuous indices of cerebrovascular reactivity were derived: PRx, PAx, RAC and LDF derived Lx. All indices were derived via moving Pearson correlation coefficients between 30 consecutive 10 second average values of relevant signals and their parameters (ie. 5 minute of data), updated every minute.

Statistics

All statistical analysis was conducted utilizing R statistical software (R Core Team (2016). R: A language and environment for statistical computing. R Foundation for Statistical Computing, Vienna, Austria. URL https://www.R-project.org/). The following packages were employed: *ggplot2*, *dplyr*, *tidyverse*, *lubridate*, *segmented*, and *pROC*. Where significance is reported, alpha was set at 0.05. The following analysis described is similar to that performed within previous studies on the LLA. This was done so as to allow comparison between the results, and potentially provide validation of the results seen within that study.[14]

Finding the LLA

In order to determine the LLA of autoregulation in the 22 animals, piecewise linear regression of the CPP versus LDF-CBF plots was employed. The LDF-CBF signal was standardized against the individual animal's baseline LDF-CBF signal, producing "% change of LDF-CBF from baseline". This is similar to other studies evaluating LDF-CBF.

The piecewise regression process employed a starting point for estimation of the break-point in LDF-CBF. This starting point was visually estimated from the ICM+ plots of CPP versus LDF-CBF. The breakpoint identified by the piece wise regression process is one in which minimized the sum residual square error (SSE) of the two linear segments, above and below this point. This was conducted for each animal, with piecewise regression plots produced denoting the 95% confidence interval (CI) for each fitted linear segment. Finally, the mean LLA for the cohort of 22 piglets was determined by averaging all 22 LLA values obtained.

Binned Cohort Data and Plot

After delineating the mean LLA for the cohort, cohort wide plots were produced to inspect the population trend of various physiologic measures against the LLA. All data was binned across 5 mm Hg bins of CPP, using R statistical software. The following error bar plots were then produced: % change in LDF-CBF From Baseline vs. CPP, PRx vs. CPP, PAx vs. CPP, and RAC vs. CPP.

Comparing CPP for Various Clinical Thresholds of PRx, PAx and RAC to LLA

To conduct a rough comparison of the CPP for clinically defined thresholds of PRx, PAx and RAC to the CPP at the LLA, piecewise regression was performed in each animal. To do so, a simplified piecewise linear regression was performed for PRx vs. CPP and PAx vs. CPP, using these models to determine the CPP in each animal for the following thresholds of PRx and PAx defined in TBI patients.[9,152] For PRx, the thresholds of 0, +0.25 and +0.35 were tested, based on previous work in TBI. For PAx, the thresholds of 0 and +0.25 were tested. Finally, for RAC, the thresholds of -0.10 and -0.05 were tested. CPP values at each threshold for PRx, PAx and RAC were compared with the CPP values at the LLA using a Pearson correlation coefficient and Bland-Altman analysis. The Bland-Altman analysis was only conducted for those thresholds reaching statistically significant correlations with the LLA (ie. PRx 0, PRx +0.25, and PRx +0.35).

Prediction of Impaired Autoregulation using Continuous Indices

As done in previous studies, receiver operating curve (ROC) analysis of PRx, PAx, RAC and Lx were performed across the cohort defined LLA. This was conducted in order to determine the ability of these indices to predict being either above or below the LLA. For each piglet, one mean value for each variable was obtained at each 5 mm Hg bin of CPP (ie. CPP = 40 mm Hg, 45 mm Hg, etc.). Five mm Hg bins of CPP were used for the ROC analysis, given this was what was conducted within the previous study by Brady et al.[14]

This data was then given the binary designation of being above the LLA, or below the LLA, based on the LLA defined previously. The data from all 22 piglets was then used for the ROC analysis. AUC for the ROC's was reported and 95% CI reported via Delong method. Significance values (ie. p-values) for the AUC's were derived from univariate logistic regression analysis. Comparison between AUC's was conducted using Delong's test.

Criteria for Measures of the LLA

In order to be able to say that a specific index provides a measure of the LLA in this particular model, the following criteria needed to be met:

1. Demonstration of cerebrovascular reactivity indices to trend towards progressively more positive values at CPP levels below the LLA.
2. Statistically significant logistic regression analysis for each cerebrovascular reactivity index in the prediction of having CPP values above or below the cohort defined LLA.

5.1.3 Results

Defining the LLA

Through piecewise linear regression analysis of each piglet, the LLA was obtained for each animal. Figure 5.1 displays an example of the recorded MAP, ICP, CPP and LDF-CBF signal during the hypotension experiment. While Figure 5.2 displays two examples of piecewise linear regression analysis of the LLA. The mean LLA was 36.2 +/- 10.5 mm Hg.

Figure 5.1: Example of Physiologic Signal Changes During Hypotension

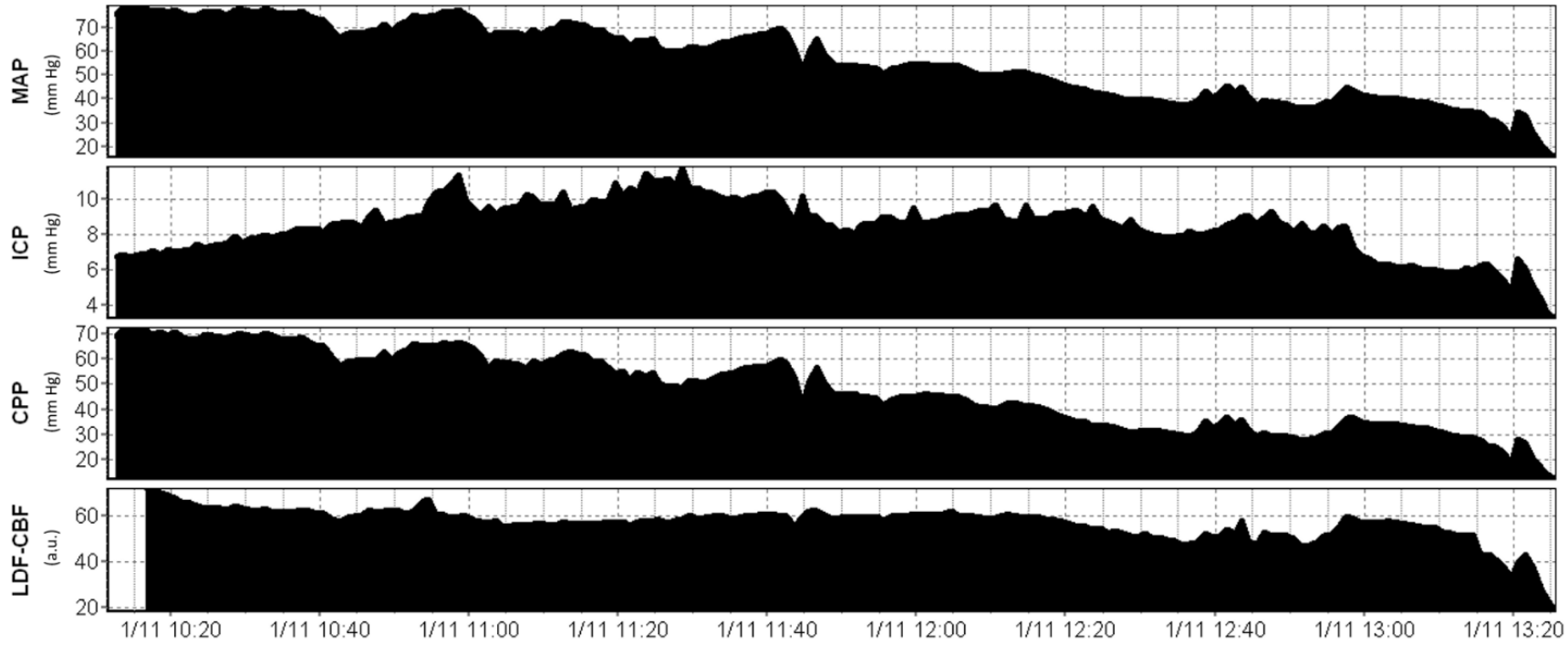

a.u. = arbitrary units, CPP = cerebral perfusion pressure, ICP = intracranial pressure, LDF-CBF = laser Doppler flowmetry cerebral blood flow, MAP = mean arterial pressure, mm Hg = millimeters of Mercury.

Figure 5.2: Examples of Piecewise Linear Regression Analysis of LLA

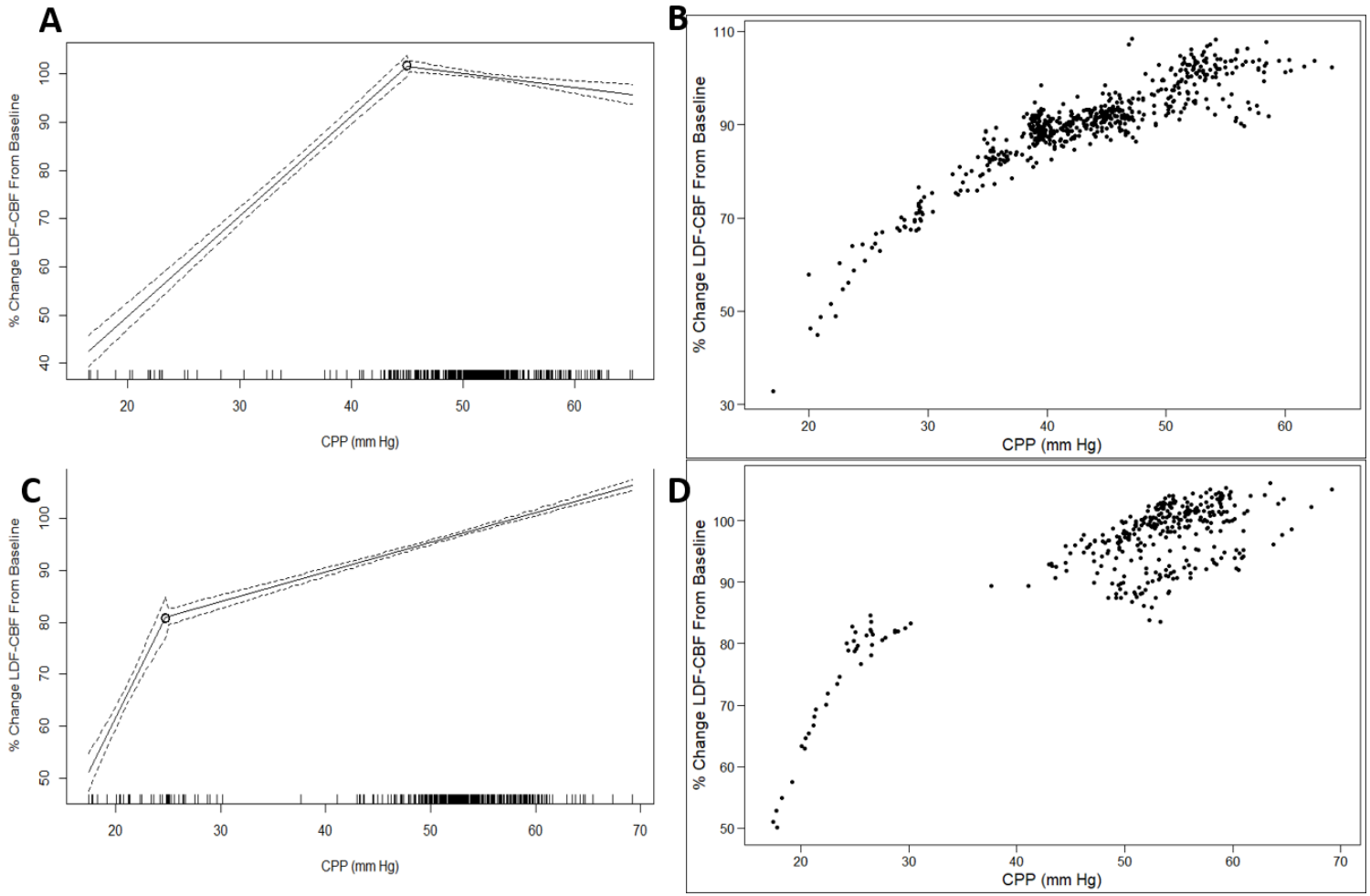

CPP = cerebral perfusion pressure, LDF-CBF = laser Doppler flowmetry cerebral blood flow, mm Hg = millimeters of Mercury. Panel A + B = Piecewise linear regression and scatter plot for one piglet. Panel C + D = piecewise linear regression and scatter plot for one piglet. NOTE: dashed line on piecewise linear regression plots represents the 95% confidence intervals for the fitted lines.

Population-Wide Trends

In order to provide a population-wide assessment of % change in LDF-CBF and the ICP derived indices during changes in CPP, various error bar plots were produced. Figure 5.3 displays the plot of CPP versus % change in LDF-CBF from baseline, with the vertical dashed line indicating the approximate mean LLA, derived above. This demonstrates that there is a precipitous drop in LDF-CBF below the LLA.

Similarly, the ICP indices were plotted across 5 mm Hg bins of CPP, producing error bar plots. Figure 5.4 displays these plots. It can be seen that PRx, PAx and RAC all correlated with the LLA, denoted by the vertical dashed line.

Figure 5.3: Population-Wide – % Change in LDF From Baseline vs. CPP

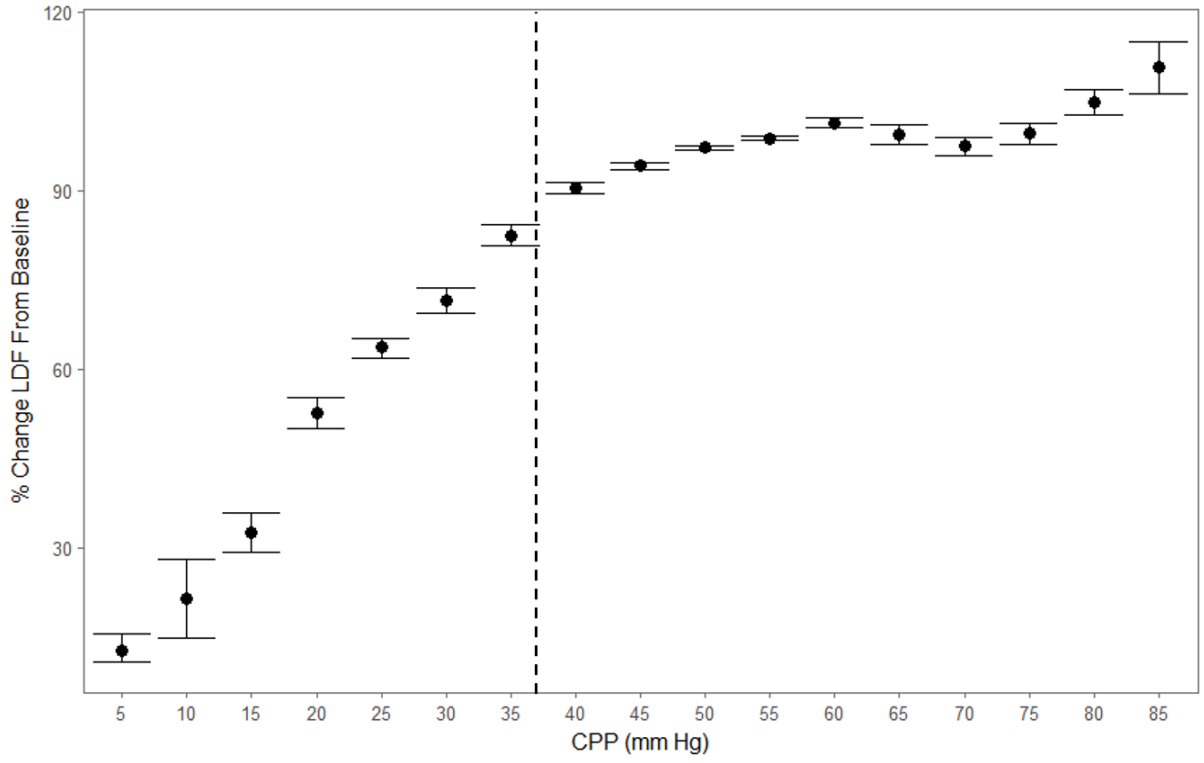

CPP = cerebral perfusion pressure, LDF = laser Doppler flowmetry, mm Hg = millimeters of Mercury. NOTE: vertical dashed line represents the approximate mean LLA for the population defined through piecewise linear regression in each animal.

Figure 5.4: Population-Wide Error Bar Plots – PRx vs. CPP, PAx vs. CPP and RAC vs. CPP

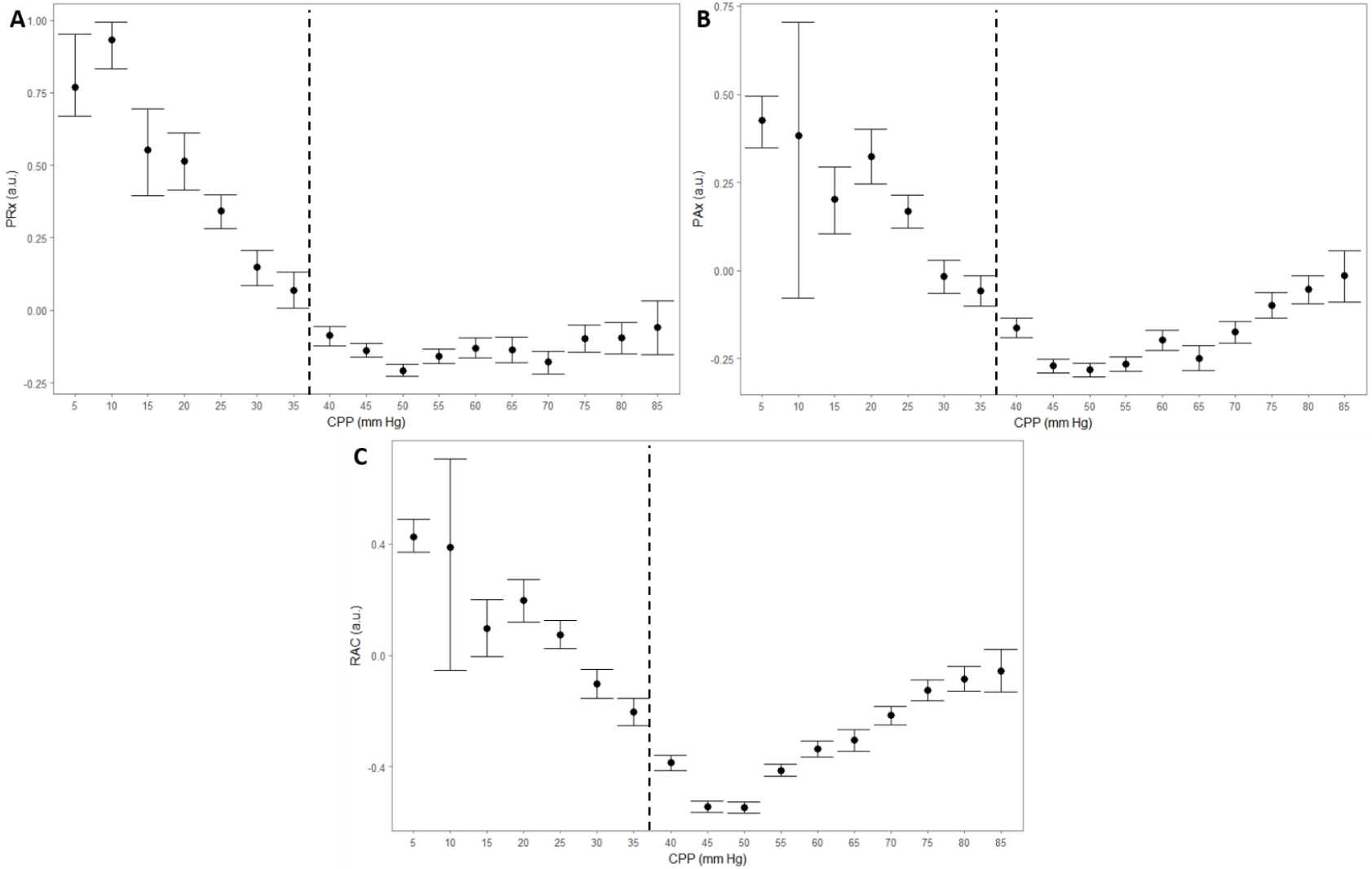

AMP = pulse amplitude of ICP, a.u. = arbitrary unite, CPP = cerebral perfusion pressure, ICP = intra-cranial pressure, PAx = pulse amplitude index (correlation between AMP and MAP), PRx = pressure reactivity index (correlation between ICP and MAP), RAC = correlation between AMP and CPP. NOTE: vertical dashed line represents the approximate mean LLA for the population, derived through piecewise linear regression in each animal.

Comparing CPP for Various Clinical Thresholds of PRx and PAx to LLA

For each animal, the CPP at each threshold for PRx, PAx and RAC was roughly derived through a simplified piecewise linear model of PRx vs. CPP, PAx vs. CPP, and RAC vs. CPP in each individual animal. These CPP values were compared to the CPP for the LLA derived in each animal, as described above. Table 5.1 displays the results for Pearson correlation between the CPP at TBI defined critical thresholds and the LLA within the cohort of piglets. Only the PRx thresholds appeared to produce statistically significant correlations, though they are weak in strength. Bland-Altman analysis comparing the CPP values at these PRx thresholds, and the CPP at the LLA, displayed poor agreement between the threshold CPP values and the CPP at the LLA.

Table 5.1: Comparison of CPP at Index Threshold to LLA – Pearson Correlation and T-test

Index Threshold Tested Against LLA	Pearson Correlation Coefficient with LLA	p-value for Pearson Correlation Coefficient
PRx = 0	**0.538**	**0.014**
PRx = +0.25	**0.571**	**0.008**
PRx = +0.35	**0.512**	**0.021**
PAx = 0	-0.078	0.745
PAx = +0.25	0.294	0.208
RAC = -0.10	0.394	0.077
RAC = -0.05	0.350	0.120

*AMP = pulse amplitude of ICP, CPP = cerebral perfusion pressure, ICP = intracranial pressure, LLA = lower limit of autoregulation, PAx = pulse amplitude index (correlation between AMP and MAP), PRx = pressure reactivity index (correlation between ICP and MAP), RAC = correlation between AMP and CPP. *Note: Bolded values are those which reached statistical significance.*

LLA ROC Analysis

Through ROC analysis across the LLA, using the data from the 22 piglets, the AUC's for each continuous index were calculated. The AUC for PRx, PAx and RAC was: 0.806 (95% CI: 0.750 – 0.863, p<0.0001), 0.726 (95% CI: 0.664 – 0.789, p<0.0001), and 0.710 (95% CI: 0.646 – 0.775, p<0.0001), respectively. Finally, the AUC for Lx was 0.809 (95% CI: 0.754 – 0.863, p<0.0001). Comparing AUC's via Delong's test, there was a statistically significant difference between the AUC's generated, when comparing PRx to PAx

(p=0.0004), and PRx to RAC (p<0.0001). However, the AUC's for PAx and RAC were not statistically different (p=0.214).

5.1.4 Discussion

Through retrospective analysis of archived experimental piglet data, a cohort of animals subjected to pure arterial hypotension, this allowed for the assessment of ICP derived continuous indices against the LLA. A few important points deserve highlighting.

First, for the first time, insight has been provided some evidence validating PAx and RAC against the LLA within a model of hypotension. This suggests that both indices provide information regarding cerebral autoregulatory capacity with a moderate accuracy. However, inconclusive evidence exists to support that the index threshold values, as defined in a TBI population,[152] measure the LLA within this current model. The Pearson correlations between the LLA and the CPP at these thresholds were poor and not statistically significant. It remains uncertain as to whether the TBI defined critical thresholds for PAx and RAC can be applied outside of the TBI population, given the poor performance of these thresholds within this model of arterial hypotension. Further, it remains unclear as to whether these thresholds represent relevant aspects of cerebral autoregulation, aside from associations with patient outcome in TBI. It is also likely that threshold values for reactivity indices may vary by individual. It must be acknowledged these results are preliminary.

Finally, confirmatory evidence has been provided that PRx correlates with the LLA within a model of hypotension. This was conducted using both the animal data from the initial publication documenting this relationship,[14] plus another 14 sham control animals from other experiments. A similar AUC (0.806, p<0.0001) in the prediction of the LLA using PRx was demonstrated. Finally, evaluating clinically relevant thresholds for PRx, all thresholds fail to produce strong correlations with the LLA within a model of arterial hypotension. This was confirmed via poor agreement with the LLA on Bland-Altman analysis for all PRx clinical thresholds tested. This is likely because these thresholds have been defined within adult TBI populations,[9,152] and thus the underlying disease and influence of ICP elevation post-injury may produce these thresholds that are disease specific. It is therefore not surprising that these thresholds do not necessarily respect the LLA in a model of pure hypotension. As with PAx and RAC, it must be stated that given the small numbers of animals within the current study, strong conclusions regarding these clinical thresholds cannot be made at this time. This work remains preliminary.

Limitations

Despite the interesting and promising results, a few limitations deserve emphasis. First, this is a retrospective analysis of an amalgamated cohort of piglets from 3 separate experiments. Though the anesthetic, procedures and experimental hypotension techniques were similar for all animals, the cohorts were not exactly identical. For example, 8 of the animals were slightly older (ie. 5 to 10 days, versus 3 to 5 days), with higher weights. This could influence the cerebrovascular response slightly. Second, despite have a sizable cohort of piglets for this retrospective analysis, it is still a relatively small number of animals, thus the conclusions drawn must be taken with caution. Third, the clinically defined thresholds for PRx, PAx, and RAC tested are defined within a TBI population.[9,152] Thus, exploring how they relate to the LLA in a model of arterial hypotension may explain why many of the thresholds for PRx, PAx and RAC don't appear to be related to the LLA. As mentioned above, the results of this analysis are preliminary and thus strong conclusions about the relationship between the clinical thresholds and the LLA cannot be made. Further validation is required. Further to this, even though the CPP at some of the clinically defined index thresholds appeared to be related to the LLA within this piglet model, one must interpret this with caution. As the LLA represents the point at which cerebral autoregulation becomes impaired (ie. not the point at which vascular reactivity is completely lost), the lack of strong associations with CPP at thresholds defined by clinical outcome is not surprising. These thresholds for the ICP defined indices were derived from TBI patient outcome at 6 months post injury. As a result, these index thresholds may represent the severe end of the autoregulation spectrum, the point of complete failure of vascular reactivity. Hence, the relationship between the CPP at thresholds and the LLA may not be robust, as they could be representing different aspects of impaired cerebrovascular reactivity. As well, one must assume that there are individual animal-based differences in vascular reactivity, introducing the influence of potential random effects. Much further interrogation of these clinically defined index thresholds is required, with the current analysis providing some preliminary insight.

5.1.5 Conclusions

The three ICP derived continuous indices of cerebrovascular reactivity, PRx, PAx and RAC were evaluated against the LLA within this experimental model of arterial hypotension. All three indices appear to respect the LLA within this model of pure arterial hypotension, with PRx being superior.

5.2 Lower Limit of Autoregulation in Rabbit Model of Intra-Cranial Hypertension

5.2.1 Introduction

Aside from literature supporting an association between continuous measures of cerebrovascular reactivity and patient outcome, there is a paucity of data to support the concept that these indices measure the limits of autoregulation (ie. become progressively more positive when CPP decreased below the LLA).[14] To date, only PRx and two NIRS derived indices (COx and HVx) have been validated against the lower LLA in an animal model of arterial hypotension.[14,173] Chapter 5.1 provides evidence to validate all ICP derived indices against the LLA in a piglet model of arterial hypotension.

However, these continuous indices have never been validated against the LLA in a model of sustained intra-cranial hypertension. Thus, this study will explore the correlation between PRx, PAx and RAC with the LLA in a rabbit model of sustained IC hypertension.

5.2.2 Methods

Animals

The animals described within this study have in part been described in previous studies related the physiologic response to intra-cranial hypertension.[145,146] The details surrounding this NZ rabbit model of IC hypertension have been provided in Chapter 3.1 of the general methods, including anesthetic administered and CSF infusion protocol for the IC hypertension experiment. In brief, all animals were placed under general anesthesia, with an isolated basilar artery fed circulation created two weeks prior to the experiment by ligation of common carotid arteries. IC hypertension was induced through an infusion of Hartmann's solution into the lumbar cistern, via intra-thecal catheter. ICP was elevated until cessation of diastolic flow on TCD. ICP, ABP, TCD CBFV from the basilar artery, and cortical LDF-CBF were recorded and linked in time-series. Arterial blood pressure (ABP) was measured through in the dorsal aorta after catheter insertion in the femoral artery (GaelTec, Dunvegan, UK). Cerebral blood velocity was measured using an 8MHz Doppler ultrasound probe (PCDop 842, SciMed, Bristol, UK) positioned over the basilar artery (accessed through a 7mm burr-hole at the bregma). ICP was monitored using an intraparenchymal microsensor (Codman and Shurtleff, Raynham, MA, USA) inserted through a right

frontal burr-hole, and a laser Doppler flowmetry (LDF) probe was placed epidurally through a further right frontal burr-hole (Moor Instruments, Axbridge, Devon, UK). The digitally recorded raw physiologic data from 12 animals from this experiment were accessed for the purpose of this study. Only 12 animals were used for this study, given the quality of the recorded LDF and TCD signals from the remaining animals were deemed unsuitable for derivation of piece-wise regression models to evaluate the LLA. Given technique related limitations for LDF and TCD during these experiments the recorded signals for animals, other than the selected 12, were: noisy, non-continuous and contained various degrees of signal artefact. As such, only the data from 12 animals were utilized.

Data Acquisition

All signals from the combined above invasive and non-invasive monitoring modalities were recorded and archived for future retrospective use. All recorded signals were digitized via A/D converters (DT300; Data Translation, Marlboro, MA), sampled at frequency of 100 Hertz (Hz), using WREC software (Warsaw University of Technology) and subsequently processed using ICM+ software (Cambridge Enterprise Ltd, Cambridge, UK, http://icmplus.neurosurg.cam.ac.uk). Signal artifacts were removed prior to further processing or analysis using tools available in ICM+.

Signal Analysis

CPP was determined as: MAP – ICP. FVs was derived by calculated the maximum FV over a 0.5 second window, updated every 0.25 seconds. FVm was calculated using the average FV over a 10 second window, updated every 10 seconds without data overlap. AMP was determined by calculating the fundamental Fourier amplitude of the ICP signal over a 10 second window, updated every 10 seconds. This was done over the frequency range consistent with the rabbits HR (ie. 100 – 400 bpm). Finally, 10 second moving averages (without data overlap) were calculated for all recorded signals: ICP, AMP, ABP (ie. producing MAP), CPP, FVm, FVs, LDF based CBF (LDF-CBF). Continuous indices of cerebrovascular reactivity were generated in a fashion consistent with that described in Chapter 3, deriving: PRx, PAx, RAC, and Lx. Update frequency for all physiologic variables was 10-seconds-by-10-seconds, given the short duration of recordings during the experiment.

The archived signals for all 28 of the animals were retrospectively interrogated and analyzed. Utilizing ICM+ software, plots for LDF versus CPP and FVm/FVs versus CPP were constructed. These were inspected visually for overall trend and the presence of a visible "break point" in LDF/FVm/FVs where future piecewise linear regression analysis would potentially be able to identify an accurate LLA. It was found that only 12 of the animals had sufficient recordings to allow for the accurate assessment of the LLA (given insufficient data after artifact removal to clearly identify an LLA), and thus only 12 animals were utilized for the remainder of the study.

Statistics

All statistical analysis was conducted utilizing R statistical software (R Core Team (2016). R: A language and environment for statistical computing. R Foundation for Statistical Computing, Vienna, Austria. URL https://www.R-project.org/). The following packages were employed: *ggplot2, dplyr, tidyverse, lubridate, segmented,* and *pROC*. Where significance is reported, alpha was set at 0.05. The following analysis described is identical to that performed by Brady et al., the only study in existence validating PRx against the LLA.[14] This was done so as to remain as to allow comparison between the results, and potentially provide validation of the results seen within that study.

Finding the LLA

In order to determine the LLA of autoregulation in the 12 animals, piecewise linear regression of either LDF-CBF versus CPP plots, or FVs versus CPP plots, was employed. In 3 of the 12 animals, the LDF-CBF signals were not adequate for piecewise regression, and thus CPP versus FVs plots were utilized to find the LLA. The LDF-CBF signal was standardized against the individual animal's baseline LDF-CBF signal, producing "% change of LDF-CBF from baseline". This is similar to other studies evaluating LDF-CBF.

The piecewise regression process employed a starting point for estimation of the break-point in either LDF-CBF or FVs. This starting point was visually estimated from the ICM+ plots of LDF-CBF versus CPP or FVs versus CPP, described above. The breakpoint identified by the piece wise regression process is one in which minimized the SSE of the two linear segments, above and below this point. This was conducted for each animal, with piecewise regression plots produced denoting the 95% CI for each fitted linear

segment. Finally, the mean LLA for the cohort of 12 rabbits was determined by averaging all 12 LLA values obtained.

Finding the "Cushing's Response Point"

Given this animal model involved sustained intra-cranial hypertension, the profound sympathetic surge seen during herniation could influence the relationship between MAP and ICP or AMP, leading to overwhelming positive trends in PRx, PAx and RAC below the LLA.[145] Thus, it was important to see if there was a distinct separation between the LLA and when the Cushing's response was seen. A separate piecewise linear regression analysis of CPP versus MAP plots was performed, looking for a break point where as CPP continues to decrease, a dramatic increase in MAP is seen, corresponding the point where the Cushing's response takes effect. The breakpoint identified by the piecewise regression process is one in which minimized the SSE of the two linear segments, above and below this point. This was conducted for each animal, with piecewise regression plots produced denoting the 95% CI for each fitted linear segment. Finally, the mean "Cushing's Point" for the cohort of 12 rabbits was determined by averaging all 12 breakpoint values of MAP versus CPP. The mean LLA was compared to the mean "Cushing's Point" via student t-test, to assess statistical significance.

Binned Cohort Data and Plot

After delineating the mean LLA for the cohort, cohort wide plots were produced to inspect the population trend of various physiologic measures against the LLA. First all data was binned across 2.5 mm Hg bins of CPP, using R statistical software. The following error bar plots were then produced: LDF-CBF vs. CPP, FVs vs. CPP, PRx vs. CPP, PAx vs. CPP, RAC vs. CPP and AMP vs. CPP.

Comparing CPP for Various Clinical Thresholds of PRx and PAx to LLA

A rough comparison of CPP for clinically defined thresholds of PRx and PAx to CPP at the LLA, defined via piecewise regression in each animal, was performed. To do so, a simplified piecewise linear regression was performed of PRx vs. CPP and PAx vs. CPP, using these models to determine CPP in each animal for the following thresholds of PRx and PAx defined in TBI patients. For PRx, the thresholds of 0, +0.25 and

+0.35 were tested. For PAx, the thresholds of 0 and +0.25 were tests. CPP values at each threshold for PRx and PAx were compared with the CPP values at the LLA, using a Bland-Altman analysis. The Bland-Altman analysis was only conducted for those index thresholds which displayed statistically significant correlation coefficients with the LLA.

Prediction of Continuous Indices for Impaired Autoregulation

As done in Brady et al., ROC analysis of PRx, PAx and Lx across the cohort defined LLA was performed. This was conducted in order to determine the ability of these indices to predict being either above or below the LLA. For each rabbit, 1 mean value for each variable was obtained at each 2.5 mm Hg bin of CPP (ie. CPP = 40 mm Hg, 45 mm Hg, etc.). We utilized 2.5 mm Hg bins of CPP for the ROC analysis, to improve ROC prediction, given the short duration of experiments and noisy data recording available in this experiment. This is in contrast to the 5 mm Hg binned data utilized within the previous study by Brady et al.,[14] where long duration of controlled induced experimental hypotension and data recording allowed for using such data binning.

This data was then given the binary designation of being above the LLA, or below the LLA, based on the LLA defined previously. The data from all 12 rabbits was then utilized for the ROC analysis. AUC for the ROC's was reported and 95% CI reported via Delong method. Significance values (ie. p-values) for the AUC's were derived from univariate logistic regression analysis. Comparison between AUC's was conducted utilizing Delong's test.

Criteria for Measures of the LLA

In order to be able to say that a specific index provides a measure of the LLA in this particular model, the following criteria needed to be met:

3. Demonstration of cerebrovascular reactivity indices to trend towards progressively more positive values at CPP levels below the LLA.
4. Statistically significant logistic regression analysis for each cerebrovascular reactivity index in the prediction of having CPP values above or below the cohort defined LLA.

5.2.3 Results

Defining the LLA

Piecewise linear regression was conducted in each rabbit. Nine of the rabbits had this analysis conducted on the LDF-CBF vs. CPP plots, while in 3 animals it was conducted on the FVs plots vs. CPP. Across all rabbits, the mean LLA was determined to be 51.5 +/- 8.2 mm Hg. Figure 5.5 displays the piecewise linear regression for two animals, with their corresponding scatter plots. Panel A displays and example of the plots for ICP, MAP, CPP, LDF and FVs over time during the experiment. Panel B and C denote an example of piecewise regression using the LDF-CBF vs. CPP plot, and Panel D and E denote the same using the FVs vs. CPP plot. Figure 5.6, displays the LDF-CBF vs. CPP error bar plot for the entire rabbit cohort, demonstrating a dramatic drop in LDF signal below the defined LLA (ie. ~50 mm Hg).

Defining the "Cushing's Point"

Piecewise linear regression of MAP vs. CPP was conducted for each rabbit. Across all rabbits the mean "Cushing's Point", where with further decrease in CPP we saw dramatic increases in MAP, was 42.4 +/- 9.8 mm Hg. Figure 5.7 displays an example of the piecewise regression between CPP and MAP, identifying the "Cushing's Point". Comparing the LLA and the Cushing's point across all animals, via the student's t-test, the LLA and Cushing's point were noted to be statistically different (t=2.396, p=0.027).

Figure 5.5: Examples of Piecewise Linear Regression Analysis

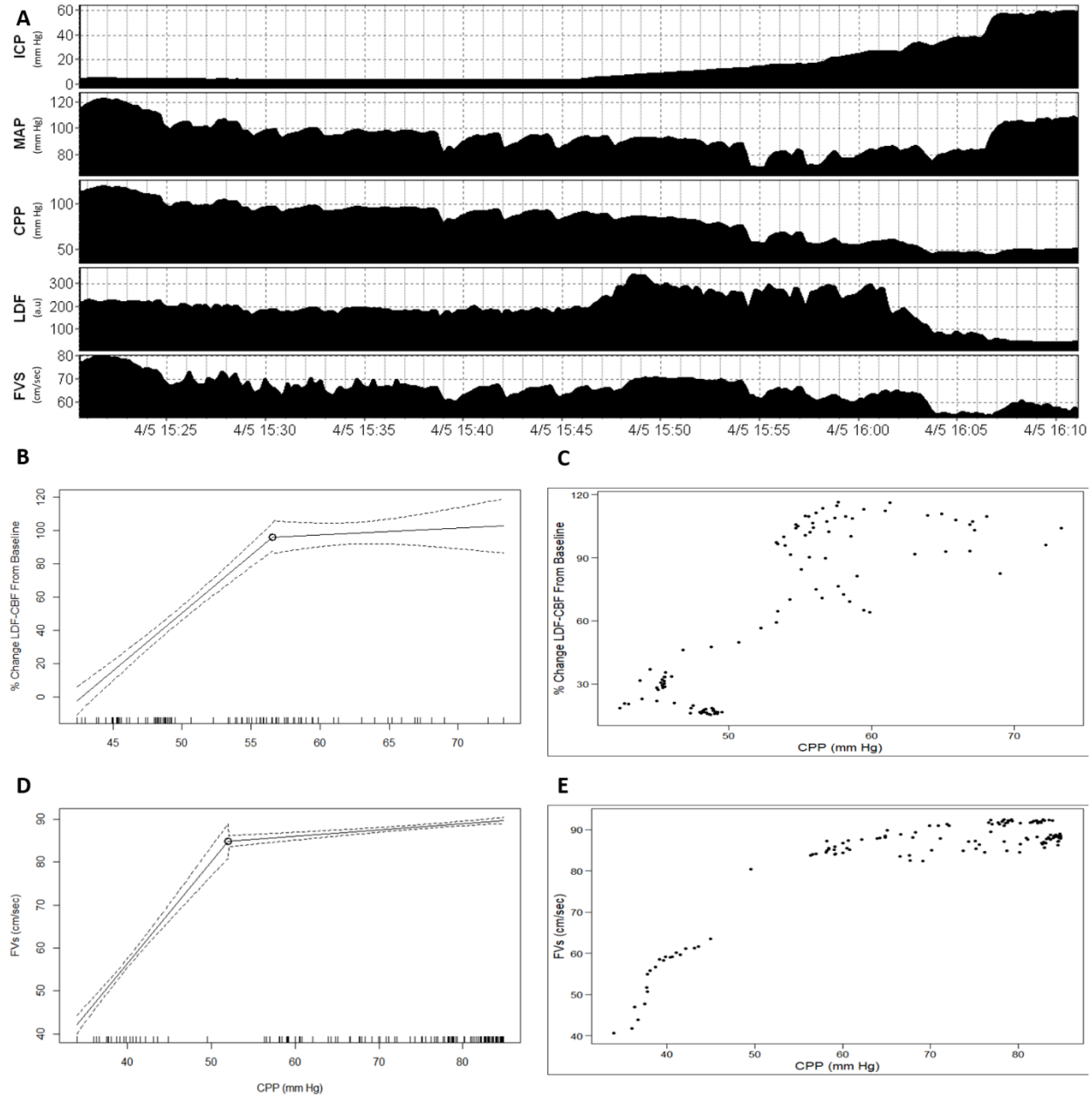

a.u. = arbitrary units, cm = centimeters, CPP = cerebral perfusion pressure, FVs = systolic flow velocity, ICP = intra-cranial pressure, LDF-CBF = laser Doppler flowmetry cerebral blood flow, MAP = mean arterial pressure, mm Hg = millimeters of Mercury, sec = second. Panel A = example of ICP, MAP, CPP, LDF-CBF and FVs over time during the experiment. Panel B = piecewise regression using the LDF-CBF vs. CPP plot, Panel C = scatterplot of LDF-CBF vs.CPP, Panel D = piecewise regression using FVs vs. CPP plot, Panel E = scatterplot of FVs vs. CPP. Note: in piecewise regression plots, the hashed lines along the x-axis denote data point density.

Figure 5.6: Error Bar Plots – % Change in LDF-CBF vs. CPP – Entire Rabbit Cohort

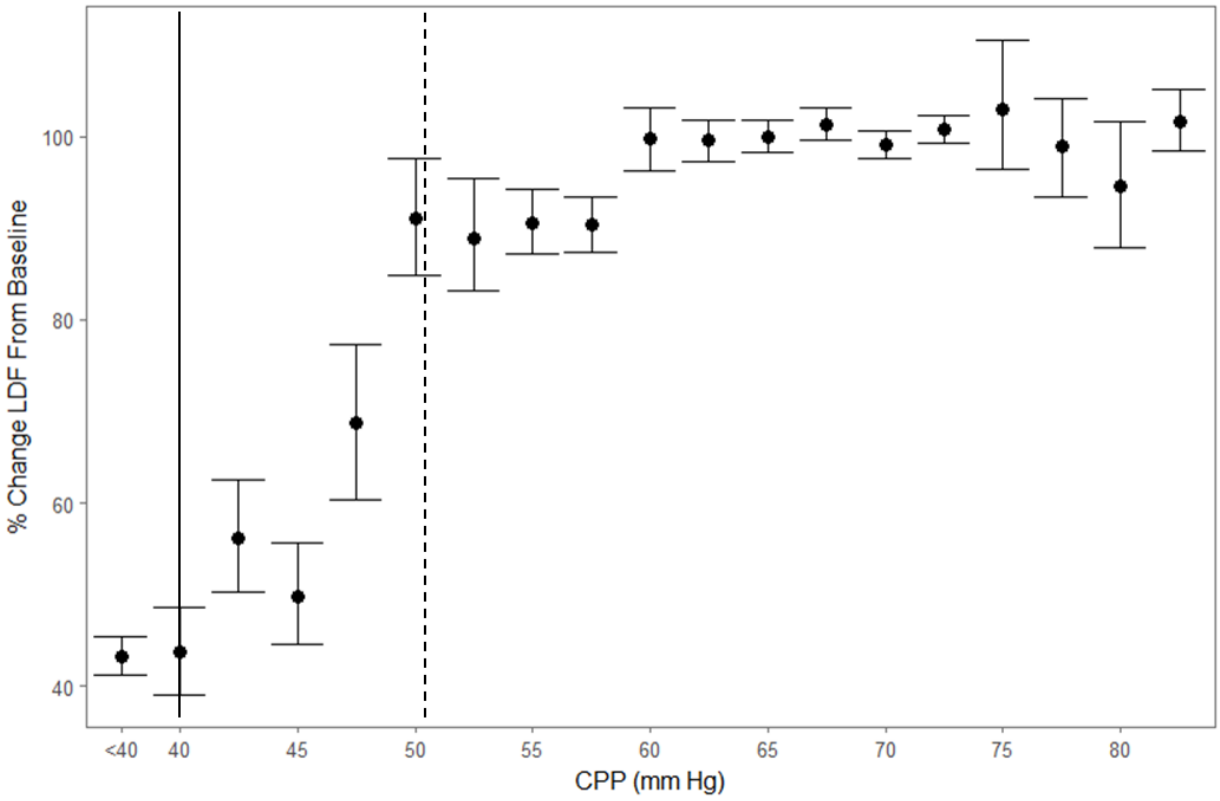

a.u. = arbitrary units, cm = centimeters, CPP = cerebral perfusion pressure, LDF-CBF = laser Doppler flowmetry cerebral blood flow, mm Hg = millimeters of Mercury. Vertical dashed line represents the approximate LLA for the entire cohort. Vertical solid line represents the approximate "Cushing's Point" for the entire cohort.

Figure 5.7: Piecewise Linear Regression Identifying Cushing's Point – Example

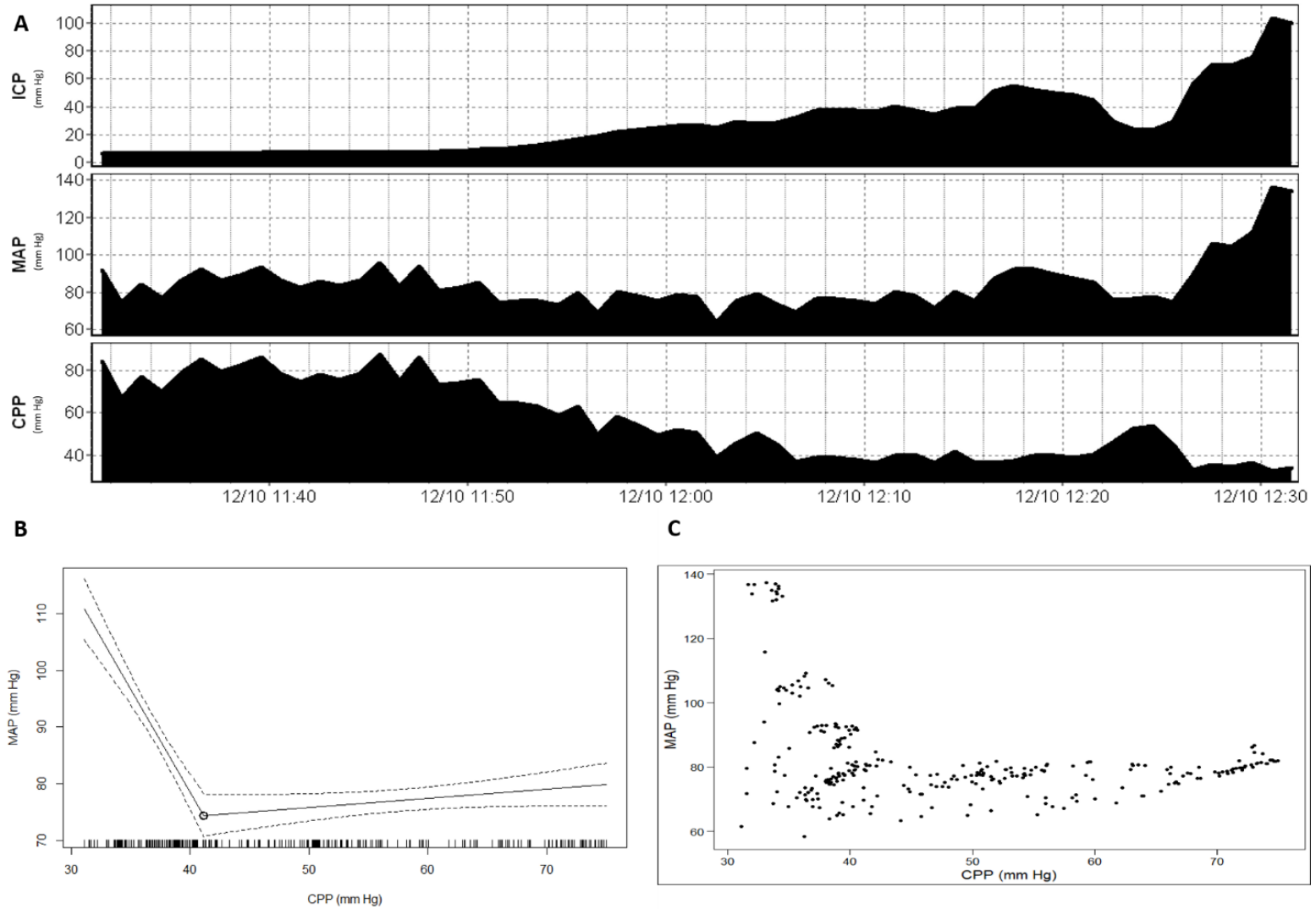

CPP = cerebral perfusion pressure, ICP = intra-cranial pressure, MAP = mean arterial pressure, mm Hg = millimeters of Mercury. Panel A = example of ICP, MAP and CPP over time during the experiment, Panel B = piecewise linear regression of MAP vs. CPP, Panel C = scatter plot of MAP vs. CPP.

Autoregulation/Cerebrovascular Reactivity across the LLA

Various cohort-wide plots of continuous indices of autoregulation/cerebrovascular reactivity across the LLA were produced. Figure 5.8 displays PRx and PAx error bar plots against binned CPP. It can be seen that, as reported in Brady et al.,[14] PRx correlates with the LLA, becoming progressively more positive (denoting "impaired" autoregulation) below the LLA of ~50 mm Hg (Panel A). Similarly, we are able to demonstrate the PAx also correlates with the LLA within this model (Panel B). Finally, given the LLA was mainly defined using LDF-CBF signal across a range of CPP, the LDF derived Lx also correlated with the LLA. Of note for all of the above relationships, these trends can be seen between the LLA (vertical dashed line) and the Cushing's point (vertical solid line), indicating that indeed these relationships to the LLA are seen before the Cushing's response develops.

RAC failed to produce reliable data within this model of intra-cranial hypertension to either confirm or refute their association with the LLA. This may be secondary to failure within this subset of animals to surpass the break-point in AMP, described in the adult TBI population of Chapter 4. Figure 5.9 displays the RAC and AMP vs. CPP error bar plots, panel B displays the failure to reach the AMP breakpoint.

Figure 5.8: Cohort Based Error Bar Plots of ICP Derived Indices across the LLA

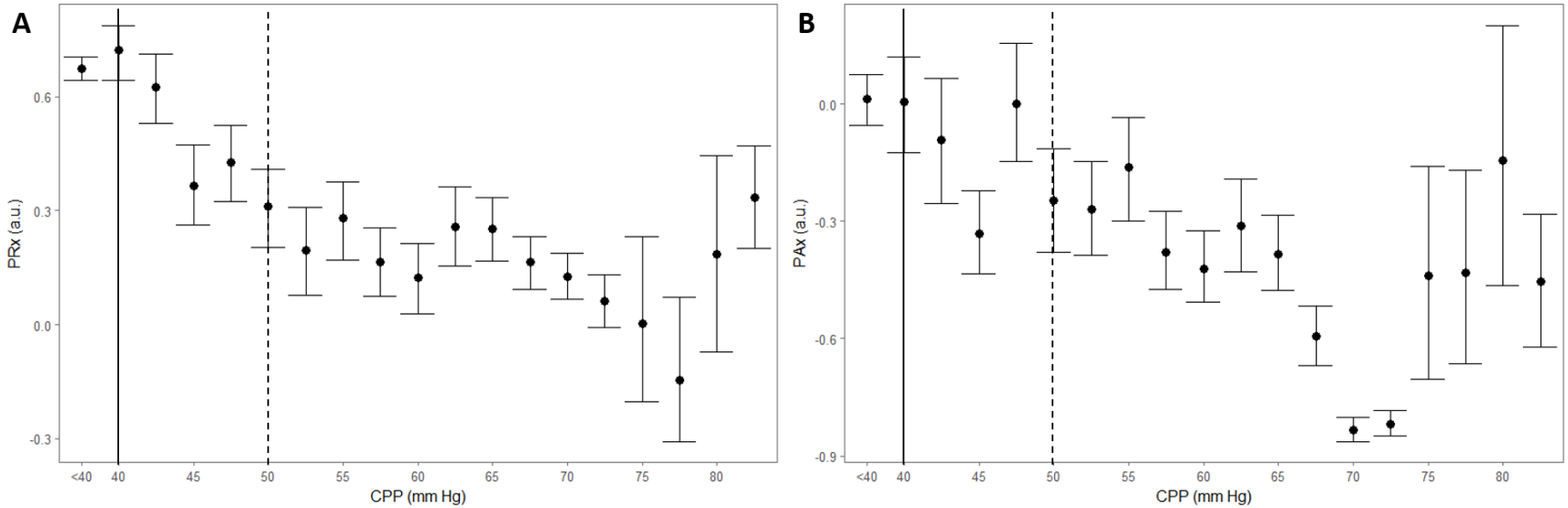

AMP = pulse amplitude of ICP, a.u. = arbitrary units, CPP = cerebral perfusion pressure, LLA = lower limit of autoregulation, MAP = mean arterial pressure, mm Hg = millimeters of Mercury, ICP = intracranial pressure, PAx = pulse amplitude index (correlation between AMP and MAP), PRx = pressure reactivity index (correlation between ICP and MAP). Panel A = PRx vs. CPP error bar plot, Panel B = PAx vs. CPP error bar plot. Note: vertical hashed line denotes the approximate LLA, while the vertical solid line represents the approximate Cushing's point.

Figure 5.9: Cohort Based Error Bar Plots of RAC and AMP across the LLA

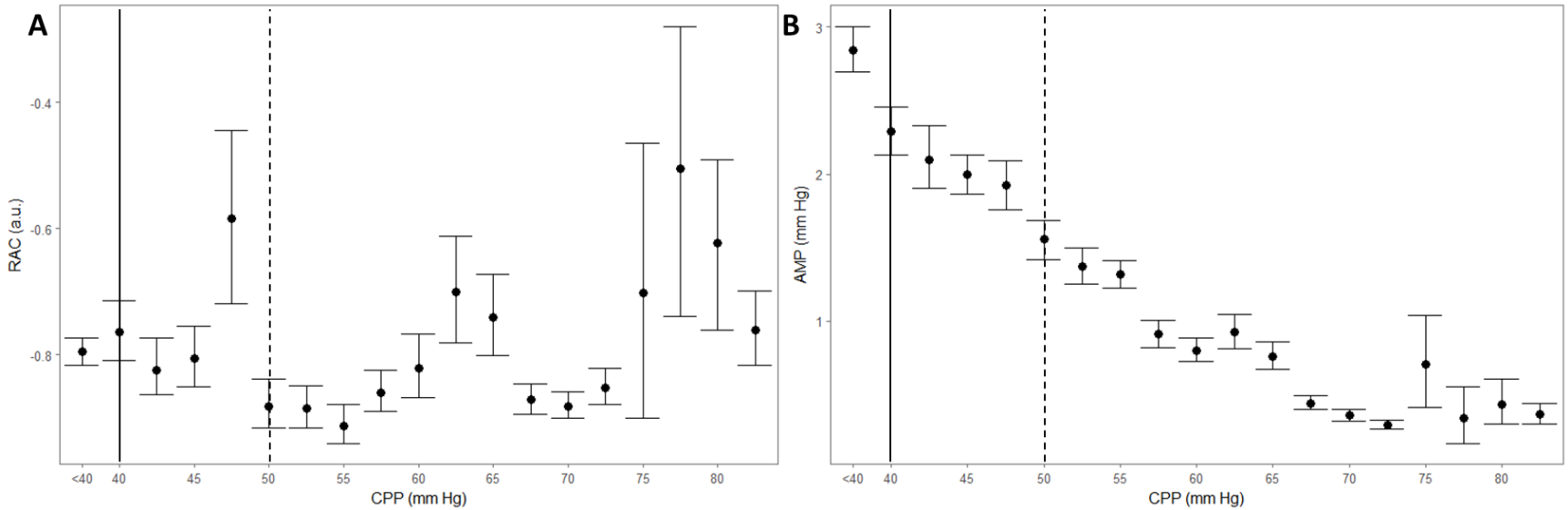

AMP = pulse amplitude of ICP, a.u. = arbitrary units, CPP = cerebral perfusion pressure, LLA = lower limit of autoregulation, mm Hg = millimeters of Mercury, ICP = intracranial pressure, RAC = correlation between AMP and CPP. Panel A = RAC vs. CPP error bar plot, Panel B = AMP vs. CPP error bar plot. Note: vertical hashed line denotes the approximate LLA, while the vertical solid line represents the approximate Cushing's point.

Comparing CPP for Various Clinical Thresholds of PRx and PAx to LLA

For each animal, the CPP at each threshold for PRx and PAx was roughly derived through a simplified piecewise linear model of PRx vs. CPP and PAx vs. CPP in each individual animal. These CPP values were compared to the CPP for the LLA derived in each animal, as described above. They were compared via Pearson correlation coefficient. Table 5.2 displays these results. RAC was not interrogated given its poor performance in the above analysis and inability to produce reliable piecewise models for RAC vs CPP.

Table 5.2: Comparison of CPP at Index Threshold to LLA – Pearson Correlation

Index Threshold Tested Against LLA	Pearson Correlation Coefficient with LLA	p-value for Pearson Correlation Coefficient
PRx = 0	0.037	0.9121
PRx = +0.25	0.429	0.1881
PRx = +0.35	**0.600**	0.0507
PAx = 0	**0.612**	**0.0454**
PAx = +0.25	**0.689**	**0.0190**

AMP = pulse amplitude of ICP, CPP = cerebral perfusion pressure, ICP = intracranial pressure, LLA = lower limit of autoregulation, PAx = pulse amplitude index (correlation between AMP and MAP), PRx = pressure reactivity index (correlation between ICP and MAP). Note: bolded values indicate those which reached statistical significance.

The Pearson correlation between the CPP values at a PRx threshold of +0.35, with the CPP at the LLA, demonstrates that this clinical threshold may represent the LLA. Similarly, the Pearson correlation between the CPP values at PAx thresholds of 0 and +0.25, with the CPP at the LLA, demonstrate that these clinical thresholds may also represent the LLA. Bland-Altman analysis for the 3 statistically significant index thresholds (ie. PRx +0.35, PAx 0, and PAx +0.25) demonstrated poor agreement with bias, when comparing the CPP at each index thresholds to the CPP at the LLA.

LLA ROC Analysis

Through ROC analysis across the LLA, using the data from the 12 rabbits, AUC's for each continuous index were identified. The AUC for PRx, PAx and RAC was: 0.795 (95% CI: 0.731 – 0.857, p<0.0001), 0.703 (95% CI: 0.631 – 0.775, p<0.0001), and 0.558 (95% CI: 0.478 – 0.637, p=0.325), respectively. Finally, the AUC for Lx was 0.740 (95% CI: 0.668 – 0.812, p<0.0001). Comparing AUC's via Delong's test, there was no significant difference between the AUC generated for PRx, PAx and Lx (all p>0.05).

5.2.4 Discussion

Through retrospective analysis of this experimental model data, validation has been provided for the previously described claims that PRx discriminates the LLA. The previous study to provide the initial data for PRx and the LLA, was by Brady et al.[14] This study focused on a piglet model of arterial hypotension, during both states of normal and slightly elevated ICP. Within this previous model, it was clearly demonstrated that PRx identified the LLA (found to be between 30 and 40 mm Hg in this animal model). Further, it was demonstrated, that PRx was superior to all other indices in the ROC analysis for detecting the LLA. This was replicated in Chapter 5.1 of this thesis. The above described study has been able to reproduce all of these results in a white NZ rabbit model of intra-cranial hypertension, which has not been described previously. Thus, further evidence has been provided to support the use of PRx in monitoring autoregulatory capacity, particularly during instances of ICP elevation. Finally, evaluation of the CPP at various clinically relevant thresholds of PRx, defined in TBI patients,[9,152] was roughly conducted. Interestingly, some preliminary results to support that the PRx threshold of +0.35 correlates with the LLA within this model of intra-cranial hypertension, though agreement on Bland-Altman was poor.

Furthermore, validating evidence has been provided to support that the ICP index PAx, also correlates with the LLA, allowing for confidence in its application as a measure of autoregulatory capacity/cerebrovascular reactivity. Thus, given the results of section 5.1 and 5.2 of this thesis, PAx measures the LLA during both arterial hypotension and IC hypertension. This has never been described previously for this index. In addition, similar to PRx, some preliminary results are provided to support that the clinically relevant PAx thresholds[152] of 0 and +0.25 correlate with the LLA within this model of

intra-cranial hypertension, though as with the PRx threshold of +0.35, the agreement on Bland-Altman analysis was poor.

Of additional interest, the ICP derived index RAC failed to demonstrate any reliable evidence that it correlated with the LLA within this model of sustained intra-cranial hypertension, where the other ICP derived indices performed well. RAC is derived from the correlation between AMP and CPP. During this intra-cranial hypertension experiment, AMP was constantly increasing, with CPP decreasing secondary to elevated ICP (ie. not a drop in MAP). Thus, the correlation derived between AMP and CPP during such a physiologic event will be negative in nature. This was seen in the persistently negative values for RAC derived in every animal. Thus, it isn't that surprising that we didn't see a dramatic response in RAC below the LLA. It may be that the failure of RAC to display a significant relationship to the LLA is a function of the particular model used, not the index. Furthermore, an upper break-point in AMP was not seen in this subpopulation of rabbits (n=12), as has been described in other animal and clinical studies.[145] This is likely secondary to the Cushing's sympathetic response seen within the animals during this experiment, which has been previously described.[145] This Cushing's response led to a preservation of, and increase in, MAP during elevation of ICP. It is possible that if this break-point in AMP were observed it may lead to a rapid rise in RAC to more positive values. Whether or not this potential physiologic event would have led to RAC correlating with the LLA is unknown, and requires further investigation.

Finally, through the use of linear piecewise regression of CPP versus MAP, the point at which the sympathetic driven Cushing's response occurred was identified, at a mean CPP of 42.4 +/- 9.8 mm Hg. This point was statistically below the mean LLA of 51.5 +/-8.2 mm Hg (p=0.027). Thus, between the LLA and the Cushing's point, the ICP derived indices were uninfluenced by the sympathetic response seen during a Cushing's response. Hence, the trend towards progressively more positive index values seen for PRx and PAx confirms that these indices respect the LLA in this model of IC hypertension.

Limitations

Despite the interesting results found within this study, there are some important limitations which should be highlighted. First, this study is a retrospective assessment of archived experimental data. Second, this rabbit model of IC hyptertension involved ligation of the common carotids bilaterally to produce an isolated basilar artery fed intra-cranial circulation. Despite a 2 week rest period between

this arterial ligation and the IC hypertension experiments, the isolated circulation may have had an impact on cerebral autoregulatory function. By ligating the common carotids, this left the entire anterior circulation dependant of posterior circulation flow and both the presence of adequate anterio-posterior communicating vessels and collarteral flow. Furthermore, the New Zealand white rabbit is also known to have significant variations in intra-cranial circulatory anatomy, with less than 30% of these rabbit cohorts displaying a normal circle of Willis.[174] As such, much of the anterior circulation may have been exhausted in terms of autoregulatory capacity at the time of the IC hypertension experiements, leading to ischemia and/or infarction in the anterior territories, and have impacted the recorded signals and derived cerebrovascular reactivity indices. However, with that said, the relationship between frontally recorded LDF and CPP displayed a clearly identifiable LLA, with both PRx and PAx demonstrating trend towards progressively positive value at CPP levels below the LLA, with significan logistic regression analysis. Third, out of the 28 rabbits included in the original experiment, only 12 had sufficient quality archived signals for defining and interrogating the LLA. Fourth, RAC, described within Chapter 4, failed to produce reliable data within this model of intra-cranial hypertension to either confirm or refute its association with the LLA. This particular model of intra-cranial hypertension may be why the other index tested (RAC) failed to produce reliable data to confirm or refute their association with the LLA. Fourth, the rate of rise in ICP was fairly rapid within this model (ie. ~30 min), this may have played a part in the relatively noisy data and fluctuations seen within the error bar plots provided. It is unknown if a longer period of rise in ICP would have led to "cleaner" data, and the ability to provide validation for the other indices. There is much further work required to confirm these results during other physiologic conditions. Finally, even though the CPP at some of the clinically defined thresholds for PRx and PAx appeared to be related to the LLA within this rabbit model, one must interpret this with caution. As the LLA represents the point at which cerebral autoregulation becomes impaired (ie. not the point at which vascular reactivity is completely lost), the lack of strong associations with CPP at thresholds defined by clinical outcome[9,152] is not surprising. These thresholds for the ICP defined indices were derived from TBI patient outcome at 6 months post injury. As a result, these index thresholds may represent the severe end of the autoregulation spectrum, the point of complete failure of vascular reactivity. Hence, the relationship between the CPP at thresholds and the LLA may not be robust, as they could be representing different aspects of impaired cerebrovascular reactivity. As well, one must assume that there are individual animal-based differences in vascular reactivity, introducing the influence of potential random effects. Much further interrogation of these clinically defined index thresholds is required, with the current analysis providing some preliminary insight. These cautions are

in corollary with the lack of association between the TBI defined clinical thresholds and the LLA seen in the piglet model of arterial hypotension in Chapter 5.1.

5.2.4 Conclusions

Validation for the ICP derived indices, PRx and PAx, against the LLA within this experimental model of intracranial hypertension has been provided. Given model limitations, it is unclear if RAC measures the LLA during extreme IC hypertension.

5.3 Upper Limit of Autoregulation in Piglet Model of Arterial Hypertension

5.3.1 Introduction

Chapter 5, subsection 5.1 and 5.2, highlight the ability of ICP derived indices of cerebrovascular reactivity to measure the LLA, during arterial hypotension and IC hypertension. However, within the current literature surrounding these indices, there lacks data to support their ability to measure the ULA. This likely stems from the fact that these physiologic indices are typically measured in adult TBI patients, where the main concern is ICP elevation with concomitant reductions in CPP, leading to hypoperfusion. Thus, the LLA has been the main interest in experimental validations studies using these indices. The focus of this study was to assess the ability of the ICP derived indices of cerebrovascular reactivity to measure the ULA, in a piglet model of arterial hypertension.

5.3.2 Methods

Animals

The neonatal piglet data described within were retrospectively amalgamated from previous experiments. Details regarding these models, including experimental treatment, has been outline in the general methodology section in Chapter 3.1. In brief, this cohort consisted of 6 sham piglets, where no cerebral insult had occurred (ie. ICP elevations, cardiac arrest or hypothermia). All of these animals underwent similar anesthetic (see Chapter 3.1), and subsequently had an esophageal balloon within the distal aorta, inflated to induce arterial hypertension until fatality. MAP increases were also supported with continuous infusions of intra-venous phenylephrine. ICP, ABP and LDF-CBF were recorded continuously throughout the experiment using ICM+.

Signal Acquisition and Processing

All signals from the combined above monitoring modalities were recorded and archived for future retrospective use. All recorded signals were digitized via A/D converter (DT9804, Data Translation, Marlboro, MA), sampled at frequency of 50 Hertz (Hz) or higher, using ICM+ software (Cambridge

Enterprise Ltd, Cambridge, UK, http://icmplus.neurosurg.cam.ac.uk). Signal artifacts, such as transducer adjustments, were removed prior to further processing or analysis using tools available in ICM+.

CPP was determined as: MAP – ICP. AMP was determined by calculating the fundamental Fourier amplitude of the ICP signal over a 10 second window, updated every 10 seconds. This was done over the range consistent with the normal range for piglet heart rate (ie. 100 – 350 bpm). Finally, 10 second moving averages (without data overlap) were calculated for all recorded signals: ICP, AMP, ABP (ie. producing MAP), CPP, and LDF-CBF. The piglets' archived signals were retrospectively interrogated and analyzed.

The following continuous indices of cerebrovascular reactivity were derived: PRx (correlation between ICP and MAP), PAx (correlation between AMP and MAP), RAC (correlation between AMP and CPP) and LDF derived Lx (correlation between LDF-CBF and CPP). All indices were derived via moving Pearson correlation coefficients between 30 consecutive 10 second average values of relevant signals and their parameters (ie. 5 minute of data), updated every minute.

Statistics

All statistical analysis was conducted utilizing R statistical software (R Core Team (2016). R: A language and environment for statistical computing. R Foundation for Statistical Computing, Vienna, Austria. URL https://www.R-project.org/). The following packages were employed: ggplot2, dplyr, tidyverse, lubridate, segmented, and pROC. Where significance is reported, alpha was set at 0.05. The following analysis described is similar to that performed within previous studies on the LLA. This was done so as to allow comparison between the results.

Finding the ULA

In order to determine the ULA of autoregulation in the 6 animals, piecewise linear regression of the LDF-CBF vs. CPP plots was employed. The LDF-CBF signal was standardized against the individual animal's baseline LDF-CBF signal, producing "% change of LDF-CBF from baseline". This is similar to other studies evaluating LDF-CBF, and that analysis conducted in Chapter 5, subsections 5.1 and 5.2.

The piecewise regression process employed a starting point for estimation of the break-point in LDF-CBF. This starting point was visually estimated from the ICM+ plots of LDF-CBF vs. CPP. The breakpoint identified by the piece wise regression process is one in which minimized the SSE of the two linear segments, above and below this point. This was conducted for each animal, with piecewise regression plots produced denoting the 95% CI for each fitted linear segment. Finally, the mean ULA for the cohort of 6 piglets was determined by averaging all 6 ULA values obtained.

Binned Cohort Data and Plot

After delineating the mean ULA for the cohort, cohort wide plots were produced to inspect the population trend of various physiologic measures against the ULA. First all data was binned across 2.5 mm Hg bins of CPP, using R statistical software. The following error bar plots were then produced: % change in LDF-CBF From Baseline vs. CPP, PRx vs. CPP, PAx vs. CPP, and RAC vs. CPP.

Prediction ability of Continuous Indices for Impaired Autoregulation

As done in previous studies, ROC analysis of PRx, PAx, RAC and Lx were performed across the cohort defined ULA. This was conducted in order to determine the ability of these indices to predict being either above or below the ULA. For each piglet, 1 mean value for each variable was obtained at each 2.5 mm Hg bin of CPP (ie. CPP = 40 mm Hg, 45 mm Hg, etc.). Five mm Hg bins of CPP were used for the ROC analysis, given this was what was conducted within the previous study by Brady et al.

This data was then given the binary designation of being above the ULA, or below the ULA, based on the ULA defined previously. The data from all 6 piglets was then used for the ROC analysis. AUC for the ROC's was reported and 95% CI reported via Delong method. Significance values (ie. p-values) for the AUC's were derived from univariate logistic regression analysis.

Criteria for Measures of the ULA

In order to be able to say that a specific index provides a measure of the ULA in this particular model, the following criteria needed to be met:

3. Demonstration of cerebrovascular reactivity indices to trend towards progressively more positive values at CPP levels above the ULA.

4. Statistically significant logistic regression analysis for each cerebrovascular reactivity index in the prediction of having CPP values above or below the cohort defined ULA.

5.3.3 Results

Defining the ULA

Through piecewise linear regression analysis of each piglet, the ULA was obtained for each animal. The mean ULA was 83.1 +/- 17.8 mm Hg, with a wide inter-piglet variation in individual ULA values seen (range: 63.4 to 109.3 mm Hg). Figure 5.10 displays the piece-wise linear regression of the % Change in LDF from baseline versus CPP, attempting to identify the ULA. All animals died secondary to heart failure during the aggressive increases in MAP using the aortic balloon and intra-venous phenylephrine.

Population-Wide Trends

In order to provide a population-wide assessment of % change in LDF-CBF and the ICP derived indices during changes in CPP, various error bar plots were produced. Figure 5.11 displays the plot of CPP versus % change in LDF-CBF from baseline, with the vertical dashed line indicating the approximate mean ULA, derived above. This demonstrates that there is initially a precipitous rise in LDF-CBF above the ULA. However, this signal subsequently saturates, failing to display the classic characteristics of pressure, or flow, passivity to increases in CPP when above the ULA.

Similarly, the ICP indices were plotted across 5 mm Hg bins of CPP, producing error bar plots. Figure 5.12 displays these plots. It can be seen that PRx, PAx and RAC initially display a trend to more positive values above the ULA (denoted by the vertical dashed line), with subsequent rapid tapering of this increase at the point of LDF-CBF saturation.

ULA ROC Analysis

Through ROC analysis across the ULA, using the data from the 6 piglets, the AUC's for each continuous index were calculated. The AUC for PRx, PAx and RAC was: 0.575 (95% CI: 0.500 – 0.651, p=0.164), 0.580 (95% CI: 0.507 – 0.653, p=0.035), and 0.716 (95% CI: 0.651 – 0.782, p<0.0001), respectively. Comparing AUC's via Delong's test, there was no statistically significant difference between the AUC's generated, when comparing PRx to PAx (p=0.877). However, the AUC for RAC was statistically different than both PRx (p<0.0001) and PAx (p<0.0001).

Figure 5.10: Piecewise Linear Regression Analysis of ULA for 6 Piglets

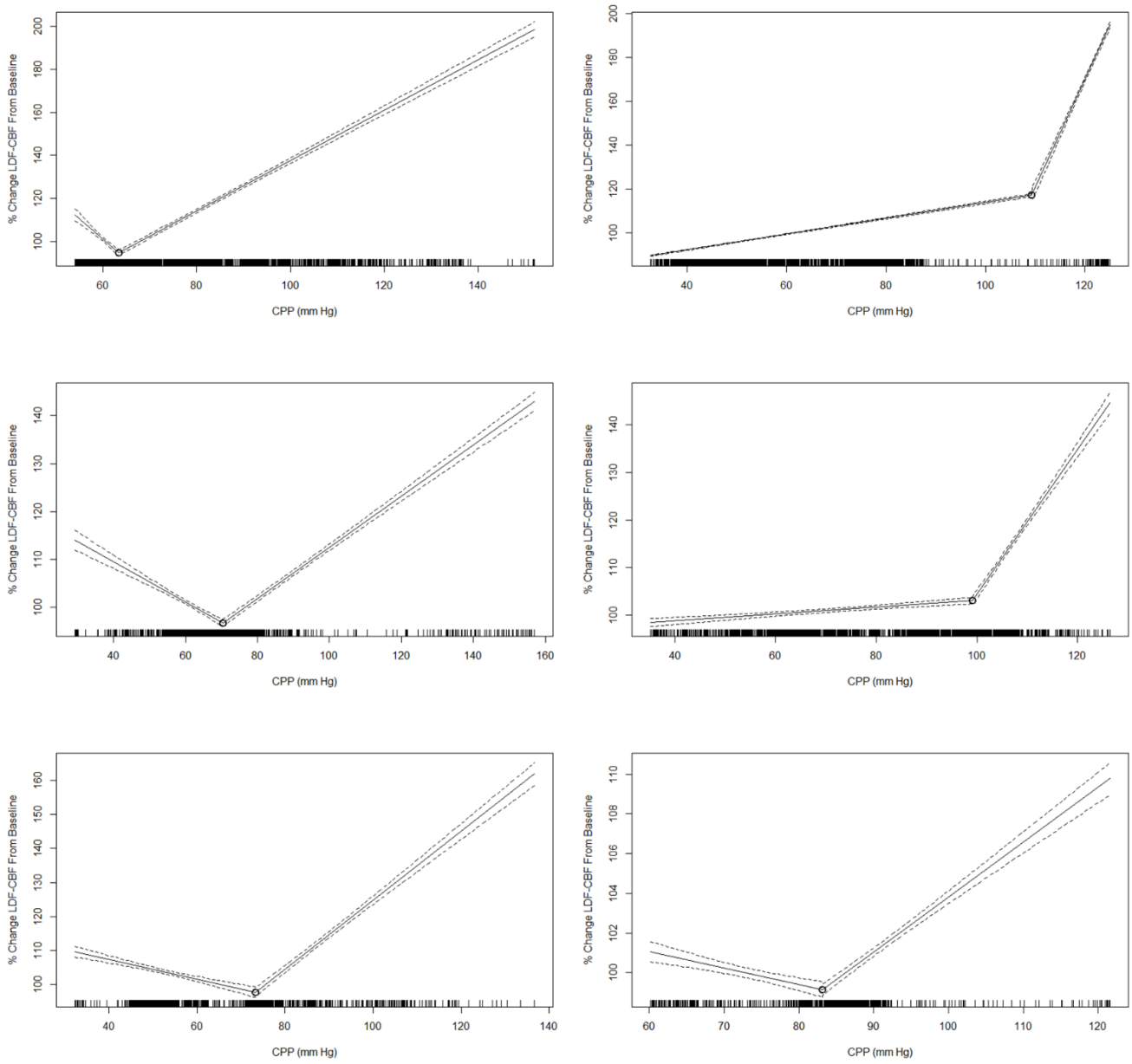

The above 6 panels depict the piecewise linear regression analysis of % LDF Change from Baseline versus CPP, attempting to determine the inflection point in LDF CBF signifying the ULA. As can be seen, there was significant heterogeneity in the identified ULA, with varying shapes and slope to the piecewise regression, highlighting the difficulting in accurately determining the ULA in this particular model of arterial hypertension.

Figure 5.11: Error Bar Plots – % Change in LDF-CBF vs. CPP – Entire Cohort

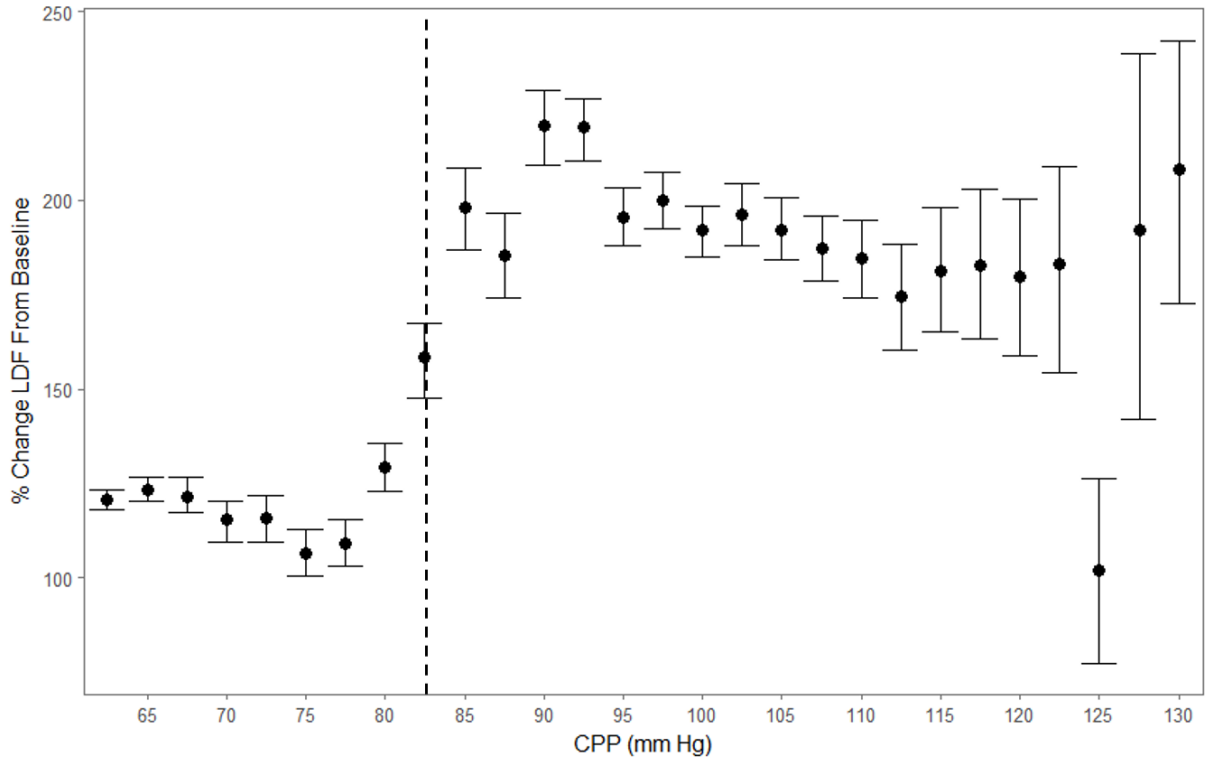

a.u. = arbitrary units, cm = centimeters, CPP = cerebral perfusion pressure, LDF-CBF = laser Doppler flowmetry cerebral blood flow, mm Hg = millimeters of Mercury. Vertical dashed line represents the approximate ULA for the entire cohort.

Figure 5.12: Cohort Based Error Bar Plots of ICP Derived Indices across the ULA

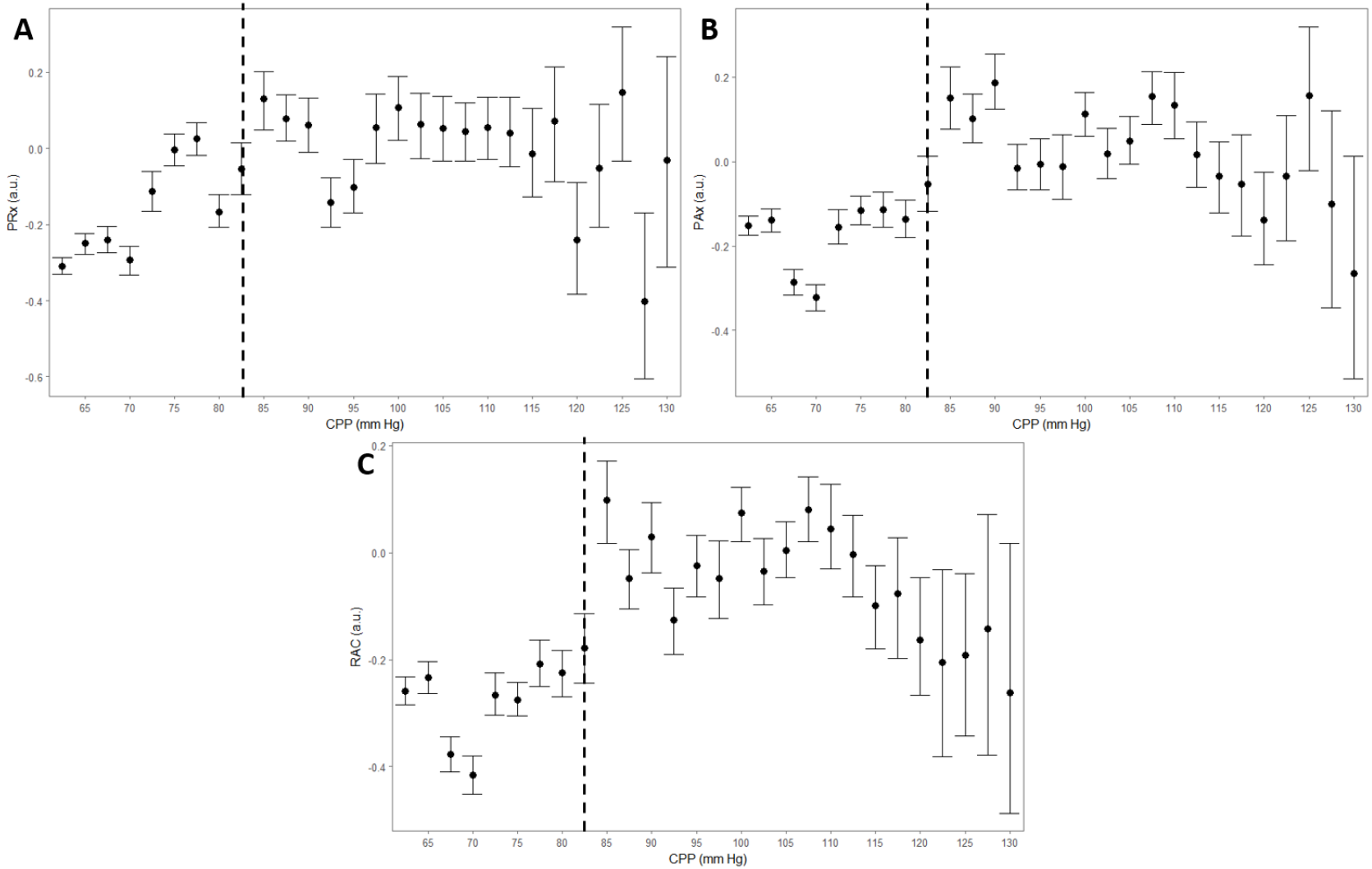

AMP = pulse amplitude of ICP, a.u. = arbitrary unite, CPP = cerebral perfusion pressure, ICP = intra-cranial pressure, PAx = pulse amplitude index (correlation between AMP and MAP), PRx = pressure reactivity index (correlation between ICP and MAP), RAC = correlation between AMP and CPP. NOTE: vertical dashed line represents the approximate mean ULA for the population, derived through piecewise linear regression in each animal.

5.3.4 Discussion

Through the retrospective analysis of the raw physiologic data from 6 piglets during induced arterial hypertension, some interesting comments/limitations should be highlighted. First, the data from this model provides no strong conclusions regarding the ability of ICP derived indices to measure the ULA. It was difficult to clearly identify the ULA in the 6 piglets for which data was available. As seen in the piece-wise regression plots, there was significant heterogeneity in the LDF response to increases in CPP, leading to a large range in ULA values determined through this regression technique (range: 63.4 to 109.3 mm Hg). Given the saturation of the LDF-CBF signal at CPP levels just past the ULA, this suggests the breakpoint in % LDF-CBF signal identified through piecewise linear regression was not the ULA. One would expect pressure/flow passivity to progressively increasing CPP values, however, this was not the case in these 6 animals. This failure to identify the ULA could be secondary to these specific animals not having a readily identifiable ULA, or inability to reach high enough MAP values to identify the ULA. This difficulty with identifying the ULA has been noted by other researchers investigating piglet CBF. Under the setting of normal ICP, it appears difficult to delineate the ULA despite aggressive increases with MAP, as most animals perish secondary to heart failure. However, sustained ICP elevations during arterial hypertension appear to shift the ULA to lower CPP values, thus allowing to identify the ULA.[175,176] Future studies of the ULA may benefit from this technique. Second, all ICP derived indices also seem to plateau during this saturation phase in LDF-CBF signal, also suggesting that this point was not the ULA. However, even if this is not the ULA, it is reasonable to accept that we use this threshold as a point at which there is a change in physiological behavior of the cerebral circulation. If so, the ROC analysis showed that both PRx and PAx were extremely poor at predicting this threshold for altered physiological response, regardless of whether it represents the ULA or not. This is in contrast to their strong performance at predicting the LLA seen in Chapter 5.1 and 5.2 of this thesis. This may indicate that these indices are poor at assessing the ULA, or just confirming that this threshold of ~83 mm Hg was not the ULA. Finally, RAC displayed the most uniform association with this threshold of 83 mm Hg. The error bar plots displayed a clear trend towards more positive index values, and the ROC analysis provided the strongest statistical significance with this index. It still remains unclear based on this small study as to whether RAC can measure the ULA, despite it showing promise over both PRx and PAx. Further experimental models for interrogating these indices with respect to the ULA are required.

One final aspect of all of the experimental models outlined in Chapters 5.1, 5.2 and 5.3 is related to the anesthetic administered. All animals were administered volatile inhalational anesthestic agents during

the induction, and also during maintanence. The rabbit models were exposed to halothane, while the piglet models were exposed to isoflurane. Both of these inhalational anesthetics have a well-documented literature body related to alteration of CBF control, leading to either hypoperfusion or hyperperfusion states.[177–179] It is unknown as to the impact that these agents had on the recorded physiology during the respective experiments, or the impact on the derived cerebrovascular reactivity indices. Such an impact related to halothane or isoflurane may have led to alterations in the observed LLA or ULA in the animal models, and thus impacted the results of the analysis related to individual cerebrovascular reactivity indices and their ability to measure the LLA or ULA. As such, future experimental models in this area will need to pay particular attention to the anesthetic agents employed, so as to avoid this potential confounding factor in the assessment of the LLA or ULA.

5.3.5 Conclusions

It is currently unclear as to whether the ICP derived indices of cerebrovascular reactivity can measure the ULA, based on this experimental model of arterial hypertension. Further investigation is required.

CHAPTER 6: MULTI-MODAL MONITORING INTER-INDEX RELATIONSHIPS IN ADULT TBI

*The information presented within this chapter can also be found detailed within the following publications:

1. Zeiler et al., *J Neurotrauma*. 2017; 34(22):3070-3080. doi: 10.1089/neu.2017.5129.[180]

2. Zeiler et al., *Neurocrit Care*. 2018; 28(2):194-202. doi: 10.1007/s12028-017-0472-x.[181]

3. Zeiler et al., *J Neurotrauma*. 2018; 35(2):314-322. doi: 10.1089/neu.2017.5364.[182]

6.1 Multi-Modal Monitoring Cohort

6.1.1 Introduction

Numerous continuous indices of cerebrovascular reactivity exist, and are derived from the different MMM devices employed for cranial monitoring within the ICU.[4,10] These devices include, but are not limited to: ICP, $PbtO_2$, TCD and NIRS. As alluded to within previous sections of this thesis, the majority of current literature on these continuous indices focuses on the ICP derived index PRx, with limited information on others. Furthermore, inter-index association studies currently are limited to the assessment of individual indices, using Pearson correlation coefficients and basic linear regression.[20,83] Thus, it can be confusing to the treating clinician as to which indices are related, and which co-vary. This information is crucial, as understanding which indices are closely associated provides the potential for future modelling of invasive indices using non-invasive surrogates. This chapter focuses on assessing the inter-index relationships between various MMM derived continuous indices of cerebrovascular reactivity, with subsection 6.1 focusing on an adult TBI population with the highest number of different monitoring devices simultaneously recording.

6.1.2 Methods

Patient Population

The patients included in this study represent a sub-population of a cohort that provide the substrate for previous publications which assessed specific NIRS based autoregulatory indices and their association with PRx.[19,20] A review of this dataset revealed that it contained raw monitoring signals which permitted the measurement of additional indices of cerebrovascular reactivity. The majority of patients in this cohort had the following monitoring: ICP, CPP, ABP, NIRS, bilateral TCD of the MCA, and $PbtO_2$. Thus, this population provided us the largest number of monitoring devices, and hence allowed assessment of relationships between the largest range of autoregulatory indices. This study was conducted as a retrospective analysis of a prospectively maintained database cohort.

All patients suffered mild to severe TBI and were admitted to the NCCU at Addenbrooke's Hospital, Cambridge. Those with mild and moderate TBI, displayed progressive deterioration in clinical status, necessitating multi-modal monitoring via a combination of invasive and non-invasive techniques. Treatment received during the recording periods included standard ICP-directed therapy, with an ICP goal of less than 20 mm Hg and CPP goal of greater than 60 mm Hg.

Signal Acquisition

ABP was measured through either radial or femoral arterial lines connected to pressure transducers (Baxter Healthcare Corp. CardioVascular Group, Irvine, CA). ICP was acquired via an intra-parenchymal strain gauge probe (Codman ICP MicroSensor; Codman & Shurtleff Inc., Raynham, MA). NIRS signals were recorded bilaterally over the frontal lobes utilizing the NIRO 200 monitoring. The following NIRS signals were recorded: HbO, HHb, TOI, THI and Hb.

$PbtO_2$ monitoring occurred via invasive parenchymal monitoring (Licox probe; Integra, Licox Brain Oxygen Monitoring System, Plainboro, NJ), typically placed in the right frontal lobe via a triple lumen bolt (Technicam Ltd).

TCD assessment of MCA CBFV was conducted via Doppler Box (DWL Compumedics, Singen, Germany). Two separate recording sessions were obtained for each patient with TCD, lasting ~60 minutes each. Bilateral MCA recordings were obtained in every patient during these sessions.

Signal Processing

All recorded signals were recorded using digital data transfer or digitized via A/D converters (DT9801; Data Translation, Marlboro, MA), where appropriate, sampled at frequency of 50 Hz or higher, using ICM+ software (Cambridge Enterprise Ltd, Cambridge, UK, http://www.neurosurg.cam.ac.uk/icmplus). Signal artifact were removed manually prior to further processing or analysis.

Post-acquisition processing of the above signals was conducted using ICM+ software. CPP was determined using the formula: CPP = MAP – ICP. Of note, the data recorded from the left TCD probe had a large amount of artifact, impeding the ability to include it in the majority of patients. Consequently, signals from the left TCD probe were excluded, and only right sided NIRS based indices are reported.

FVs was determined by calculating the maximum FV over a 1.5 second window, updated every second. FVd was calculated using the minimum FV over a 1.5 second window, updated every second. FVm was calculated using average FV over a 10 second window, updated every 10 seconds (ie. without data overlap). AMP was determined by calculating the fundamental Fourier amplitude of the ICP pulse waveforms over a 10 second window, updated every 10 seconds.

Ten second moving averages (updated every 10 seconds to avoid data overlap) were calculated for all recorded signals: ICP, ABP (which produced MAP), CPP, FVm, FVs, FVd, TOI, and THI. For the $PbtO_2$ signal, 30 second means were calculated, as previously described by Jaeger et al.

Autoregulation indices were derived in a similar fashion across modalities, as detailed in Chapter 3, table 3.3. The following continuous indices were derived: PRx, PAx, RAC, Mx, Mx_a, Sx, Sx_a, Dx, Dx_a, TOx, TOx_a, THx, THx_a, ORx-5, ORx-30 and ORx-60.

Data for this analysis were provided in the form of a minute by minute time trends of the parameters of interest for each patient. This was extracted from ICM+ in to CSV datasets, which were collated into one continuous data sheet (compiled from all patients). Thirty-minute moving averages (non-overlapping) for every index, and individual patient grand means for each index, were determined. The statistical analysis was performed on all 3 data sheets for each data sheet: minute-by-minute, 30 minute moving averaged, and grand means. Three separate data sheets were employed given the currently unknown autocorrelative structure within each of these physiologic indices. Furthermore, given $PbtO_2$ based indices are typically calculated over varying window lengths (such as 30 minutes or longer), which are

longer than all other ICP/TCD/NIRS based indices, multiple data sheets were utlizedto ensure that there was no difference in the results based on the calculation windows and averaging process of the data.

Statistics

General Statistics

Statistics were performed utilizing XLSTAT (Addinsoft, New York, United States; https://www.xlstat.com/en/) add-on package to Microsoft Excel (Microsoft Office 15, Version 16.0.7369.1323) and R statistical software (R Core Team (2016). R: A language and environment for statistical computing. R Foundation for Statistical Computing, Vienna, Austria. URL https://www.R-project.org/).

Tests for normality were performed using the Shapiro-Wilks test for all indices and measured variables. All indices and variables were determined to be non-parametric in nature. Alpha was set at 0.05 for all results describing a p-value. All statistical tests were performed on each of these data sheets, resulting in three sets of results.

We employed a Pearson correlation coefficient matrix to assess correlation between the various indices, which was conducted after performing a Fisher transformation (formula 6.1) to the data set (which normalizes the correlation coefficient distribution). This was the only test in which transformed data was utilized within the analysis.

Grouped variance between different combinations of indices was assessed using the Friedman test with and without multiple sampling, to account for within subject variation. The main assumption for the use of this test was that all indices were measuring the same physiologic variable (ie. autoregulation). The Friedman test was performed on the following combinations of data: all indices, ICP derived indices (PRx, PAx, RAC), $PbtO_2$ derived indices (ORx-5, ORx-30, ORx-60), NIRS derived indices (THx, TOx, THx_a, TOx_a), and TCD derived indices (Mx, Sx, Dx, Mx_a, Sx_a, Dx_a). The results for both the with and without multiple comparisons were identical, hence only the Friedman test with multiple sampling is mentioned within the results section.

Multivariate Clustering and Assessment of Co-variance

Finally, multivariate statistics were performed to delineate further the associations between the various indices. Currently, it is unclear as to which multivariate clustering technique is superior in the exploration of time series based physiologic variables. Consequently, an array of testing techniques were chosen. Three different multi-variate methods were employed in order to assess the co-variance within various combinations of indices. This was done, so as to be comprehensive and to provide confirmation of the potential clustering seen in any individual given test.

First, Principal Component Analysis (PCA) was performed using a Spearman type PCA, chosen to account for the non-parametric data distribution in the dataset (with significance set at $p<0.05$). PCA has been described in detail in other publications, and is ideally suited as an "exploratory" statistic for small patient cohorts with large numbers of variables. The purpose of PCA is to highlight which combinations of variables explain the overall variance within the entire dataset, and thus which variables may be related and of further interest to study via other methods. [159–161]

Second and third, agglomerative hierarchal clustering (AHC) and k-means based cluster analysis (KMCA) (using Euclidean distance) were also performed.[159] These tests provide an overall assessment of the similarity between variables, grouping them into clusters (or stems on a dendrogram, as seen within AHC) based on the mean distance away from one another, as assessed by Euclidean distance.

For the AHC, the statistical strength of the correlation between the clusters produced in the dendrograms was quantified using cophenetic correlation coefficients. Cophenetic correlations coefficients were produced by the Spearman correlation between the original Euclidean distance matrix calculated for the ACH, and the cophenetic distance matrix. The cophenetic distance is defined as the distance between two clusters that contain two indices individually and the point where both clusters are merged (ie. it represents the height on the dendrogram at which the branch points occur). The cophenetic correlation coefficient is believe to be an estimate of how well the AHC dendrogram maintains pairwise distances when compared with the original data set (ie. the baseline distance matrix between variables).[162]

With the KMCA, the number of clusters can be set by the investigator. The "Elbow method" of KMCA was utilized in order to determine the appropriate number of clusters for the final analysis.[159] The Elbow method consists of computing all possible k-means clusters. Subsequently, a plot of the within-group sum of squares versus cluster number, allowed selection of an inflection point (or "elbow") at which the

plot showed the most dramatic slope change. This is deemed the "most appropriate" cluster number for the final analysis.

6.1.3 Results

Patient Demographics

The median age of the patients within this retrospective TBI cohort was 33 years (range: 16 to 76 years), with a median admission GCS of 7 (range: 3 to 14). Three patients underwent surgical evacuation of mass lesions upon admission to hospital. There were a total of 37 patients included in the final analysis.

Inter-Index Correlation

The Pearson correlation coefficient matrix for the grand mean data set can be seen in Table 6.1. The Pearson correlation matrices for the 30-minute average and minute-by-minute data sheets provided very similar results and are hence not shown. In the grand mean data set, PRx was noted to display strong correlations with PAx, RAC and Sx/Sx_a. PRx displayed weak correlations with the remaining indices, with r-values less than 0.3 ($p<0.0001$ for all). PAx and RAC displayed similar correlation patterns to PRx.

$PbtO_2$ based indices (ORx-5/ORx-30/ORx-60) failed to display strong correlations with any of the other indices of autoregulatory assessment within the grand mean data set. However, strong correlations were seen between ORx-30 and ORx-60. All r-values were 0.250 or less, with most failing to reach statistical significance. The only exception to this was with the correlation between ORx-60 and THx ($r= -0.341$, $p=0.039$). This raises the question as to whether ORx-30 or ORx-60 can safely be utilized as a surrogate for cerebrovascular reactivity assessment.

The TCD based indices (Mx, Sx and Dx) displayed interesting correlation patterns within the grand mean data set. Robust correlations were observed for Mx vs. Dx ($r=0.911$, $p<0.0001$), and Mx vs Sx ($r=0.726$, $p<0.0001$) were seen. Furthermore, the TCD indices derived using correlations against CPP (Mx, Sx, and Dx) were strongly correlated with those derived using MAP (Mx_a, Sx_a, and Dx_a). Mx displayed a moderate correlation with the ICP derived indices (PRx, PAx, and RAC) with r-values ranging from 0.3 to 0.4. Mx was strongly correlated with the spatially resolved NIRS indices (TOx and THx): TOx ($r=0.618$,

p<0.0001) and THx (r=0.487, p=0.002). Sx and Sx_a were correlated with the ICP derived indices, Mx and Dx (as previously mentioned), with the remaining correlations being weak. Finally, Dx and Dx_a only displayed strong correlations between Mx and Sx, with the remaining index correlations being weak.

The NIRS based spatially resolved indices displayed strong intra-technique correlations. Only the statistically significant strong correlations are reported, with the remaining displaying weak correlations (r-values <0.3) (the exact r-values can be seen in Table 6.1). TOx displayed moderate-to-strong correlations with THx, PRx, Mx, Sx and Dx. THx displayed moderate-to-strong correlations with TOx, RAC, Mx, Sx and Dx. Of note, most NIRS based autoregulatory indices displayed weak, or absent, correlation to ICP derived indices (such as PRx, PAx or RAC). Importantly, NIRS based indices displayed moderate-to-weak correlation with PRx, with most r-values around 0.3 or less.

Table 6.1: Pearson Correlation Coefficient Matrix – Grand Mean Data Set

Variables	PRx	PAx	RAC	Mx	Mx_a	Sx	Sx_a	Dx	Dx_a	TOx	TOx_a	THx	THx_a	ORx_5	ORx_30	ORx_60
PRx	**1**	**0.682**	**0.677**	**0.356**	**0.412**	**0.531**	**0.538**	0.119	0.168	**0.393**	0.217	0.257	0.058	-0.013	-0.135	-0.054
PAx	**0.682**	**1**	**0.825**	0.296	**0.479**	**0.554**	**0.668**	0.014	0.160	0.255	0.227	0.159	0.025	0.188	0.038	0.111
RAC	**0.677**	**0.825**	**1**	**0.368**	**0.349**	**0.584**	**0.507**	0.133	0.110	0.288	0.183	**0.342**	0.150	0.164	-0.009	0.031
Mx	**0.356**	0.296	**0.368**	**1**	**0.723**	**0.726**	**0.373**	**0.911**	**0.695**	**0.618**	**0.460**	**0.487**	**0.434**	0.316	0.085	0.053
Mx_a	**0.412**	**0.479**	**0.349**	**0.723**	**1**	**0.490**	**0.552**	**0.531**	**0.825**	**0.551**	**0.524**	**0.332**	**0.326**	0.322	0.089	0.148
Sx	**0.531**	**0.554**	**0.584**	**0.726**	**0.490**	**1**	**0.791**	**0.626**	**0.426**	**0.558**	**0.346**	0.284	0.158	0.253	-0.024	0.012
Sx_a	**0.538**	**0.668**	**0.507**	**0.373**	**0.552**	**0.791**	**1**	0.242	**0.422**	**0.347**	0.221	-0.015	-0.139	0.196	-0.026	0.115
Dx	0.119	0.014	0.133	**0.911**	**0.531**	**0.626**	0.242	**1**	**0.732**	**0.518**	0.303	**0.421**	**0.389**	0.275	0.154	0.100
Dx_a	0.168	0.160	0.110	**0.695**	**0.825**	**0.426**	**0.422**	**0.732**	**1**	**0.454**	**0.352**	0.289	**0.326**	**0.348**	0.277	0.306
TOx	**0.393**	0.255	0.288	**0.618**	**0.551**	**0.558**	**0.347**	**0.518**	**0.454**	**1**	**0.863**	**0.516**	**0.456**	0.172	-0.096	-0.140
TOx_a	0.217	0.227	0.183	**0.460**	**0.524**	**0.346**	0.221	0.303	**0.352**	**0.863**	**1**	**0.412**	**0.473**	0.133	-0.085	-0.088
THx	0.257	0.159	**0.342**	**0.487**	**0.332**	0.284	-0.015	**0.421**	0.289	**0.516**	**0.412**	**1**	**0.885**	0.009	-0.264	**-0.341**
THx_a	0.058	0.025	0.150	**0.434**	**0.326**	0.158	-0.139	**0.389**	**0.326**	**0.456**	**0.473**	**0.885**	**1**	-0.012	-0.216	-0.260
ORx_5	-0.013	0.188	0.164	0.316	0.322	0.253	0.196	0.275	**0.348**	0.172	0.133	0.009	-0.012	**1**	**0.654**	**0.529**
ORx_30	-0.135	0.038	-0.009	0.085	0.089	-0.024	-0.026	0.154	0.277	-0.096	-0.085	-0.264	-0.216	**0.654**	**1**	**0.920**
ORx_60	-0.054	0.111	0.031	0.053	0.148	0.012	0.115	0.100	0.306	-0.140	-0.088	**-0.341**	-0.260	**0.529**	**0.920**	**1**

*The described indices are Pearson correlation coefficients between various variables: PRx (between ICP and MAP), PAx (between AMP and MAP), RAC (between AMP and CPP), ORx (between $PbtO_2$ and CPP; 5 = 5 minutes calculation window, 30 = 30 minute calculation window, 60 = 60 minute calculation window), Mx (between FVm and CPP), Mx_a (between FVm and MAP), Sx (between FVs and CPP), Sx_a (between FVs and MAP), Dx (between FVd and CPP), Dx_a (between FVd and MP), TOx (between TOI and CPP), TOx_a (between TOI and MAP), THx (between THI and CPP) and THx_a (between THI and MAP). *Values in bold typeface are those which reached statistical significance ($p<0.05$).*

Friedman Test (with multiple sampling) for Grouped Similarity Between Indices

A Friedman test, with multiple sampling, was conducted on different groups of indices, in order to assess if similar variance existed between the means in each group. The main assumption made for this statistical test was that each index measured the same physiologic parameter (ie. cerebrovascular reactivity) with the same range of measurement.

In the grand mean sheet, the Friedman test on the whole group of indices (ie. 16 variables in total), indicated that these indices were dissimilar ($p<0.0001$, $Q = 249.797$). Testing of clusters of indices based on the modality they were derived from showed that, even within clusters, there was clear lack of similarity between the ICP based indices (ie. PRx, PAx and RAC; $p<0.0001$, $Q = 48.054$), the TCD based indices (ie. Mx, Mxa, Sx, Sxa, Dx and Dxa; $p<0.0001$, $Q = 141.046$), and the NIRS-based indices ($p<0.0001$, $Q = 38.849$). However, the $PbtO_2$ based indices (ORx-5, ORx-30 and ORx-60) were found to share substantial commonality based on the Friedman test ($p=0.155$, $Q = 3.722$). Similar results were found for the 30-minute mean and minute-by-minute data sheets.

Inter-Index Relationships - Multivariate Tests (PCA, AHC and KMCA)

Principal Component Analaysis (PCA)

For the grand mean data, the PCA test was performed utilizing a Spearman type PCA (given the non-parametric nature of the dataset). Twenty principal components (PC) (also referred to as factors (F)) were identified, with the first 8 PC's composing ~90% of the overall variance in the dataset. PC eigenvalue data, Scree plots, and variable specific loadings can be seen in Appendix A.

A loading biplot for PC1 (denoted F1) and PC2 (denoted F2) can be seen in Figure 6.1. As can be seen in Figure 6.1, the ICP derived indices (PRx, PAx and RAC) are clustered in the same quadrant of the biplot, contributing to the overall variance of both PC's. Furthermore, PRx/PAx/RAC appeared to be associated with TCD based Sx and Sx_a, in terms of their contributions to the variance of the whole data set. Similarly, the TCD based indices (Mx, Mx_a, Dx and Dx_a) were co-located within the area of the biplot most associated with PC1. NIRS based spatially resolved THx, THx_a, TOx and TOx_a were co-located with the Sx/Sx_a TCD indices. Of note, ORx-/ORx-30/ORx-60 were all co-located, but separated from the other variables, indicating they are essentially unrelated to all the other indices. Furthermore, ORx-5/ORx-30/ORx-60 were located close to the origin of the biplot, indicating that they contribute little

variance to the two main principal components of the data sheet. The 30-minute mean and minute-by-minute data sets displayed similar results, and can be found in Appendix A.

Figure 6.1: PCA Loading Biplot of F1 (PC1) vs. F2 (PC2) – Minute-by-Minute Data Set

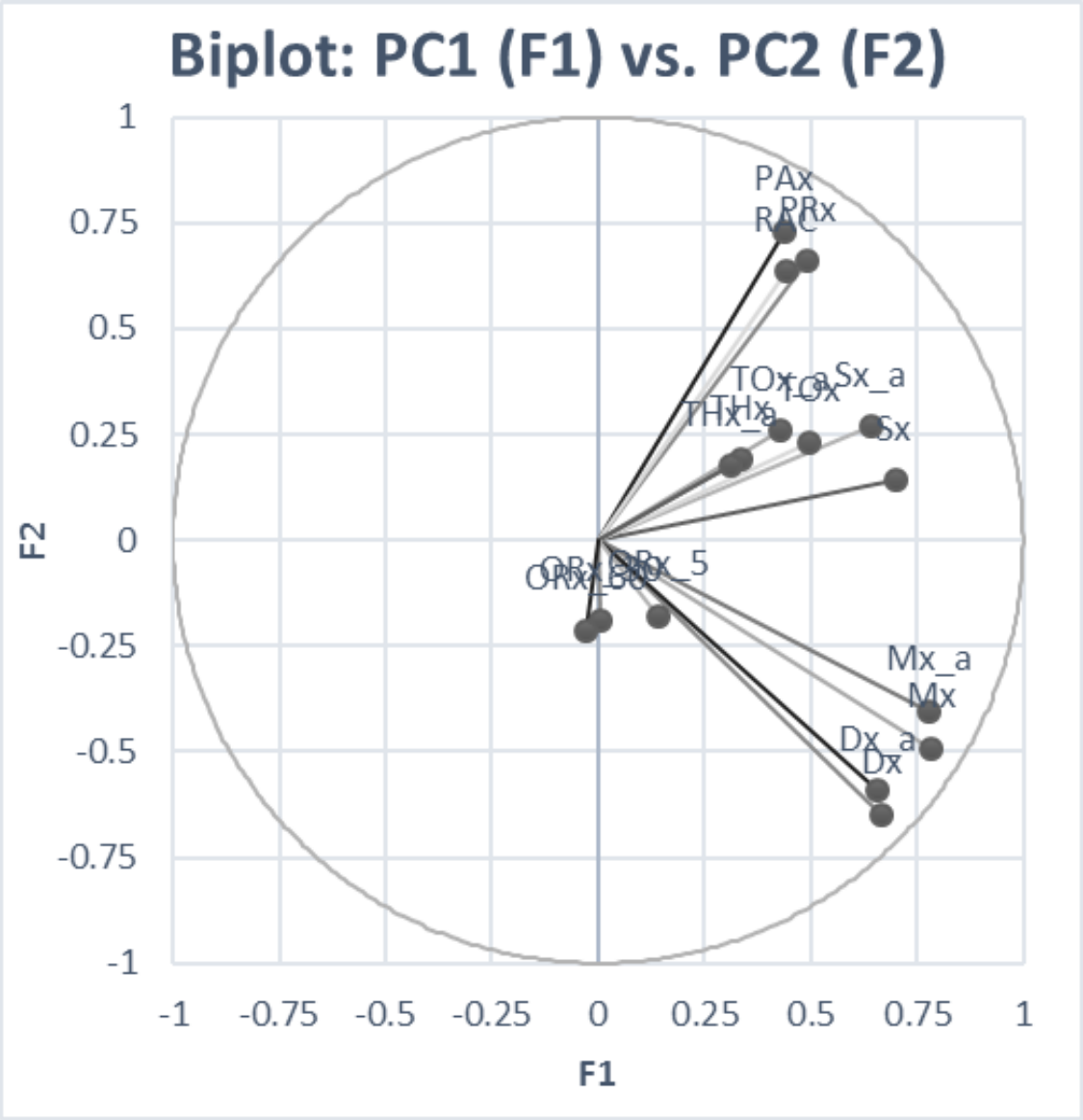

PCA = principal component analysis, F = factor, PC = principal component, F1 = PC1 = principal component #1, F2 = PC2 = principal component #2. PC1 and PC2 are the two components which contribute the largest amount of variance to the entire data set. The above biplot of PC1 vs. PC2 displays which variables contribute variance to PC1 and PC2. The longer the arm connecting (0,0) to the variable (such as PRx), the larger the contribution of that variable. Similarly, the quadrant on the biplot in which the variable falls correlates to its contribution to a particular PC. The upper left quadrant is primarily PC2; lower left quadrant is neither PC1 or PC2; the upper right quadrant is PC1 and PC2; the lower right quadrant is primarily PC1.

Agglomerative Hierarchal Clustering (AHC)

To further assess the inter-index relationships, AHC was applied to see if different associations appeared. Figure 6.2 displays the hierarchal dendrogram generated from this analysis on the minute-by-minute data. As can be seen within the dendrogram, the TCD based indices, ICP based indices, $PbtO_2$ based indices and NIRS based indices seem to co-cluster under similar branches. Another relation of interest is that of Sx/Sxa with PRx/PAx/RAC, where these indices arise from the same limb of the dendrogram. This is concordant with the results of the Pearson correlation matrix and the PCA. In addition, the spatially resolved NIRS indices (THx, THx_a, TOx and TOx_a) appear to co-localize with the Sx/Sx_a TCD indices on the dendrogram (similar to the Pearson correlation testing and PCA).

An interesting association was observed between the NIRS indices and PRx and PAx. This was seen in the PCA (and KMCA; see next section), but was not robustly demonstrated by the Pearson correlation coefficients. Finally, ORx-5/ORx-30/ORx-60 clustered on a separate limb of the dendrogram, having little association with the other indices. The cophenetic correlation coefficient derived for the AHC dendrogram displayed in Figure 6.2 was 0.822, indicating a statistically robust clustering. Applying AHC to the 30 minute and grand mean data sets resulted in similar hierarchical dendrograms with similar clustering of indices (cophenetic correlation coefficients of r=0.812 and r=0.746 respectively), confirming the relations/clustering seen in the minute-by-minute data set

Figure 6.2: AHC Dendrogram - Minute by Minute Data

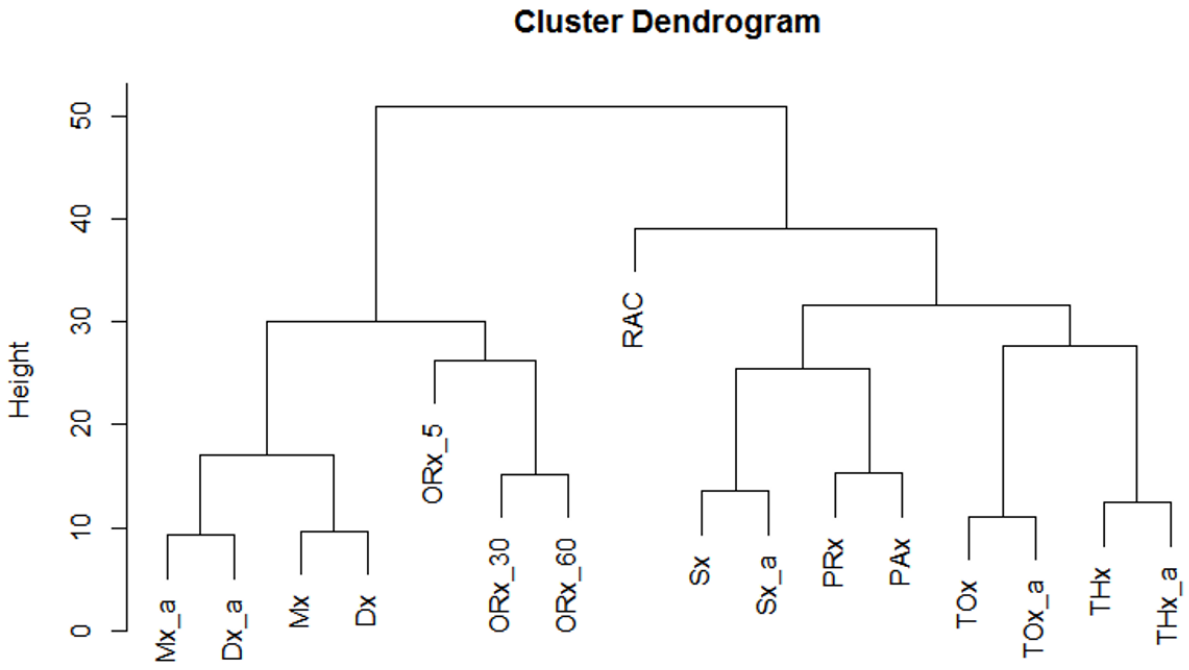

AHC = agglomerative hierarchal clustering; The described indices are Pearson correlation coefficients between various variables: PRx (between ICP and MAP), PAx (between AMP and MAP), RAC (between AMP and CPP), ORx (between $PbtO_2$ and CPP; 5 = 5 minutes calculation window, 30 = 30 minute calculation window, 60 = 60 minute calculation window), Mx (between FVm and CPP), Mx_a (between FVm and MAP), Sx (between FVs and CPP), Sx_a (between FVs and MAP), Dx (between FVd and CPP), Dx_a (between FVd and MAP), TOx (between TOI and CPP), TOx_a (between TOI and MAP), THx (between THI and CPP) and THx_a (between THI and MAP).

K-Mean Cluster Analysis (KMCA)

KMCA was employed, using seven centers of cluster (based on Euclidean distance and the Elbow method of cluster number determination). Table 6.2 displays the KMCA cluster groupings based on cerebrovascular reactivity index from the grand mean data sheet, with the clusters displaying similar patterns to the AHC described above. Figure 6.3 displays the "elbow method" plot confirming the selection of 7 centroids within the KMCA. Identical findings were seen with the 30-minute mean and minute-by-minute data sheets.

Table 6.2: KMCA Clusters – Grand Mean Data Set

Cluster 1	Cluster 2	Cluster 3	Cluster 4	Cluster 5	Cluster 6	Cluster 7
PRx	RAC	Mx	Mx_a	TOx	THx	ORx-5
PAx		Dx	Dx_a	TOx_a	THx_a	ORx-30
Sx						ORx-60
Sx_a						

KMCA = k-means cluster analysis, PRx (between ICP and MAP), PAx (between AMP and MAP), RAC (between AMP and CPP), ORx (between PbtO2 and CPP; 5 = 5 minutes calculation window, 30 = 30 minute calculation window, 60 = 60 minute calculation window), Mx (between FVm and CPP), Mx_a (between FVm and MAP), Sx (between FVs and CPP), Sx_a (between FVs and MAP), Dx (between FVd and CPP), Dx_a (between FVd and MAP), TOx (between TOI and CPP), TOx_a (between TOI and MAP), THx (between THI and CPP) and THx_a (between THI and MAP).

Figure 6.3: KMCA "Elbow Method" Plot for Centroid Confirmation – Grand Mean Data Set

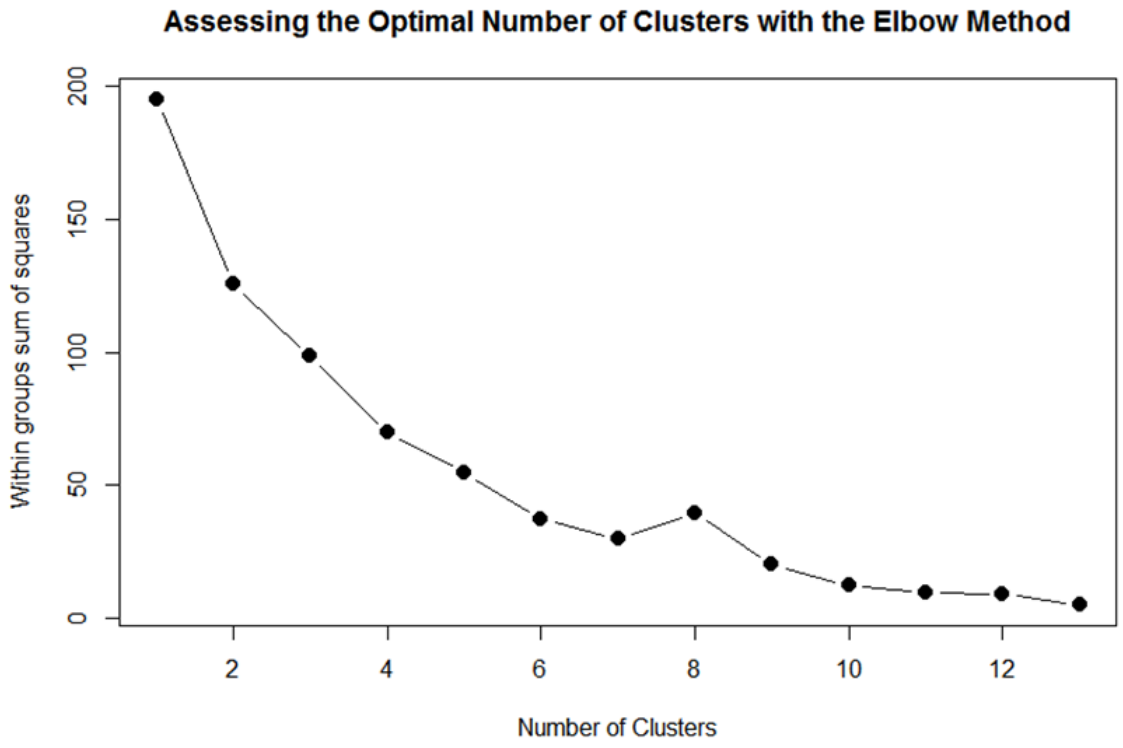

Plot denotes sequential KMCA performed on grand mean data set. For each number of centroids/clusters, the within group sum of square distance is calculated. The "elbow method" involves evaluating this plot and selecting the centroid/cluster number where there is an "elbow", transitioning to a relative plateau in the within group sum of square distance. Hence in this figure, centroid/cluster number of 7 fits these criteria, and is subsequently the most appropriate cluster number for final KMCA.

6.1.4 Discussion

This retrospective analysis of a small cohort of adult TBI patients with ICP, MAP, TCD, NIRS and $PbtO_2$ monitoring provides interesting insights into these inter-index associations, with concordant results across three distinct data sheets. A few important relationships are highlighted below.

First, and most importantly, these indices are not all related. This is clear based on all forms of analysis performed: Pearson correlation test, Friedman test (with and without multiple sampling), PCA, AHC and KMCA. Thus, for the treating clinician, it is critical to understand that these indices are derived from different invasive/non-invasive cranial and systemic monitoring metrics and may measure different aspects of physiology. One cannot simply substitute a less commonly described index for one that has been well defined, such as PRx. With that said, the analysis produced some interesting relationships which could drive further study.

Second, PRx displayed strong correlations with PAx and RAC across Pearson correlation test, PCA, AHC and KMCA. It is not surprising that these indices are related, since they are all derived from ICP or AMP. Of note, PRx was not found to be strongly correlated to Mx ($r=0.356$, $p<0.0001$), a finding confirmed in all three data sheets across the short recordings. This is in contradiction to a previously defined moderate correlations between PRx and Mx.[83] The reason for this may be related to the small patient numbers, short monitoring duration and impact of injury/treatment heterogeneity.

Third, TCD based indices (regardless if calculated via CPP or MAP) are associated and co-cluster during formal cluster analysis. This is unsurprising, and has been previously described in larger cohorts.[83] What was interesting was the strong association of Sx/Sx_a with the ICP derived indices across all of the analyses. This strong relationship with PRx/PAx/RAC may stem from the contribution of systolic peaks in CBF to ICP and its derivatives (ie. AMP), suggesting Sx/Sx_a may be closely associated with PRx/PAx/RAC. This is in contrast to Mx/Dx (and their MAP derivatives), which may more closely relate to CBV, and therefore do not strongly associate with PRx/PAx/RAC on Pearson test, PCA, AHC and KMCA. These relationships require further investigation and physiologic validation. However, the strong association between Sx/Sx_a with PRx/PAx/RAC may imply that Sx/Sx_a might be the best surrogate for PRx/PAx/RAC, compared to the other invasive/non-invasive indices.

Fourth, $PbtO_2$ based indices (ORx-5/ORx-30/ORx-60) all failed to display strong correlations with any of the other indices, as assessed through Pearson correlation, KW, PCA, AHC and KMCA. This was confirmed across the minute-by-minute, 30 minute, and grand mean data. Notably, but not surprisingly,

ORx-5, ORx-30, and ORx-60 were found to be co-related on Pearson correlation, PCA, ACH and KMCA across all data sheets and recording lengths. The divergence of ORx from the other indices measured likely stems from the fact the $PbtO_2$ is a slowly changing parameter, at a frequency that is lower than most slow waves. Taking all of this into consideration, ORx may be a questionable tool for assessment of autoregulatory capacity, and should be utilized with caution in the clinical setting. Derivation of patient specific CPP optimal values based on ORx, as described in some studies,[128,183] should be interpreted with caution, as $PbtO_2$ can be greatly influenced by many systemic factors, and since these indices do not appear to be associated strongly with any of the other indices, including the thoroughly studied PRx/Mx. Moreover, using thresholds defined by other indices (ie. PRx or Mx)[8,9] with ORx should be avoided entirely, since it appears that this index is not the same as PRx or Mx.

Finally, NIRS based indices displayed variable correlation with indices derived from ICP, $PbtO_2$ and TCD signals, especially PRx and Mx. The NIRS indices display intra-modality correlation of varying degrees (increasing in the 30 minute and grand mean data sets). Further, these NIRS indices seem to co-cluster on PCA, AHC and KMCA. Of interest, with both PCA and AHC, TOx/THx (and their MAP based equivalents) appear to cluster with the ICP derived indices. Based on the animal studies validating PRx and TOx against the lower limit of the Lassen curve, the association between ICP derived indices and TOx/TOx_a is not that surprising. The cluster of THx and THx_a with the ICP derived indices has not been well documented. It is possible that the spatially resolved NIRS indices, with parent signals designed to exclude the contamination of extracranial blood flow, may represent frontal lobe pulsatile cortical blood flow through the small arteries/arterioles. This may explain the clustering and association with PRx/PAx/RAC/Sx/Sx_a, and not Mx/Dx which are potentially more representative of CBV. In addition, the 'classic' clustering of these indices has been to group TOx/Mx group together (CBF effects) and THx/PRx together (CBV effects). The multi-technique analysis performed in this study provides inference that are not concordant with these classical views, and suggest that the NIRS based spatially resolved indices are more closely related to ICP (for both THx and TOx). These NIRS indices may therefore both be metrics of CBV (perhaps oxygenated and deoxygenated versions). This relation was confirmed on every test (PCA, ACH and KMCA) across all data sheets. Further to this, the relationships described within the manuscript are statistically robust. The ACH dendrogram, for example, is a statistically significant and robust outcome based on a strong cophenetic correlation coefficient (r=0.822). This indicates a quite strong AHC intra-cluster association, and essentially means the clusters on this test are not by chance. This was of course confirmed with the grouped variances within PCA and grouped clustering on KMCA testing. However, despite these results, further exploration of these relationships is

required in order to better understand the physiology and associations between indices of autoregulation.

Limitations

Despite these interesting results, some critical limitations within this study must be addressed. First, this is a retrospective cohort study. The patient population is composed of those with heterogenous injury patterns, ICU/hospital courses and potentially varied ICU therapies during the recorded signals. This impacts the inter-patient signal variability and potentially the results of the analysis. This may be exemplified by the lack of "strong" correlation between PRx and Mx, which has been previously seen in larger cohorts of TBI patients with TCD recordings.[83] Therefore, the results are only hypothesis generating and by no means definitive in terms of the relationships between the various autoregulatory indices.

Second, the population was small, consisting of only 37 patients. Third, the duration of signal recording was quite limited for each patient within the short recording cohort, with typically only two sessions lasting one hour each in duration. Thus, depending on the individual patient events (ie. suctioning, ICP therapies, etc.) during these period, various segments of data were either too artefactual to include in the final analysis (such as during suctioning or turning), or significantly impacted by administered therapies (such as hypertonic saline boluses). Furthermore, weaker correlation was demonstrated between THx_a and PRx, than in a previously published study, based on similar recordings. The reason for the weaker correlation coefficient stems from the fact that the population of this current study is only a sub-population the original group (i.e. those with all the monitoring modalities available). Also, we only used the short (1-2 hour) recordings, given these were the only recordings available with TCD.

Third, the instability of spontaneous slow waves may be the main driving factor as to why some indices failed to produce reproducible relationships. It may be that in the continuous measure of these indices within the ICU, we should apply filters related to slow wave power,[129] focusing only on those periods in which power and signal coherence meet a certain threshold. This could potentially improve some of the relationships seen. Longer recording sessions would be required for this, ideally throughout the entirety of the patient's ICU stay.

Fourth, even the metric of cerebrovascular reactivity provided by individual indices are dissimilar, it is important to highlight that this does not indicate that CPP-optimum derived from these indices is

divergent as well. This would need to be explored in patients with all of the above monitoring modalities, across much longer recording intervals.

Fifth, the use of multivariate statistical tests, such as PCA, are meant as "exploratory" methods of analyzing small patient cohorts with many recorded variables. PCA, AHA and KMCA are not definitive tests, in that they do not indicate statistically significant associations or correlations between various combinations of variables. These tests are merely designed to provide some idea on groupings of variables across the entire data set and serve only to drive further directed studies of specific relationships identified. Thus, the associations of Sx/Sx_a and the NIRS indices with PRx/PAx/RAC require further investigation in order to better understand the physiologic link between these indices.

6.1.5 Conclusions

Continuously indices of cerebrovascular reactivity, derived from various MMM devices, are different, and can be poorly correlated with one another. However, these indices cluster in several groupings, which provide insights regarding the pathophysiology that underlies their production. Caution must be advised when utilizing less commonly described autoregulation indices (such as ORx) for the clinical assessment of autoregulatory capacity, as they appear to not be related to commonly measured/establish indices, such as PRx.

6.2 Laser Doppler, ICP and Transcranial Doppler Indices

6.2.1 Introduction

PRx and Mx are the two most commonly quoted continuous indices of cerebrovascular reactivity in TBI, with moderate inter-index correlation (r values quoted up to 0.58).[83] Given the different monitoring techniques utilized to produce these indices, these carry different physiologic information, and may not provide similar information regarding cerebral autoregulation/vessel reactivity (as demonstrated in the previous study, section 6.1).[180]

Though no longer employed clinically, cortical LDF affords the ability to obtain continuous direct measure of small vessel/microvascular CBF. This device requires insertion of a fibreoptic probe into the subdural space, and uses the Doppler shift in the reflected light signal to calculate cortical CBF in the region of the probe.[122] Given the availability of this direct measure of cerebral cortical microvascular flow, it becomes possible to ask a key question: How do Mx and other TCD derived indices of cerebrovascular reactivity relate to cortical microvascular autoregulatory capacity?

A previous study displayed interesting differences between Lx and Mx,[125] but did not address relationships with other TCD- based indices (such as Sx or Dx). Further, the existing data provide no guidance on how PRx (and other ICP derived indices of cerebrovascular reactivity based on "global" ICP), relate to cortical microvascular autoregulatory capacity? While focal continuous measurement of microvascular cerebral blood flow is possible with thermal diffusion catheters, their use in the assessment of microvascular behavior over extended periods is limited, given the need for repeated re-calibration and moderate noise in the parent signal.[142] However, given that, of all the continuous bedside monitors available, the microvascular flow best approximates nutritive perfusion, such relationships are critically important in helping validate and interpret less direct metrics of vascular biology in the injured brain.

The goal of this study was to explore the relationship between various commonly used bedside autoregulatory/cerebrovascular reactivity indices in order to determine which indices best approximate cortical small-vessel/microvascular autoregulatory capacity. Various tests of multi-variate assessment of co-variance were employed in order to assess these relationships, identical to the previous study in section 6.1.

6.2.2 Methods

Patient Population

The patient population included in this study is a sub-population of a cohort that has been previously described.[122,125] This patient cohort was one in which the main goal of the initial prospective study was to assess regional CBF via LDF in TBI patients, where local Cambridge Health Authority research ethics committee approval was obtained. Through retrospective analysis of this cohort, it was identified that the raw monitoring signals included data that would allow the determination of various indices of cerebrovascular reactivity, assessing the relationship between those derived from different monitoring devices. All recording sessions included in this study had the following monitors: ICP, MAP, CPP, LDF-CBF and TCD based CBFV of the MCA ipsilateral to the ICP and LDF monitors.

This study was conducted as a retrospective analysis of a prospectively maintained database cohort, in which 61 separate recordings were analyzed. Most recordings were approximately 30 minutes to 1 hour in duration. All patients in both cohorts suffered moderate-severe TBI, or deteriorated after an initial admission with mild TBI and required sedation and mechanical ventilation for clinical care in the NCCU at Addenbrooke's Hospital, Cambridge. Treatment received during the recording periods included standard ICP-directed therapy, with an ICP goal of less than 20 mm Hg and CPP goal of greater than 60 mm Hg.

Signal Acquisition

Various signals were obtained through a combination of invasive and non-invasive methods. ABP was obtained through either radial or femoral arterial lines connected to pressure transducers (Baxter Healthcare Corp. CardioVascular Group, Irvine, CA). ICP was acquired via an intra-parenchymal strain gauge probe (Codman ICP MicroSensor; Codman & Shurtleff Inc., Raynham, MA).

LDF based CBF was obtained via placement of a MBF3D dual channel laser LDF (Moor Instrument Ltd, Devon UK) in the subdual space, ipsilateral to the ICP monitor. The LDF probe employed a low energy laser (0.5 to 1.5 mW) with light generated in the near infrared spectrum (780 to 820 nm). LDF signals were recorded at a frequency of 14.6 kHz. All probes were pre-calibrated prior to insertion.

Finally, TCD assessment of MCA CBFV was conducted via Doppler Box (DWL Compumedics, Singen, Germany) or Neuroguard (Medasonic, Fremont, CA, USA). Unilateral MCA recordings (ipsilateral to the ICP and LDF monitors) were obtained in every patient during these sessions.

All recorded signals were digitized via A/D converters (DT9801; Data Translation, Marlboro, MA), sampled at frequency of 50 Hz or higher and recorded using WREC software (Warsaw University of Technology) and analyzed retrospectively using ICM+ software (Cambridge Enterprise Ltd, Cambridge, UK, http://www.neurosurg.cam.ac.uk/icmplus). All signal artifacts were removed prior to further processing or analysis.

Signal Processing

Post-acquisition processing of the above described signals was conducted utilizing ICM+ software. CPP was determined utilizing the virtual signals by: CPP = MAP – ICP. FVs was determined by calculating the maximum FV over a 1.5 second window, updated every second. FVd was calculated using the minimum FV over a 1.5 second window, updated every second. FVm was calculated using average FV over a 10 second window, updated every 10 seconds (ie. without data overlap). AMP was determined by calculating the fundamental amplitude of the ICP signal over a 10 second window, updated every 10 seconds. Ten second moving averages (updated every 10 seconds to avoid data overlap) were calculated for all recorded signals: ICP, ABP (which produced MAP), CPP, FVm, FVs, FVd, and LDF-CBF.

Cerebrovascular Reactivity Indices

The cerebrovascular reactivity indices were derived in an identical fashion to the description in Chapter 3, and in the previous study (section 6.1.2). The following cerebrovascular reactivity indices were derived: PRx, PAx, RAC, Mx, Mx_a, Sx, Sx_a, Dx, Dx_a, Lx, and Lx_a. A 10 second update period was chosen given the short duration of the recordings.

Statistics

The analysis conducted is identical to that performed in the previous study, outlined in section 6.1.2. The only difference for this study is that there are slightly larger patient/recording numbers, no $PbtO_2$ or

NIRS monitoring, and the availability of LDF signal. As well, given the short recording duration, instead of 3 data sheets utilized in chapter 6.1, only 2 were employed (ie. grand mean data, and 10-second-by-10-second data). For more details on the statistical methods please see 6.1.2 “Statistics” section.

6.2.3 Results

Patient Demographics

A total of 40 patients, with 61 recordings, were included within this study. The average age was 31.1 +/- 15.3 years, with a median admission GCS of 5 (IQR: 4 to 7). The median 6-month Glasgow Outcome Score (GOS) for these patients was 2 (range: 1 to 5).

Cerebrovascular Reactivity Index Analysis

Inter-Index Correlation

We compared the inter-index correlation via a Pearson correlation matrix, for both the 10 second-by-10 second data and the grand mean data. Of note, the ICP derived indices (PRx, PAx and RAC) display moderate to strong inter-technique correlation ($r\sim >0.5$ in all, $p<0.05$ in all). A similar trend was noted with the TCD derived indices (Mx, Mx_a, Dx, Dx_a, Sx, Sx_a). Mx and PRx were not strongly correlated ($r=0.346$, $p=0.006$). Sx and Sx_a were moderately correlated with the ICP derived indices. Finally, the LDF derived indices were correlated more with TCD indices (Mx: $r=0.561$, $p<0.0001$; Dx: $r=0.492$, $p<0.0001$). Thus, it appears that cortical small-vessel/microvascular autoregulatory capacity may be better approximated by TCD derived Mx/Mx_a and Dx/Dx_a, then other indices. These relationships were confirmed in both data sheets. Table 6.3 displays the grand mean Pearson correlation matrix.

Table 6.3: Pearson Correlation Coefficient Matrix for Autoregulatory Indices – Grand Mean Data

Variables	PRx	PAx	RAC	Mx	Mx_a	Sx	Sx_a	Dx	Dx_a	Lx	Lx_a
PRx	**1**	**0.496**	**0.600**	**0.356**	**0.433**	**0.382**	**0.393**	-0.203	-0.204	0.139	0.189
PAx	**0.496**	**1**	**0.644**	0.077	**0.379**	**0.279**	**0.612**	-0.161	0.076	-0.067	0.182
RAC	**0.600**	**0.644**	**1**	0.119	**0.319**	**0.352**	**0.369**	-0.230	-0.017	0.051	0.167
Mx	**0.356**	0.077	0.119	**1**	**0.707**	**0.670**	**0.398**	**0.753**	**0.473**	**0.561**	0.171
Mx_a	**0.433**	**0.379**	**0.319**	**0.707**	**1**	**0.469**	**0.717**	**0.486**	**0.713**	**0.400**	0.250
Sx	**0.382**	**0.279**	**0.352**	**0.670**	**0.469**	**1**	**0.646**	**0.301**	0.178	0.255	0.062
Sx_a	**0.393**	**0.612**	**0.369**	**0.398**	**0.717**	**0.646**	**1**	0.158	**0.417**	0.095	0.107
Dx	-0.203	-0.161	-0.230	**0.753**	**0.486**	**0.301**	0.158	**1**	**0.739**	**0.492**	0.095
Dx_a	-0.204	0.076	-0.017	**0.473**	**0.713**	0.178	**0.417**	**0.739**	**1**	**0.329**	0.165
Lx	0.139	-0.067	0.051	**0.561**	**0.400**	0.255	0.095	**0.492**	**0.329**	**1**	**0.556**
Lx_a	0.189	0.182	0.167	0.171	0.250	0.062	0.107	0.095	0.165	**0.556**	**1**

*AMP = fundamental amplitude of ICP, CPP = cerebral perfusion pressure, Dx = diastolic flow index (between FVd and CPP), Dx_a = arterial diastolic flow index (between FVd and MAP), FVd = diastolic flow velocity, FVm = mean flow velocity, FVs = systolic flow velocity, ICP = intracranial pressure, Lx = laser Doppler flow index (between LDF-CBF and CPP), Lx_a = arterial laser Doppler flow index (between LDF-CBF and MAP), Mx = mean flow index (between FVm and CPP), Mx_a = arterial mean flow index (between FVm and MAP), PAx = between AMP and MAP, PRx = pressure reactivity index (between ICP and MAP), RAC = between AMP and CPP. *Note: all values in bold type face are those which reached statistical significance (ie. p<0.05).*

Grouped Variance Analysis – Friedman Test

Similarity between various groups of autoregulatory indices was assessed by the Friedman test (with and without multiple sampling), with the pre-test assumption that each index was assessing the same aspect of physiology, autoregulation. In both the 10 second-by-10 second and grand mean data sheets, Friedman testing confirmed that the indices were not all the same ($p<0.0001$, $Q = 301.204$). Further Friedman tests were applied to groups of monitor specific indices (ie. derived indices were grouped based on their monitoring signal source: ICP, TCD, etc). The within monitor Friedman testing also confirmed each index was in fact demonstrably different.

Principal Component Analysis (PCA)

Spearman PCA was conducted on both data sheets, with similar results. Eleven principal components (PC) (also referred to as factors (F)) were identified, with the first 5 PC's composing ~90% of the overall variance in the dataset. PC eigenvalue data, Scree plots, and variable specific loadings can be seen in Appendix B of the supplementary materials.

A loading biplot for PC1 (denoted F1) and PC2 (denoted F2) can be seen in Figure 6.4. As can be seen within the biplot, the ICP derived indices (PRx, PAx and RAC) are clustered in the same quadrant of the biplot, contributing to the overall variance of both PC1 and PC2. Furthermore, PRx/PAx/RAC appeared to be associated with TCD based Sx and Sx_a, in terms of their contributions to the variance of the whole data set. Similarly, the TCD based indices (Mx, Mx_a, Dx and Dx_a) were co-located within the area of the biplot most associated with PC1. LDF indices (Lx, Lx_a) co-varied with TCD derived Mx/Mx_a/Dx/Dx_a, confirming the correlations seen in the Pearson test analysis.

Figure 6.4: Spearman Type Principal Component Analysis of Autoregulatory Indices – Biplot of PC1 vs. PC2 (Grand Mean Data)

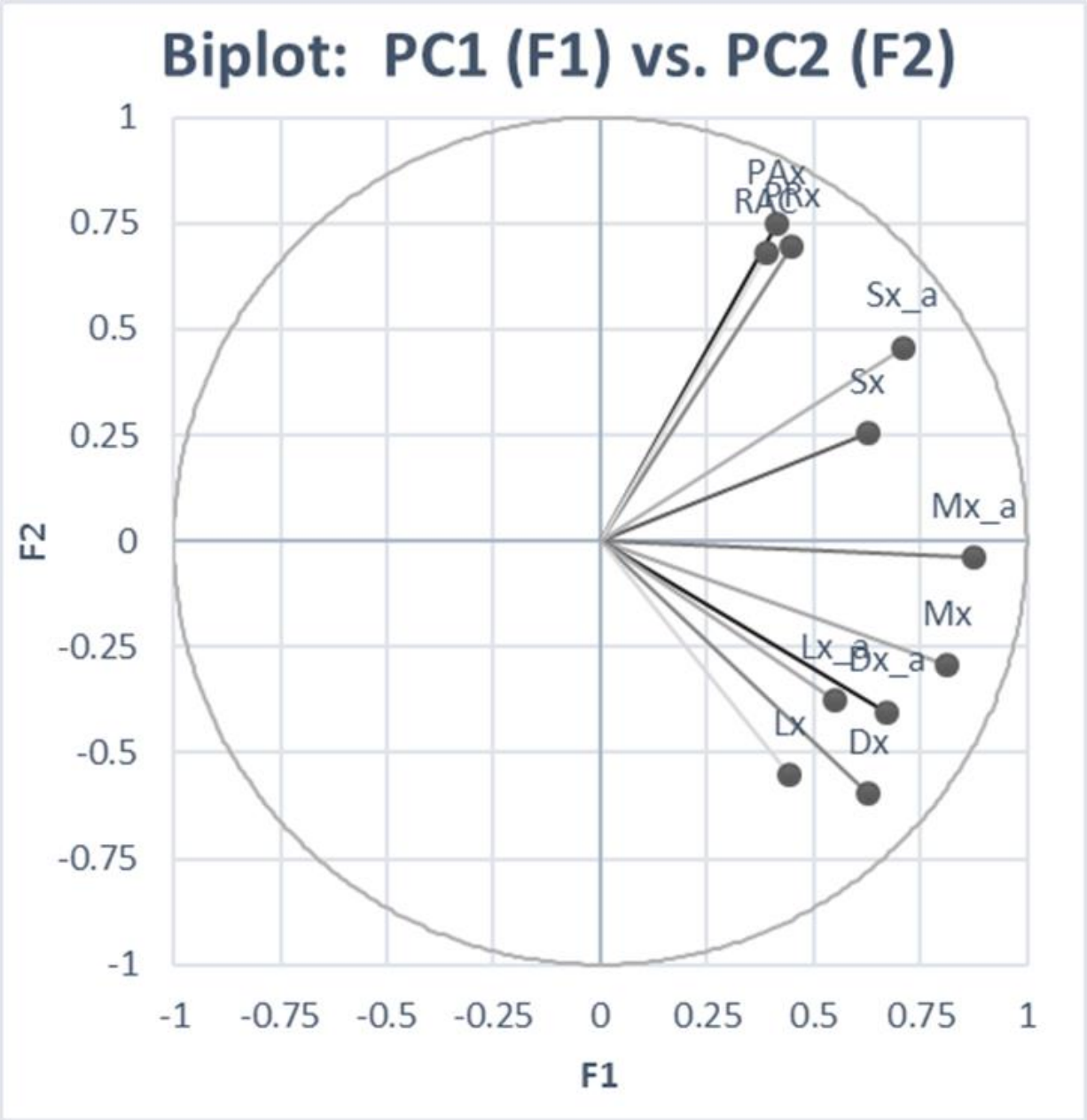

PCA = principal component analysis, F = factor, PC = principal component, F1 = PC1 = principal component #1, F2 = PC2 = principal component #2. PC1 and PC2 are the two components which contribute the largest amount of variance to the entire data set. The above biplot of PC1 vs. PC2 displays which variables contribute variance to PC1 and PC2. The longer the arm connecting (0,0) to the variable (such as PRx), the larger the contribution of that variable. Similarly, the quadrant on the biplot in which the variable falls correlates to its contribution to a particular PC. The upper left quadrant is primarily PC2; lower left quadrant is neither PC1 or PC2; the upper right quadrant is PC1 and PC2; the lower right quadrant is primarily PC1.

Agglomerative Hierarchal Clustering (AHC)

AHC was performed on both data sheets, yielding identical results. Figure 6.5 demonstrates the dendrogram produced. Of note is the clustering of ICP, TCD and LDF based indices. ICP indices co-cluster with Sx and Sx_a, as displayed in both Pearson and PCA testing. Similarly, TCD based Mx/Mx_a and Dx/Dx_a co-cluster with Lx/Lx_a, as seen in the Pearson and PCA testing. The cophenetic correlation coefficient for the grand mean AHC was 0.77, indicating moderate-to-strong significance of the clustering.

Figure 6.5: AHC Dendrogram of Cerebrovascular Reactivity Indices – Grand Mean Data

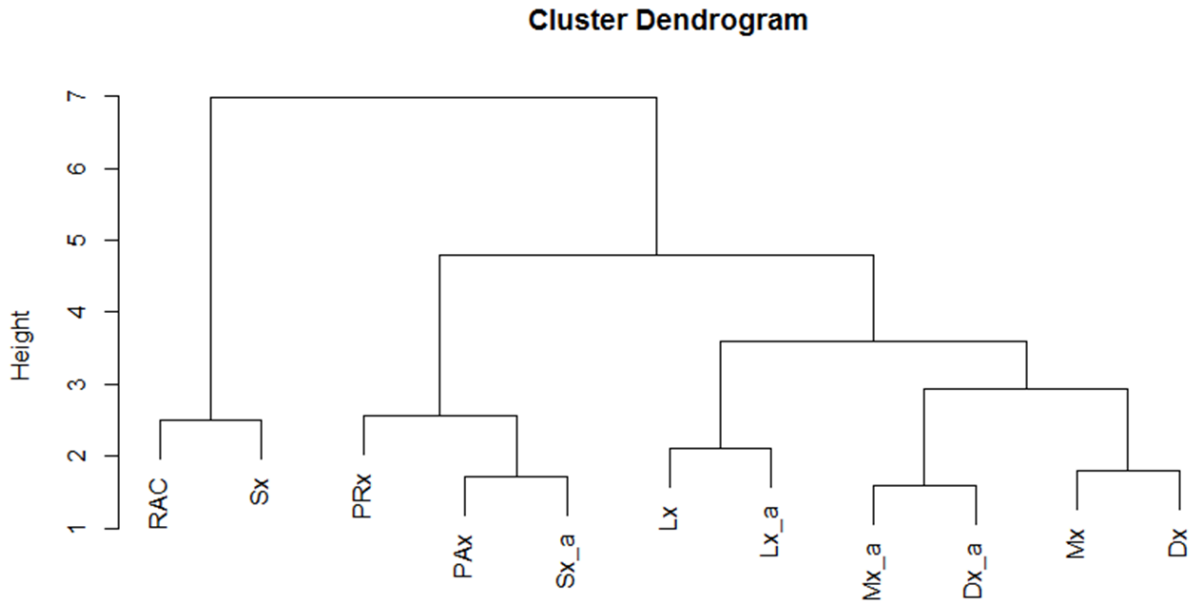

AHC = agglomerative hierarchal clustering, AMP = fundamental amplitude of ICP, CPP = cerebral perfusion pressure, Dx = diastolic flow index (between FVd and CPP), Dx_a = arterial diastolic flow index (between FVd and MAP), FVd = diastolic flow velocity, FVm = mean flow velocity, FVs = systolic flow velocity, ICP = intracranial pressure, Lx = laser Doppler flow index (between LDF-CBF and CPP), Lx_a = arterial laser Doppler flow index (between LDF-CBF and MAP), Mx = mean flow index (between FVm and CPP), Mx_a = arterial mean flow index (between FVm and MAP), PAx = between AMP and MAP, PRx = pressure reactivity index (between ICP and MAP), RAC = between AMP and CPP.

K-Means Cluster Analysis (KMCA)

KMCA was performed on both data sheets, producing identical clustering results. Based on the "Elbow Method", the optimal number of centroids for the KMCA was determined to be 4. The clustering of the indices was similar to that seen in the AHC, PCA and Pearson correlation testing and hence not discussed further.

6.2.4 Discussion

Through the analysis of this TBI LDF data set, the relationships between various ICP/TCD/LDF cerebrovascular reactivity indices in humans have been better defined. First, intra-technique correlations were seen for ICP, TCD and LDF-CBF derived indices across a using a range of statistical approaches, including the Pearson correlation test, PCA, ACH and KMCA. This result isn't surprising, given indices derived from the same signals would be expected to be inter-related. Second, LDF-CBF based Lx and Lx_a were found to be more closely associated with TCD based Mx/Mx_a and Dx/Dx_a, than with Sx/Sx_a or the ICP derived indices. This was confirmed on all forms of the analysis. This suggests that TCD "vascular" based measures (Mx/Mx_a and Dx/Dx_a) are a better approximation of cortical small-vessel/microcirculatory autoregulation. Further to this, Lx and Lx_a were not correlated with ICP-derived indices of cerebrovascular reactivity (ie. including PRx) in any of the analyses conducted. This is another important finding as it suggests that that ICP-derived indices may not measure cortical pial/microcirculatory vascular reactivity. This lack of association with metrics derived from continuously measured CBF requires further evaluation. Third, Sx/Sx_a appear to be more closely associated with the ICP derived indices (PRx, PAx and RAC), as confirmed on all forms of the analysis. This was also seen in the study in section 6.1. This likely stems from the peak pulsatile systolic component of CBFV yielding a stronger contribution to the ICP signal, than mean or diastolic CBFV's. Further, it isn't surprising that by the time that CBF reaches the small cortical vessels, that the peak systolic pulsatile component has less of an impact on regional LDF-CBF signal, where it is more likely to be dependent on mean flow or diastolic flow parameters. This requires confirmation however.

Limitations

Some important limitations should be highlighted. First, this is a small retrospective cohort of patients that were studied. The patients had heterogeneous injury patterns and were subject to variations in ICU therapies/treatments during the short recording sessions. This could have impacted signal heterogeneity and quality, leading to a direct influence on both the results of the slow wave and autoregulatory index analysis. Therefore, the strength of conclusions that can be drawn from the analysis is limited. However, with that said, the analysis conducted provides more than anecdotal insight into the co-variance and inter-index relationship, providing valuable information all involved in the critical care management of moderate/severe TBI patients.

Second, LDF-CBF probes are no longer in clinical use in humans. Consequently, despite interesting results in this chapter, it will be difficult to confirm the analysis with newer and larger patient cohorts. Therefore, unfortunately, only retrospective data sets exist to analyze relationships between LDF based cortical/small-vessel CBF and common monitors in current use. The decline in the use of LDF stemmed from cost, maintenance, invasive placement and focality of measure, as well as the relatively noisy signal generated from red blood cell flux measurements. With that said, the technique provided useful and unique information on cortical cerebral blood flow, and subsequent cerebrovascular reactivity.

Finally, the statistics utilized within the autoregulatory index analysis are mainly exploratory and not confirmatory of the relationships described. The use of PCA, AHC and KMCA are exploratory multi-variate statistical techniques designed to highlight potential relationships of interest within an entire dataset, which would then drive further prospective focused assessment of the individual relationships identified. Given the limitations mentioned around the clinical use of LDF, the analysis will have to remain “exploratory” for human data. With that said, the relationships were all confirmed across Pearson correlation test, PCA, AHC and KMCA, potentially indicating that the various clustering/correlations are more than just by chance within an individual multi-variate test. Further to this, future prospective evaluation of the index relations can be carried out within controlled animal studies, given the continued application of LDF within this setting.

6.2.5 Conclusions

Mx is most closely related to LDF derived measures of microvascular flow (Lx/Lx_a). Both Sx/Sx_a and the ICP derived indices appear to be dissociated from LDF based cortical small vessel cerebrovascular reactivity, leaving Mx/Mx_a/Dx/Dx_a as a better surrogate for the assessment of cortical small vessel/microvascular cerebrovascular reactivity. Sx/Sx_a co-cluster/co-vary with ICP derived indices, as seen in previous work described in this thesis.

6.3 Relationships between ICP and Transcranial Doppler Indices

6.3.1 Introduction

Based on the results of the studies detailed in sections 6.1 and 6.2,[180,181] it is apparent within these small patient cohorts that Sx/Sx_a preferentially co-vary with the ICP derived indices of cerebrovascular reactivity. Confirming that Sx/Sx_a do indeed co-cluster with the ICP derived indices would provide confidence in utilizing them as a potential surrogate for the more invasive ICP indices. Furthermore, given Sx_a can be derived through entirely non-invasive means (ie. with MAP recording by non-invasive finger-cuff techniques), ICP indices (such as PRx), could be estimated or even forecasted (ie. predicted) if this relationship with Sx/Sx_a is validated. Thus, the goal of this study was to provide validation for the ICP and TCD derived inter-index relationships seen in sections 6.1 and 6.2, using a substantially larger adult TBI cohort with both continuous high-frequency ICP and TCD recordings.

6.3.2 Methods

Patient Population and Demographic Data Acquisition

A large retrospective database cohort of TBI patients with simultaneous TCD and ICP recording was utilized. TCD signal acquisition in TBI patients was conducted intermittently within the NCCU at Addenbrooke's Hospital, Cambridge between the period from January 1992 up to and including September 2011. The timing to application of TCD based monitoring varied from patient to patient, typically initiated between 24 hours to 10 days post-TBI. The duration of recording also varied between patients, subject to the technical limitations of long-term TCD monitoring.

TCD based CBFV, ICP and ABP were all linked in time series and prospectively stored. We performed a retrospective analysis of this prospectively maintained database. A large portion of this population was previously utilized in the determination of critical thresholds for Mx and Mx_a.[8]

Most patients included in this analysis had sustained moderate/severe TBI, but also included a few patients who were initially classified as mild TBI (as defined by the admission GCS), but experienced subsequent clinical deterioration leading to invasive monitoring and admission to the NCCU. Treatment

received during the recording periods included standard ICP-directed therapy, with an ICP goal of less than 20 mm Hg and CPP goal of greater than 60 mm Hg.

For the purpose of confirming the co-variance and co-clustering relationships previously discovered, minimum recording lengths of 30 minutes were utilized for analysis. A total of 347 patients were included, with 410 recordings of 30 minutes or greater in duration. The following patient demographic data was obtained from the database: age, sex, admission GCS, and patient outcome at 6 months.

Signal Acquisition

Various signals were obtained through a combination of invasive and non-invasive methods. ABP was obtained through either radial or femoral arterial lines connected to pressure transducers (Baxter Healthcare Corp. CardioVascular Group, Irvine, CA). ICP was acquired via an intra-parenchymal strain gauge probe (Codman ICP MicroSensor; Codman & Shurtleff Inc., Raynham, MA). Finally, TCD assessment of MCA CBFV was conducted via Doppler Box (DWL Compumedics, Singen, Germany) or Neuroguard (Medasonic, Fremont, CA, USA).

All recorded signals were digitized via A/D converters (DT9801; Data Translation, Marlboro, MA), sampled at frequency of 50 Hz or higher, using ICM+ software (Cambridge Enterprise Ltd, Cambridge, UK, http://www.neurosurg.cam.ac.uk/icmplus). All signal artifact was removed prior to further processing or analysis.

Signal Processing

Post-acquisition processing of the above described signals was conducted utilizing ICM+ software. CPP was determined as: CPP = MAP – ICP. FVs was determined by calculating the maximum FV over a 1.5 second window, updated every second. FVd was calculated using the minimum FV over a 1.5 second window, updated every second. FVm was calculated using average FV over a 10 second window, updated every 10 seconds (ie. not data overlap). AMP was determined by calculating the fundamental Fourier amplitude of the ICP signal over a 10 second window, updated every 10 seconds. Ten second

moving averages (updated every 10 seconds to avoid data overlap) were calculated for all recorded signals: ICP, ABP (which produced MAP), CPP, FVm, FVs, and FVd.

Cerebrovascular Reactivity Indices

The autoregulation/cerebrovascular reactivity indices were derived in a similar fashion, as highlighted in Chapter 3. The following indices of cerebrovascular reactivity were derived: PRx, PAx, RAC, Mx, Mx_a, Sx, Sx_a, Dx, and Dx_a.

Statistics

The analysis conducted is identical to that performed in the previous studies, outlined in section 6.1.2. The only difference for this study is that there are larger patient/recording numbers, with ICP and TCD signals. Three data sheets were employed for the analysis (ie. grand mean, 30-minute mean and minute-by-minute data). For more details on the statistical methods please see 6.1.2 "Statistics" section.

6.3.3 Results

Patient Demographics

A total of 347 patients, with 410 recordings, constituting 419.6 hours of monitoring, were included for the co-variance/cluster analysis. The mean age was 33.7 +/- 16.4 years, with 250 males. The median admission GCS was 6 (IQR: 4 to 8). The mean length of recording was 1.02 hours (range: 0.50 to 3.26 hours).

Cerebrovascular Index Co-Variance/Clustering Analysis

Inter-index correlation was compared via a Pearson correlation matrix, for all three data sheets: grand mean, 30-minute mean and minute-by-minute data. Table 6.4 displays the Pearson correlation matrix for the grand mean data sheet. Of note is the strong inter-index correlation of the ICP indices. In

addition, Sx and Sx_a display stronger correlation with the ICP indices, compared to Mx/Mx_a/Dx/Dx_a. This was confirmed across all 3 data sheets.

Table 6.4: Pearson Correlation Coefficient Matrix for Autoregulatory/Cerebrovascular Reactivity Indices – Entire TBI TCD Cohort – Grand Mean Data

Variables	PRx	PAx	RAC	Mx	Mx_a	Dx	Dx_a	Sx	Sx_a
PRx	**1**	**0.665**	**0.490**	**0.434**	**0.440**	**0.303**	**0.365**	**0.448**	**0.488**
PAx	**0.665**	**1**	**0.631**	**0.234**	**0.357**	0.085	**0.197**	**0.368**	**0.562**
RAC	**0.490**	**0.631**	**1**	**0.332**	**0.277**	**0.176**	**0.156**	**0.544**	**0.344**
Mx	**0.434**	**0.234**	**0.332**	**1**	**0.777**	**0.934**	**0.732**	**0.738**	**0.479**
Mx_a	**0.440**	**0.357**	**0.277**	**0.777**	**1**	**0.728**	**0.898**	**0.599**	**0.695**
Dx	**0.303**	0.085	**0.176**	**0.934**	**0.728**	**1**	**0.805**	**0.580**	**0.340**
Dx_a	**0.365**	**0.197**	**0.156**	**0.732**	**0.898**	**0.805**	**1**	**0.446**	**0.487**
Sx	**0.448**	**0.368**	**0.544**	**0.738**	**0.599**	**0.580**	**0.446**	**1**	**0.754**
Sx_a	**0.488**	**0.562**	**0.344**	**0.479**	**0.695**	**0.340**	**0.487**	**0.754**	**1**

*AMP = fundamental amplitude of ICP, CPP = cerebral perfusion pressure, Dx = diastolic flow index (between FVd and CPP), Dx_a = arterial diastolic flow index (between FVd and MAP), FVd = diastolic flow velocity, FVm = mean flow velocity, FVs = systolic flow velocity, ICP = intracranial pressure, Mx = mean flow index (between FVm and CPP), Mx_a = arterial mean flow index (between FVm and MAP), PAx = between AMP and MAP, PRx = pressure reactivity index (between ICP and MAP), RAC = between AMP and CPP. *all values in bold type face are those which reached statistical significance (ie. p<0.05)*

Grouped Variance Analysis – Friedman Test

Similarity between various groups of indices was assessed by the Friedman test (with and without multiple sampling), with the pre-test assumption that each index was assessing the same aspect of physiology, cerebrovascular reactivity. Friedman testing showed significant inter-index differences, indicating that these indices were non-identical. Further Friedman tests were applied to groups of monitor specific indices (ie. Separately within the two clusters of ICP- and TCD-derived indices). This within-modality Friedman testing also confirmed that each index was in fact different.

Principal Component Analysis (PCA) – Entire TBI TCD Cohort

Spearman PCA was conducted on all three data sheets, all with similar results. Nine principal components (PC) (also referred to as factors (F)) were identified, with the first 5 PC's composing ~96% of

the overall variance in the dataset. PC eigenvalue data, Scree plots, and variable specific loadings can be seen in Appendix C of the supplementary materials. A loading biplot for PC1 (denoted F1) and PC2 (denoted F2) can be seen in Figure 6.6, based on the grand mean data. The ICP derived indices (PRx, PAx and RAC) are clustered in the same quadrant of the biplot, contributing to the overall variance of both PC1 and PC2. Furthermore, PRx/PAx/RAC appeared to be associated with TCD based Sx and Sx_a, in terms of their contributions to the variance of the whole data set. Similarly, the TCD based indices (Mx, Mx_a, Dx and Dx_a) were co-located within the area of the biplot most associated with PC1. This was confirmed on all 3 data sheets.

Agglomerative Hierarchal Clustering (AHC) – Entire TBI TCD Cohort

AHC was performed on all three data sheets, yielding similar results. Figure 6.7 demonstrates the AHC dendrogram for the grand mean data from the entire TBI TCD cohort. As was seen in the two previous sections, Sx/Sx_a co-clustered with the ICP derived indices. The cophenetic correlation coefficient for the grand mean data AHC analysis was 0.76, indicating a moderate-to-strong significance of the clustering.

K-Means Cluster Analysis (KMCA)

KMCA was performed on all data sheets for both cohorts, producing identical clustering results. For the entire TBI TCD cohort, based on the "Elbow Method", the optimal number of centroids for the KMCA was determined to be 3. This was also similar to that seen in the AHC, PCA and Pearson correlation testing.

Figure 6.6: Spearman Type Principal Component Analysis of Autoregulatory/Cerebrovascular Reactivity Indices – Biplot of PC1 vs. PC2 (Entire TBI TCD Cohort - Grand Mean Data)

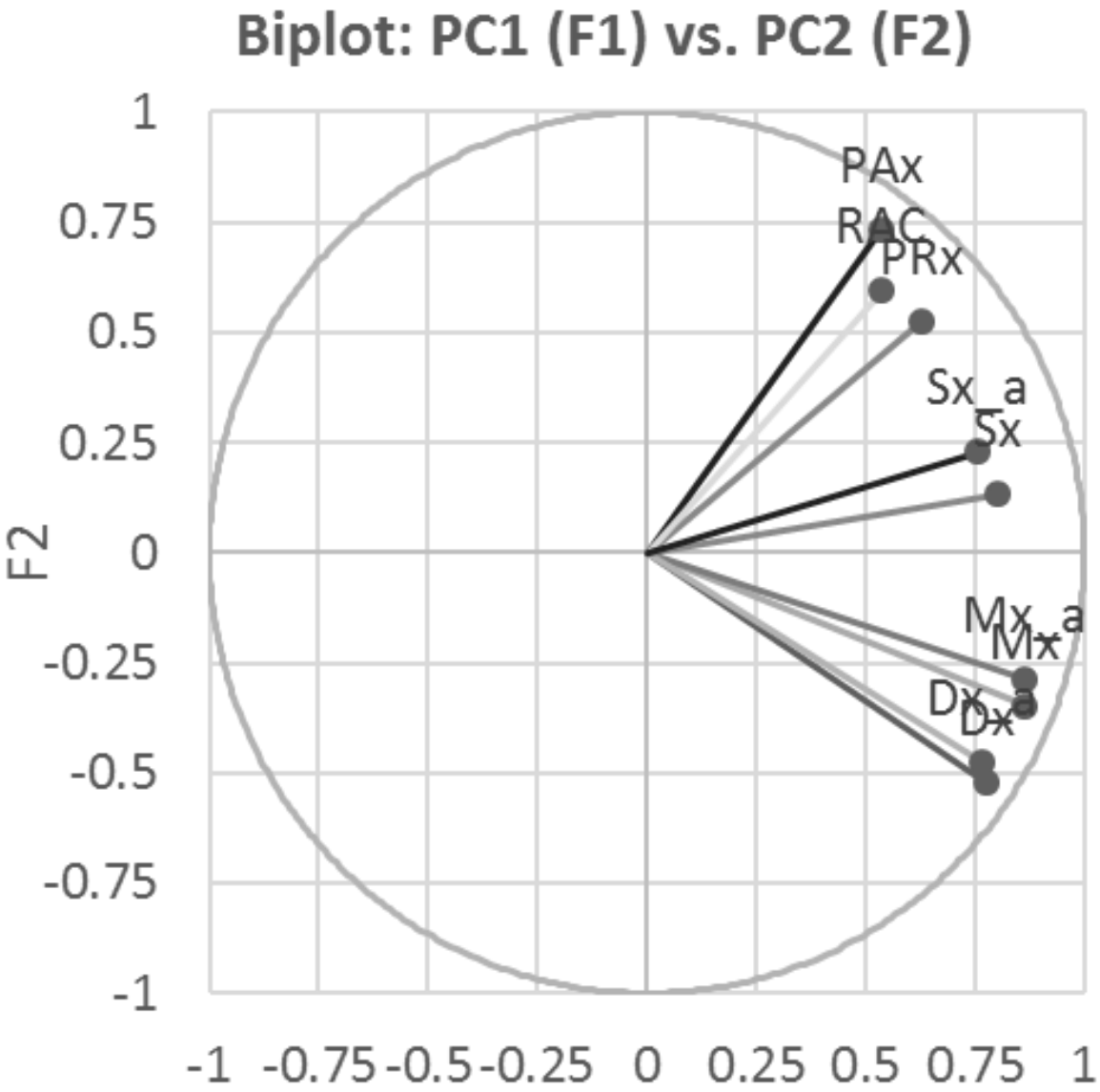

PCA = principal component analysis, F = factor, PC = principal component, F1 = PC1 = principal component #1, F2 = PC2 = principal component #2. PC1 and PC2 are the two components which contribute the largest amount of variance to the entire data set. The above biplot of PC1 vs. PC2 displays which variables contribute variance to PC1 and PC2. The longer the arm connecting (0,0) to the variable (such as PRx), the larger the contribution of that variable. Similarly, the quadrant on the biplot in which the variable falls correlates to its contribution to a particular PC. The upper left quadrant is primarily PC2; lower left quadrant is neither PC1 or PC2; the upper right quadrant is PC1 and PC2; the lower right quadrant is primarily PC1.

Figure 6.7: Entire TBI TCD Cohort – AHC Dendrogram – Grand Mean Data

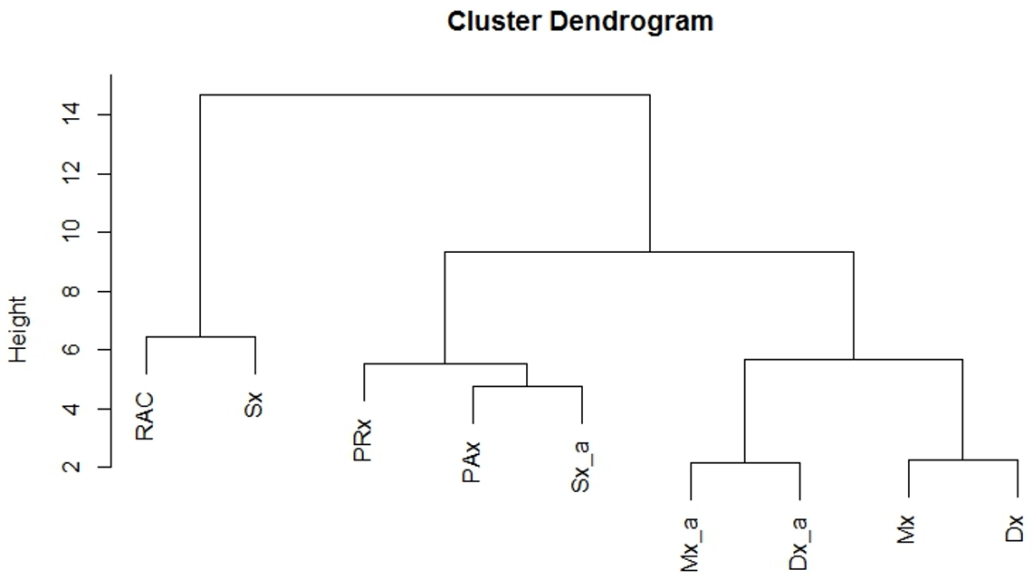

AHC = agglomerative hierarchal clustering, AMP = fundamental amplitude of ICP, CPP = cerebral perfusion pressure, Dx = diastolic flow index (between FVd and CPP), Dx_a = arterial diastolic flow index (between FVd and MAP), FVd = diastolic flow velocity, FVm = mean flow velocity, FVs = systolic flow velocity, ICP = intracranial pressure,, Mx = mean flow index (between FVm and CPP), Mx_a = arterial mean flow index (between FVm and MAP), PAx = between AMP and MAP, PRx = pressure reactivity index (between ICP and MAP), RAC = between AMP and CPP.

6.3.4 Discussion

These results replicate the previously described multi-variate clustering analysis of continuous autoregulation indices in a larger cohort of TBI patients with TCD, providing confirmatory evidence for the co-clustering/co-variance of Sx/Sx_a with the ICP derived indices (PRx, PAx, RAC). The current results based on 410 recordings of at least 30 minutes duration, provide this confirmatory evidence. Thus, it appears that Sx/Sx_a may be more representative of the ICP derived indices, compared to Mx/Mx_a/Dx/Dx_a. This was confirmed with the Pearson correlation test, PCA, AHC and KMCA in all three data sheets analyzed. This may stem from the peak pulsatile systolic component of CBFV yielding a stronger contribution to the ICP signal, than mean or diastolic CBFV's. This concept requires confirmation.

It is important to identify which TCD-based indices are associated with ICP derived indices, in particular PRx. Only a few indices have been validated in animal models with respect to the lower limit of autoregulation (such as PRx). Thus, strong co-variance and association between "non-validated" indices with PRx potentially allow for the use of these indices as a "surrogate" measure for the validated PRx. Sx and Sx_a may be these surrogate measures, with Sx_a potentially derived through entirely non-invasive means.

Limitations

Despite the interesting results, some important limitations should be highlighted. First, a retrospective cohort of patients were studied. The patients had heterogeneous injury patterns and were subject to variations in ICU therapies/treatments during the short recording sessions. This could have impacted signal heterogeneity and quality, leading to a direct influence on both the results of the slow wave and autoregulatory/cerebrovascular reactivity index analysis. Further, these varying treatments may have impacted patient outcomes seen at 6 months. Adding to this, given the varied time frame to application of TCD monitoring within this population, it limits the ability to make definitive comments regarding the "time-dependent" change in predictive power for these indices with respect to 6-month outcome. This aspect would definitively benefit from a prospective study, analyzing the application of TCD recording throughout the course of the patient's ICU stay, leading to standardized and longer recording periods. With this type of data, one would be able to comment on the whether there exists a variation in the predictive power of the TCD based indices, based on the time frame post-injury from which the recordings were obtained.

Second, given this was a retrospective analysis of a database, data was limited to that recorded at the time of entry. Details regarding patient co-morbidities and CT based injury patterns/burden were not recorded in these patients. These details may prove important in terms of an individual patient's cerebrovascular response to injury and the development of impaired autoregulatory capacity. Further prospective studies would benefit from a detailed account of these variables in order to determine their impact on cerebrovascular reactivity post-TBI.

Third, the statistics utilized within the index co-variance/cluster analysis are mainly exploratory and not 100% confirmatory of the relationships described. The use of PCA, AHC and KMCA are exploratory multi-variate statistical techniques designed to highlight potential relationships of interest within an

entire dataset, which would then drive further prospective focused assessment of the individual relationships identified. With that said, the relationships were all confirmed across Pearson correlation test, PCA, AHC and KMCA, potentially indicating that the various clustering/correlations are more than just by chance within an individual multi-variate test.

Finally, as mentioned in previous studies (6.1 and 6.2), the erratic nature of spontaneous slow waves may impact the strength of the relationships seen. Thus, future prospective analysis will require longer recording sessions to allow for the application of slow wave power filters. Ideally this would take place over the course of a patient's ICU stay, in order to confirm that these relationships hold true throughout the acute phase of illness.

6.3.5 Conclusions

TCD based Sx, and Sx_a, are both more closely associated with the ICP derived indices (PRx, PAx and RAC), compared to Mx (or Mx_a) and Dx (or Dx_a). Thus, Sx and Sx_a likely provide a better approximation of PRx and other ICP derived indices, compared to Mx/Mx_a/Dx/Dx_a.

CHAPTER 7: NON-INVASIVE MODELLING OF PRESSURE REACTIVITY USING TCD IN ADULT TBI

*The results of the studies detailed in section 7.1, 7.2 and 7.3 can also be found detailed in the following publications:

1. Zeiler et al., *J Neurotrauma*. 2018; 35(14):1559-1568. doi: 10.1089/neu.2017.5596.[184]

2. Zeiler et al., *Crit Ultrasound J.* 2018; 10(1):16. doi: 10.1186/s13089-018-0097-0.[185]

3. Zeiler et al., *Acta Neurochir (Wein).* 2018; 60(11):2149-2157. doi: 10.1007/s00701-018-3687-5.[186]

4. Zeiler et al., *J Neurotrauma*. 2018 Sep 27. doi: 10.1089/neu.2018.5987. [Epub ahead of print][187]

7.1 Estimation of Pressure Reactivity Index Using TCD

7.1.1 Introduction

PRx is the one continuous measure of autoregulatory capacity that has received the most attention in the TBI population.[3,11] Numerous studies have been published linking abnormal PRx values to poor outcome in TBI. Further to this, thresholds associated with 6-month outcomes have been defined for PRx in the TBI population.[9,152] Finally, PRx is one of few indices that have been validated in an animal model against the LLA.[14]

Despite the promising nature of PRx, the major limitation in its acquisition is the need for invasive measure of ICP. Non-invasive autoregulatory indices based on transcranial Doppler (TCD) exist, including: Mx_a and Sx_a. These TCD-derived indices display a positive linear relationship with PRx. In addition, based on the studies performed in Chapter 6 in three separate patient populations, robust statistical co-variance and co-clustering of the non-invasively derived Sx_a with the invasively derived PRx has been demonstrated.[180–182] Thus, the question remains: Can we estimate PRx using non-invasive TCD based autoregulatory indices?

The main issues with modelling PRx are the fact that the high frequency data used are autocorrelated violating the assumption of statistical independence implicit in simple linear regression techniques and limiting the literature in this area to date. The goal of this study was to provide for the first time, a non-invasive method of estimating PRx using formal time series analysis and linear mixed effects modelling.

7.1.2 Methods

Patient Population

A large retrospective database of TBI patients with simultaneous TCD and ICP recording were studied. All high frequency signals from monitoring devices were archived prospectively between the periods for January 1992 up to and including September 2011, with all patients being admitted to the neurosciences critical care unit (NCCU) at Addenbrooke's Hospital, Cambridge. This was the identical TCD cohort described in section 6.3.[182] For further details refer to section 6.3.2.

Similar to the previous study on co-variance (Chapter 6.3), we were only interested in continuous recording lengths of 30 minutes or longer, for use in linear mixed effects (LME) modelling of PRx. A total of 410 recordings from 347 patients were included. Details of the study population are provided in the results section.

Signal Acquisition, Processing and Definitions of Cerebrovascular Reactivity Indices

This was conducted identically to the methods described in section 6.3.2.

Statistics

Minute-by-minute time series data were utilized for the entirety of the analysis described below. Statistical significance was set at an alpha of less than 0.05. All statistical analysis was conducted using R statistical software (R Core Team (2016). R: A language and environment for statistical computing. R Foundation for Statistical Computing, Vienna, Austria. URL https://www.R-project.org/). The following packages were utilized during the analysis: *dplyr, ggplot2, ggthemes, tseries, forecast, lubridate* and *lme4*.

The statistical methods sections to follow will outline the techniques employed to: A. estimate the autocorrelative structure of PRx in time series, B. estimate PRx using non-invasive TCD indices of cerebrovascular reactivity via application of linear mixed effects (LME) modelling (with embedded PRx ARIMA error structure) to, and C. assess the correlation and agreement between model based estimated PRx and the observed PRx values.

Autocorrelative Structure of PRx

Prior to being able to model PRx using TCD based indices, it was necessary to determine the autocorrelation structure of PRx. We used autoregressive integrative moving average (ARIMA) modelling PRx to determine: the autoregressive structure of order "p", the differencing factor or order "d", and the moving average component of order "q"; commonly denoted "(p,d,q)".[163,164,166] The autoregressive structure refers to the dependence of PRx at time t (denoted PRx_t) on previous measures of PRx (ie. called "lags"), say at time t-1 (ie. PRx_{t-1}), and so forth (ie. say to PRx_{t-p}), with the order "p" indicating how many previous PRx measures PRx_t is dependent on. The differencing component refers to the need to make a non-stationary signal stationary, with seasonal or trending structure within a time series indicating non-stationary character. Stationarity is defined as the presence of a stable variance, autocorrelative structure and mean over time. Stationarity can be introduced by differencing previous PRx measures from current measures, thus removing seasonality or trending structure to a time series and allowing further modelling to occur. The differencing order "d" refers to how many previous terms should be included in the differencing process. Finally, the moving average term refers to the need to include the error in the model at time "t" (ie. e_t) based on its association in previous measured error terms (ie. e_{t-q}). The order "q" for the moving average component refers to how many previous error terms are to be included within the ARIMA model. Assuming stationarity (ie. no "d" order), a general ARMA model can be represented by the following formula:

$$PRx_t = c + \varepsilon_t + \sum_{i=1}^{p} \varphi PRx_{t-i} + \sum_{i=1}^{q} \theta \varepsilon_{t-i} \qquad (7.1)$$

Where: PRx_t = PRx at time t, PRx_{t-i} = PRx at time t-i, ε_t = error at time t, ε_{t-i} = error at time t-i, c = constant, ϕ and θ are coefficient parameters at time t, p = autoregressive order, and q = moving average order.

Initially, the following process was conducted on 10 representative patient recordings (I.e. the longest continuous recordings), in order to derive the optimal ARIMA structure for PRx time series. The following process was only conducted on the 10 longest representative patient recordings, so as to provide insight into the approximate best ARMA structure for future population wide LME models.

First, data had already been artifact cleared and had a 10-second moving average filter applied to the data, leading to some data smoothing (as described above in the signal processing section). Thus, the initial step for the ARIMA modelling focused on determining stationarity of the signal. This was assessed, and confirmed, using 3 methods. First, the autocorrelation function (ACF) correlogram for PRx was assessed, looking for a rapid decline in significant lags, indicating a stationary signal. Second, the Augmented Dickey Fuller (ADF) test was applied to assess for stationarity. Finally, the auto.arima function in R was employed to see if the automated process confirmed the results of the above two steps. All above process confirmed stationarity within the patient examples.[159,163,164]

Second, the autoregressive structure of PRx was assessed using the ACF correlograms and partial autocorrelation function (PACF) correlograms. ACF correlograms were assessed to see how many previous consecutive terms (ie. "lags") PRx may be dependent upon. Similarly, the PACF correlograms were assessed to see how many non-consecutive previous lags, PRx may be dependent upon. Significant level on ACF/PACF correlograms is set at a correlation level of $+/-(2/N^{1/2})$, where N = sample size. Sequential ARMA models were run for PRx by varying the order "p" from 0 to 3, while also varying the moving average order "q" from 0 to 3. Given the analysis for stationarity confirming a stationary signal within the 10 patient examples, the differencing order "d" was fixed at 0. In doing so 16 separate ARMA models for PRx were generated within the 10 patient examples. Model superiority was assessed by Akaike Information Criterion (AIC) and Log-Likelihood (LL), with the lowest AIC and highest LL indicating the best ARMA model for PRx. In addition, model superiority was assessed via residuals, model ACF and PACF correlograms, with an adequate model represented by random residuals, and ACF/PACF failing to display any lags reaching significance. Finally, the auto.arima function was employed to assess if there would be a difference in the automated ARIMA structure process from the manual process. The auto.arima algorithm within R produced the same final ARIMA model for PRx as identified by the manual iterative process.

LME Modelling of PRx Using TCD Derived Indices

LME modelling was conducted in a step-wise fashion on the entire patient population.[159,163,165] Initially LME modelling involved a fixed linear model represented by PRx ~ Sx_a, and a random component introduced into the intercept only (based on individual patient). The PRx ARIMA structure was embedded within the LME model. This model (ie. PRx ~ Sx_a) was used to confirm the ARMA model

structure identified in the 10 patient examples. Iterative LME models were run with various permutations of embedded ARIMA structure for PRx. Again, 16 separate models were run, varying autoregressive order "p" from 0 to 3, and the moving average order "q" from 0 to 3. Given stationarity of signal identified within the patient examples, no differencing order "d" was introduced.

Having confirmed that the LME model residuals structure follows the PRx ARIMA model, this model was used in the subsequent search for a parsimonious model of the relationship between various TCD derived parameters and PRx. This analysis was done on the full data set, deriving LME models for each patient as well as for the entire population. The following LME models were assessed, initially with random intercept only (stratified by patient), as above: PRx ~ Sx_a, PRx ~ Mx_a, PRx ~ Dx_a, PRx ~ Sx_a + Mx_a, PRx ~ Sx _a + Dx_a, PRx ~ Sx_a + Mx_a + Dx_a. Finally, these LME models were run again, introducing random effects into the slope parameters for each of the included independent variables: Sx_a, Mx_a and Dx_a. All models were corrected using maximum likelihood estimation method. Adequacy of the LME model was assessed via QQ plots and the residuals distribution plot, with linear shape to the QQ plots and normally distributed residuals confirming validity of the model.

Models were compared using AIC, Bayesian Information Criterion (BIC), LL and ANOVA testing. Superior models were attributed to the lowest AIC, lowest BIC and highest LL. Significance between models as assessed by ANOVA testing was set at a $p < 0.05$. The top two LME models were reported in detail, with a final assessment of model adequacy through ACF/PACF plots of the model residuals, observing for a minimal number of significant lags which decay rapidly.[159,163]

Generalized fixed effect model versions of the two superior LME models were evaluated by removing the random components of the LME model. This was conducted via generating models for each patient, with the ARMA structure coefficients determined per patient. Finally, a generalized model was also determined for population. Generalized fixed effects models were compared to their LME versions via AIC, BIC, LL and ANOVA testing.

Observed versus Estimated PRx

Finally, the correlation between the observed (minute-by-minute) PRx values in the population versus those estimated from the optimal two LME models were evaluated using Pearson correlation coefficient. Linear regression plots were then produced between observed and estimated PRx for the best two LME models, using grand mean data (ie. mean value per patient). Finally, Bland-Altman plots were produced

to assess agreement between the observed and estimated PRx values, using grand mean Fisher transformed data (ie. Fisher transform applied to both observed and estimated PRx). Bland-Altman determination was conducted via the following method: estimated PRx – observed PRx.

Generalized fixed effects model estimated PRx was compared against the observed PRx in a similar fashion, however are not reported given the results were poor.

7.1.3 Results

The results are described in three sections. The first of these ([A]) characterizes the study population, the second ([B]) the building blocks used for developing TCD based PRx modelling, and the third ([C]) addressing the development and testing of the accuracy of modelled PRx.

A. Study Population

Patient Demographics

As in section 6.3, there were 347 patients with 410 recordings analyzed. The mean age was 33.7 +/- 16.4 years, 250 male subjects. Median admission GCS was 6 (IQR: 4 to 8). Mean recording length was 1.02 hours (range: 0.50 to 3.26 hours).

B. Building the Model to Estimate PRx

The initial step was to confirm the expected relationship between TCD flow indices and PRx in the data, understand the autocorrelative structure of PRx time series data in order to provide a rigorous framework for modelling PRx from TCD data, and then confirm that the models for PRx time series data were generalizable across the populations of study. These results are addressed in the next three sections of results

Linear Relation between PRx, Sx_a and Mx_a – Population Level

In order to confirm the linear relationship between PRx, Sx_a and Mx_a, simple linear regression was employed using grand mean data (ie. one average value for each index per patient over the entire recording period), allowing the use of linear principals (ie. ensuring independence of measures). Figure 7.1 displays the linear relationship between PRx versus Sx_a (panel A) and PRx versus Mx_a (panel B).

Figure 7.1: Linear Relationship between PRx vs. Sx_a and PRx vs. Mx_a – Grand Mean Population Data

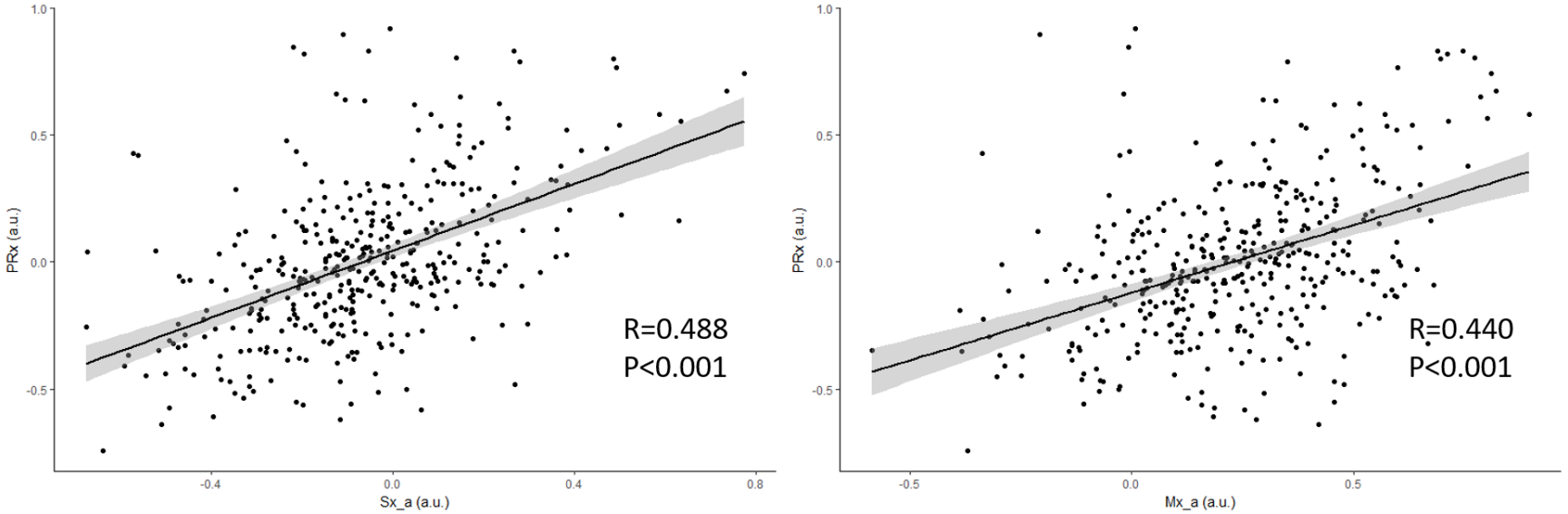

a.u. = arbitrary units, FVm = mean velocity, FVs = systolic flow velocity, ICP = intra-cranial pressure, MAP = mean arterial pressure, Mx_a = mean flow index (correlation between FVm and MAP), p = p-value, PRx = pressure reactivity index (correlation between ICP and MAP), R = Pearson correlation coefficient, Sx_a = systolic flow index (correlation between FVs and MAP).

ARIMA Modelling of PRx – Patient Example

Ten patients, with the longest continuous recordings, were initially analyzed to determine the ARIMA structure of PRx. All patients were deemed to display stationary signals for PRx, as assessed by ACF correlograms, ADF testing and auto.arima algorithmic testing. Thus, no differencing factor was employed. Figure 7.2 displays a patient example of the ACF and PACF correlograms on the raw PRx data, indicating rapid decay of significant lags on the ACF (panel A) and PACF (panel B) correlograms, confirming stationarity (ADF test = -4.456, p-value = 0.01).

Running sequential iterative ARIMA models for PRx within the patient examples, the appropriate autoregressive order "p" and moving average order "q" for the PRx ARIMA model were assessed. Autoregressive order, "p", varied from 0 to 3, and moving average order, "q", varied from 0 to 3, assessing 16 separate ARIMA models for PRx. All models and their AIC's and LL can be seen in Appendix D. The most robust ARIMA structure for PRx, across the 10 patient examples, was deemed to be (2,0,2), with p = 2, d = 0, and q = 2. This model had the lowest AIC of -69.3, and amongst the highest LL of 39.65. Furthermore, the residuals for this PRx ARIMA model appear random, with ACF/PACF correlograms indicating a lack of significant lags (Figure 7.3). This ARIMA structure was confirmed with the auto.arima algorithm in R across all patient examples.

Figure 7.2: PRx ACF and PACF Correlograms - Patient Example

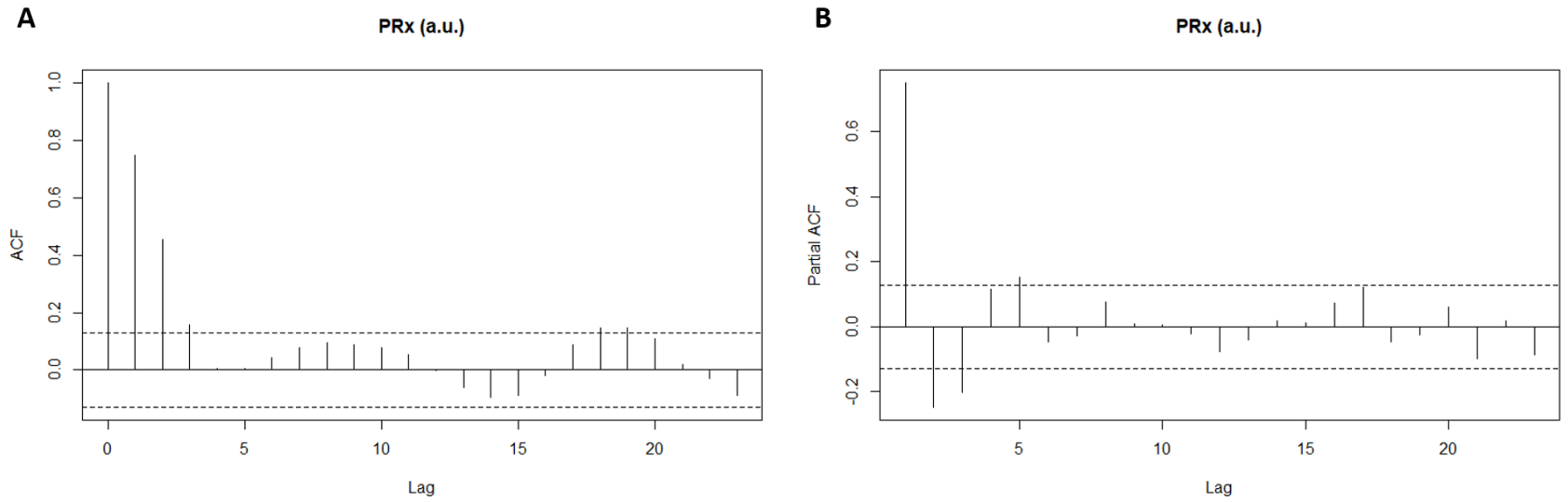

ACF = autocorrelation function, a.u. = arbitrary units, ICP = intracranial pressure, MAP = mean arterial pressure, PACF = partial autocorrelation function, PRx = pressure reactivity index (correlation between ICP and MAP). Panel A = ACF correlogram, Panel B = PACF correlogram. Confidence intervals on correlograms (dotted lines) = +/-(2/$N^{1/2}$), where N = sample size.

Figure 7.3: PRx ARIMA Model (2,0,2) Residual Plot, ACF and PACF Correlograms – Patient Example

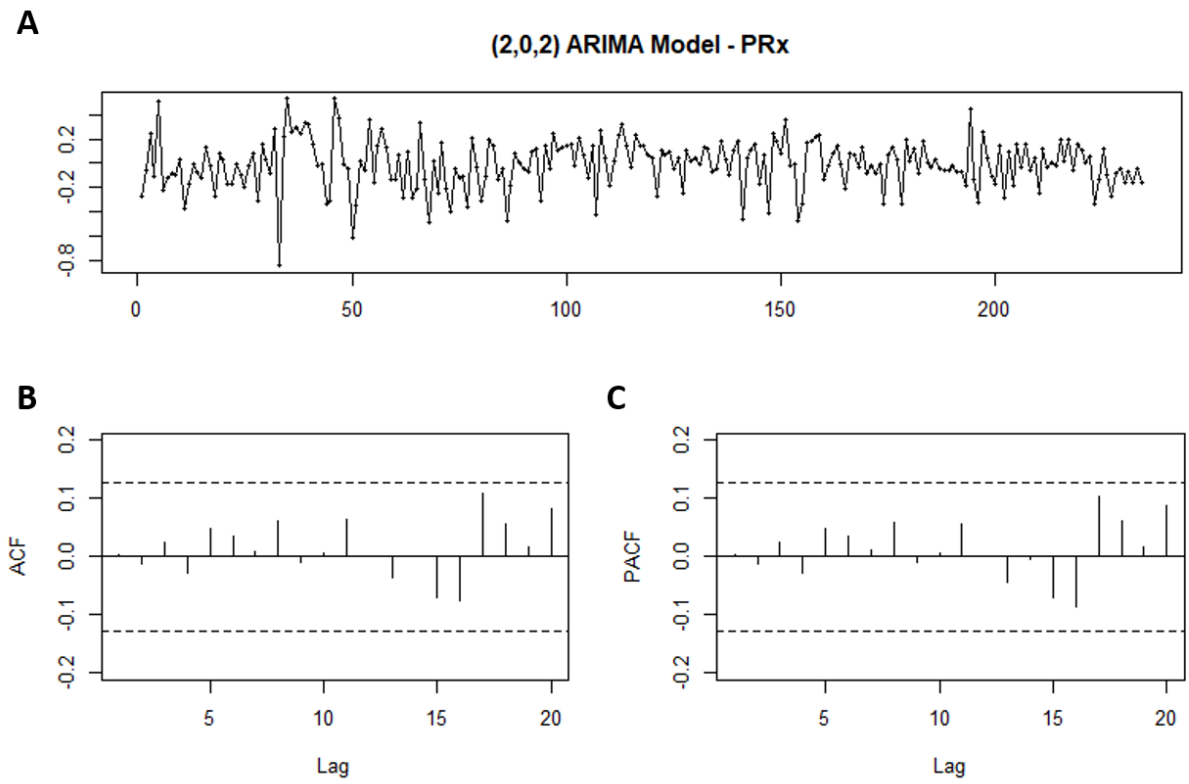

ACF = autocorrelation function, a.u. = arbitrary units, ARIMA = autoregressive integrative moving average, MAP = mean arterial pressure, PACF = partial autocorrelation function, PRx = pressure reactivity index (correlation between ICP and MAP)

Confirmation of PRx ARIMA Structure Via Sequential LME Modelling

In order to confirm that the PRx (2,0,2) ARIMA model structure was adequate for the modeling across the entire dataset, sequential LME models were employed based on the fixed effects PRx ~ Sx_a, and random effects within the intercept (based on patient), with varied embedded PRx ARIMA structures. The same 16 ARIMA model structures utilized within the patient examples were then run, assessing the AIC, BIC and LL of the LME models, with the goal of parsimony in the ARIMA structure. The data for AIC, BIC and LL in each LME with the varied embedded PRx ARIMA error structures can be found in Appendix D. The best model was again deemed to be that with a PRx ARIMA error structure of (2,0,2), with an AIC of -9797.294, BIC of -9735.699 and LL of 4906.647. The residual density for this model was normally distributed.

C. Model Development and Accuracy Assessment

Modelling of PRx using TCD derived variables was conducted in two stages. First, modelling of PRx using the optimal autocorrelative structure that we identified in the previous section of results was conducted. Then measured (ie. observed) and estimated PRx were compared to determine how well te observed PRx values correlated with estimates from the top two models.

LME Modelling of PRx Using TCD Indices

After confirming that ARIMA (2,0,2) error structure was adequate for continued LME modelling of PRx of the population, several different LME models were fitted to the whole data set, first varying the fixed effects model structure and then the random effects, as described within the methods section. The AIC, BIC and LL values for each LME model tested is presented in Table 7.1. The two best models, based on lowest AIC/BIC values, highest LL, and normally distributed residuals were: PRx ~ Sx_a, and PRx ~ Sx_a + Mx_a, with random effects (based on patient) introduced into both the independent variables and intercept. In addition, ANOVA testing indicated these two models were superior, with the multi-variable model (with Sx_a and Mx_a) performing significantly better. The QQ plots and residual density plots for both models can be seen in Figure 7.4, indicating adequacy of the model. ACF and PACF plots of the residuals form each of these models displayed a number of significant lags each LME model (ie. ~10).

To evaluate further the impact of patient-by-patient variation on the LME model, random effects were removed from these models. Doing so produced inferior models, with larger AIC and BIC values. Furthermore, comparing these population wide generalized fixed effects models to the LME models via ANOVA, the LME models described above were statistically superior.

Figure 7.4: QQ Plot and Residual Density Plot for Two Superior LME Models

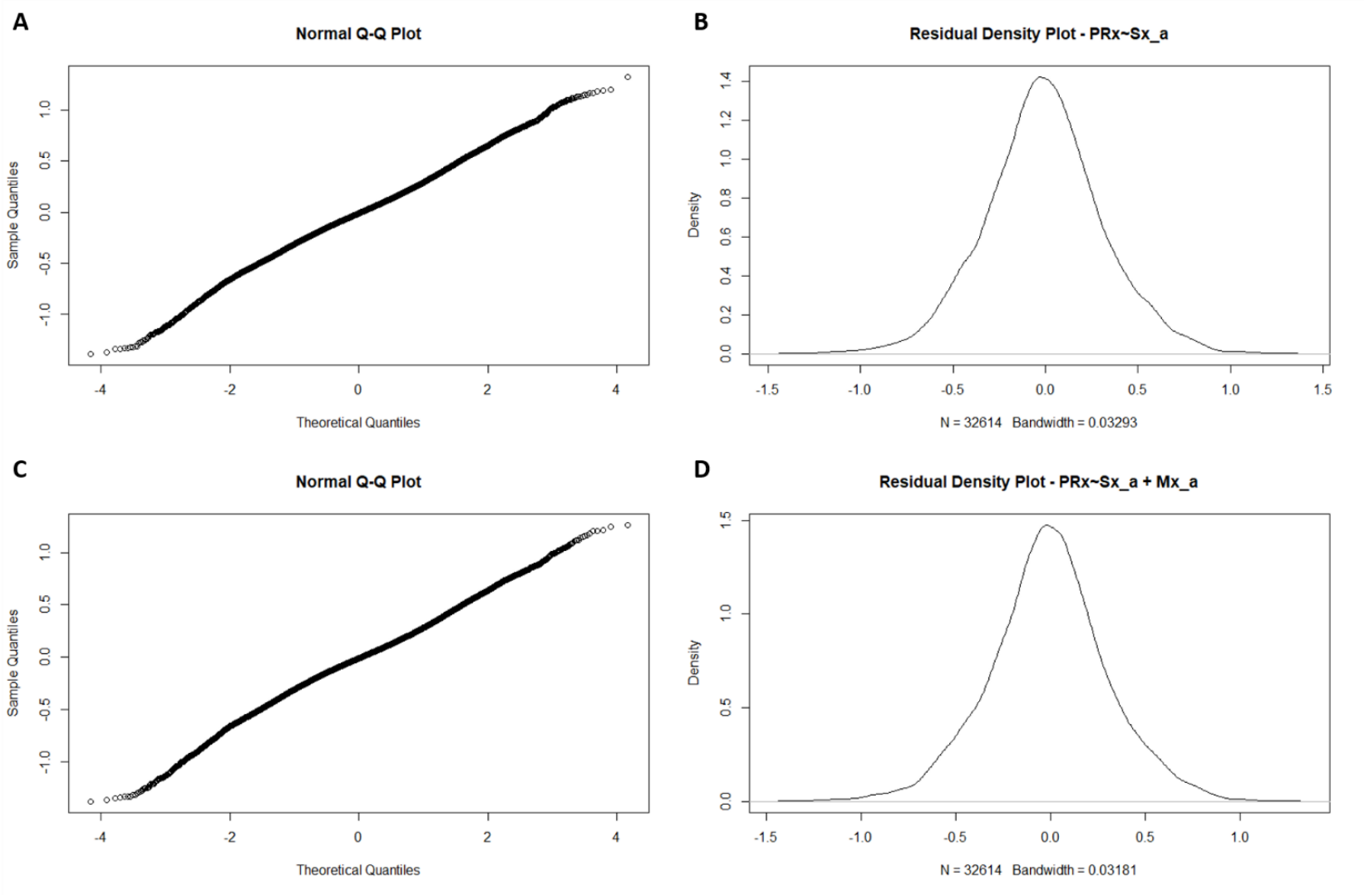

QQ = quantile quantile. Panel A = QQ plot for LME model PRx ~ Sx_a, Panel B = residual density plot for LME PRx ~ Sx_a, Panel C = QQ plot for LME PRx ~ Sx_a + Mx_a, Panel D = residual density plot for LME PRx ~ Sx_a + Mx_a. QQ and Density plots for both models indicate normally distributed residuals, and thus model adequacy.

Table 7.1: LME Models with PRx (2,0,2) ARIMA Structure – Entire Population

LME Model		**PRx ARIMA Structure**		**AIC**	**BIC**	**LL**
Fixed Effects	**Random Effects**	**p**	**q**			
PRx ~ Sx_a	intercept	2	2	-9797.294	-9735.699	4906.647
PRx ~ Mx_a	intercept	2	2	-8530.042	-8468.447	4273.021
PRx ~ Dx_a	intercept	2	2	-7865.311	-7803.716	3940.655
PRx ~ Sx_a + Mx_a	intercept	2	2	-9821.206	-9751.912	4919.603
PRx ~ Sx_a + Dx_a	intercept	2	2	-9804.395	-9735.101	4911.198
PRx ~ Sx_a + Mx_a + Dx_a	intercept	2	2	-9822.731	-9745.737	4921.365
PRx ~ Sx_a	**Intercept + Sx_a**	**2**	**2**	**-10806.43**	**-10729.44**	**5413.404**
PRx ~ Mx_a	Intercept + Mx_a	2	2	-9928.451	-9851.458	4974.226
PRx ~ Dx_a	Intercept + Dx_a	2	2	-9239.414	-9162.420	4629.707
PRx ~ Sx_a + Mx_a	**Intercept + Sx_a + Mx_a**	**2**	**2**	**-11798.81**	**-11691.02**	**5913.404**
PRx ~ Sx_a + Dx_a	Intercept + Sx_a + Dx_a	2	2	FTC	FTC	FTC
PRx ~ Sx_a + Mx_a + Dx_a	Intercept + Sx_a + Mx_a + Dx_a	2	2	FTC	FTC	FTC

*AIC = Akaike Information Criterion, ARIMA = auto-regressive integrative moving average, BIC = Bayesian Information Criterion, Dx_a = diastolic flow velocity (correlation between TCD based FVd and MAP), FTC = "failure to converge" for the model, FVd = TCD based diastolic flow velocity, FVm = mean TCD flow velocity, FVs = TCD based systolic flow velocity, ICP = intra-cranial pressure, LL = log likelihood, LME = linear mixed effects model, p = auto-regression parameter for ARIMA model, MAP = mean arterial pressure, PRx = pressure reactivity index (correlation between ICP and MAP), q = moving average parameter for ARIMA model, Sx_a = systolic flow index (correlation between TCD based FVs and MAP), TCD = transcranial Doppler. *Note: bolded value represents the most appropriate ARIMA structure and LME model for the patient population tested, based on principal of parsimony, lowest AIC and BIC. There was no integrative parameter (ie. "d" parameter) included within the ARIMA models, given stationarity testing during patient examples (see appendix A and Methodology section of manuscript).*

Population Based Estimation of PRx Using Sx_a and Mx_a

Assessing the correlation between observed PRx and estimated PRx using the various models, it confirmed that the above-mentioned superior LME models, with embedded PRx ARIMA structure of (2,0,2), displayed the best correlation between observed and estimated values. The model based on fixed effects of PRx ~ Sx_a (with random effects in the slope and intercept based on patient) had a correlation of 0.794 ($p<0.0001$, CI = 0.788 to 0.799). The model based on fixed effects of PRx ~ Sx_a + Mx_a (with the same random effects) displayed a correlation of 0.814 ($p<0.0001$, CI = 0.809 to 0.819). All correlations between observed and estimated PRx for the LME models tested can be seen in Table 7.2.

Table 7.2: Correlation Between Observed PRx and LME Model Based Predicted PRx

LME Model		**Correlation Between**
Fixed Effects	**Random Effects**	**Observed PRx and Model Predicted PRx**
PRx ~ Sx_a	intercept	0.770
PRx ~ Sx_a + Mx_a	intercept	0.770
PRx ~ Sx_a + Dx_a	intercept	0.770
PRx ~ Sx_a + Mx_a + Dx_a	intercept	0.770
PRx ~ Sx_a	**Intercept + Sx_a**	**0.794**
PRx ~ Sx_a + Mx_a	**Intercept + Sx_a + Mx_a**	**0.814**
PRx ~ Sx_a + Dx_a	Intercept + Sx_a + Dx_a	NA
PRx ~ Sx_a + Mx_a + Dx_a	Intercept + Sx_a + Mx_a + Dx_a	NA

*Dx_a = diastolic flow velocity (correlation between TCD based FVd and MAP), FTC = "failure to converge" for the model, FVd = TCD based diastolic flow velocity, FVm = mean TCD flow velocity, FVs = TCD based systolic flow velocity, ICP = intra-cranial pressure, LL = log likelihood, LME = linear mixed effects model, p = auto-regression parameter for ARIMA model, MAP = mean arterial pressure, PRx = pressure reactivity index (correlation between ICP and MAP), q = moving average parameter for ARIMA model, Sx_a = systolic flow index (correlation between TCD based FVs and MAP), TCD = transcranial Doppler. *Note: bolded value represents the most appropriate ARIMA structure and LME model for the patient population tested, based on principal of parsimony, lowest AIC and BIC.*

Figure 7.5 displays the linear relationship between observed and estimated grand mean PRx (ie. average per patient) from the two optimal models: PRx ~ Sx_a (Figure 7.5A), and PRx ~ Sx_a + Mx_a (Figure 7.5B). As can be seen, each model shows a strong linear correlation between observed PRx and model estimated PRx, with a slope almost equal to that of line "y = x" (dotted straight line in Figure 7.5A and 7.5B).

Figure 7.5: Linear Regression Between Observed and Estimated PRx – Using Estimated PRx From Two Best LME Models

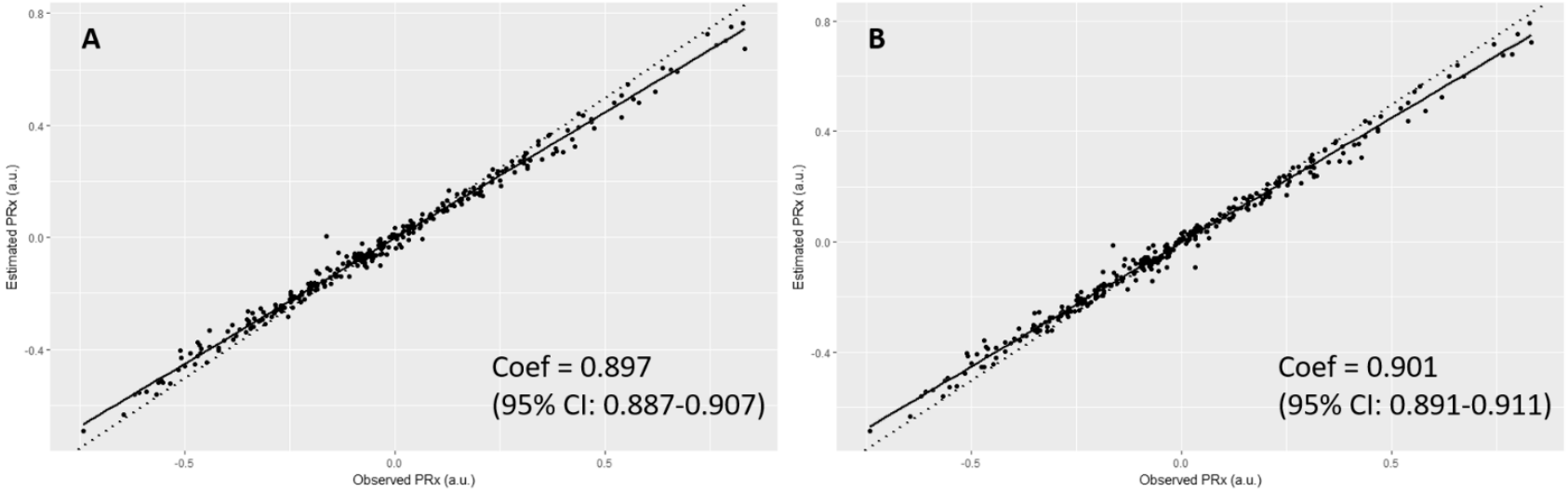

a.u. = arbitrary units, ICP = intracranial pressure, LME = linear mixed effects, MAP = mean arterial pressure, PRx = pressure reactivity index (correlation between ICP and MAP). Panel A: LME model – PRx ~ Sx_a (random effects with intercept and Sx_a), Panel B: LME model – PRx ~ Sx_a + Mx_a (random effects with intercept, Sx_a and Mx_a). Coef = coefficients, form linear model between observed PRx and model estimated PRx. Dotted straight line – represents the relationship "y = x", for comparison the two models.

Finally, Figure 7.6 displays the Bland-Altman plots for Fisher transformed grand mean data (ie. average per patient), assessing the difference between observed and estimated PRx for each model (Figure 7.6A and Figure 7.6B). Both plots display good agreement between the observed and estimated PRx values for each model, within limits. Of note, that the model estimates PRx well for values between +0.50 and -0.50 (approximately +0.46 and -0.46 in un-transformed data; the common clinical range), where outside of that the agreement deteriorates.

Figure 7.6: Bland-Altman Plots – Top Two LME Models – Observed versus Estimated PRx (FT Grand Mean Data)

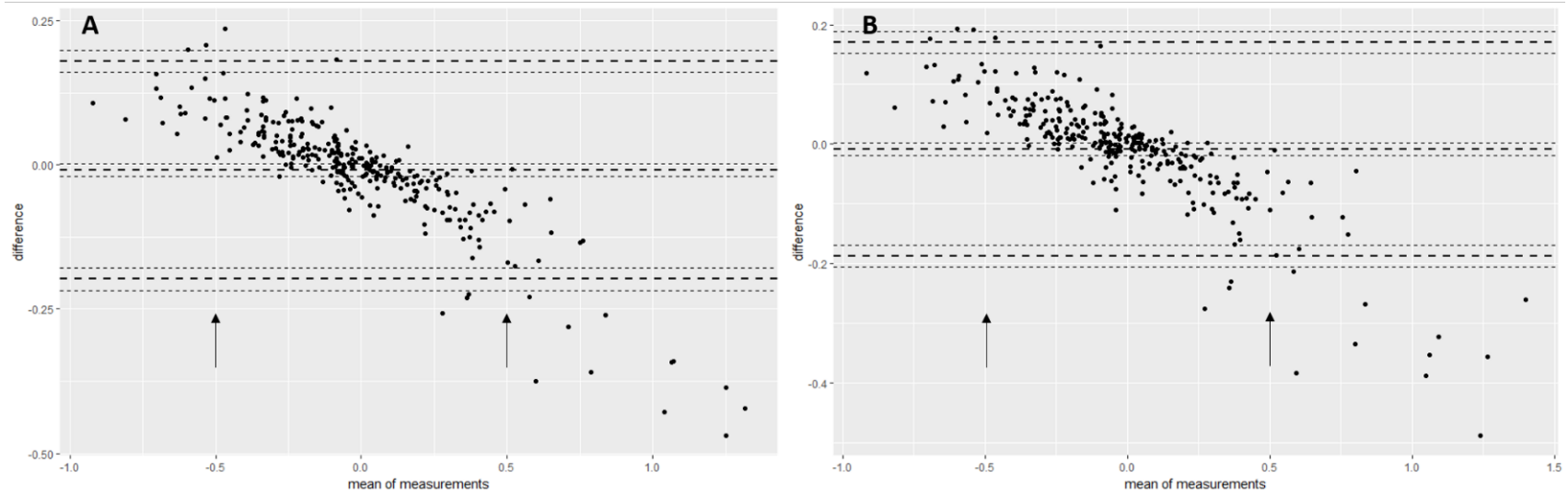

*FT = Fisher transformed, LME = linear mixed effects. Panel A: Bland-Altman plot comparing observed versus estimated PRx for LME model – PRx ~ Sx_a (random effects in intercept and Sx_a), Panel B: Bland-Altman plot comparing observed versus estimated PRx for LME model – PRx ~ Sx_a + Mx_a (random effects in intercept, Sx_a and Mx_a). Horizontal bold dotted lines represent +/- 2 standard deviations in difference. Arrows denote margins of acceptable agreement between observed and estimated PRx, where outside of this range the agreement deteriorates. *NOTE: These values are FT values, where a transformed value of 0.5 is ~0.46 in un-transformed data.*

7.1.4 Discussion

Through the application of linear mixed effects modelling and accounting for the autocorrelative structure of PRx, via employing ARIMA modeling, models were produced which theoretically estimated PRx using non-invasive TCD autoregulation indices in TBI patients, Sx_a and Mx_a. Furthermore, PRx was estimated with a correlation between observed and estimated of ~0.80, with acceptable agreement on linear regression and Bland-Altman analysis. This is the first attempt at applying time series and linear mixed effects modelling of PRx, and has laid the ground for further exploration of complex time series analysis of high frequency data in TBI patients.

Some important points should be highlighted in this study. First, this is the first attempt at estimating an invasive autoregulation index, PRx, using non-invasive TCD measures, Sx_a and Mx_a. This is preliminary attempt at incorporating the complexities of time series analysis in the modelling of PRx. Models have been produced for estimating PRx, however, these are very preliminary and should be interpreted with caution. These results are promising for the future ability to estimate the "gold standard" PRx via non-invasive means. Further, a strong relationship between non-invasive TCD derived measures of cerebrovascular reactivity and the invasive derived "gold-standard" PRx has been displayed, demonstrating that in fact PRx may be expressed in terms of these non-invasive measures. As well, this paper identifies the strong link between two aspects of cerebral autoregulation, measures of cerebral blood flow (ie. TCD based CBFV) and measures of cerebral blood volume (ie. ICP). Previous literature has displayed variable correlation between these measures. This study provides a highly important evidence of a strong link between the two and offers explanation of that relatively poor correlation. Second, the complexity of these models displays the difficulties in incorporating time series "real-time" analysis of high frequency physiological data from ICU monitoring. The application of ARIMA modelling is complex and labor intensive to find the most parsimonious model for the variable of interest, PRx. In order to ensure the appropriate modeling was applied, various iterative techniques were employed in both representative patient examples and a basic LME in the entire dataset. Third, given the poor performance of the generalized fixed effects versions of the models, it is clear that there exists patient-by-patient variability that impacts the ability to model PRx, supporting the application of LME modelling. This cannot be ignored, as see within the analysis. This was confirmed via AIC, BIC, LL, ANOVA and correlation with observed PRx values. An important point for those wishing to employ generalized fixed effects models. Thus, the application of a generalized fixed effects model is limited, based on the results from this dataset. Fourth, the BA analysis provided further confirmation that the estimated PRx from the

top 2 models, were in good agreement with the observed PRx values in the patients. However, there is some bias evident within the BA plots (ie. the negative linear pattern seen), despite being within agreement throughout the normal range of PRx values typically encountered within the clinical setting (ie. -0.5 to +0.5). This particular bias indicates that the models slightly underestimate PRx. Thus, the model is not perfect, but still closely estimates PRx within acceptable degrees of agreement. Finally, again this is preliminary work and these models should not be employed clinically at this time to estimate PRx using non-invasive TCD measures. Further analysis of these models and improvements need to occur before the reliability of their estimation can be determined.

Limitations

Some important limitations need to be highlighted. First, this is a retrospective analysis of a heterogeneous patient cohort. Thus, patient co-morbidity, injury pattern/burden and treatment heterogeneity may have impacted the recorded and archived high frequency signals utilized in the derivation of these autoregulation indices.

Second, the ARIMA structure identified for PRx is only valid in this TBI patient sample. The (2,0,2) ARIMA structure may not apply to other cohorts of TBI patients, or even other, perhaps longer recordings in the same patients. It is possible that the autoregressive order "p" as well as the moving average order "q" may be much higher in other cohorts, depending on dynamical composition of time series. Furthermore, the ARIMA structure of PRx based on different update periods, averaging process and grouped averages (ie. mean hourly values, mean daily values, etc.) has not been explored within this study.

Third, this cohort the signals appeared to fulfill the criteria for stationarity, based on various aspects of assessment. Thus, a differencing order "d" was not applied in the ARIMA structure for PRx. However, stationarity was only assessed within the 10 longest patient recordings, generalizing the results of the stationarity assessment to the rest of the patient dataset. Thus, the short recordings not assessed could potentially have seasonality/trend which we did not account for. Futhermore, it is possible that different populations of TBI patients, different methods of acquiring PRx and different averaging of the PRx data may introduce seasonality and trend to the data such that the signals become non-stationary. As well, the recordings were short, it may be that seasonality and trend were not appreciated in such short duration recordings, and longer recordings may display the need for a differencing order within

the ARIMA structure for PRx. Much further evaluation of the autocorrelative structure for PRx and other high frequency physiologic variables in TBI is required.

Fourth, the inclusion of PRx ARIMA structure within the LME modelling adds significant complexity to the final models derived for the general population. This is a significant limitation to the application of these models broadly at this time. If further studies confirm and improve upon the preliminary results displayed here, there is potential to automate this modelling and PRx estimation so that it is may become more accessible.

Fifth, one could argue that the top 2 LME models displaying approximately 10 significant residual lags on the ACF plot indicates the model isn't perfect. This is correct, and possible a consequence of the short nature of the TCD recordings. However, with p-values less than 1 $X10^{-16}$, there exists confidence that 10 residual lags would not inflate the p-values so much that statistical significance could be questioned within the LME models.

Finally, the fact the generalized fixed effects models fail to display superiority to the LME models is a major limitation. This indicates that there is substantial patient-to-patient variability, limiting the ability to apply these models to other patients and datasets. Thus, at the current time, no general model can be offered for widespread use.

7.1.5 Conclusions

Through employing linear mixed effects modelling and accounting for the autocorrelative structure of PRx with ARIMA modelling, one can theoretically estimate PRx using non-invasive TCD based indices of cerebrovascular reactivity.

7.2 Application of New Robotic Doppler Technology

Introduction

The results of the studies detailed in 6.1, 6.2 and 6.3 provide a comprehensive assessment of the inter-index relationships between cerebrovascular reactivity indices derived from MMM. Importantly, the association between Sx/Sx_a and the invasive ICP derived indices (PRx, PAx, and RAC) was highlighted in the relevant chapters.[180–182] Furthermore, the results of 7.1 further confirm the strong relationship between PRx and Sx_a.[184]

Based on these results, the only major limitation regarding this identified relationship is that the TCD recordings were short in nature, limited by the technique. One potential last aspect to explore is the relationship between ICP and TCD derived indices in longer recordings, in order to assess the impact of recording length on the co-variance and improve our models of PRx estimation using non-invasive TCD indices. Finally, such data could allow for prediction of PRx using non-invasive TCD measures.

Recent advances in robotics have led to the development of robotically driven TCD probes for extended duration recordings, integrated with automated algorithms for MCA CBFV detection and optimization of recorded signal intensity. To date, these devices have not been applied the neurocritically ill. To obtain longer recordings, this technology was applied in moderate/severe TBI patients within the NCCU at Addenbrooke's Hospital for the purpose of this thesis. This section highlights this newly applied technology, with the results of the prospective validation study of PRx and Sx_a inter-index relationships/modelling found in the section to follow, section 7.3.

Methods:

From of November 2017 to April 2018, in place of the regular TCD devices (Doppler Box (DWL Compumedics, Singen, Germany) or Neuroguard (Medasonic, Fremont, CA, USA)), the Delica EMS 9D robotic TCD (Delica EMS 9D System, Shenzen Delica Medical Equipment Co. Ltd., China; http://www.delicasz/com) system was applied for bilateral MCA CBFV recording in moderate and severe TBI patients within the NCCU at Addenbrooke's Hospital, University of Cambridge. TCD monitoring is considered part of standard NCCU patient care, as such formal patient or proxy consent was not required. The timing to application of TCD based monitoring varied from patient to patient, typically

initiated between 24 hours to 10 days post-TBI. A total of 20 patients were able to be recorded with the device during the 6-month trial period.

All patients were intubated and sedated given the severity of their TBI, with ICP target of less than 20 mm Hg, and CPP greater than 60 mm Hg. ABP was obtained through radial arterial lines connected to pressure transducers (Baxter Healthcare Corp. CardioVascular Group, Irvine, CA). All patients had a frontally situated cranial bolt (Technicam Ltd, Newton Abbot, UK), for parenchymal ICP monitoring (Codman ICP MicroSensor; Codman & Shurtleff Inc., Raynham, MA), and cerebral microdialysis (M Dialysis AB, Stockholm, Sweden). Finally, bifrontal near infrared spectroscopy was also applied (NIRO-200 or NIRO-200NX, Hamamatsu Photonics Ltd, Japan).

We recorded all physiologic signals in digital high frequency format (50 Hertz (Hz) or higher) using ICM+ software (Cambridge Enterprise Ltd, Cambridge, UK, http://icmplus.neurosurg.cam.ac.uk). This was installed and run directly off the Delica monitor.

The following sections will describe the device and outline the advantages/disadvantages of the system within the moderate/severe TBI population. Finally, summary conclusion regarding the device are made.

The Device – An Overview:

The Probes/Robotic Drive

The Delica EMS 9D robotic TCD system is a portable TCD system allowing for bilateral simultaneous MCA insonation. The standard probes available with the system are 1-2 MHz Doppler ultrasound probes, each attached to a separate robotic drive. The entire drive/probe construct is encased within a tough plastic shell and supported using a head-band type frame (Figure 7.7A). An option exists for the probes to be surrounded by a small rubber ring around its periphery, which is designed to hold ultrasound gel for longer, allowing for preserved signal quality. Figure 7.7 displays various pictures of the Delica EMS 9D system.

Figure 7.7: Delica EMS 9D Robotic TCD Probe and Headband

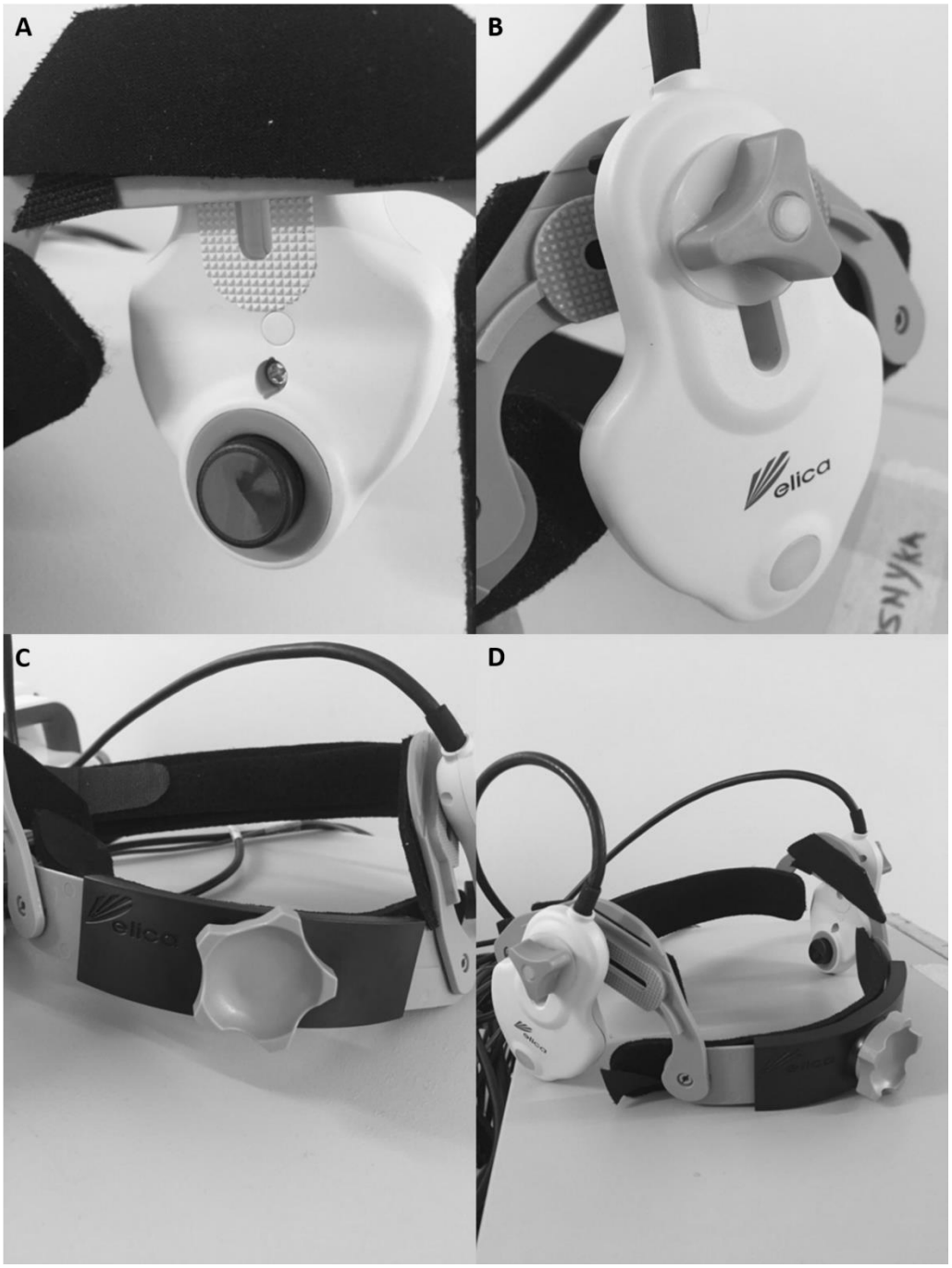

TCD = transcranial Doppler. Panel A: TCD probe (black circular object) held with robotic drive as one construct within plastic casing. Medial view – where probe contacts patient for transtemporal insonation of the middle cerebral artery. Neoprene pad is also seen on medial aspect of head-band. Panel B: Lateral view of robotic drive/TCD probe construct. Displays wing-nut attachment to head-band holder, via "inverted U-shaped" plastic bracket. Panel C: Anterior view of head-band displaying plastic component and wheel ratchet system for tightening. Panel D: Full view of head-band with bilateral robotic drive/TCD probes attached.

The head-band frame is a composite of plastic and Velcro straps with fabric (Figure 6.8C and 6.8D). The diameter of the head-band may be adjusted using either the Velcro straps, or the ratcheting wheel located on the front of the head band (Figure 7.7C). Ideal location of the band is just above the orbital margins. Near the temporal windows, the head-band frame contains plastic inverted "U-shaped" pieces following the course of the superior temporal line, meant for mounting the robotic drive/TCD probe construct (Figure 7.7B). The is accomplished using wing-nut fasteners. The entire head-band is padded with exchangeable Neoprene inserts, for comfort (Figure 7.7A).

The Delica TCD Software

The Delica EMS 9D comes with its own specially design software for recording TCD signal. This provides both an easy to use interface with the robotic drive system, and continuously updating CBFV waveforms and M-mode signals. Furthermore, the left side of the screen provides both simultaneous left and right CBFV waveforms at various depths of insonation, allowing for selection of the optimal depth for recording. Various other more complex functions are available within the software, such as microemboli detection, however focus will not be on these, given the goal was to assess the basic ability to record in critically ill TBI patients. Figure 7.8 Displays the software interface.

Figure 7.8: Delica EMS 9D TCD Software Interface

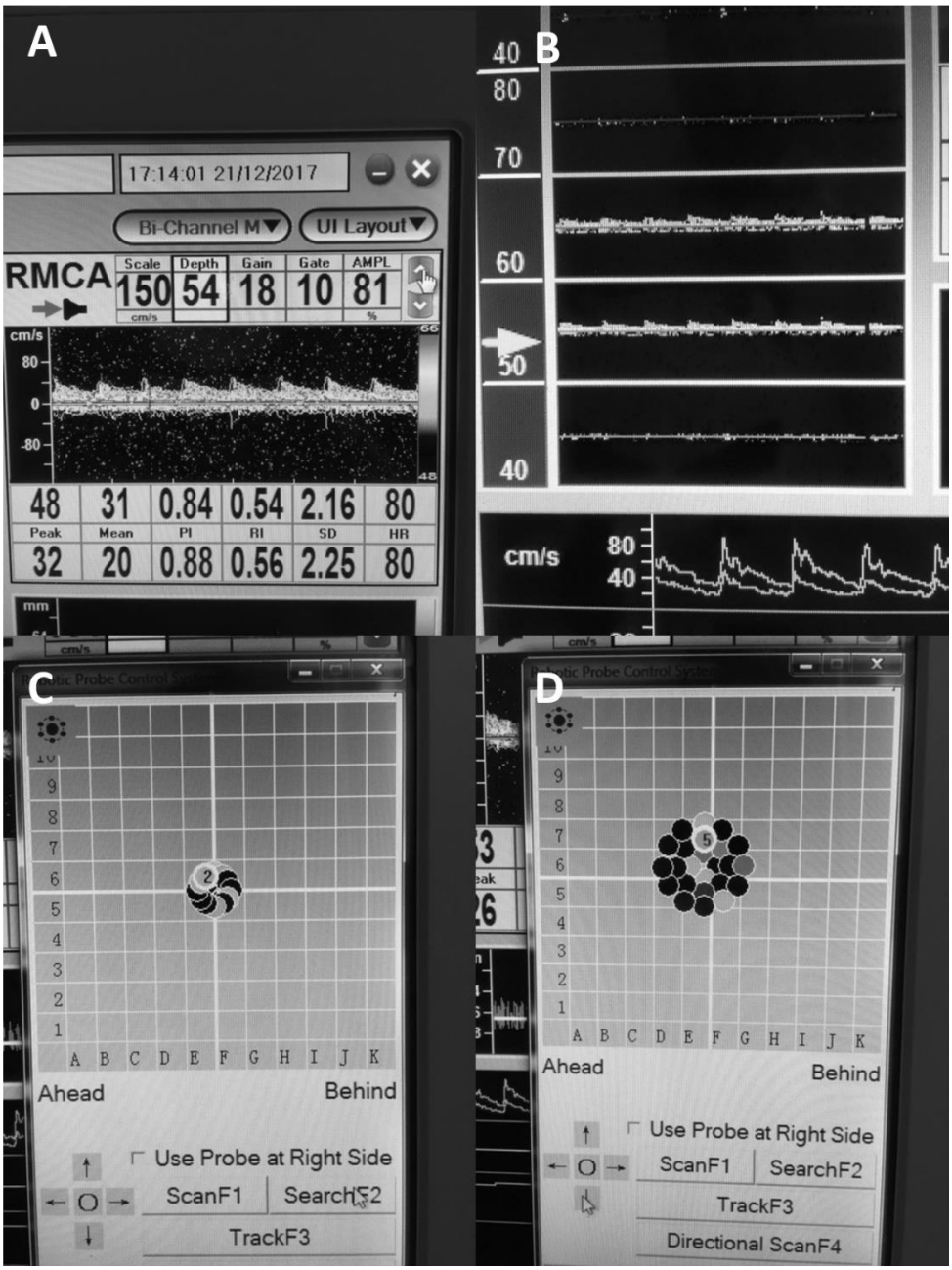

TCD = transcranial Doppler. Panel A: Displays right middle cerebra artery real time blood flow velocity waveform. Panel B: Displays sequential "look ahead" view of right middle cerebral artery, providing sequential real time cerebral blood flow velocity waveforms at various depths of insonation. Panel C: Search robotic signal acquisition function window, displaying the pattern at which the TCD probe is automatically moved. Panel D: Directional robotic signal acquisition function window, displaying the patter which the TCD probe is moved, changing the angle of insonation. Note: panel C and D, the various points of insonation are color coded to represent strength of signal, this can be appreciated via different shadings in this greyscale picture.

Finally, the robotic drive system carries 4 main functions: scan, search, direction, and track. Scan is an automated algorithm which moves the TCD probe position in a square grid pattern, insonating at each spot, assessing for MCA CBFV signal intensity and providing a color code for its findings (black = poor/no signal found, red = good; with colors ranging from blue, to green, to yellow, to orange, to red). It must be acknowledged that the amount that the probe can change in position is limited, so large position corrections still required manual manipulation. After completion of the grid, the proprietary automated algorithm then chooses the best position. The search function provides an automated circular search pattern around the initial starting point, changing both probe position and insonation angle. As with the scan function, it insonates each spot, finding the optimal signal intensity for a final position. The directional function alters the TCD probe angle, using an automated algorithm, with the goal of finding the optimal insonation angle. It should be noted, at any point, the operator can manually change the probe position using the direction touch pad on the screen.

Finally, the track function is enabled after the user selects the optimal position of insonation. This function is designed to automatically detect any deterioration in signal quality/intensity, and then automatically adjust the TCD probe (both via position and angle), using a proprietary algorithm, to restore optimal signal. Figure 7.9, demonstrates TCD CBFV signal recorded over a 4-hour period, displaying continuous uninterrupted acquisition of maximum envelope flow velocity signal which retained good quality without the need of any manual adjustments over the whole duration of recording.

Figure 7.9: TCD CBFV Signal – Over 4 Hour Recording Session

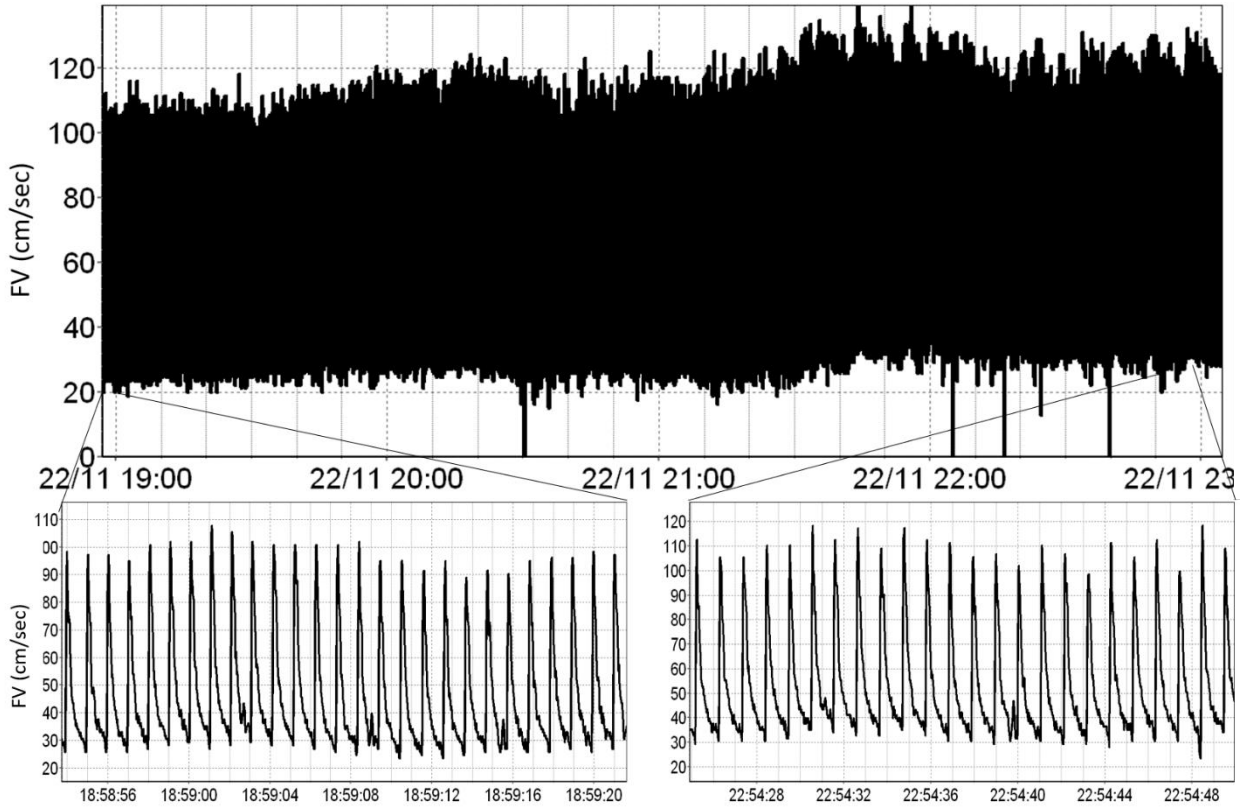

*CBFV = cerebral blood flow velocity, cm = centimeter, FV = flow velocity, sec = seconds, TCD = transcranial Doppler. *Diagram depicts continuous uninterrupted FV signal over 4+ hours of recording. Two windows on bottom of image depict signal waveforms from beginning (bottom left) and end (bottom right) of the recording, demonstrating preserved high-quality signal throughout the duration of the lengthy recording period.*

<u>Application in Moderate/Severe TBI – Initial Impression - Advantages and Disadvantages</u>

The Delica EMS 9D system was applied in moderate/severe TBI patients who were intubated, sedated and had other multi-modal monitoring in situ (ie. both invasive and non-invasive). The typical patient set-up can be seen in Figure 7.10, including a triple-bolt (ICP, Licox, and microdialysis) with bifrontal NIRS.

Figure 7.10: Application of Robotic TCD System in TBI Patient with Multi-modal monitoring

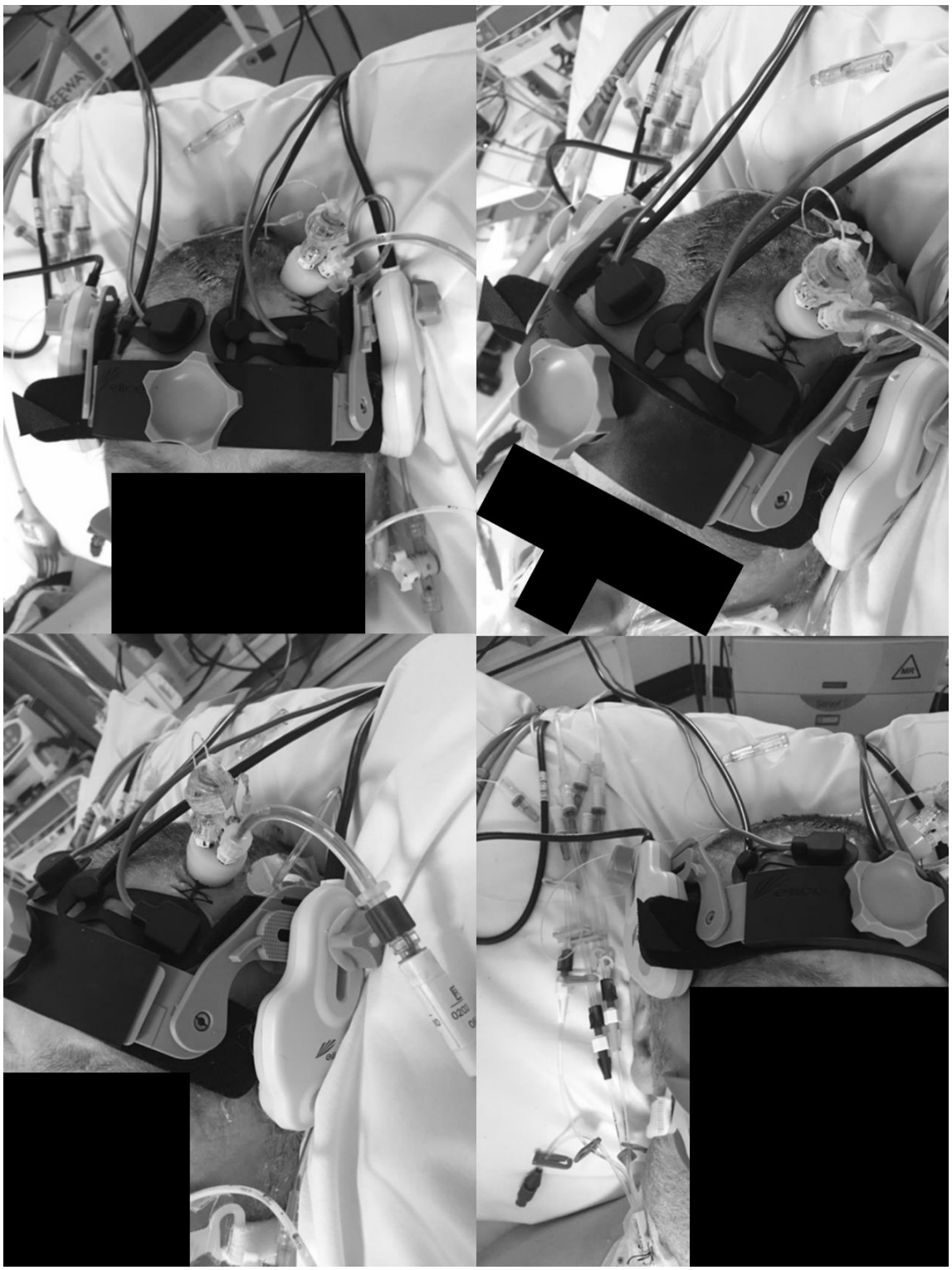

Patient has triple bolt located in left frontal area, with bifrontal NIRS pads applied (all images). Delica TCD head-band can be seen crossing the forehead, just above the orbital rims. Wheel for ratchet tightening of headband can be seem (both upper left and right images). Robotic drive/TCD probe can be seen over transtemporal window, insonating the MCA (upper right and lower left images).

Advantages

With above described set-up, extended length recordings were possible, with non-interrupted, good quality TCD signals. The TCD probe held ultrasound gel for 4 hours without any drying issues or need for re-application. Both the recording length and gel integrity duration are far longer than most standard TCD systems can provide. Furthermore, bilateral MCA TCD was captured, in the presence of all other multi-modal monitoring devices described, confirming its applicability in the multi-monitoring moderate/severe TBI patient.

The head-band appeared to be comfortable, with the padding protecting surgical wounds from injury, and rarely moving once secured. Once in situ, the head-band, with attached robotic drive/TCD probes tolerated patient turning in each patient, without loss of CBFV waveform or intensity. Furthermore, two patients underwent portable chest x-ray while recording, with no change in signal intensity throughout this procedure. Finally, one patient underwent a bedside chest-tube insertion without change in signal quality.

The robotic drive system worked well, with the search and directional functions aiding with set-up and re-acquisition of signal if it needed to be optimized. The algorithms for these two functions appeared to work well, finding the optimal angle and position of insonation.

Disadvantages

The system suffered from a few important initial issues/limitations, which require highlighting. The main issues stemmed from initial poor real-time functioning of certain aspects of the robotic drive system. As mentioned above, the search and direction functions appear to work satisfactorily. However, the two other functions (scan and track), within the initial version of the system, were less useful. The scan function, within all patients recorded, failed to select automatically the appropriate optimal position for insonation. This occurred during repeated attempts. As a result, it was elected to manually position the probe using the CBFV waveform and M-mode, selecting an appropriate starting position and depth for insonation. The search and direction functions were then applied, which provided improvement and overall optimization of the signal acquired. This issue was raised with the manufacturer, who responded promptly with a software update, leading to a remedy to the scan function. This was subsequently trialed on additional patients, confirming its functionality and fix to the previous issues.

As well, with the initial software version, the track function rarely appeared to work. This was a disappointment, as the hope with this function is that the drive would automatically correct for any shift in the probe during recording. There were two issues we found with this function in the initial software version. First, despite being enabled, it was rarely triggered, even in the rare case when the headframe/probe shifted and lost signal. Second, when the track function was triggered, one could audibly identify that the robotic drive was attempting to move the TCD probe, however it never appeared to accurately correct the probe for signal loss. Both issues were likely a result of inefficiencies in the embedded algorithm for the track function. As with the scan function, concerns were raised with the manufacturer and resolved with a subsequent, more recent version of the software. Trialing this updated software version on additional patients, the track function was correctly engaged during shift of the probe, and corrected the probe position/angle, optimizing the CBFV signal.

Finally, as observed that in one patient with scalp soft tissue bruising, the ratcheting head-band triggered a sustained intra-cranial pressure elevation above 20 mm Hg lasting 5 minutes, with an initial baseline ICP of 10 to 15 mm Hg. This was promptly resolved by re-adjusting the head-band. In this one patient however, the sedation was relatively light, and thus the ICP elevation was likely secondary to pain experienced during the head-band tightening. Nevertheless, this is an important potential complication to highlight.

Summary of Experience:

The current Delica EMS 9D robotic TCD system provides the ability to obtain 4+ hours of continuous, uninterrupted bilateral TCD recordings in critically ill TBI patients, undergoing other various invasive/non-invasive multi-modal monitoring. Further, the automated algorithms aid in TCD set-up and optimization of signal intensity.

7.3 Predicting Pressure Reactivity Index Using TCD

7.3.1 Introduction

Given the results of section 7.1 of this thesis,[184] the next natural step is to explore the ability to predict PRx using non-invasive TCD measures, such as Sx_a and/or Mx_a. This has never been attempted before, given complexity of analysis and limitations surrounding acquisition of continuous longer uninterrupted TCD recordings. The goal of this study was to outline the first experience at predicting PRx using non-invasive Sx_a, derived from extended duration robotic TCD recordings (see section 7.2 for description of set-up).

7.3.2 Methods

Patient Population

The data utilized in study consisted of part of a prospective observational study conducted over a 6-month period. All patients suffered from moderate to severe TBI and were admitted to the neurosciences critical care unit (NCCU) at Addenbrooke's Hospital, Cambridge, during the period of November 2017 to May 2018. Patients were intubated and sedated given the severity of their TBI. Invasive ICP monitoring was conducted in accordance with the BTF guidelines.[150] Therapeutic measures were directed at maintaining ICP less than 20 mm Hg and CPP greater than 60 mm Hg.

Ethics

TCD monitoring is a part of standard intermittent cerebral monitoring within the NCCU. The application of the newer robotic TCD device (see description below) was therefore in alignment with usual care, negating the need for formal direct or proxy consent. All data related to patient admission demographics and high frequency digital signals from monitoring devices were collected in an entirely anonymous format, negating the need for formal consent, as in accordance with institutional research committee policies.

Signal Acquisition

This was conducted identically to the methods described in section 6.3.2. TCD assessment of MCA CBFV was conducted via a robotic TCD system, the Delica EMS 9D (Delica, Shenzhen, China, www.delicasz.com). This system allows for continuous extended duration recording of MCA CBFV, using robotically controlled TCD probes, with automated correction algorithms for probe shift.

The goal of the initial study from which this data was analyzed was to obtain extended duration recording of ICP, near infrared spectroscopy (NIRS) and TCD. This study aimed to record 3 to 4 hours of continuous data from all devices simultaneously, given the previous work on inter-index relationships focused on recording durations of only 0.5 to 1-hour duration due to limitation of conventional TCD. As such, this data set also proved to be ideal for complex time series modelling and forecasting analysis. Only patients with 3 or more hours of continuous, uninterrupted, ICP and TCD recordings were utilized for this study. Thus, only a sub-population of the group from the original study were utilized for this analysis.

Signal Processing

This was conducted identically to the methods described in section 6.3.2.

Cerebrovascular Reactivity Indices

This was conducted identically to the methods described in section 6.3.2. Diastolic flow index (Dx_a) was not derived in this study, given the previous work documenting poor time series and linear mixed effects (LME) model performance in relation to PRx (section 7.1.3). Data for this analysis were provided in the form of a minute by minute time trends of the parameters of interest for each patient. This was extracted from ICM+ in to comma separated values (CSV) datasets, which were collated into one continuous data sheet (compiled from all patients).

Statistical Analysis

Similar statistical modelling approach as seen in the previous work for time series data and LME model creation were followed with this data set (section 7.1.2), and almost identical statistical description to this work will be found below.[184] Minute-by-minute time series data was utilized for the entirety of the analysis described below. Statistical significance was set at an alpha of less than 0.05. All statistical analysis was conducted using R statistical software (R Core Team (2016). R: A language and environment for statistical computing. R Foundation for Statistical Computing, Vienna, Austria. URL https://www.R-project.org/). The following packages were utilized during the analysis: dplyr, ggplot2, ggthemes, tseries, forecast, lubridate and lme4.

The statistical methods sections to follow will outline the techniques employed to: A. estimate the autocorrelative structure of PRx in time series, B. create an accurate model estimating PRx using non-invasive TCD indices of cerebrovascular reactivity via application of linear mixed effects (LME) modelling (with embedded PRx autocorrelative error structure) , C. assess the correlation and agreement between model based estimated PRx and the observed PRx values, and D. forecast PRx using the derived LME models and estimated PRx time series data. For LME model creation/training the 1st 80% of the data was utilized for each patient, with the remaining 20% utilized for the prediction of PRx using the LME models.

Autocorrelative Structure of PRx

Prior to being able to model PRx using TCD based indices, it was necessary to determine the autocorrelation structure of PRx. Box-Jenkin's autoregressive integrative moving average (ARIMA) modelling was employed for PRx to determine: the autoregressive structure of order "p", the differencing factor or order "d", and the moving average component of order "q"; commonly denoted "(p,d,q)".[163,164] The autoregressive structure refers to the dependence of PRx at time t (denoted PRx_t) on previous measures of PRx (ie. called "lags"), say at time t-1 (ie. PRx_{t-1}), and so forth (ie. say to PRx_{t-p}), with the order "p" indicating how many previous PRx measures PRxt is dependent on. The differencing component refers to the need to make a non-stationary signal stationary, with seasonal or trending structure within a time series indicating non-stationary character. Stationarity is defined as the presence of a stable variance, autocorrelative structure and mean over time. Stationarity can be introduced by differencing previous PRx measures from current measures, thus removing seasonality or trending

structure to a time series, and allowing further modelling to occur. The differencing order "d" refers to how many previous terms should be included in the differencing process. Finally, the moving average term refers to the need to include the error in the model at time t (ie. ε_t) based on its association in previous measured error terms (ie. ε_{t-q}). The order "q" for the moving average component refers to how many previous error terms are to be included within the ARIMA model. Assuming stationarity (ie. no "d" order), a general ARMA model can be represented by the following formula:

$$PRx_t = c + \varepsilon_t + \sum_{i=1}^{p} \varphi PRx_{t-i} + \sum_{i=1}^{q} \theta \varepsilon_{t-i} \quad (7.1)$$

Where: PRxt = PRx at time t, PRxt-i = PRx at time t-i, εt = error at time t, εt-i = error at time t-i, c = constant, ϕ and θ are parameters at time t-i, p = autoregressive order, and q = moving average order.

The following process was conducted on all patient recordings, in order to derive the optimal ARIMA structure for PRx time series. This would provide insight into the approximate best ARMA structure for future LME models.

First, data had already been artifact cleared and had a 10-second moving average filter applied to the data, leading to some data smoothing (as described above in the signal processing section). Thus, the initial step for the ARIMA modelling focused on determining stationarity of the signal. This was assessed, and confirmed, using 3 methods. First, the autocorrelation function (ACF) correlogram was assessed for PRx, looking for a rapid decline in significant lags, indicating a stationary signal. Second, the Augmented Dickey Fuller (ADF) test was employed to assess for stationarity. Third, seasonal decomposition was employed using the like-named function in R for each PRx time series, which employs locally weighted scatterplot smoothing (LOESS) to identify seasonal and trend components to a time series. All above processes confirmed stationarity within the patient examples.

Second, the autoregressive structure of PRx was assessed using the ACF correlograms and partial autocorrelation function (PACF) correlograms. ACF correlograms were assessed to see how many previous consecutive terms (ie. "lags") PRx may be dependent upon. Similarly, the PACF correlograms were assessed to see how many non-consecutive previous lags, PRx may be dependent upon. Significant level on ACF/PACF correlograms is set at a correlation level of $+/-(2/N^{1/2})$,[163] where N = sample size. Sequential ARMA models for PRx we run, by varying the order "p" from 0 to 3, while also varying the moving average order "q" from 0 to 3. Given the analysis for stationarity confirmed a stationary signal

within the 10 patient examples, we fixed the differencing order "d" at 0. In doing so, 16 separate ARMA models were generated for PRx within each patient. Model superiority was assessed by Akaike Information Criterion (AIC) and Log-Likelihood (LL), with the lowest AIC and highest LL indicating the best ARMA model for PRx.[159,163,164,166,188] In addition, model superiority was assessed via residuals, model ACF and PACF correlograms, with an adequate model represented by random residuals, and ACF/PACF failing to display any lags reaching significance.

LME Modelling of PRx Using TCD Derived Indices

LME modelling was conducted on the entire patient population. LME modelling involved various fixed linear models, and a random component introduced into the intercept and independent variable coefficient (based on individual patient). The PRx ARIMA structure was embedded within the LME models (ie. (2,0,2)). This analysis was done on the full data set, deriving LME models for each patient as well as for the entire population. The following LME models were assessed, initially with random intercept only (stratified by patient), as above: PRx ~ Sx_a, PRx ~ Mx_a, and PRx ~ Sx_a + Mx_a. All models were corrected using maximum likelihood estimation method. Adequacy of the LME model was assessed via QQ plots and the residuals distribution plot, with linear shape to the QQ plots and normally distributed residuals confirming validity of the model.

Models were compared using AIC, Bayesian Information Criterion (BIC), LL and analysis of variance (ANOVA) testing. Superior models were attributed to the lowest AIC, lowest BIC and highest LL. Significance between models as assessed by ANOVA testing was set at a $p < 0.05$. The top 2 superior LME models were reported in detail, with a final assessment of model adequacy through ACF/PACF plots of the model residuals, observing for a minimal number of significant lags which decay rapidly.[163,164,166]

Generalized fixed effects models were also created based on the top two LME models. However, these models performed poorly, with substantially inferior AIC, BIC and LL values. In addition, these general fixed effects models maintained continuous significant lags in the residuals, further indicating poor modelling of PRx. Hence, these models will not be discussed further.

Observed versus Estimated PRx

The correlation between the observed (minute-by-minute) PRx values in the population versus those estimated from our optimal two LME models was assessed using Pearson correlation coefficient. Linear regression plots were then produced between observed and estimated PRx for the best two LME models, using grand mean data (ie. mean value per patient). Finally, Bland-Altman plots were produced to assess agreement between the observed and estimated PRx values, using grand mean Fisher transformed data (ie. Fisher transform applied to both observed and estimated PRx). Bland-Altman determination was conducted via the following method: estimated PRx – observed PRx.

Predicting PRx

PRx was then predicted based on the top two LME models from the above discussed methods. Using the LME models themselves and the remaining 20% patient data not used in LME creation, predicted PRx (pPRx) values were derived from observed Sx_a and Mx_a values within this data subset. The predicted values were then compared to the actual observed PRx values during this period using Pearson correlation, linear modelling and Bland-Altman analysis. Bland- Altman determination was conducted via the following method: pPRx – observed PRx.

7.3.3 Results

a. Patient Demographics

A total of 10 patients with moderate/severe TBI had sufficient quality TCD signals (ie. at least 3 – 4 hours duration and uninterrupted). The mean age for this population was 34.5 +/- 17.0 years, with 8 patients being male. The median admission GCS was 7 (IQR 4 to 8), with median admission GCS motor score of 4 (IQR 2 to 5). The mean duration of ICP/TCD recording was 223.2 +/- 38.4 minutes. Only 80% of the total recording duration for each patient was utilized for model formation and training, with the remaining 20% reserved for predictive testing.

b. Building the Model to Estimate PRx

ARIMA Modelling of PRx

In all 10 patients the ARIMA structure of PRx was investigated in order to determine the appropriate structure for future LME modelling of the entire population. Upon inspection of the ACF/PACF plots, ADF test results and seasonal decomposition techniques, it was determined that no significant trend or seasonality were present in any of the 10 patient recordings. Thus, no differencing order "d" was introduced. Next, sequential ARMA models were produced for each patient, varying the autoregressive order "p" and moving average order "q", from 0 to 3. Across all patients the optimal ARMA model for PRx was deemed to be a p of 2 and q or 2 (ie. (2,0,2)), based on the principal of parsimony, and the lowest AIC and highest LL. Figure 7.11 displays the ACF and PACF plots of PRx for one patient with 4 hours of continuous recording, demonstrating a rapid decay in significant lags (implying stationarity). Figure 7.12 demonstrates the ARMA model for PRx in the same patient, with an ARMA structure of (2,0,2). This figure demonstrates a lack of significant lags on ACF and PACF plots, with randomly distributed residuals, confirming adequacy of the model.

Figure 7.11: ACF and PACF for PRx – Patient Example

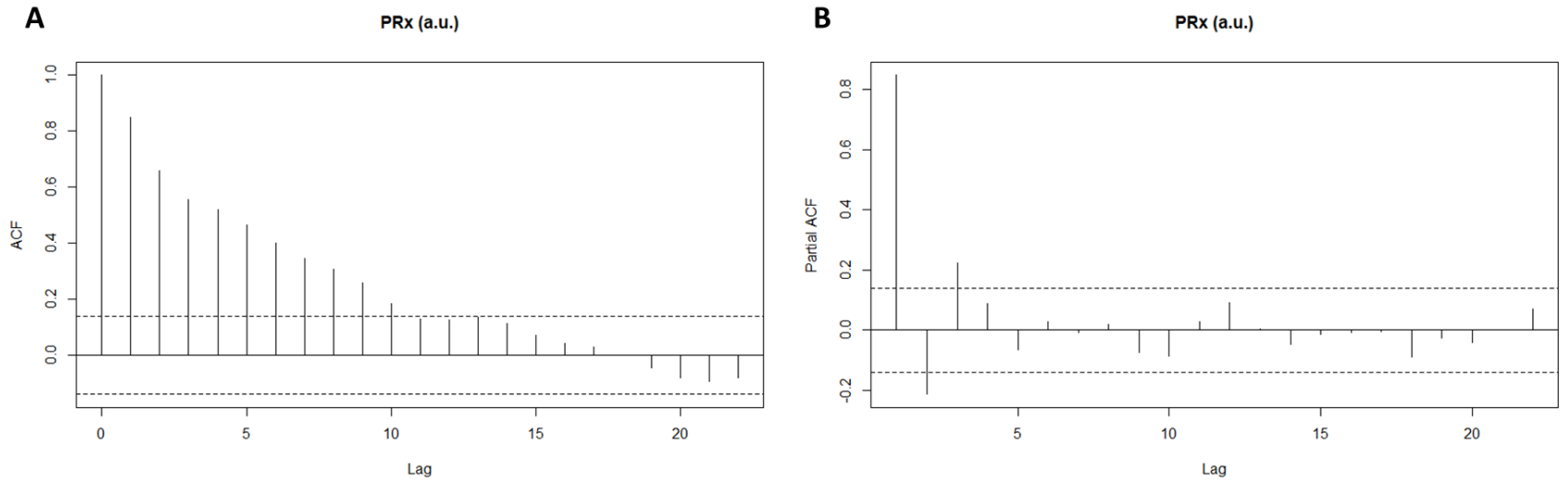

ACF = autocorrelation function, a.u. = arbitrary units, PACF = autocorrelation function, PRx = pressure reactivity index (correlation between intracranial pressure and mean arterial pressure). Panel A: ACF plot displaying a rapid decay of significant PRx lag, suggesting stationarity. Panel B: PACF plot, also displaying rapid decay of significant PRx lags.

Figure 7.12: ACF, PACF and Residual Plots for PRx (2,0,2) ARIMA Model – Patient Example

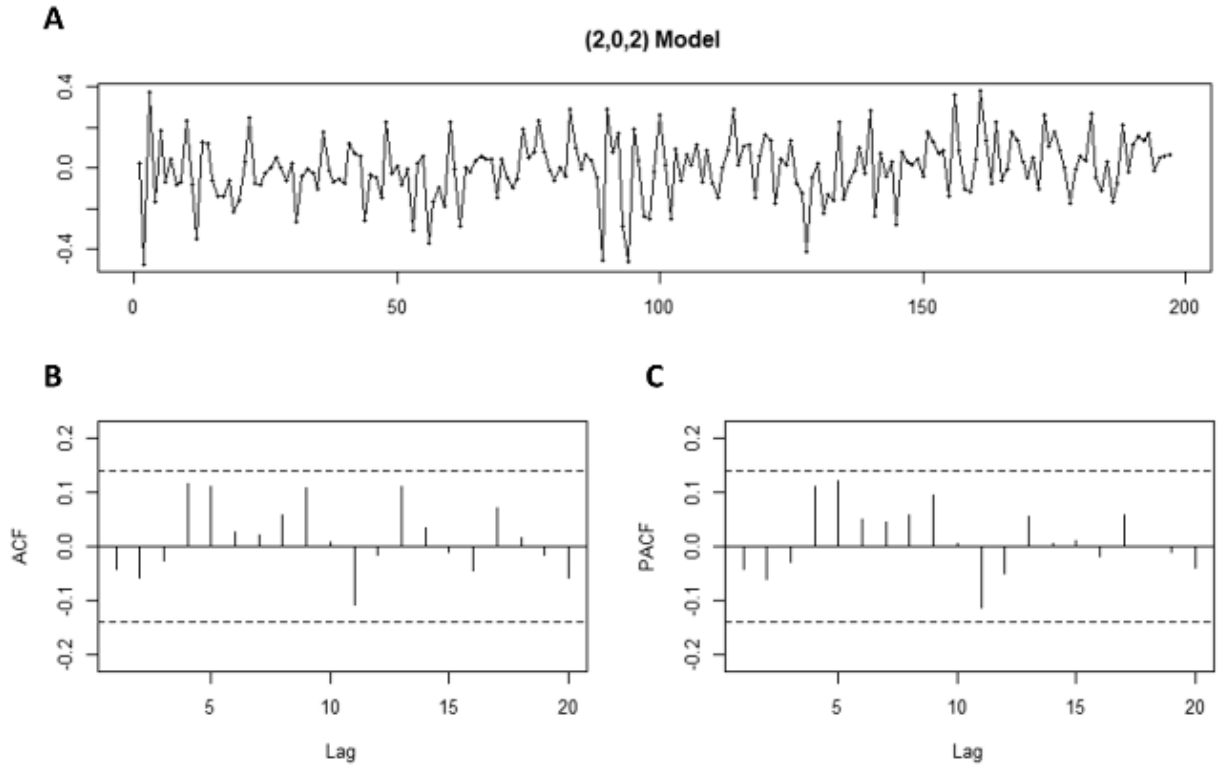

ACF = autocorrelation function, PACF = autocorrelation function, PRx = pressure reactivity index (correlation between intracranial pressure and mean arterial pressure). Panel A: displays the residual plot for the ARIMA model in this patient example. Panel B: ACF plot displaying no significant lags with (2,0,2) ARIMA model for PRx. Panel C: PACF plot, also no significant lags with (2,0,2) ARIMA model for PRx.

c. Model Development and Accuracy Assessment

LME Modelling of PRx Using TCD Indices

Using the (2,0,2) PRx ARMA structure identified within the individual patients, various LME models were produced, embedding the PRx ARMA structure within. Table 7.3 displays the model characteristics for those LME models derived from Sx_a and Mx_a, introducing random effects by patient into the intercept and coefficients. Model superiority was confirmed via ANOVA testing, with the lowest AIC/BIC and highest LL, indicating superiority. The top two LME models were: PRx ~ Sx_a (AIC = -1564.957, BIC = -1510.159, LL = 792.4786) and PRx ~ Sx_a + Mx_a (AIC = -1597.345, BIC = -1520.627, LL = 812.6726); with random effects by patient introduced into both the coefficients and intercept. The QQ and residual density plots for these top two LME models can be seen in Appendix E, displaying normally distributed residuals, indicating model adequacy. The ACF and PACF plots for these two models can also be found in Appendix E, displaying acceptable rapid decay of significant lags.

Population Based Estimation of PRx Using Sx_a and Mx_a

Using the top two LME models described above, PRx was estimated using the available Sx_a and Mx_a measures in the training data set. Grand mean values were calculated per patient and plotted against the observed PRx values from the data. A strong linear relationship was seen between estimated and observed PRx using both LME models. Figure 7.13 displays estimated versus observed PRx plots for each model. The PRx ~ Sx_a model displayed a correlation between estimated and observed values of 0.998 (95% CI = 0.990 – 0.999; $p<0.0001$), while the PRx ~ Sx_a + Mx_a model had a correlation between estimated and observed PRx values of 0.997 (95% CI = 0.988 – 0.999; $p<0.0001$). Bland-Altman analysis on Fisher transformed results displayed acceptable agreement, with slight underestimation bias in the estimated PRx for both models. This bias in the Bland-Altman plots was seen in our previous work as well. Appendix E contains the results of the Bland-Altman analysis comparing the estimated to observed PRx for both LME models.

Table 7.3: LME Models with PRx (2,0,2) ARIMA Structure – Entire Population

LME Model		**PRx ARIMA Structure**		**AIC**	**BIC**	**LL**
Fixed Effects	**Random Effects**	**P**	**q**			
PRx ~ Sx_a	intercept	2	2	-1543.672	-1499.833	779.8362
PRx ~ Mx_a	intercept	2	2	-1502.348	-1458.509	759.1738
PRx ~ Sx_a + Mx_a	intercept	2	2	-1550.704	-1501.385	784.3520
PRx ~ Sx_a	**Intercept + Sx_a**	**2**	**2**	**-1564.957**	**-1510.159**	**792.4768**
PRx ~ Mx_a	Intercept + Mx_a	2	2	-1516.367	-1461.569	768.1836
PRx ~ Sx_a + Mx_a	**Intercept + Sx_a + Mx_a**	**2**	**2**	**-1597.345**	**-1520.627**	**812.6726**

*AIC = Akaike Information Criterion, ARIMA = auto-regressive integrative moving average, BIC = Bayesian Information Criterion, FVm = mean TCD flow velocity, FVs = TCD based systolic flow velocity, ICP = intra-cranial pressure, LL = log likelihood, LME = linear mixed effects model, p = auto-regression parameter for ARIMA model, MAP = mean arterial pressure, PRx = pressure reactivity index (correlation between ICP and MAP), q = moving average parameter for ARIMA model, Sx_a = systolic flow index (correlation between TCD based FVs and MAP), TCD = transcranial Doppler. *Note: bolded value represents the most appropriate ARIMA structure and LME model for the patient population tested, based on principal of parsimony, lowest AIC and BIC. There was no integrative parameter (ie. "d" parameter) included within the ARIMA models, given stationarity testing during patient examples (see appendix A and Methodology section of manuscript).*

Figure 7.13: Linear Regression Between Observed and Estimated PRx – Using Estimated PRx From Two Best LME Models

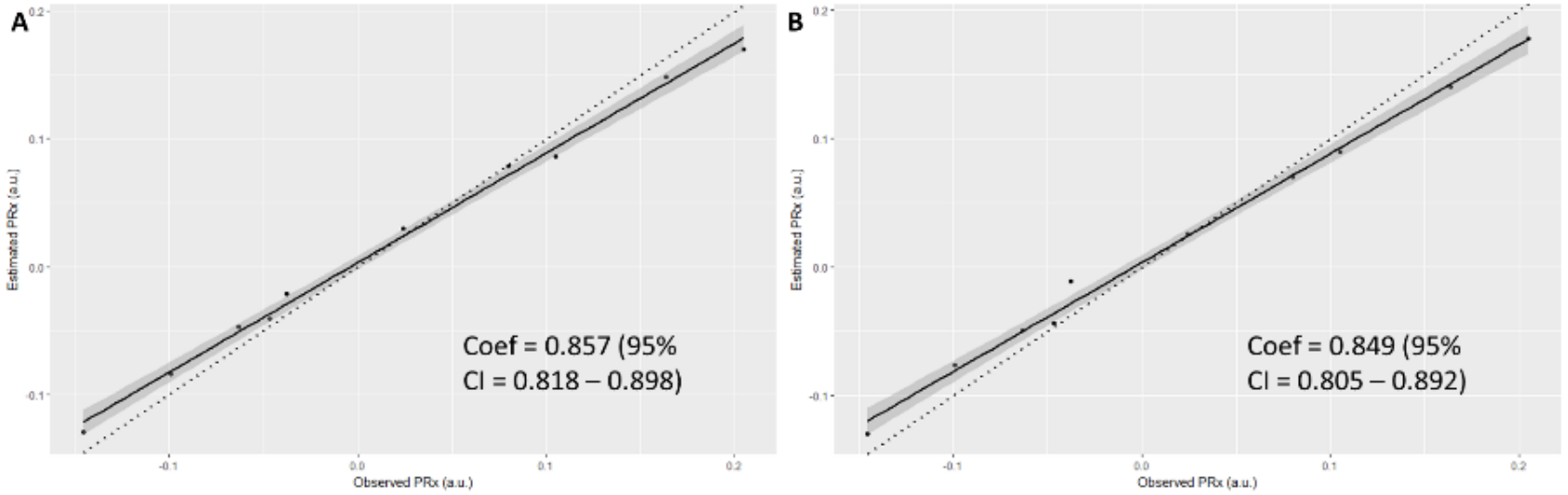

a.u. = arbitrary units, ICP = intracranial pressure, LME = linear mixed effects, MAP = mean arterial pressure, PRx = pressure reactivity index (correlation between ICP and MAP). Panel A: LME model – PRx ~ Sx_a (random effects with intercept and Sx_a), Panel B: LME model – PRx ~ Sx_a + Mx_a (random effects with intercept, Sx_a and Mx_a). Coef = coefficients, form linear model between observed PRx and model estimated PRx. Dotted straight line – represents the relationship "y = x", for comparison to our two models.

d. Predicting PRx Using Non-Invasive TCD Parameters

Using the top two LME models derived above, predicted PRx (pPRx) was derived via the 20% of data not used in model construction/training. Each patient had 20% of their recording data excluded from the prior model formation/training, each with ICP and TCD derived variables, amounting to ~30 to 60 minutes of minute-by-minute data per patient. For each LME model, the Sx_a and Mx_a values from this new data were entered into the models to derive pPRx. Grand mean values were then calculated per patient. For the model PRx ~ Sx_a, the correlation between predicted and observed PRx values was 0.797 (95% CI = 0.336 – 0.949; p=0.006). Similarly, for the model PRx ~ Sx_a + Mx_a, the correlation between predicted and observed PRx was 0.763 (95% CI = 0.258 – 0.941; p=0.011). Predicted and observed PRx values displayed a linear association, though not 1:1. Figure 7.14 displays the predicted versus observed PRx plots for the top two LME models. Bland-Altman analysis of Fisher transformed data demonstrated acceptable agreement between predicted and observed PRx values, with similar underestimation of the predicted PRx values as seen in the training data previously. All Bland-Altman test results for comparing pPRx to observed PRx can be found in Appendix E.

Figure 7.14: Linear Regression Between Observed and Predicted PRx – Using Predicted PRx From Two Best LME Models

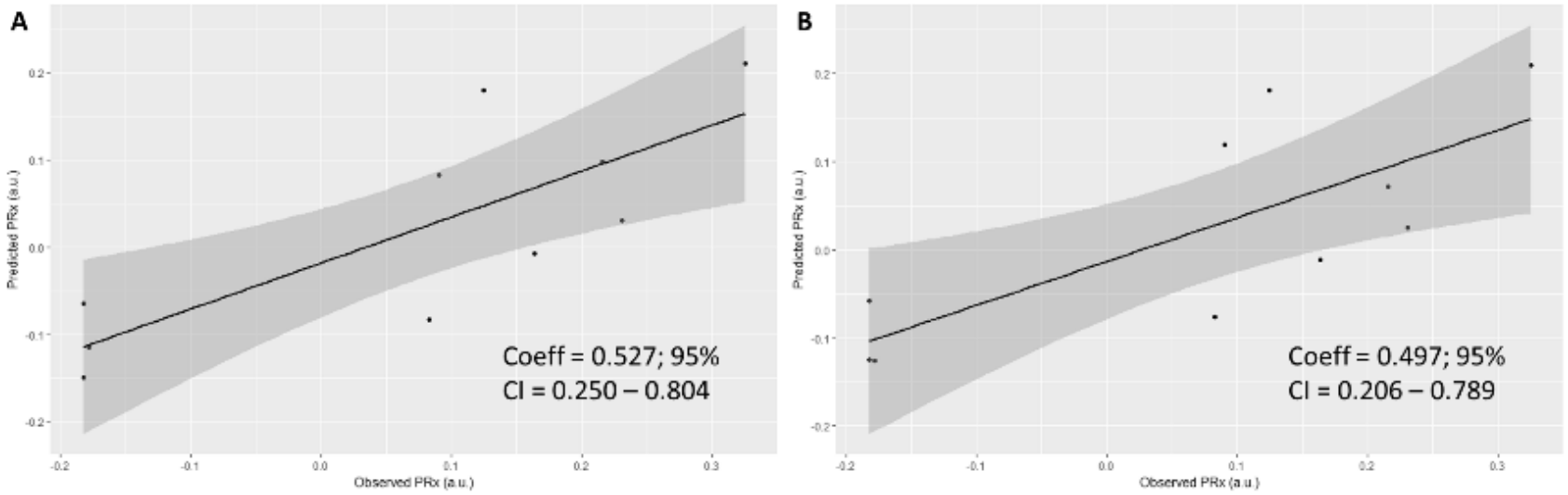

a.u. = arbitrary units, ICP = intracranial pressure, LME = linear mixed effects, MAP = mean arterial pressure, PRx = pressure reactivity index (correlation between ICP and MAP). Panel A: LME model – PRx ~ Sx_a (random effects with intercept and Sx_a), Panel B: LME model – PRx ~ Sx_a + Mx_a (random effects with intercept, Sx_a and Mx_a). Coef = coefficients, form linear model between observed PRx and model estimated PRx.

7.2.4 Discussion

Through the application of time-series ARMA and LME modelling in this pilot study, for the first time the prediction of PRx using non-invasive TCD measures (ie. Sx_a and Mx_a) has been described. Some important aspects of this preliminary pilot work require highlighting.

First, through the application of ARMA modelling of PRx, and LME modelling of PRx using TCD measures, in this unique cohort of patients with extended duration continuous TCD recordings, LME models that accurately estimate observed PRx can be produced. This is similar to prior retrospective work in a large TB population with TCD.[184] Further, the superior two models from this current cohort were of similar ARMA and mixed-effects structure to those discovered in the prior work, as confirmed through the principal of parsimony. This provides some validation of the previous work, and also provides some evidence to support these models regardless of the duration of TCD recording analyzed. In addition, the bias on Bland-Altman analysis comparing observed to estimated PRx displayed the same underestimation bias seen in the previous work, with acceptable agreement. Finally, is provides prospective confirmatory evidence of the strong relationship between PRx and Sx_a in longer duration recordings.

Second, as with the previous work,[184] the general fixed effects versions of the top two models performed poorly in estimating PRx, with continuous significant autocorrelation in the model residuals. As mentioned within the methods section, these models were subsequently not reported further. This again confirms patient-by-patient heterogeneity, limiting the extrapolation of this work to other general TBI populations.

Third, for the first time in the literature the ability to predict PRx using non-invasive TCD surrogates has been demonstrated. Comparing pPRx to the observed PRx values in the top two models, the correlation is of moderate strength with a linear relationship between the two and acceptable agreement on Bland-Altman analysis. However, a similar underestimation bias for pPRx is present on Bland-Altman analysis. Further, the relationship between pPRx and the observed PRx was not 1:1, indicating the prediction is not perfect. Further work is required to optimize the prediction models.

Finally, this work is based on only 10 patients and is entirely preliminary with results that are not generalizable at this time. Thus, this type of modelling and prediction of PRx should not be conducted outside of a research setting. Much further work is required for validation.

Limitations

Despite the interesting results of this analysis, there are some important limitations which require highlighting.

First, as with the previous work in this area, the patient population was heterogeneous in terms of age, intra-cranial injury patterns and therapies directed at ICP/CPP goals. These heterogeneities could impact signal fluctuations and the results obtained for the time series modelling conducted. Though in comparison to the larger time series work in TBI, the results of the modelling within this preliminary pilot study were similar, as described above.[184]

Second, patient numbers were small, at only 10. For the purpose of this type of analysis the desire was to only look at patients with 3 to 4 hours of completely uninterrupted ICP and TCD recordings. This limited the size of this unique patient population, given technical limitations around TCD. Thus, the results here are quite preliminary and should be considered experimental at this point. This requirement for interrupted continuous TCD is a significant limitation with the described modelling and forecasting processes, as conventional TCD is currently heavily limited by artifact and signal loss. The application of robotic TCD mitigated this in the study, however this technology is relatively new and not without limitations, including patient eligibility (ie. no decompressive craniectomy, no cervical spine immobilisation collars, etc.) and substantial cost. Furthermore, even with the application of robotic TCD, it still posed difficult to obtain continuous extended duration recordings. As robotic and automatic TCD technology improves, it is expected to be able to obtain extended duration uninterrupted recordings throughout a patient's ICU stay. Thus, even though the current results are limited given patient numbers, they provide the platform for future applications once technology catches up with the demands of this type of modelling/prediction.

Third, the ARIMA structure highlighted for PRx, and the LME models within this study may not be widely applied outside this population. This was also mentioned in the previous publication on this topic.[184] There exists the potential for patient specific ARIMA structures, and thus the models described in these studies should not be applied clinically. Furthermore, as mentioned above, the general fixed effects versions of the top two models performed poorly in the estimation of PRx, with continuous significant residual lags. This also suggests significant patient-by-patient heterogeneity, negating the extrapolation of these results to other general TBI populations at this time. Much further work on PRx, amongst other

physiologic measures in TBI, is required in larger patient populations in order to determine the exact high frequency time series behavior. This is a work in progress for us currently.

Finally, the statistical methodology employed within this study is quite complex, requiring numerous steps, and is fraught with difficulties. Thus, the wide spread applicability of these techniques is currently limited. However, based on the results of this work with time series data in TBI, the plan is to develop custom functions for ICM+ software, allowing for a much more user-friendly application of such modelling and forecasting/prediction techniques. Such functions will automate much of the analysis described in these works on time series (ie. sections 7.1 and 7.3), requiring limited user input. This will hopefully bring this type of work to the wider clinical world for future multi-center validation studies.

7.2.5 Conclusions

Through the application of ARMA and LME modelling, it is possible to predict PRx using non-invasive TCD measures, such as Sx_a and Mx_a. This is the first preliminary attempts at doing so. Much further work is required prior to application within a clinical setting, as this the current work should be considered experimental at this time.

CHAPTER 8: CRITICAL THRESHOLDS FOR CEREBROVASCULAR REACTIVITY INDICES AND OUTCOME PREDICTION IN ADULT TBI

*The study results described in sections 8.1 and 8.2 can also be found detailed in the following respective publications:

1. Zeiler et al., *J Neurotrauma*. 2018; 35(10):1107-1115. doi: 10.1089/neu.2017.5472.[152]

2. Zeiler et al., *J Neurotrauma*. 2018; 35(2):314-322. doi: 10.1089/neu.2017.5364.[182]

8.1 ICP Derived Indices of Cerebrovascular Reactivity

8.1.1 Introduction

ICP derived continuous indices of cerebrovascular autoregulation are currently employed in some ICU's, particularly in the MMM of TBI patients.[11,12] The two most quoted ICP derived indices are PRx[3] and PAx.[15] As well, within Chapter 4 of this thesis, a new index of cerebrovascular reactivity, RAC, was explored.[21] All three of these ICP based indices have been interrogated in experimental models, as described in Chapter 5 of this thesis, with some preliminary evidence to suggest they provide some measure of the LLA.

To date, PRx has received most attention, both in terms of published literature and clinical application. PRx has displayed strong associations with patient outcome, with published thresholds of PRx associated with mortality and morbidity at 6 months in a mixed TBI population.[9] The use of PRx as a surrogate assessment of cerebral autoregulatory status has received support from recent multi-modal monitoring consensus statements,[11] and has been applied in the estimation of individual patient "optimal" CPP.[144]

However, the basis for such use of PRx leaves some issues unanswered. The PRx thresholds for poor functional outcome at 6-months (ie. PRx > 0) and mortality (ie. PRx > +0.25) were derived from a large cohort or heterogenous TBI patients, including some who were post-DC.[9] PRx calculation is known to be impacted by craniectomy in TBI, making its reliability uncertain, at least initially, after removal of the calvarium.[22] Furthermore, recent literature supports a potential superior capability of PAx over PRx in the prediction of patient outcome, within the subgroup of patients with "low" ICP (defined as less than

15 mm Hg).[15] However, the literature addressing PAx in TBI is limited, with few studies suggesting an association with outcome, and no definition of clear threshold values that predict outcome. Finally, based on the results from Chapters 4 and 5 of this thesis, RAC shows promise as an index of cerebrovascular reactivity.[21]

Most critically for clinical use, there is no documented comparison of these three ICP-derived indices as they relate to mortality and functional outcome at 6 months, and the critical thresholds of each of these indices which are associated with poor outcome. Furthermore, all descriptions of outcome associations and threshold values for these indices is confounded inclusion of patients following DC, and their performance has not been described in a purely non-DC TBI patient population, potentially mitigating the poorly understood impact of craniectomy on these continuous indices of cerebrovascular reactivity.

The goal of this study in non-DC TBI patients was to: A. compare the association to outcome of all three ICP derived indices (PRx, PAx and RAC), B. compare the thresholds of each index which are most associated with morbidity and mortality, C. conduct both outcome and threshold analysis for these indices across various timeframes/lengths of signal recording.

8.1.2 Methods

Patient Population and Demographic Data Acquisition

This population is identical to the one described in Chapter 4.[21] All patients (n=358) were admitted to the NCCU at Addenbrooke's Hospital, Cambridge, during the period of March 2005 to December 2016. In addition, only patients with at least 6 hours of recorded signals were included in this study. Patients suffered either moderate to severe TBI, or mild TBI and subsequently deteriorated to a point where they required ICP monitoring and sedation and mechanical ventilation as part of ICP management. Treatment received during the recording periods included standard ICP-directed therapy, with an ICP goal of less than 20 mm Hg and CPP goal of greater than 60 mm Hg.

The following patient demographic data was obtained from the database: age, sex, admission Glasgow Coma Scale (GCS), and patient outcome at 6 months. Patient outcome was assessed via the Glasgow Outcome Score (GOS) at 6 months and stored prospectively within the database. For purpose of the outcome and threshold analysis, we dichotomized the GOS into two binary outcomes of interest: A. Favourable (GOS of 4 or 5) vs. Unfavourable (GOS of 3 or less), and B. Alive vs. Dead.

Signal Acquisition

See Chapter 4.2 for details on signal acquisition.

Signal Processing

See Chapter 4.2 for details on signal processing. The following variables were derived: ICP, MAP, AMP, PRx, PAx, RAC and RAP.

Finally, data for this analysis were provided in the form of a minute by minute time trends of the parameters of interest for each patient. This was extracted from ICM+ in to CSV datasets, which were collated into one continuous data sheet (compiled from all patients). From this, separate data sheets for: entire recording period for each patient (n=358), 1st 24 hours of recording (n= 340), 1st 72 hours of recording (n=277), 1st 5 days of recording (n=217), 1st 7 days of recording (n=163), and 1st 10 days of recording (n=101) were produced in order to assess the association to outcome, and thresholds, across various durations of recording. The difference in patient numbers between time periods of analysis is secondary to both death and discontinuation of high-resolution physiologic recording.

This staged analysis was conducted in order to determine if the outcome relationships and thresholds seen in the total recording period (as used in previous works on PRx and PAx), continue to hold true within various recording periods after TBI. Within these separate data sheets, a grand mean per patient was calculated for each index across the duration of that recording period and subsequently utilized for the final statistical analysis.

Statistics

Statistics were performed utilizing XLSTAT (Addinsoft, New York, United States; https://www.xlstat.com/en/) add-on package to Microsoft Excel (Microsoft Office 15, Version 16.0.7369.1323) and R statistical software (R Core Team (2016). R: A language and environment for statistical computing. R Foundation for Statistical Computing, Vienna, Austria. URL https://www.R-project.org/). For all statistical tests described, alpha was set at 0.05 for significance.

General Statistics

Simple descriptive statistics for the non-DC cohort were utilized to summarize the patient demographics.

Outcome Analysis

First, a univariate binary logistic regression (ULR) analysis was performed utilizing the three indices (PRx, PAx, and RAC) and two binary outcomes of interest: A. Favourable vs. Unfavourable, and B. Alive versus Dead; both at 6 months post-TBI.

Second, multi-variate binary logistic regression (MLR) was performed using a "baseline" model, including: age, sex, admission GCS, mean ICP, mean AMP, MAP and mean CPP. This "all inclusive" baseline model was selected in order to include all physiologic variables monitored during the patient's ICU stay. This multi-variate analysis was exploratory only, designed to determine which ICP derived cerebrovascular reactivity index was superior in outcome prediction when all other physiologic variables were taken into account. Database records did not contain information regarding pupillary response, GCS motor response, extra-cranial injury burden or admission CT scan injury characteristics. Thus, in the absence of this data, used in current TBI prognostic models, we focused on the demographic data available to us (ie. Age, cumulative GCS and Sex) in addition to the physiologic variables. The goal was not to produce the most significant model for overall outcome prediction, with the minimum number of variables. The goal was, based on the available data, determine which ICP derived index of cerebrovascular reactivity was superior, taking into account as much demographic and physiologic information available. Subsequently, each index was added individually to the baseline model in order to see the difference in both outcomes of interest. Then all indices were added to the baseline model in order to determine which indices remained statistically significant. Finally, PAx and RAP were added to the baseline model, to allow for comparison with the RAC based model – given it is believed that RAC contains both information pertaining to cerebrovascular reactivity and compensatory reserve, based on the results from Chapter 4.

Both of ULR and MLR techniques described above were performed for each recording period: entire recording, 1st 24 hours, 1st 72 hours, 1st 5 days, 1st 7days and 1st 10 days. Strength of relationship to the outcomes of interest were reported via AUC, with bold AUC's reaching a $p<0.05$. For ULR, statistically significant differences in AUC's between PRx, PAx and RAC were tested via Delong's test.

Threshold Analysis

A sequential chi-square method of thresholding was conducted. This technique for threshold analysis has been described in detail within other publications on continuous autoregulation/cerebrovascular reactivity indices in TBI, including PRx. Sequential 2 by 2 binary outcome contingency tables were constructed for each outcome: 6-month dichotomized Favourable vs. Unfavourable GOS, and 6 month Alive vs. Dead. Patients were grouped by Favourable vs. Unfavourable GOS, and Alive vs. dead status based on PRx, PAx or RAC index values above or below sequential thresholds (in 0.05-point steps in the index value). Pearson chi-square was then determined for each 2 by 2 table.

The chi-square test statistic value was then plotted against index threshold (PRx, PAx or RAC). The index threshold value with the largest statistically significant ($p<0.05$) Chi-square value was then deemed the threshold for that outcome of interest (ie. 6-month Favourable vs. Unfavourable outcome, or 6-month mortality). Patients with index values above these thresholds are at highest risk of worse outcome (Unfavourable GOS or mortality).

This entire process was repeated for each index (PRx, PAx and RAC) during each monitoring period: entire recording period, 1st 24hours, 1st 72 hours, 1st 5 days, 1st 7 days and 1st 10 days. This was done to determine the potential variation in PRx, PAx and RAC thresholds associated with different lengths of recording.

8.1.3 Results

Patient Demographics

In total, there were 358 patients included for analysis. All patients suffered mild to severe TBI. In addition, all patients had at least 6 hours of high frequency signals recorded. The mean age was 40.6 +/- 17.2 years (range: 16 to 89) with a median admission Glasgow Coma Scale score of 7 (IQR = 3 to 9; range: 3 to 13). There were 272 males (76.0%), and the mean length of signal recording was 189.1 +/-151.1 hours (range: 8.5 to 1033.0 hours; median = 152.7 hours). The mean ICP, MAP, CPP, AMP, PRx and RAC were: 14.057 +/-7.6 mm Hg, 91.3 +/- 7.9 mm Hg, 77.5 +/- 8.5 mm Hg, 2.3 +/- 1.4 mm Hg, 0.046 +/-0.173, and -0.350 +/- 0.254; respectively. A further breakdown of patient demographics can be seen in Table 8.1, based on the recording period analyzed.

Table 8.1: Patient Demographics by Recording Length Analyzed

	Recording Period					
	Total	**1st 24hr**	**1st 72hr**	**1st 5d**	**1st 7d**	**1st 10d**
N	358	340	277	217	163	101
Mean Age (yrs)	40.6 +/- 17.2	40.6 +/- 17.2	40.2 +/- 17.0	38.78 +/- 15.8	39.2 +/- 15.1	38.4 +/- 14.0
Number of Males	272	258	212	169	124	83
Median Admission GCS (IQR)	7.0 (3 to 9)	7.0 (3 to 10)	7.0 (3 to 9)	6.0 (3 to 9)	7.0 (3 to 9.5)	7.0 (3 to 9)
Mean ICP (mm Hg)	14.1 +/-7.6	15.6 +/- 8.6	14.9 +/- 7.4	15.1 +/- 6.2	15.4 +/- 4.5	15.9 +/- 4.2
Mean AMP (mm Hg)	2.34 +/- 1.39	2.63 +/- 1.67	2.68 +/- 1.43	2.44 +/- 1.15	2.48 +/- 1.12	2.41 +/- 0.96
Mean CPP (mm Hg)	77.5 +/- 8.5	75.2 +/- 9.0	76.3 +/- 7.4	77.4 +/- 7.3	78.8 +/- 5.9	80.2 +/- 5.8
MAP (mm Hg)	91.2 +/- 7.9	90.5 +/- 9.3	91.2 +/- 1.4	92.5 +/- 7.7	94.2 +/- 7.4	96.1 +/- 7.2
Mean PRx	0.05 +/- 0.17	0.01 +/- 0.22	0.00 +/- 0.19	0.00 +/- 0.16	0.01 +/- 0.15	0.00 +/- 0.12
Mean PAx	-0.06 +/- 0.20	-0.07 +/- 0.24	-0.07 +/- 0.20	-0.08 +/- 0.18	-0.07 +/- 0.16	-0.07 +/- 0.14
Mean RAC	-0.35 +/- 0.25	-0.36 +/- 0.29	-0.38 +/- 0.26	-0.38 +/- 0.23	-0.38 +/- 0.20	-0.40 +/- 0.18

AMP = pulse amplitude of ICP, CPP = cerebral perfusion pressure, d = day, GCS = Glasgow Coma Scale, hr = hours, ICP = intra-cranial pressure, MAP = mean arterial pressure, mm Hg = millimeters of Mercury, N = number, yrs = years, PAx = pulse amplitude index (correlation between AMP and MAP), PRx = pressure reactivity index (correlation between ICP and MAP), RAC = correlation between AMP and CPP.

Association with 6-Month Outcome – PRx, PAx and RAC

Univariate Binary Logistic Regression (ULR)

A summary of the ULR AUC's for each index, during each recording period can be seen in Table 8.2 (bolded AUC's indicate a $p<0.05$). In summary, RAC demonstrated superior AUC's for prediction of both unfavourable outcome and for mortality; across all periods of recording analyzed. In analyzing the entire recording period, the AUC's for prediction of unfavourable outcome were: PRx (0.573, $p<0.0001$), PAx (0.606, $p<0.0001$), and RAC (0.655, $p<0.0001$). Similarly, the AUC's for mortality were: PRx (0.651, $p<0.0001$), PAx (0.705, $p<0.0001$), and RAC (0.722, $p<0.0001$). The AUC differences between RAC vs.

PRx, and PAx vs. PRx reached statistical significance (ie. $p<0.05$) in all recording periods (except the "1st 10 days" recording group) tested, using Delong's test. However, the difference in AUC between RAC and PAx, failed to reach statistical significance, regardless of the recording period analyzed. The "1st 10 days" recording group failed to display statistically significant relationships between the indices and the two binary outcomes.

Multivariate Binary Logistic Regression (MLR)

Table 8.3 displays the AUC's for the various prognostic models tested: baseline model, baseline + PRx, baseline + PAx, baseline + RAC and baseline + "All Indices"; across all time periods of recording that were analyzed (bold AUC's indicate $p<0.05$). In summary, the baseline model demonstrated significance for ICP, Age and admission GCS for both binary outcomes, across the majority of the recording periods analyzed. This also held true in the majority of the models in which one or more of the cerebrovascular reactivity indices was added, across all time periods. Only the "1st 10 days" recording group failed to reach statistical significance between any of the models and the binary outcomes analyzed.

Table 8.2: Univariate Binary Logistic Regression – A/D and F/U AUC's Based on Various Recording Periods

Recording Period	PRx				PAx				RAC			
	A/D AUC	p-value	F/U AUC	p-value	A/D AUC	p-value	F/U AUC	p-value	A/D AUC	p-value	F/U AUC	p-value
Total	0.651	***<0.0001***	0.573	***0.002***	0.705	***<0.0001***	0.606	***0.0001***	0.722	***<0.0001***	0.655	***<0.0001***
1st 24hr	0.650	***<0.0001***	0.580	***0.002***	0.688	***<0.0001***	0.612	***0.0001***	0.677	***<0.0001***	0.632	***<0.0001***
1st 72hr	0.613	***0.0001***	0.517	0.144	0.671	***<0.0001***	0.579	***0.011***	0.693	***<0.0001***	0.603	***0.001***
1st 5d	0.596	***0.003***	0.508	0.279	0.667	***0.001***	0.591	***0.007***	0.700	***<0.0001***	0.621	***0.001***
1st 7d	0.583	0.038	0.550	0.221	0.660	***0.009***	0.621	***0.006***	0.704	***0.0001***	0.660	***0.0001***
1st 10d	0.546	0.643	0.519	0.793	0.585	0.265	0.548	0.186	0.630	0.086	0.612	***0.050***

A/D = alive/dead, AMP = pulse amplitude of ICP, AUC = area under the receiver operating curve, CPP = cerebral perfusion pressure, d = day, F/U = favourable/unfavourable GOS (Favourable = 4 or 5; Unfavourable = 3 or less), hr = hour, ICP = intracranial pressure, MAP = mean arterial pressure, PAx = pulse amplitude index (moving correlation coefficient between AMP and MAP), PRx = pressure reactivity index (moving correlation coefficient between ICP and MAP), RAC = moving correlation coefficient between AMP and CPP.
**NOTE: bold values are those p-values which reached the threshold of statistical significance (p<0.05).*

Table 8.3: Multivariate Logistic Regression – A/D and F/U AUC's Based on Various Recording Periods

MODEL	**Recording Period**											
	Total (n=358)		**1st 24hr (n=340)**		**1st 72hr (n=277)**		**1st 5d (n=217)**		**1st 7d (n=163)**		**1st 10d (n=101)**	
	A/D AUC	**F/U AUC**	**A/D AUC**	**F/U AUC**	**A/D AUC**	**F/U AUC**	**A/D AUC**	**F/U AUC**	**A/D ACU**	**F/U AUC**	**A/D AUC**	**F/U AUC**
Baseline	**0.802**	**0.718**	**0.765**	**0.716**	**0.759**	**0.710**	**0.780**	**0.720**	**0.755**	**0.730**	0.741	0.743
+ PRx	**0.822**	**0.727**	**0.804**	**0.732**	**0.802**	**0.717**	**0.807**	**0.718**	**0.803**	**0.734**	0.741	0.752
+ PAx	**0.836**	**0.728**	**0.798**	**0.728**	**0.797**	**0.720**	**0.796**	**0.723**	**0.790**	**0.740**	0.739	0.744
+ RAC	**0.863**	**0.745**	**0.811**	**0.742**	**0.821**	**0.725**	**0.820**	**0.733**	**0.817**	**0.764**	0.744	0.740
+ All Indices Included	**0.862**	**0.748**	**0.816**	**0.738**	**0.823**	**0.723**	**0.825**	**0.735**	**0.819**	**0.763**	0.751	0.761
+PAx and RAP	**0.847**	**0.741**	**0.806**	**0.739**	**0.819**	**0.722**	**0.803**	**0.727**	**0.803**	**0.760**	0.743	0.743

*A/D = alive/dead, AMP = pulse amplitude of ICP, AUC = area under the receiver operating curve, CPP = cerebral perfusion pressure, d = day, F/U = favourable/unfavourable GOS (Favourable = 4 or 5; Unfavourable = 3 or less), hr = hour, ICP = intracranial pressure, MAP = mean arterial pressure, n= number, PAx = pulse amplitude index (moving correlation coefficient between AMP and MAP), PRx = pressure reactivity index (moving correlation coefficient between ICP and MAP), RAC = moving correlation coefficient between AMP and CPP, RAP = moving correlation coefficient between AMP and ICP. *NOTE: bold values are those p-values which reached the threshold of statistical significance (p<0.05). **All "MODEL's" contained: Age, Sex, admission Glasgow Coma Scale (GCS), mean ICP, mean CPP, MAP, mean AMP. ***All Indices Included model – despite including PRx, PAx and RAC, RAC was the only index to reach statistical significance in the model across all recording periods (except 1st 10d – given nothing reached significance secondary to patient numbers in this cohort), with PRx and PAx both dropping out of the model.*

In evaluating the baseline model with the addition of PRx, PAx or RAC, RAC displayed superior AUC's for both binary outcomes, across all periods analyzed. Furthermore, when all indices were added into the MLR, both PRx and PAx failed to reach significance, with RAC being the only ICP derived cerebrovascular reactivity index that remained significant. Finally, the RAC multivariate model also outperformed the PAx + RAP multivariate model across all time periods analyzed. This held true across all time periods analyzed.

Critical Thresholds Associated with Morbidity and Mortality – PRx, PAx and RAC

The sequential chi-square thresholding was conducted for each index with each binary outcome, across all recording periods. Appendix F displays the chi-square versus index threshold plots for each index, in each recording period. In summary, using the entire recording period, PRx displayed a threshold of +0.35 for both unfavourable outcome ($p=0.0001$) and mortality ($p<0.0001$). This is contradictory to the previous thresholding study (which included DC patients), displaying thresholds of +0.05 and +0.25, respectively.[9] For the same recording period, PAx displayed a threshold of +0.05 for unfavourable outcome ($p<0.0001$) and +0.25 for mortality ($p<0.0001$). Finally, for the same recording period, RAC displayed a threshold of -0.10 for unfavourable outcome ($p<0.0001$), and -0.05 for mortality ($p<0.0001$). Figure 8.1 displays the chi-square value vs. index threshold plots for PRx, PAx and RAC, using data from the entire recording period.

Figure 8.1: Threshold Plots for PRx, PAx and RAC – Entire Recording Period

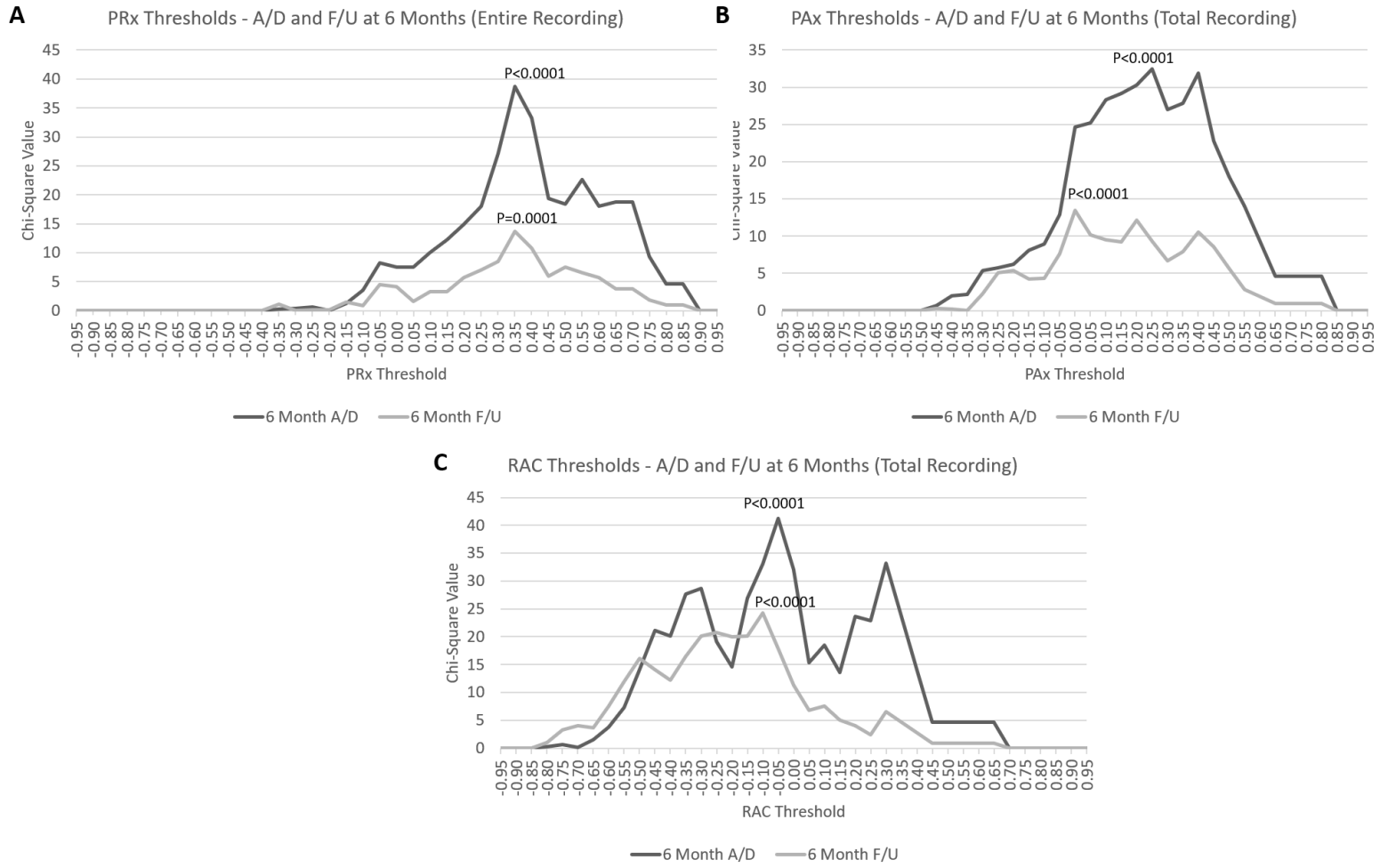

A/D = Alive/Dead outcome (black line), AMP = pulse amplitude of ICP, CPP = cerebral perfusion pressure, F/U = favourable/unfavourable outcome (grey line), ICP = intra-cranial pressure, MAP = mean arterial pressure, P = p-value, PAx = pulse amplitude index (correlation between AMP and MAP), PRx = pressure reactivity index (correlation between ICP and MAP), RAC = correlation between AMP and CPP.

Critical Thresholds of PRx, PAx and RAC Based on Length of Recording Analyzed

Given that the duration of signal recording varies significantly between patients, we were interested to explore differences in critical thresholds of PRx, PAx and RAC across various durations of recording. Figure 8.2 displays the critical thresholds for PRx, PAx and RAC (for both binary outcomes) plotted against the duration of recording used for analysis. Of interest is the significant variation in thresholds of both PRx (Figure 8.2A) and PAx (Figure 8.2B), with loss of significance of some threshold values using 7 and 10 days of recording. In contrast, RAC (Figure 8.2C) displayed more consistent and stable critical thresholds, for both binary outcomes, regardless of the length of recording period utilized within the analysis.

Figure 8.2: Critical Thresholds of PRx, PAx and RAC – Based on Length of Recording Analyzed

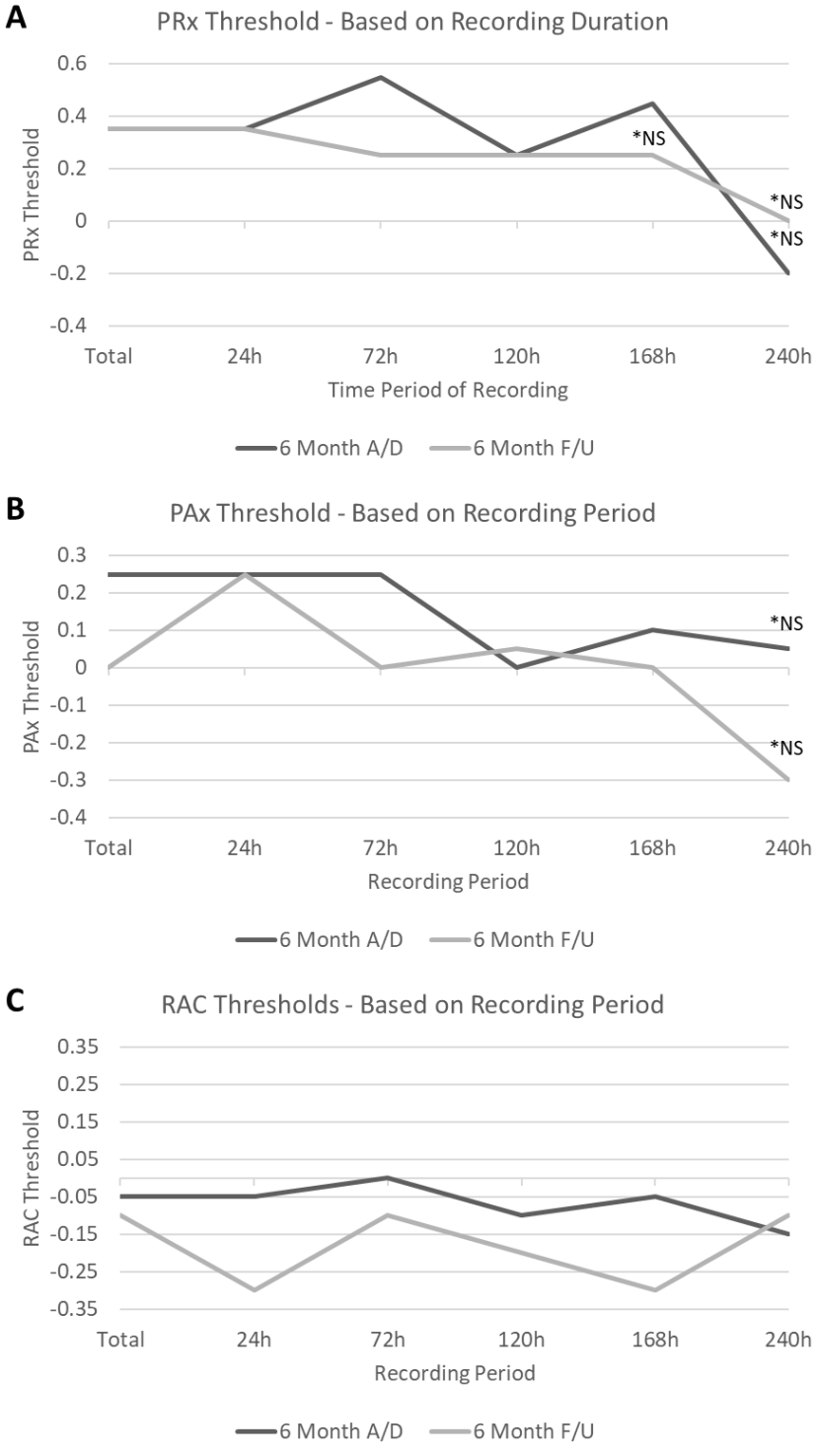

*A/D = Alive/Dead outcome, AMP = pulse amplitude of ICP, CPP = cerebral perfusion pressure, F/U = favourable/unfavourable outcome, ICP = intra-cranial pressure, MAP = mean arterial pressure, P = p-value, PAx = pulse amplitude index (correlation between AMP and MAP), PRx = pressure reactivity index (correlation between ICP and MAP), RAC = correlation between AMP and CPP. *NS = not statistically significant threshold value for this period of recording analyzed. Number of patients in each time period analyzed: Total = 358, 1st 24 hours = 340, 1st 72 hours = 277, 1st 5 days = 217, 1st 7 days = 163, 1st 10 days = 101.*

8.1.4 Discussion

Using both univariate logistic regression and multi-variate logistic regression, and critical threshold analysis of PRx, PAx and RAC in a solely non-DC TBI cohort, some important relationships have been identified which need to be emphasized.

First, RAC, explored in Chapter 4, displays the highest AUC for prediction of both mortality and unfavourable outcome, when compared to PRx and PAx. This was replicated across all periods of recording that were analyzed. This finding is critical, given that PRx is the most commonly quoted continuous autoregulation index in TBI. The fact that RAC may be superior to PRx for outcome prediction warrants its consideration for further evaluation in terms of clinical application.

Second, RAC also displayed superior AUC's for both binary outcomes using MLR, compared to the models including PRx or PAx. This was again replicated across all recording periods analyzed. Furthermore, when all three indices were added into the MLR modelling, RAC was the only one to remain statistically significantly associated with both mortality and unfavourable outcome, across all recording periods analyzed. Finally, the RAC model also outperformed the PAx + RAP model across all time periods analyzed. RAP is the moving correlation coefficient between AMP and ICP, and is believed to represent pure compensatory reserve and not cerebrovascular reactivity. RAC is believed to represent an index which carries information regarding both cerebrovascular reactivity and cerebral compensatory reserve, as demonstrated in Chapter 4. Thus, the multivariate model including PAx (an index of cerebrovascular reactivity) and RAP (an index of compensatory reserve) should theoretically carry similar or superior outcome prediction capacity compared to a multivariate model with RAC alone. The MLR model with RAC alone outperformed all other multi-variate models tested, including the model with PAx and RAP, indicating that RAC appears superior and carries additional outcome predictive capabilities. These models with RAP alone are not discussed in detail given they do not focus on cerebrovascular reactivity/autoregulation, as the goal of this study was to explore the outcome predictive capabilities of ICP derived indices of cerebrovascular reactivity/autoregulation.

Third, critical thresholds of cerebrovascular reactivity indices for both mortality and unfavourable outcome vary depending on the length of recording utilized. This holds true for all three indices. Using the entire recording period (which has been described in previous autoregulation index thresholding studies), the thresholds for both Favourable/Unfavourable and Alive/Dead were: +0.35/+0.35 for PRx, 0/+0.25 for PAx, and -0.10/0 for RAC. The ~0.34 to 0.45 lower value for the threshold of RAC, compared

to PRx, is not surprising given previous literature demonstrating this approximate relationship across ~2.7 million data points.

Fourth, the important point of these thresholds, regardless of which time period is utilized, is the fact that DC patients were excluded. The literature supporting aberrations in PRx post-craniectomy[22] raise concerns around the previously defined critical thresholds.[9] Thus, these new thresholds may be more reliable for outcome prediction in those patients not undergoing a decompressive craniectomy. For DC patients, it still remains unclear the utility of PRx, at least in the initial phases, post-craniectomy and the reliability of the critical thresholds in this population.

Fifth, the chi-square critical threshold analysis indicated that RAC had more consistent and stable critical thresholds for favourable/unfavourable and Alive/Dead binary outcomes at 6 months. Compared to PRx and PAx, which display greater variation in critical threshold values based on the duration of recordings analyzed, RAC may prove to be more stable, at least in the non-DC TBI population, for the application of critical thresholds for mortality and unfavourable outcome. In addition, PRx and PAx had issues with statistical significance of their critical thresholds for recording lengths of 7 and 10 days, while RAC did not. Thus, for critical threshold analysis of long recording periods (ie. greater than 7 days), RAC may be superior. However, it must be acknowledged that the number patients who had at least 7 days or 10 days of recording, in order to be included in those analysis groups, were much less than the "all comers" entire recording, or 1st 24 hours of recording, groups. Thus, it is possible that we were underpowered to reach significance in these specific recording periods.

Finally, the "grey" zone of PRx, as defined by previous thresholding analysis as the index value range between the two critical thresholds of +0.05 and +0.25, was not identified within this cohort of 358 non-DC patients. This raises suspicion of the potential influence that the DC patients had on the previous critical threshold analysis.[9] Thus, the thresholds identified for PRx within this current study, may represent the true thresholds for non-DC patients.

Limitations

Despite the interesting results, there are some important limitations to highlight. First, this study was conducted retrospectively on a prospectively collected database of mild to severe TBI patients, with archived high frequency signal data. Thus, there exists significant heterogeneity in injury pattern, systemic injury, co-morbidities and treatment within the NCCU, all of which could significantly impact

the outcome and threshold analysis. Furthermore, while on the NCCU, patients were actively undergoing ICP and CPP directed therapies which would influence both the parent recorded signals, and the subsequently derived autoregulatory indices.

Second, the results of both the outcome and threshold analysis for the "1st 10 days" recording period should be interpreted with caution. This analysis was underpowered in this sub-group of patients, with only 101 included. This would account for the failure to reach statistical significance in the ULR, MLR and thresholding studies described.

Third, the study presents promising results related to RAC in both ULR/MLR outcome prediction and consistency/stability in critical thresholds, with better prognostic associations in the cohort. However, the exploration of RAC in this context is very limited, and the definitive superiority of RAC over either PRx or PAx remains unproven and requires further confirmation. Similarly, while the data suggest that RAC may have benefits for measurement of optimum CPP, its performance needs to be formally compared to PRx.

Fourth, the use of the sequential chi-square technique for critical threshold analysis could be considered controversial. It was elected to proceed with this method for two main reasons. First, sharply defined thresholds for the indices were desired, which is not afforded through standard ROC analysis. Second, given the previous work on critical thresholds for continuous autoregulation indices in TBI, similar threshold analysis was conducted to allow for comparison with prior results.

8.1.5 Conclusions

In this cohort of non-DC TBI patients, RAC appears to be superior to PRx and PAx in 6-month outcome prediction, using both univariate and multivariate logistic regression; across all time periods of recording analyzed. Further, RAC displayed more consistent and stable critical thresholds associated with mortality and unfavourable outcomes at 6 months, compared to PRx and PAx.

8.2 TCD Systolic Flow Index

8.2.1 Introduction

Chapters 6 and 7 detailed the strong association between TCD based Sx/Sx_a and the ICP derived indices of cerebrovascular reactivity.[180–182,184] Regardless of the ability to model the "gold standard" PRx via Sx_a, there still exists the potential to utilize Sx/Sx_a as a primary measure of cerebrovascular reactivity. Currently, the only TCD index with defined critical thresholds is Mx, despite previous literature suggesting Sx has a stronger association with 6-month outcome in adult TBI. Thus, the aim of this study was to explore and provide critical thresholds for 6-month outcomes in adult TBI patients.

8.2.2 Methods

Patient Population and Demographic Data Acquisition

The identical patient cohort described in sections 6.3 and 7.1 was utilized for this study.[182,184] Details surrounding this cohort can be found in these sections. Only 281 patients had outcome information available for this study. The following patient demographic data was obtained from the database: age, sex, admission GCS, and patient outcome at 6 months. Patient outcome was assessed using the GOS at 6 months, and stored prospectively within the database. For purpose of the outcome and threshold analysis, we dichotomized the GOS into two binary outcomes of interest: A. Favourable (GOS of 4 or 5) vs. Unfavourable (GOS of 3 or less), and B. Alive vs. Dead.

Signal Acquisition

Refer to section 6.3 and 7.1 for details.

Signal Processing

Refer to section 6.3 and 7.1 for details.

Cerebrovascular Reactivity Indices

The cerebrovascular reactivity indices were derived in a similar fashion, as described in Chapter 3. The following indices were used for this outcome analysis: PRx, PAx, RAC, Mx, Mx_a, Sx, Sx_a, Dx and Dx_a.

Statistics

General Statistics

Data were provided on a minute-by-minute basis for the duration of the recordings, for each recording. Data was also extracted into CSV documents. We then produced individual recording grand means for each index. Statistical analyses were performed in XLSTAT (Addinsoft, New York, United States; https://www.xlstat.com/en/) add-on package to Microsoft Excel (Microsoft Office 15, Version 16.0.7369.1323) and R statistical software (R Core Team (2016). R: A language and environment for statistical computing. R Foundation for Statistical Computing, Vienna, Austria. URL https://www.R-project.org/). Tests for normality were performed using the Shapiro-Wilks test for all indices and measured variables. All indices and variables were determined to be non-parametric in nature. Alpha was set at 0.05 for all results describing a p-value.

Outcome Analysis and Critical Thresholds

To assess the association with patient 6-month outcome, two binary outcomes were of interest: A. Favourable (GOS 4 or 5) vs. Unfavourable (3 or less), and B. Alive vs. Dead. Initially simple univariate logistic regression was performed, comparing each of the ICP indices (PRx, PAx, RAC) and the TCD indices (Mx, Mx_a, Sx, Sx_a, Dx, and Dx_a) to both binary outcomes. We reported area under the receiver operating curve (AUC) and p-values for each.

Next, to define critical thresholds for Sx and Sx_a, a sequential chi-square method of thresholding was conducted. This technique for threshold analysis has been described in detail within other publications on continuous autoregulation indices in TBI, including PRx and Mx. It was conducted identical to that described in section 8.1.2.

8.2.3 Results

Univariate Logistic Regression

A univariate logistic regression analysis was performed for each index with both binary outcomes. A summary of the AUC's and p-values for each index and binary outcome can be seen in Table 8.4.

These results support previously described univariate logistic regression analysis results for TCD based indices. Sx displayed AUC's of 0.630 (p=0.005) and 0.646 (p=0.001) for its association with alive/dead and favourable/unfavourable outcomes at 6 months, respectively. Sx_a displayed AUC's of 0.582 (p=0.068) and 0.632 (p=0.001) for its association with alive/dead and favourable/unfavourable outcomes at 6 months. Thus, Sx is superior to Mx and Dx, and Sx_a is superior to Mx_a and Dx_a. Further, Sx_a appears worse at outcome prediction, compared to Sx. Finally, Sx displayed broadly similar AUC magnitude to the ICP derived indices for both binary outcomes.

Dx displayed an AUC of 0.592 (p=0.012) for unfavourable outcome at 6 months. Dx failed to reach significance in univariate logistic regression for its association with 6-month mortality (AUC = 0.560, p = 0.215). Similarly, Dx_a failed to reach significance in logistic regression for both 6-month mortality and unfavourable outcome (AUC = 0.494, p = 0.792; AUC = 0.563, p = 0.116, respectively).

Table 8.4: Binary Univariate Logistic Analysis – Comparing Indices of Autoregulation to Dichotomized Outcomes

	"Favourable" vs. "Unfavourable" Outcome – AUC	**"Favourable" vs. "Unfavourable" Outcome – p value**	**"Alive" vs. "Dead" Outcome – AUC**	**"Alive" vs. "Dead" Outcome – p value**
"Invasive" Indices				
PRx	**0.560**	**0.035**	**0.593**	**0.004**
PAx	**0.613**	**0.002**	**0.648**	**0.001**
RAC	**0.579**	**0.028**	**0.640**	**0.002**
Mx	**0.640**	**0.001**	**0.614**	**0.010**
Sx	**0.646**	**0.001**	**0.630**	**0.005**
Dx	**0.592**	**0.013**	0.560	0.216
"Non-invasive" Indices				
Mx_a	**0.617**	**0.001**	0.559	0.213
Sx_a	**0.632**	**0.001**	0.582	0.068
Dx_a	0.563	0.118	0.494	0.792

AUC = area under the receiver operating curve, The described indices are Pearson correlation coefficients between various variables: PRx (between ICP and MAP), PAx (between AMP and MAP), RAC (between AMP and CPP Mx (between FVm and CPP), Mx_a (between FVm and MAP), Sx (between FVs and CPP), Sx_a (between FVs and MAP), Dx (between FVd and CPP), Dx_a (between FVd and MP).

Critical Thresholds for Sx and Sx_a

The sequential chi-square thresholding was conducted for both Sx and Sx_a, with each binary outcome. Using the entire recording period, Sx displayed a threshold of -0.15 for unfavourable outcome ($p<0.0001$) and -0.20 for mortality ($p<0.0001$). This is a much lower threshold compared to those described for Mx/Mx_a in previous publications. Figure 8.3 displays the chi-square vs. threshold plot for Sx.

Similarly, Sx_a displayed thresholds of +0.05 ($p=0.019$) and -0.10 ($p=0.0001$) for alive/dead and favourable/unfavourable outcomes, respectively. Of note, the chi-square test statistic and p-values for Sx_a were much worse across the entire sequential threshold analysis for Sx_a, compared to Sx. This indicates that the strength of relationships for the thresholds defined for Sx_a are much less than those described for Sx. Figure 8.4 displays the chi-square value vs. index threshold plot for Sx_a, using data from the entire recording period.

Figure 8.3: 6 Month Outcome Thresholds – Sx

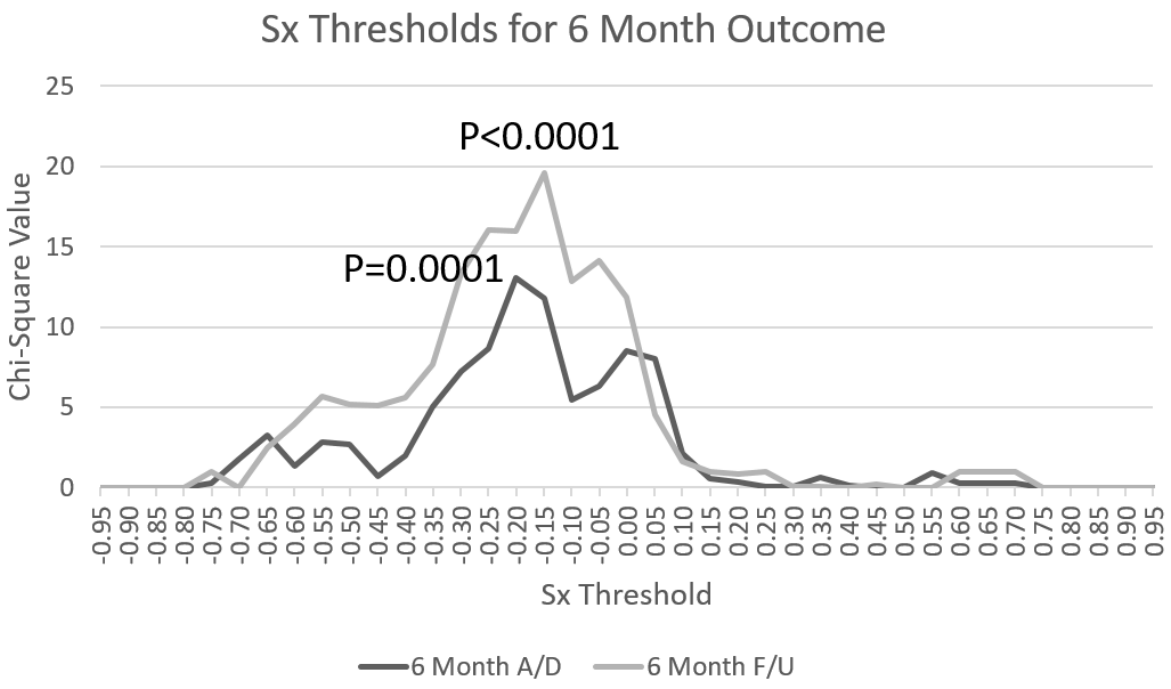

A/D = Alive/Dead outcome, CPP = cerebral perfusion pressure, FVs = systolic flow velocity, F/U = favourable/unfavourable outcome, MAP = mean arterial pressure, P = p-value, Sx = systolic flow index (correlation between FVs and CPP).

Figure 8.4: 6 Month Outcome Thresholds – Sx_a

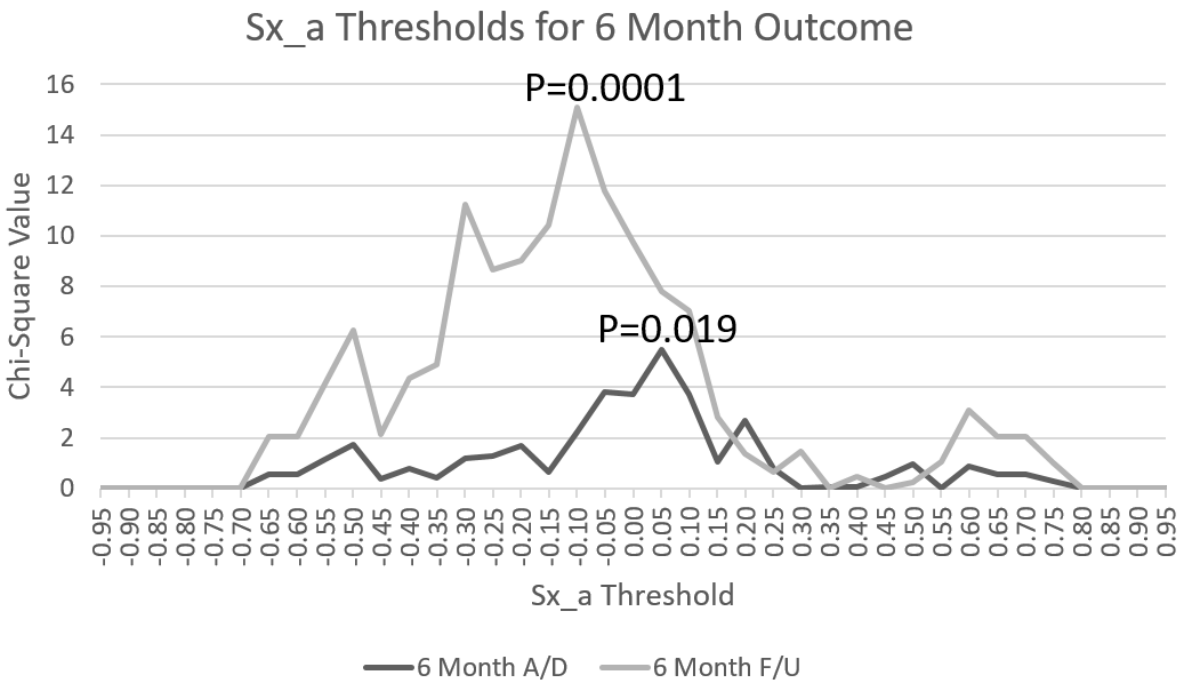

A/D = Alive/Dead outcome, CPP = cerebral perfusion pressure, FVs = systolic flow velocity, F/U = favourable/unfavourable outcome, MAP = mean arterial pressure, P = p-value, Sx_a = systolic flow index based on MAP (correlation between FVs and MAP).

8.2.4 Discussion

Univariate Logistic Regression Outcome Analysis

Univariate logistic regression analysis displayed that Sx is superior to Mx and Dx in its association with both binary 6-month outcomes. Similarly, Sx_a displayed superiority to Mx_a and Dx_a in its association with both binary 6-month outcomes. This confirms previously described results.[84,180] Of further interest, Sx displayed similar AUC's to the ICP derived indices (PRx, PAx, and RAC) for both binary 6 month outcomes. This univariate regression analysis confirms similarity in outcome prediction between Sx and the ICP derived indices, PRx/PAx/RAC.

Critical Thresholds Analysis

Critical thresholds associated with 6-month outcome have been defined for both Sx and Sx_a. Some important points require highlighting. First, the thresholds for mortality and unfavourable outcome with Sx is -0.20 and -0.15 respectively. These are lower than those previously describe for Mx, with mortality and unfavourable outcome thresholds defined at +0.05 and +0.30, using an identical process. Thus, one cannot apply the same Mx based thresholds[8] to other TCD based autoregulation indices. Furthermore, the threshold for worse outcomes with Sx are not located near zero or in positive values, meaning disrupted autoregulatory capacity of a magnitude likely to impact outcome may be present even with negative values for Sx. This is not seen in the two commonly quoted indices, PRx and Mx, where negative values are believed to denote "preserved autoregulation", and thresholds for outcome association are always at or above zero. This emphasizes that "intact" cerebral autoregulation in TBI is a spectrum, not a binary phenomenon, with varying degrees of "intact" and "impared" autoregulation which may be detected differently via different MMM based measures.

Second, there is a difference between the thresholds for Sx and Sx_a, with Sx_a displaying thresholds for mortality and unfavourable outcome at +0.05 and -0.10, respectively. It appears the use of MAP during the calculation of Sx_a, shifts the thresholds for 6-month outcome towards more positive index values. Thus, even within Sx and Sx_a, we cannot assume that the thresholds associated with 6-month outcome are interchangeable. However, it must be acknowledged that the chi-square test statistic and p-values for the Sx_a threshold analysis were less significant for all thresholds tested, compared to Sx. Thus, the strength of the relationship with respect to the Sx_a thresholds is not as robust as those described for Sx. This difference between Sx and Sx_a was mirrored within the univariate logistic regression analysis, which revealed that Sx was superior in both mortality and unfavourable outcome prediction at 6 months. The results from the logistic regression analysis for Sx and Sx_a mirror those previously published.[84,180]

Limitations

Despite having 281 patients included for the outcome and critical threshold analysis, the length of TCD recordings are relatively short. "Short" recordings, defined as less than 30 minutes duration, were removed from the analysis in order to prevent limited recording periods from confounding the outcome and threshold analysis. Thus, the grand mean calculations for all indices were based on recordings

ranging from 30 minutes up to 2 or 3 hours in maximum duration. However, despite using only the "longer" recordings, they only provide a "snap-shot" into autoregulation/cerebrovascular reactivity. Thus, using these limited recordings for outcome association studies is fraught with issues since the global outcomes used for threshold analysis reflect the constellation of physiologic and pathologic events suffered during the patient's entire hospital course.

8.2.5 Conclusions

Sx and Sx_a provide superior 6-month outcome prediction, compared to Mx and Mx_a, with defined critical thresholds different than those described for Mx. Both systolic indices better differentiate between favourable-unfavourable outcome than alive-deead.

CHAPTER 9: INJURY BURDEN AS A DRIVER OF IMPAIRED CEREBROVASCULAR REACTIVITY IN ADULT TBI

*The results of this study can also be found detailed in the publication: Zeiler et al., *J Neurotrauma*. 2018, 35(14):1569-1577. doi: 10.1089/neu.2017.5595..[189]

9.1 Introduction

Chapter 8 focuses on the association between various MMM derived cerebrovascular reactivity indices and thresholds with patient outcome in adult TBI.[152,182] These thresholds may therefore characterize critical points in the loss of autoregulatory capacity/cerebrovascular reactivity, beyond which the burden of abnormal physiology impacts outcome. However, despite a growing body of literature on these continuous ICP derived indices of cerebrovascular reactivity, very little is understood with regards to what drives impaired vascular reactivity after TBI. Potential drivers of such a relationship include the severity and type of IC injury, the severity of EC injury, and/or the physiological response to injury.

As mentioned in Chapter 2, one past study from Cambridge evaluated the association between intracranial injury burden and autoregulatory function in 126 patients post-TBI, and showed that PRx was more commonly abnormal in patients with Diffuse Injury Grade III, as compared to other diffuse and focal injury classifications, on the Marshall Scale.[107] However, the Marshall grading system is just one of many available, and its summary descriptions do not provide a full characterization of the type, extent and severity of intracranial injury. Further, the PRx outcome threshold of >0 used in this analysis may have been non-optimal, since a recent re-analysis suggests that its derivation may have been heavily confounded by inclusion of patients with decompressive craniectomy where different intracranial conditions apply. Consequently, there exists an imperfect understanding of how intracranial injury impacts on autoregulation following TBI, and there are no publications relating the severity of extracranial injury or post-injury physiology to the incidence of abnormal cerebral autoregulation.

Understanding such relationships is important, since their elucidation could allow early patient stratification, and potentially reveal mechanistic targets for therapy. Therefore, this study details exploration of these relationships in a large non-DC TBI patient population with archived high frequency digital ICU signals. There were two main goals of this study:

1. Determine the association between admission IC injury burden (assessed by recognized CT scoring systems in TBI and an extensive CT based IC lesion database) and impaired cerebrovascular reactivity.

2. Determine how the burden of EC injury relates to impaired cerebrovascular reactivity.

9.2 Methods

Patient Population and Demographic Data Acquisition

This population is identical to that described in Chapters 4 and 8.1.[21,152] Details regarding the population specifics can be found there.

Intra-Cranial (IC) Injury Burden Data Acquisition

All admission CT-head scans were accessed and archived retrospectively. These scans were assessed by a qualified specialist neurosurgeon (the author of this thesis) for a variety of injury characteristics. There was a vast amount of admission CT scoring systems and injury scales determined from the admission CT scans. As such, this study was designed to be a very preliminary analysis into admission injury characteristics associated with impaired vascular reactivity, with the described associations to be considered exploratory in nature. This image analysis will be assessed in future prospective studies as part of CENTER-TBI.[190] This IC CT injury database has been described in detail within Chapter 3.4 of the general methods.

Extra-Cranial (EC) Injury Burden Data Acquisition

As part of standard trauma and NCCU care, the admission total Injury Severity Score (ISS)[191] and Acute Physiology And Chronic Health Evaluation II (APACHE II)[192] score were determined for each patient as part of national audit requirements and were retrospectively available for this study.

Signal Acquisition

See Chapter 4.2 for details on signal acquisition.

Signal Processing

See Chapter 4.2 for details on signal processing. PRx, PAx and RAC were derived for every patient. Finally, data for this analysis were provided in the form of a minute by minute time trends of the parameters of interest for each patient. From this, data was extracted for; entire recording period for each patient (n=358), 1st 24 hours of recording (n= 340), and 1st 72 hours of recording (n=277) were produced in order to assess the association between IC and EC injury burden and cerebrovascular reactivity, across various durations of recording. Within these separate datasets, a grand mean was calculated per patient for each index across the duration of that recording period and subsequently utilized for the final statistical analysis. Furthermore, in each of these sheets we evaluated the following binary thresholds for PRx, PAx and RAC: A. PRx: >0, >0.25, >0.35; B. PAx: >0, >0.25; and C. RAC: > -0.05, > -0.10. These are the critical thresholds associated with patient outcome previously defined in the literature and within Chapter 8.1. Finally, for the entire recording dataset, we calculated the percentage of recording time (% time) spent above each threshold for every patient.

Statistics

Statistics were performed utilizing XLSTAT (Addinsoft, New York, United States; https://www.xlstat.com/en/) add-on package to Microsoft Excel (Microsoft Office 15, Version 16.0.7369.1323) and R statistical software (R Core Team (2016). R: A language and environment for statistical computing. R Foundation for Statistical Computing, Vienna, Austria. URL https://www.R-project.org/). For all statistical tests described, alpha was set at 0.05 for significance, with correction for multiple comparisons.

General Statistics

Simple descriptive statistics were utilized to summarize the patient demographics. Box plots were also employed to summarize the cerebrovascular reactivity indices, with respect to IC and EC injury scoring

systems. A Shapiro Wilks test found significant non-normality in the distributions of all continuous variables of interest and non-parametric tests were used.

The burden of IC and EC injury, quantified using widely accepted scoring systems,[153–156] were related to differences in PRx, PAx and RAC based on category of injury burden. All scoring systems are summarized in Chapter 3, section 3.5.1. Using the entire recording period datasets, first correlations between ICP derived indices (PRx, PAx and RAC) and the IC and EC injury scores were examined using Spearman's test. Similarly, the % time spent above index threshold was correlated with IC and EC injury scores. Finally, mean PRx, PAx and RAC values across each category of IC injury scoring system were compared for: Marshall,[153] Rotterdam,[154] Helsinki[155] and ordinal Stockholm[156] scores; using the Kruskal-Wallis (KW) test for the Marshall CT grade, and a one-way Jonckheere-Terpstra (JT) test for the ordinal Rotterdam, Helsinki and Stockholm (converted from continuous) scores. This was repeated for % time above thresholds of PRx, PAx and RAC. The KW test was chosen for the Marshall system, given this system is not an ordinally arranged grading system. The JT test was chosen for the Rotterdam, Helsinki and ordinal Stockholm graded, given these systems are ordinal in nature and we wished to test if there was statistically significant increase in mean values as the ordinal IC CT score increased. The JT test was performed in a one-way method, testing for increasing mean values, running 1000 permutations, yielding a p-value.

Next, the difference between individual patient demographics and injury characteristics for those patients above and below various thresholds in PRx, PAx and RAC (using above defined thresholds) were evaluated. Using the entire recording period data sheet, continuous variables were compared using the Mann-Whitney U test, while categorical variables were compared via chi-square testing.

Injury Burden Association with Impaired Cerebrovascular Reactivity

Impaired cerebrovascular reactivity was defined using the above-mentioned critical thresholds for PRx, PAx, and RAC. Each threshold was tested, for every demographic and injury variable.

First, a univariate binary logistic regression (ULR) analysis was performed utilizing the three datasets; evaluating all patient demographics and injury characteristics, comparing to the following binary

outcomes of interest: A. PRx Above 0, B. PRx above +0.24, C. PRx above +0.35, D. PAx above 0, E. PAx above +0.25, F. RAC above -0.05, and G. RAC above -0.10.

Second, multivariable binary logistic regression (MLR) was performed using the above thresholds for PRx, PAx and RAC as binary outcomes. Any variables reaching statistical significance (or close to it: p-values <=0.100) in the ULR were entered into the initial MLR model, yielding unique multivariable models for each index threshold tested. Running sequential multivariable models, through a backward elimination method, deleting those variables which were grossly insignificant (ie. p>0.100), the best potential model was derived (based on highest AUC, statistical significance p<0.05, and individual component variables reaching p<0.100 within the model). This was conducted for each index threshold tested.

Both of ULR and MLR techniques described above were performed for each recording period: entire recording, 1st 24 hours, and 1st 72 hours. Only the results of the entire recording period are reported, given the other two periods displayed confirmatory results. Strength of relationship to the outcomes of interest were reported via AUC, with bold AUC's reaching a p<0.05.

9.3 Results

Patient Demographics

Patient demographics for each of the 3 data sheets are summarized in Table 9.1. A total of 358 patients were included in the entire recording period cohort, with a mean recording period length of 189.1 +/- 151.1 hour (range: 8.5 to 1033.0 hours duration). There were 340 and 277 patients in the 1st 24 hours of recording and 1st 72 hours of recording cohorts, respectively. Injury data are summarized in Appendix G for the entire cohort.

Table 9.1: Patient Demographics by Recording Length Analyzed

	Total	**1st 24hr**	**1st 72hr**
N	358	340	277
Mean Age (yrs)	40.6 +/- 17.2	40.6 +/- 17.2	40.2 +/- 17.0
Number of Males	272	258	212
Median Admission GCS (IQR)	7.0 (3 to 9)	7.0 (3 to 10)	7.0 (3 to 9)
Mean ICP (mm Hg)	14.1 +/-7.6	15.6 +/- 8.6	14.9 +/- 7.4
Mean AMP (mm Hg)	2.34 +/- 1.39	2.63 +/- 1.67	2.68 +/- 1.43
Mean CPP (mm Hg)	77.5 +/- 8.5	75.2 +/- 9.0	76.3 +/- 7.4
MAP (mm Hg)	91.2 +/- 7.9	90.5 +/- 9.3	91.2 +/- 1.4
Mean PRx	0.05 +/- 0.17	0.01 +/- 0.22	0.00 +/- 0.19
Mean PAx	-0.06 +/-0.20	-0.07 +/- 0.24	-0.07 +/- 0.20
Mean RAC	-0.35 +/- 0.25	-0.36 +/- 0.29	-0.38 +/- 0.26

AMP = pulse amplitude of ICP, CPP = cerebral perfusion pressure, d = day, GCS = Glasgow Coma Scale, hr = hours, ICP = intra-cranial pressure, MAP = mean arterial pressure, mm Hg = millimeters of Mercury, N = number, yrs = years, PAx = pulse amplitude index (correlation between AMP and MAP), PRx = pressure reactivity index (correlation between ICP and MAP), RAC = correlation between AMP and CPP.

IC Injury Scores and Cerebrovascular Reactivity

No significant correlation was detected between any of the ICP indices (PRx, PAx and RAC) and any of the IC injury burden scores (Spearman's correlation). Comparing the indices to the IC injury scores, all coefficients were positive, however failed to reach r-values greater than 0.250 (however with most reaching $p<0.05$). When comparing the % time spent above threshold for PRx, PAx and RAC with the IC injury scores, we found identical trends.

Given the non-ordinal nature of the Marshall CT grading system, Kruskal Wallis (KW) test was used to compare the mean PRx, PAx and RAC values across individual IC score categories. For the Rotterdam, Helsinki and ordinal Stockholm score we compared the mean PRx, PAx and RAC values across each ordinal category using a one-way JT test. Marshall CT grade displayed no statistically significant association with the mean PRx, PAx or RAC on KW testing. Similarly, the Marshall CT grade was not significantly associated with % time above thresholds for PRx, PAx and RAC, with the only exception being the percentage of time spent with a PRx threshold above 0.

The Rotterdam CT score displayed some statistically significant association with mean PRx ($p=0.001$), PAx ($p=0.001$) and RAC ($p=0.001$). Similar results were seen for the % time spent above threshold, with most PRx and RAC % times above threshold reaching significance. The JT testing confirmed a statistically significant increase in the mean values of the indices and % time above threshold, with increasing Rotterdam score.

The Helsinki CT score displayed the most significant association, comparing mean index values and % time above threshold across score categories using the JT test. All mean index values and % times above threshold were significantly different between ordinal Helsinki score categories (all $p<0.002$), with increasing mean values seen with increasing Helsinki score values. The mean PRx, PAx, and RAC vs Helsinki CT score can be seen in Figure 9.1.

Figure 9.1: Box Plots of PRx, PAx and RAC versus Helsinki CT Score

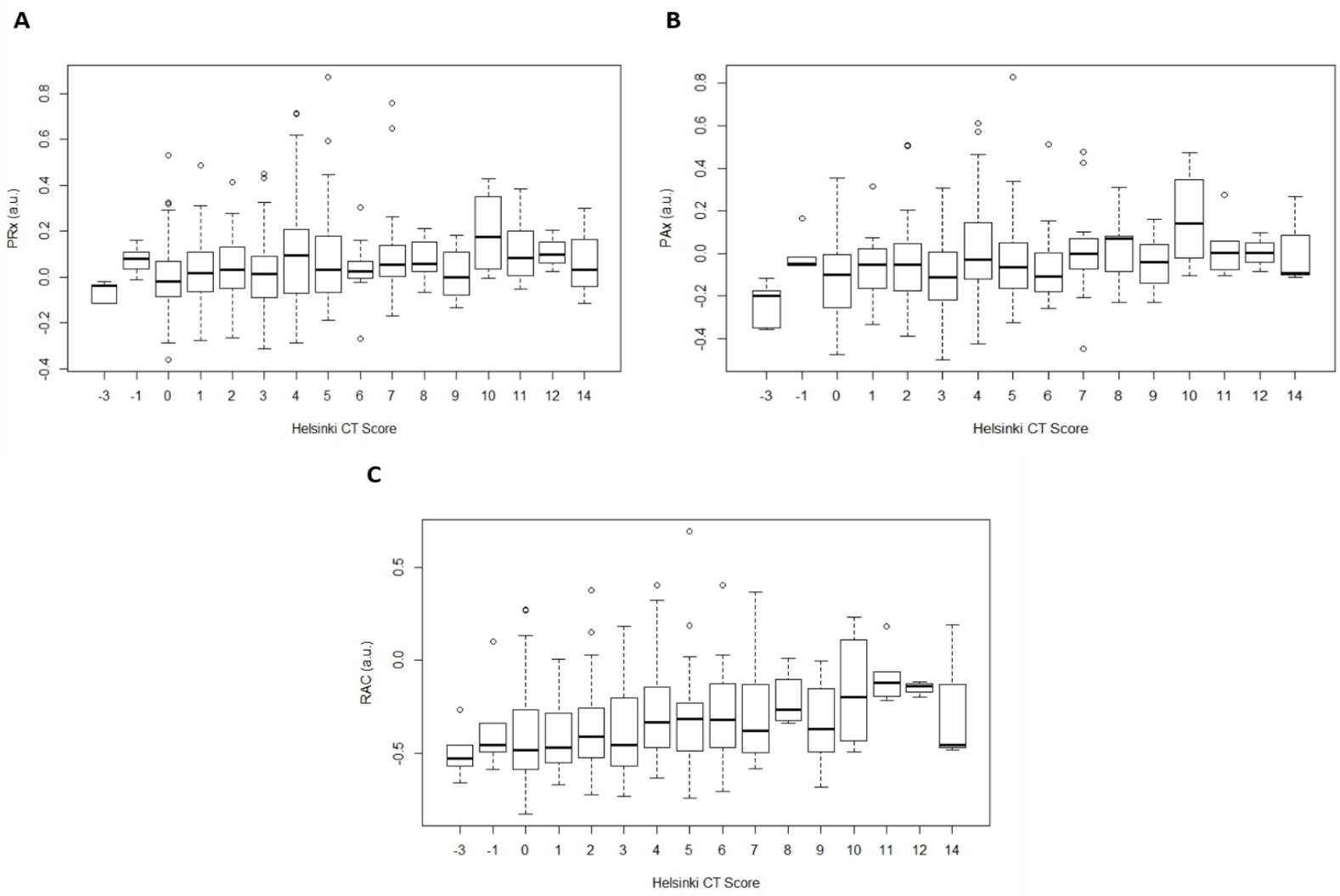

a.u. = arbitrary units, CT = computed tomography, PAx = pulse amplitude index (correlation between pulse amplitude of ICP (AMP) and MAP), PRx = pressure reactivity index (correlation between ICP and MAP), RAC = correlation between AMP and CPP. Panel A: PRx vs. Helsinki Score (p=0.01 on JT testing), Panel B: PAx vs. Helsinki Score (p=0.001 on JT testing), Panel C: RAC vs. Helsinki Score (p=0.001 on JT testing).

Finally, the ordinally arranged Stockholm score seemed to display significant association between mean index values and % time above thresholds for RAC only. The JT testing confirmed a statistically significant increase in the mean values of RAC with increasing ordinal Stockholm score value. All mean values for indices and % time above thresholds, for each IC scoring system category can be seen in Appendix H of the Supplementary Materials.

EC Injury Scores and Cerebrovascular Reactivity

We evaluated the EC injury scores (ISS and APACHE) in a similar manner. As with the majority of the IC injury scores, the ISS EC injury score failed to reach any statistically significant relationship with any of the ICP indices of cerebrovascular reactivity. Out of all IC and EC injury scores, the APACHE score displayed the strongest correlation with PRx ($p = 0.016$), PAx ($p=0.001$) and RAC ($p=0.001$), with r-values up to 0.285. Similar trends were found when comparing the % time spent above threshold for PRx, PAx and RAC with the IC and EC injury scores. Figure 9.2 displays box plots of the PRx, PAx and RAC values compared to ISS and APACHE scores.

Figure 9.2: Box Plots of PRx, PAx and RAC versus APACHE and ISS Scores

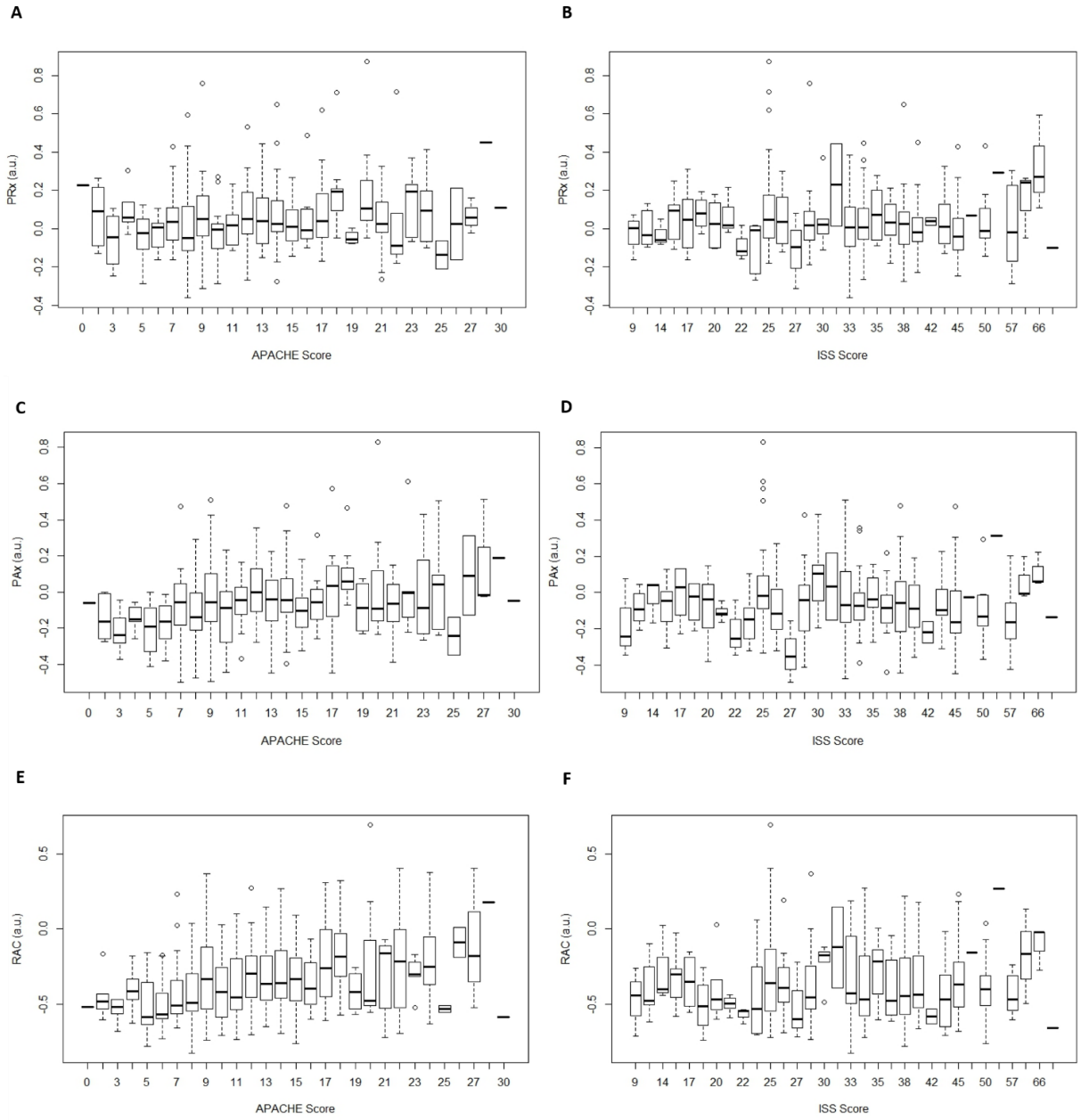

APACHE = APACHE injury score, a.u. = arbitrary units, ISS = injury severity score, PAx = pulse amplitude index (correlation between pulse amplitude of ICP (AMP) and MAP), PRx = pressure reactivity index (correlation between ICP and MAP), RAC = correlation between AMP and CPP. Panel A: PRx vs. APACHE (r=0.130; p=0.016), Panel B: PRx vs. ISS (r=0.-0.018; p= 0.762), Panel C: PAx vs. APACHE (r=0.257; p=0.001), Panel D: PAx vs. ISS (r=-0.064; p=0.264), Panel E: RAC vs. APACHE (r=0.285; p=0.001), Panel F: RAC vs. ISS (r=0.027; p=0.644).

Patient Demographics and Injury Characteristics – Across Binary Index Thresholds

Table 9.2 displays the results of the Mann-Whitney U testing for across the various binary outcome thresholds for RAC, with similar results found for PRx and PAx (Appendix I). Various variables displayed statistical significance between those below versus above threshold. Of note, age and APACHE scores were the two variables consistently different between those patients below and above the index thresholds, with higher age and APACHE scores seen in those above the thresholds.

The ISS and IC scoring systems were rarely statistically different between those patients below and above threshold. Those patients with PRx, PAx, and RAC values above threshold were most likely to display significantly higher Helsinki CT score values.

Patients with PRx values above 0 displayed more contusions, higher largest lesion volume, higher total contusion volume and more midline shift. A similar pattern was seen for patients with PAx values above 0. The other index thresholds tested rarely displayed a statistically significant difference in the continuous variable IC injury characteristics.

Table 9.2: RAC Thresholds – Non-Binary Demographics and Injury Characteristics

Demo (Mean and Medians with Std Dev/IQR)	RAC		p-value	RAC		p-value
	<-0.05	**≥-0.05**		**<-0.10**	**≥-0.10**	
N	314	44	-	302	56	-
Age	39.2 (16.7)	50.6 (17.5)	**<0.0001**	38.9 (16.7)	49.7 (17.0)	**<0.0001**
GCS	7 (4-10)	5 (3-8.25)	0.078	7 (4-10)	6 (3-8.25)	0.143
Marshall	2 (2-3)	3 (2-4)	0.433	2 (2-3)	3 (2-3.25)	0.455
Rotterdam	2 (2-3)	2 (2-4)	0.252	2 (2-3)	2 (2-4)	0.135
Helsinki	2 (0-4.75)	4 (2-6.25)	**0.016**	2 (0-4.75)	4 (2-6)	**0.005**
Stockholm	2.06 (0.89)	2.35 (0.95)	0.055	2.05 (0.89)	2.32 (0.91)	**0.034**
Stockholm Range	2 (2-3)	3(2-3)	0.088	2 (2-3)	3 (2-3)	**0.041**
ISS	32.6 (11.2)	35.2 (12.3)	0.384	32.8 (11.2)	33.9 (12.2)	0.829
APACHE II	11.7 (5.5)	14.4 (5.7)	**0.006**	11.6 (5.5)	14.6 (5.6)	**0.001**
MLS (mm)	1.6 (3.4)	3.0 (5.2)	0.051	1.6 (3.4)	2.6 (4.7)	0.166
Largest Lesion Volume	12.3 (22.1)	18.7 (32.1)	0.055	12.4 (22.4)	17.0 (29.2)	0.091
# Contusions	0.44 (0.87)	0.43 (0.73)	0.684	0.42 (0.85)	0.52 (0.83)	0.204
# DAI Lesions	1.1 (2.8)	0.5 (1.6)	**0.021**	1.2 (2.9)	0.43(1.4)	**0.005**
Total Contusion Volume	4.0 (8.7)	6.3 (17.2)	0.797	5.9 (17.0)	6.1 (13.3)	0.257

 # = number, N = number of patients, CPP = cerebral perfusion pressure, DAI = diffuse axonal injury, MLS = midline shift, mm = millimeters, ISS = injury severity score, GCS = Glasgow Coma Scale, RAC = correlation between pulse amplitude of ICP (AMP) and cerebral perfusion pressure (CPP).

Univariate Logistic Regression (ULR) Analysis – Prediction of Impaired Cerebrovascular Reactivity

Further evaluation of the association between all patient demographics, EC injury and IC injury characteristics with the development of impaired cerebrovascular reactivity was undertaken. Using the defined thresholds for PRx, PAx and RAC for impaired cerebrovascular reactivity, we employed ULR techniques to evaluate each variable in relation to its ability to predict impairment in the entire recording period dataset. Each threshold was evaluated against each variable. Table 9.3 displays the ULR AUC's and p-values for the patient demographic data and both the IC and EC scoring systems tested, while Appendix J displays the ULR AUC's and p-values for the individual IC injury characteristics tested. Similar results were seen for the 1st 24 hours and 1st 72 hours recording datasets.

Various patterns of statistically significant relationships with impaired cerebrovascular reactivity were seen. Of note, the most commonly seen statistically significant association (with the highest AUC's and lowest p-values) with impaired cerebrovascular reactivity was patient age (AUC = 0.606 to 0.783; $p<0.025$ for all) and the APACHE score (AUC = 0.619 to 0.704; $p<0.032$ in all except the PRx >0 threshold). IC CT scores were mostly not significantly associated with impaired cerebrovascular reactivity, although some evidence for association was detected for the Stockholm CT score being the most significant scoring system for PAx >0.25, RAC > -0.10 and RAC > -0.05 thresholds. Of note, for most thresholds tested, admission GCS, sex, ISS and pupillary reactivity were not related to impaired cerebrovascular reactivity.

There were some noteworthy patterns from the evaluation of the individual IC CT-based lesions. Associations depended on the threshold chosen, but in general, across all index thresholds tested, the most commonly seen associations were between markers of diffuse IC injury, rather than macroscopic parenchymal damage. The following injury characteristics were most commonly statistically associated with impaired cerebrovascular reactivity: presence of convexity SDH, presence of falcine SDH, presence of bilateral SDH, thickness of tSAH and the presence of SC DAI lesions. Some important characteristics rarely associated with impaired cerebrovascular reactivity: MLS, largest lesion volume, # of contusions, total contusion volume, basal cistern compression, lateral ventricle compression, 4th ventricle compression and gyral compression.

Table 9.3: Univariate Logistic Regression of Admission Demographics and Scores with ICP Index – Grand Mean Data

	PRx >0		PRx >0.25		PRx >0.35		PAx >0		PAx >0.25		RAC >-0.05		RAC>-0.10	
	AUC	P	AUC	P	AUC	P	AUC	P	AUC	P	AUC	P	AUC	P
Age	**0.606**	**0.001**	**0.637**	**0.007**	**0.655**	**0.025**	**0.720**	**<0.0001**	**0.783**	**<0.0001**	**0.685**	**<0.0001**	**0.679**	**<0.0001**
Sex	0.495	0.850	**0.640**	**0.040**	0.663	0.204	0.555	0.526	0.699	0.073	0.586	0.335	0.534	0.621
Admission GCS	0.592	0.551	0.633	0.983	0.722	0.977	0.621	0.374	0.620	0.994	0.651	0.723	0.625	0.773
Admission Pupil Reactivity	0.564	0.241	**0.628**	**0.012**	**0.675**	**0.003**	0.558	0.648	**0.695**	**0.013**	0.600	0.050	0.577	0.098
Admission Marshall CT Grade	**0.584**	**0.029**	0.596	0.537	0.656	0.361	0.581	0.392	0.665	0.192	0.562	0.748	0.531	0.905
Admission Rotterdam CT Grade	0.562	0.157	**0.656**	**0.032**	0.689	0.107	0.569	0.443	0.689	0.140	0.628	0.149	0.570	0.332
Admission Helsinki CT Score	0.634	0.335	0.685	0.540	0.773	0.488	0.644	0.213	0.709	0.577	0.661	0.525	0.656	0.396
Admission Stockholm CT Score	0.544	0.072	0.519	0.601	0.650	0.063	0.550	0.147	**0.640**	**0.022**	**0.594**	**0.045**	**0.585**	**0.030**
Admission Stockholm CT "Range"	0.556	0.473	0.578	0.754	0.675	0.324	0.557	0.875	**0.670**	**<0.0001**	0.642	0.152	0.612	0.192
ISS	0.518	0.734	**0.598**	**0.027**	0.560	0.375	0.545	0.393	0.565	0.521	0.553	0.192	0.514	0.545
APACHE II	0.526	0.406	**0.619**	**0.032**	**0.702**	**0.002**	**0.652**	**<0.001**	**0.704**	**0.001**	**0.633**	**0.004**	**0.651**	**0.001**

*AUC = area under the receiver operative curve, p = p-value, GCS = Glasgow Coma Scale, CT = computed tomography, ISS = injury severity score, PRx = pressure reactivity index (correlation between ICP and MAP), PAx = pulse amplitude index (correlation between pulse amplitude of ICP (AMP) and MAP), RAC = correlation between AMP and CPP. *NOTE: bolded values are those which have reached statistical significance (p<0.05).*

Multivariable Logistic Regression (MLR) Analysis

Based on the results of the ULR analysis, we created individualized multivariable models for each binary threshold outcome, performing a sequential "elimination method" of MLR analysis in order to arrive at the best predictive model for each index threshold (see methods section). For each model, we included only those variables reaching statistical significance (or close to it: p<=0.100) in ULR, as highlighted in Tables 9.3 and Appendix J. Similar results were seen for the 1st 24 hours and 1st 72 hours recording data sheets.

The MLR models for the binary PRx threshold outcomes displayed similar trends to those mentioned in the ULR section, markers of systemic injury and diffuse IC injury seem to predominate over those of IC parenchymal damage. For the binary threshold outcome of PRx above 0, the best model was that composed of age (p=0.093), presence of bilateral SDH (p=0.009), convexity tSAH thickness over 5mm (p=0.049) and the presence of subcortical (SC) DAI lesions (p=0.001); with an AUC for the model of 0.670 (p<0.0001). For the binary threshold outcome of PRx above +0.25, the best model was composed of sex (p=0.015), APACHE II score (p=0.032), presence of convexity SDH (p=0.016), presence of falcine SDH (p=0.051) and the presence of bilateral convexity SDH (p=0.023); with an AUC for the model of 0.758 (p=<0.0001). Finally, for the binary threshold outcome of PRx above +0.35, the best model was composed of APACHE II score (p=0.003), presence of convexity SDH (p=0.072), presence of bilateral convexity SDH (p=0.062) and complete filling of the basal cisterns with tSAH (p=0.025); with an AUC for the model of 0.791 (p<0.0001).

For the binary threshold outcome of PAx above 0, the best model contained age (p<0.0001), presence of any basal cistern compression (p=0.011), presence of bilateral contusions (p=0.062) and the presence of SC DAI lesions (p=0.019); with an AUC for the model of 0.752 (0<0.0001). For the binary threshold outcome of PAx above +0.25, the best model contained age (p=0.001), presence of convexity SDH (p=0.099), presence of falcine SDH (p=0.067) and the presence of bilateral SDH (p=0.015); with an AUC for the model of 0.871 (p<0.0001).

Finally, the multi-variate models for the binary RAC threshold outcomes displayed similar results to those of PRx and PAx. For the binary threshold outcome of RAC above -0.05, the best model contained age (p=0.016), APACHE II (0.092), presence of tentorial SDH (p=0.048), presence of tSAH filling the basal cisterns (p=0.028) and the presence of SC DAI lesions (p=0.051); with an AUC for the model of 0.744 (p<0.0001). Similarly, for the model with RAC above -0.10 as an outcome, the best model contained age

(p=0.027), Stockholm Score (0.062), APACHE II score (p=0.032), any gyral compression (p=0.017), tSAH amount in the basal cisterns (p=0.087) and the presence of SC DAI lesions (p=0.009); with an AUC for the model of 0.756 (p<0.0001).

9.4 Discussion

Through a detailed analysis of both admission IC and EC injury burden, as it relates to cerebrovascular reactivity during the ICU phase of TBI care, some interesting and important trends have been identified for the first time.

First, whilst the admission IC CT scores (Marshall,[153] Rotterdam,[154] Helsinki,[155] Stockholm[156]) are well validated as predictors of outcome, overall, they appear to show little association with impaired cerebrovascular reactivity after TBI. Some statistically significant differences between categories of the IC scoring systems for both: A. raw mean values of PRx, PAx and RAC; and B. mean % time spent above index threshold; using KW and JT testing were seen. The Helsinki and Rotterdam scoring systems appear to display the strongest relationship to some of the indices of cerebrovascular reactivity. Similarly, through JT testing, it appears that the various scoring categories for the Helsinki score display statistically different mean values for the indices and % time above threshold, with increasing values seen as the ordinal score increases. Among the CT scoring systems, the Helsinki score provides the greatest role for large mass lesions as both basal cistern compression and mass lesions >25 cm^3 greatly increase the score, suggesting that these space occupying lesions may affect cerebral autoregulation. However, when evaluating the ability of the Helsinki score to predict "impairment" of cerebrovascular reactivity, ULR and MLR analysis display that the Helsinki score falls out of statistical significance. This was also seen with the Marshall, Rotterdam and Stockholm score in ULR and MLR analysis. The Stockholm CT score had the strongest correlations to RAC and PAx. The tSAH burden is the main outcome predictor in the Stockholm CT score, as recently shown in comparison to the other CT scoring systems. This could indicate that RAC and PAx are more strongly associated with wide spread tSAH which presumably is a driver for several secondary injury cascades following TBI.

Secondly, the EC injury scores (ISS and APACHE) displayed interesting trends. The ISS failed to be associated with either the indices or impaired cerebrovascular reactivity. Thus, the combined IC and EC trauma burden, as assessed by the ISS does not appear to be associated with impairment of

autoregulation/cerebrovascular reactivity. In contrast, the APACHE score was the most strongly, out of both the IC and EC scoring systems, associated with both raw index values and % time spent above thresholds. Furthermore, the APACHE reaches statistical significance in ULR for its association with all thresholds of ICP indices of cerebrovascular reactivity (except for the PRx >0 threshold). This predictive value for impaired reactivity is even maintained in some the multi-variate models tested for the thresholds of: PRx > +0.35 and RAC > -0.10. Examining the differences between the ISS and APACHE, it can be seen that the APACHE provides a much more robust assessment of the patient's systemic response to injury, including accounting for: A. age, B. hemodynamic response, C. core temperature, and D. laboratory values. Thus, the patient's individual "host response" to injury, appears to be most associated with impaired cerebrovascular reactivity, not the tallied gross injury burden. This raises the question of systemic host response to injury, not cumulative injury burden, as a potential driver of autoregulatory failure/cerebrovascular dysfunction post-TBI. This requires investigation. It is possible that diffuse IC injury patterns, which were more associated with impaired cerebrovascular reactivity, are also more likely to be associated with severe systemic multi-system trauma, and hence worse APACHE scores. Thus, the association between APACHE and impaired autoregulation/cerebrovascular reactivity may be reflective of this relationship, and not necessarily the host systemic biochemical/metabolic or inflammatory response, driving impaired vascular reactivity. As discussed in a recent review of literature, these relationships may be modulated by host genotype.[28,193] Much further work is required to explore this relationship.

Thirdly, diffuse IC injury patterns, not gross macroscopic parenchymal injury, appear to be most associated with impaired cerebrovascular reactivity. This was seen in both the ULR and MLR analysis of the detailed admission IC injury characteristics. The presence of a convexity SDH, falcine SDH, bilateral convexity SDH, thickness of convexity tSAH, amount of tSAH in the basal cisterns and presence of SC DAI lesions, appear to be the most significant predictors of impaired cerebrovascular reactivity, regardless of the ICP-related autoregulatory index threshold tested. All of these markers are those of diffuse injury, implicating a mechanism of high energy, with both acceleration/deceleration and angular acceleration/shearing forces applied to the parenchyma. This implies that "diffuse" injury, other than what is captured by the CT scoring systems, is more predictive of impaired reactivity. Furthermore, all markers of gross macroscopic parenchymal injury failed to be associated with autoregulatory failure. In aggregate, this could explain the lack of significance of IC CT scoring systems in predicting impaired cerebrovascular reactivity. Given these results, diffuse microscopic injury burden, not visible on admission CT scans, may be a driver of impaired cerebrovascular reactivity. Magnetic resonance imaging

(MRI) based assessment of IC injury in the acute phase may shed light on this injury pattern, and requires further investigation.

Finally, age appears to be robustly associated with both the raw indices and % time spent above index thresholds. In addition, age was a strong predictor of impaired cerebrovascular reactivity in both ULR and MLR analysis. This relationship between advancing age and impairment of autoregulatory capacity has been described in part before, and the analysis in this non-DC cohort confirms this variable as a key player in an individual patient's cerebrovascular reactivity post-TBI. Age is also included within the APACHE score calculation, and thus may play a role in why the APACHE scores were statistically significant in their associations with impaired cerebrovascular reactivity. From this data set, it cannot be determined if this was that case given the amalgamated single score that was stored within the NCCU database. Age may play a role in the baseline ability of the cerebrovascular tree to autoregulate, and/or the host response to injury. Further investigation into local and global biochemical/metabolic response and inflammatory response to TBI is required, in order to fully understand how age impacts autoregulatory function/cerebrovascular reactivity post-TBI.

Limitations

Despite the interesting results, there are some important limitations to highlight. First, this is a retrospective cohort of non-DC patients. The treatments received during the patient's ICU phase directly influenced the physiologic variables and signals recorded. Furthermore, this treatment may not have been homogenous throughout all patients included in this study. This could not be taken into account within the analysis, given the lack of information available on treatments received.

Second, this cohort is a non-DC cohort only. This was chosen specifically to avoid the confounding introduced post-DC, during which ICP and ICP derived indices of cerebrovascular reactivity are impacted. Thus, the results of this analysis only apply to non-DC patients. Similar analysis is required for DC patients, analyzing the associations while taking into account the influence of craniectomy on the physiologic variables measured.

Thirdly, the ISS included in this study is the total ISS, thus including injury to the body as well as the head and brain, not making it an exclusive score for the EC injury burden. Head ISS is based on anatomical localization of lesions on admission head CT scans, similar to many of the CT scoring systems included and, depending on the presence of polytrauma, will contribute significantly to the total ISS variable used

in this study. Moreover, APACHE II contains admission GCS which is commonly used to assess the severity of brain injury, similar to the IC CT scoring systems. Thus, the EC injury variables used in this study will to different degrees be influenced by the IC injury burden. Future studies may avoid this by only using non-head ISS components, unfortunately not available for the current cohort.

9.5 Conclusions

Diffuse IC injury markers (such as thickness of SAH, presence of sub-cortical DAI lesions, and the presence of a SDH) and systemic injury response (as assessed via APACHE II) are most associated with dysfunction in cerebrovascular reactivity after TBI. Standard IC CT scoring systems and evidence of macroscopic parenchymal damage are poor predictors, implicating potentially both microscopic injury patterns and host response as drivers of dysfunctional cerebrovascular reactivity. Age remains a major variable associated with cerebrovascular reactivity.

CHAPTER 10: SUMMARY AND CONCLUSIONS

Through the studies and data presented in Chapters 4 through 9 of this thesis, some important new insights into continuous MMM of cerebrovascular reactivity in adult TBI have been made. The following questions were addressed: A. Do other ICP derived indices exist? B. Do ICP derived indices actually measure autoregulation? C. What are the inter-index relationships between various MMM techniques? D. Can one estimate/predict the "gold standard" invasive PRx using non-invasive means? E. What are the critical thresholds associated with outcome for ICP derived indices? F. Which ICP derived index is superior for outcome prediction? and G. What role does IC and EC injury burden play in driving autoregulatory function in TBI? These questions were addressed using data from various experimental models and populations of adult TBI patients.

The following hypotheses were addressed:

***Hypothesis I:* The moving correlation coefficient between slow-wave fluctuations in AMP and CPP, defined as RAC, will provide information regarding cerebrovascular reactivity, and may be used in place of existing ICP based reactivity indices in adult TBI patients.**

Chapter 4 provided the first description of this new index in adult TBI, providing confirmatory evidence that it provides information regarding cerebrovascular reactivity. Furthermore, RAC appears to carry additional information regarding cerebral compensatory reserve (similar to RAP). The interpretation of this index is somewhat complex, however it appears to have a clearer parabolic relationship with CPP over the range of clinically seen CPP values, compared to PRx and PAx. Thus, RAC can potentially be utilized for monitoring cerebrovascular reactivity.

***Hypothesis II:* PRx, PAx and RAC will measure the LLA in an experimental piglet model of arterial hypotension.**

Chapter 5.1 outlined the experimental validation of PRx, PAx and RAC as a measure of the LLA in a model of arterial hypotension. This study provided very preliminary confirmatory evidence for PRx. In

addition, for the first time in the literature, this study provided a similar validation for PAx and RAC. These results provide some degree of confidence in the clinical use of these indices for monitoring cerebral autoregulation, though further experimental validation of these indices is required. As such Hypothesis II is not fully confirmed.

***Hypothesis III:* PRx, PAx and RAC will measure the LLA in an experimental rabbit model of sustained IC hypertension.**

Chapter 5.2 outlined the experimental validation of PRx and PAx as a measure of the LLA in and experimental model of IC hypertension. This study, for the first time, provides preliminary confirmation that PRx and PAx measure autoregulation during sustained ICP elevations. These results provide some further confidence in the clinical use of these indices to measure autoregulation, particularly in pathologic states prone to elevated ICP, such as TBI. RAC, however, failed to conclusively measure the LLA within this model, which is likely a limitation of the model and failure to reach the break-point in AMP within the 12 animals. Despite the promsing results from this analysis, further experimental evaluation of these indices as measures of the LLA during IC hypertension is required. As such Hypothesis III is not fully confirmed.

***Hypothesis IV:* PRx, PAx and RAC will measure the ULA in an experimental piglet model of arterial hypertension.**

Chapter 5.3 outlined the attempts at experimental validation of the ICP derived indices against the ULA in a piglet model of arterial hypertension. The results of the analysis within the 6 animals were inconclusive. Saturation of LDF-CBF signal, with failure to display pressure/flow passivity with increasing CPP, questions the CPP values identified as the ULA via piecewise regression. Currently it remains unclear as to whether these indices can accurately measure the ULA.

***Hypothesis V:* Continuous indices derived from MMM are not all the same, and display specific covariance structure between monitoring devices used, which is reproducible across populations.**

Chapter 6.1, 6.2, and 6.3 outlined the studies into MMM inter-index relationships, explored via multivariate clustering and co-variance analysis techniques. The strong relationships between PRx and

Sx_a seen in these sections were echoed in the results from section 7.1 and 7.3. This work, for the first time, explores the inter-index relationships of all concomitantly monitored continuous indices of cerebrovascular reactivity, across four separate adult TBI populations. Several specific relationships were seen amongst the indices examined. First, we observed intra-technique clustering, suggesting than different metrics provided by a single technique provide shared information. Second, the results demonstrate a strong, and recurrent, association between TCD based Sx/Sx_a and the ICP derived indices (PRx, PAx, and RAC). Third, the data show an association between measures of cortical pial/microvascular cerebrovascular reactivity indices and TCD based Mx/Mx_a., implicating Mx/Mx_a as potential surrogate measures of cortical vessel reactivity. Finally, the stong PRx and Sx_a relationships also hold up during extended duration recordings, as seen with the modelling in chapter 7.1 and 7.3.

***Hypotheses VI and VII:* PRx can be accurately estimated and predicted via non-invasive TCD alternatives, systolic flow index (Sx_a) and mean flow index (Mx_a).**

Chapters 7.1 and 7.3 outlined the studies into the estimation of PRx via non-invasive TCD based surrogates (Sx_a and Mx_a). Employing complex time-series ARMA models and LME modelling, it was demonstrated that PRx can be estimated using non-invasive TCD surrogates. Furthermore, this estimation closely follows observed PRx values. Further, even if the data are preliminary, given limitations with extended duration TCD recording, using time-series ARMA and LME modelling, it was demonstrated in a small pilot cohort that PRx can be predicted non-invasively with an acceptable degree of agreement. Despite these promising results, it must be acknowledged that these analyses are some of the first of their type in the literature and require substantial validation. Further, large scale, studies need to be conducted to confirm these results. As such, the results should be considered very preliminary and exploratory in nature, with Hypotheses VI and VII not fully yet confirmed.

***Hypothesis VIII:* Outcome prediction with ICP-derived indices are not equal, with RAC providing superior predictive capabilities for 6-month patient outcomes.**

Chapter 8.1 outlined the studies into outcome prediction and critical thresholds of ICP derived indices of cerebrovascular reactivity in adult TBI. It was demonstrated that RAC provides superior 6-month outcome prediction over both PRx and PAx, via both univariate and multivariate models. This was

observed for both mortality and favourable/unfavourable outcomes. These results confirm the superiority of RAC over PRx and PAx for outcome assessment.

<u>Hypothesis IX:</u> Critical thresholds for 6-month outcome in adult TBI in ICP derived reactivity indices are not all the same, with some indices displaying more "stable" thresholds over time.

As studied in Chapter 8.1, critical thresholds associated with outcome at 6-months were evaluated for all ICP indices in a non-DC cohort. Thresholds for mortality and unfavourable outcome were provided for PRx, PAx and RAC. It has demonstrated that the PRx thresholds for these outcomeswere substantially different compared to previous work on a heterogenous TBI population (which included DC patients), suggesting that alterations in post-DC cerebrovascular physiology may have confounded previous results. Furthermore, RAC consistently provided significant predictive thresholds for outcome, regardless of time period analyzed, which was not the case for PRx or PAx. Finally, RAC displayed the most stable critical thresholds over time, when compared to those for PRx and PAx. These results implicate RAC as a having potentially more reliable critical thresholds for outcome in adult TBI.

<u>Hypothesis X:</u> Both Sx and Sx_a have well defined critical thresholds associated with 6-month outcome in adult TBI.

Chapter 8.2 outlined the studies to determine critical thresholds for Sx/Sx_a. The results of this analysis demonstrate, for the first time, significant thresholds for Sx/Sx_a to predict both 6-month mortality and unfavourable outcome, based on GOS. Furthermore, these thresholds are drastically different compared to thresholds previously defined for Mx/Mx_a. These results provide a framework and clinically relevant outcome prediction thresholds derived from monitoring of Sx/Sx_a in adult TBI.

<u>Hypothesis XI:</u> Specific patterns of IC injury are associated with impaired cerebrovascular reactivity in TBI.

Chapter 9 outlined the studies conducted to evaluate the link between IC injury pattern/burden and its link with impaired cerebrovascular reactivity. The results, for the first time, suggest that IC markers of diffuse injury are linked to impaired reactivity. These markers included: thickness of SAH, presence of

SDH, and presence of DAI. This implicates acceleration/deceleration or angular forces suffered by the brain to be a potential driver of impaired vascular reactivity in adult TBI.

***Hypothesis XII:* EC injury burden will be associated with cerebral vascular reactivity in polytrauma patients.**

Chapter 9 also attempted to address the association between EC injury burden and vascular reactivity post-TBI. Given out access to records and data on EC injury was limited, the conclusions are also limited. The results did demonstrate a strong link with impaired reactivity and both age and APACHE II. The link with age has been previously documented. The association with APACHE II has never been described previously. The ISS failed to demonstrate a significant association with impaired reactivity. This implicates systemic host response (ie. APACHE II), and not the tallied systemic injury burden (ie ISS), as a potential driver of impaired cerebrovascular reactivity in adult TBI.

Clinical Implications

Clinically, the results of this thesis carry some potentially important implications which may lead to changes in future patient care. First, the results of these studies suggest RAC may: provide information regarding both cerebrovascular reactivity and cerebral compensatory reserve, have some ability of measure the LLA and appears to display stronger associations with global patient outcome. This may translate to improve prognostic models with the inclusion of such an index. This index carries some complexity in interpretation, as outlined in Chapter 4, which highlights difficulties with its implementation as a continuously displayed and interpreted bedside physiologic metric in TBI. However, the strong outcome association and stability in critical thresholds supports its promising role in the development of next generation prognostic models in moderate and severe TBI, which will be the focus of upcoming studies from CENTER-TBI.[190] Further to this, RAC appears to have a clearer parabolic relationship with CPP at the population level. This implies that RAC carries potential to be superior in the determination of individual patient optimal CPP values, improving percent yield of these CPP estimations. With future work, if such superiority of RAC based optimal CPP estimation is confirmed, this will lead to improved continuity in individualized CPP optimum estimation and potential confidence in the derived optimal CPP value that is being suggested as a target.

Second, the preliminary results of the experimental models, despite requiring much future validation, do provide some added confidence that some of these metrics of cerebrovascular reactivity employed clinically, do in fact measure aspects of the LLA. This is important, as previously, there was limited literature to suggest metrics such as PRx, do indeed provide surrogate measures for the LLA.[14]

Third, some further clarity regarding the various MMM derived cerebrovascular reactivity indices has been provided. The previous literature base suffered from small individual index comparisons between monitoring modalities. This was insufficient and led to confusion as to if all of these metrics were measuring the same aspect of cerebral physiology. Through the various analytical techniques applied in Chapters 6 and 7, it was demonstrated the certain modalities provide specific information regarding cerebrovascular reactivity, which may be carried forward in the future to guide clinical assessment. ICP, NIRS and TCD systolic flow indices appear to carry similar information regarding cerebrovascular reactivity. These were distinct from TCD mean flow-based indices which appear to provide more information regarding cortical pial/microcirculatory cerebrovascular reactivity. Finally, uncertainty regarding the utility of $PbtO_2$ derived cerebrovascular reactivity indices was provided, suggesting extreme caution in the clinical application of such measures.

Fourth, non-invasive estimation and prediction of invasively derived cerebrovascular reactivity measures has been demonstrated as feasible. These are the first preliminary attempts at such work, but provide great promise if further validated. Such non-invasive estimation carries important implications for long-term follow-up assessment using TCD, and confidence in systolic flow-derived metrics in the non-invasive assessment of cerebrovascular reactivity. Further, with the delineation of critical thresholds associated with global outcome for these TCD metrics, there now exists defined values of systolic flow indices which are associated with negative outcomes. Overall, though preliminary and exploratory in nature, this thesis work provides important implications for the future potential transition to more non-invasive monitoring modalities in adult TBI, without the sacrifice in critical information related to cerebrovascular physiology or prognostication.

Fifth, previous studies on ICP-derived indices of cerebrovascular reactivity may have been clouded by included heterogeneous populations consisting of both DC and non-DC TBI patients. The results of the ICP index critical threshold studies in this thesis suggest that DC may have had significant impacts on previously defined, and current clinically applied, critical thresholds associated with outcome.[9,152] This

implies there is a need to re-evaluate our current clinical thresholds and spend time to better understand the impact of DC on cerebrovascular physiology, raising questions as to the applicability of cerebrovascular reactivity monitoring in the setting of a craniectomy.

Finally, the association between IC and EC admission injury metrics and impaired cerebrovascular reactivity is an important finding. Though preliminary findings, requiring further validation, they suggest that specific injury characteristics predispose patients to the development of impaired vascular reactivity. This carries important implications for future ability to predict those at highest risk, and stratify them accordingly for any potential future therapies that may be directed at prevention and treatment of impaired autoregulation in TBI.

Conclusions

In conclusion, this thesis provides important results which fill in many current holes in the knowledge regarding continuous measures of cerebrovascular reactivity in adult TBI. The data and results presented in this thesis describe a new ICP derived index of cerebrovascular reactivity in adult TBI, provide validation for ICP indices as measures of the LLA, highlight important inter-index relationships, demonstrate the ability to non-invasively model invasive measures, accurately define critical thresholds for 6-month outcome, demonstrate superiority of the new ICP index, and provide the first evidence to suggest a link between specific IC injury patterns, and physiological markers of the host response, with impaired cerebrovascular reactivity. These results will provide confidence in the clinical application of MMM measures of vascular reactivity in adult TBI, while laying the platform for future exploration into drivers of impaired reactivity.

CHAPTER 11: FUTURE DIRECTIONS

11.1 Experimental Validation – LLA and ULA

The studies within this thesis provided validation of the ICP indices as measures of the LLA. However, this was conducted using the two extremes of CPP change: pure arterial hypotension, and pure IC hypertension. There still exists the possibility that these indices fail to measure the LLA when ICP is moderately elevated (ie. 20 to 40 mm Hg) – the context in which most clinical care is undertaken. Thus, further models are required to explore physiology when ICP is moderately elevated and/or arterial hypotension is present.

Regarding the ULA, this thesis failed to validate the ICP indices of cerebrovascular reactivity as measures of the ULA. Thus, it remains unclear as to whether these indices actually measure the ULA, despite some of them being employed clinically for calculation of the optimal CPP (CPPopt). Experimental models of arterial hypertension are required for to address this question, both in the setting of normal and elevated ICP. One might consider models of sustained ICP elevation during arterial hypertension, so as to shift the ULA to lower CPP values, allowing to interrogate these indices across the ULA prior to animals succumbing to cardiac failure.[175] Further, given the inability to determine the ULA easily within piglets suggests the need for a different animal model.

11.2 Validation for RAC

Despite the promising results presented in this thesis, further work is required to validate the findings for the newly defined index RAC. First, the assessment of RAC in experimental models IC hypertension requires further evaluation, given the inconclusive results seen from the studies in this thesis. It is possible that the failure to demonstrate that RAC can provide measure of the LLA during IC hypertension (as seen in Chapter 5.2) may be secondary to limitations of the model. The rate of increase in ICP was precipitous and may have led to the lack of AMP break-point seen in the 12 animals studied. Furthermore, the Cushing's response seen within these animals may have driven AMP to increase without an identifiable break point.[145] If this break point was reached, RAC would likely have measured the LLA within this model. Hence, further evaluation in this context is required, where ICP is elevated in a more controlled and prolonged fashion.

Regarding the clinical application of RAC, validation studies are required to confirm the superiority of RAC over PRx and PAx. These studies would require similar univariate and multivariate models evaluating 6-month outcomes in adult TBI, as employed in this thesis. However, added value would be found in evaluating the additional variance when each of these indices is added to the IMPACT-core[194] variables. One would expect the IMPACT + RAC to provide superior outcome prediction capabilities. However, this has yet to be demonstrated. This assessment of IMPACT plus vascular reactivity monitoring would also provide much need information regarding the overall additional benefit of monitoring cerebrovascular reactivity in adult TBI. This is currently planned using the CENTER-TBI[190] high resolution patient cohort.

Finally, the calculation of CPPopt using PRx, PAx and RAC needs further assessment. The results from this thesis displayed a more symmetric parabolic relationship between RAC vs. CPP, compared to PRx vs. CPP or PAx vs. CPP, suggesting RAC may be superior in CPPopt estimation. This requires investigation. Further, evaluating the association between the percentage of time spent outside of CPPopt and outcome, requires investigation (comparing PRx, PAx and RAC). This study is also planned using the CENTER-TBI[190] high resolution patient cohort.

11.3 Time-Series Techniques for Cerebrovascular Reactivity

This thesis provided the first described attempts at modelling cerebrovascular reactivity indices using time-series analysis techniques. Despite being adapted from the financial sector;[163,164,166] these techniques have wide reaching implications for monitoring in TBI. Applications exist for based forecasting/predictions of physiologic events, and for Bayesian state space models[166] of the entire patients clinical "state". Given the complexity of these forms of statistical modelling, the application of artificial neural networks is a natural avenue to explore with this type of modelling. The implications of these techniques could mean accurate future forecasting of events and clinical states for patients.

11.4 Critical Thresholds for DC Populations

Results from this thesis defined critical thresholds for 6-month outcomes in non-DC adult TBI patients.[152] These results provide thresholds for PRx that are substantially different compared to those that have

previously been defined, and are currently clinically used.[9] It is highly likely that these discrepancies arise from the inclusion of physiologic data from DC patients in earlier studies on the outcome associations of PRx thresholds. The physiologic response to DC likely led to the overall thresholds for the entire population (DC and non-DC) to be lower than that found in the studies of this thesis. Thus, future work is required to both better understand the changes in PRx, PAx and RAC after DC, and also define critical thresholds for DC patients.

11.5 Drivers of Impaired Cerebrovascular Reactivity

Injury Burden

IC and EC injury burden were explored as drivers of impaired cerebrovascular reactivity in adult TBI. It was demonstrated in this thesis that specific IC injury patterns were associated with impaired reactivity. This analysis is the first to explore this relationship, and needs replication. This is currently planned using the CENTER-TBI high resolution cohort.

EC injury burden was only preliminarily assessed in this thesis, with the results suggesting that the burden of abnormal physiology measured by APACHE II (which probably integrates injury severity and systemic host response) as a potential diver of impaired reactivity. This requires much further investigation. Additional assessment of systemic markers of inflammation and biomarkers of injury would prove useful. Similarly, a breakdown of organ system injury burden and its association with cerebrovascular reactivity might prove interesting. These studies are currently planned using the CENTER-TBI[190] high resolution cohort.

Understanding the IC and EC injury associations to impaired reactivity will allow us to properly risk stratify patients and improve outcome prediction capabilities.

Genetics

Recent review of literature has outlined the current literature addressing the association between genetic variation and impaired reactivity post-TBI.[28,193] More specifically, published data suggest a link between NOS3 polymorphisms and impaired reactivity,[195] and literature outside of TBI has implicated

numerous SNP's associated with systemic vascular reactivity. A theoretical framework for candidate genetic polymorphisms linked to cerebrovascular biology has been outlined in one of the publications associated with literature review for this thesis.[28] These candidate genes are currently being investigated as part of the genome wide association analysis for the CENTER-TBI[190] high resolution cohort. Potential associations with cerebrovascular reactivity will be analyzed.

If specific genes are identified, the study will be underpowered to make significant conclusions. However, this will provide the platform for future directed genetics studies related to cerebrovascular reactivity. These genetic associations will provide insight into the mechanisms involved in impaired vascular reactivity. These analyses will provide insights into potential molecular mechanisms that underpin impaired cerebrovascular reactivity, and allow the design of therapeutic interventions aimed at improving autoregulation with the aim of reducing mortality and improving patient outcome in TBI.

REFERENCES

1 Lassen NA. Cerebral blood flow and oxygen consumption in man. *Physiol Rev* 1959; **39**: 183–238.

2 Fog M. THE RELATIONSHIP BETWEEN THE BLOOD PRESSURE AND THE TONIC REGULATION OF THE PIAL ARTERIES. *J Neurol Psychiatry* 1938; **1**: 187–97.

3 Czosnyka M, Smielewski P, Kirkpatrick P, Laing RJ, Menon D, Pickard JD. Continuous assessment of the cerebral vasomotor reactivity in head injury. *Neurosurgery* 1997; **41**: 11–7; discussion 17-19.

4 Zeiler FA, Donnelly J, Calviello L, Smielewski P, Menon DK, Czosnyka M. Pressure Autoregulation Measurement Techniques in Adult Traumatic Brain Injury, Part II: A Scoping Review of Continuous Methods. *J Neurotrauma* 2017; **34**: 3224–37.

5 Budohoski KP, Czosnyka M, Kirkpatrick PJ, Smielewski P, Steiner LA, Pickard JD. Clinical relevance of cerebral autoregulation following subarachnoid haemorrhage. *Nat Rev Neurol* 2013; **9**: 152–63.

6 Oeinck M, Neunhoeffer F, Buttler K-J, *et al.* Dynamic cerebral autoregulation in acute intracerebral hemorrhage. *Stroke* 2013; **44**: 2722–8.

7 Czosnyka Z, van den Boogaard F, Czosnyka M, Momjian S, Gelling L, Pickard JD. The relationship between CSF circulation and cerebrovascular pressure-reactivity in normal pressure hydrocephalus. *Acta Neurochir Suppl* 2005; **95**: 207–11.

8 Sorrentino E, Budohoski KP, Kasprowicz M, *et al.* Critical thresholds for transcranial Doppler indices of cerebral autoregulation in traumatic brain injury. *Neurocrit Care* 2011; **14**: 188–93.

9 Sorrentino E, Diedler J, Kasprowicz M, *et al.* Critical thresholds for cerebrovascular reactivity after traumatic brain injury. *Neurocrit Care* 2012; **16**: 258–66.

10 Zeiler FA, Donnelly J, Calviello L, Menon DK, Smielewski P, Czosnyka M. Pressure Autoregulation Measurement Techniques in Adult Traumatic Brain Injury, Part I: A Scoping Review of Intermittent/Semi-Intermittent Methods. *J Neurotrauma* 2017; **34**: 3207–23.

11 Czosnyka M, Miller C, Participants in the International Multidisciplinary Consensus Conference on Multimodality Monitoring. Monitoring of cerebral autoregulation. *Neurocrit Care* 2014; **21 Suppl 2**: S95-102.

12 Le Roux P, Menon DK, Citerio G, *et al.* The International Multidisciplinary Consensus Conference on Multimodality Monitoring in Neurocritical Care: evidentiary tables: a statement for healthcare professionals from the Neurocritical Care Society and the European Society of Intensive Care Medicine. *Neurocrit Care* 2014; **21 Suppl 2**: S297-361.

13 Fraser CD, Brady KM, Rhee CJ, *et al.* The frequency response of cerebral autoregulation. *J Appl Physiol Bethesda Md 1985* 2013; **115**: 52–6.

14 Brady KM, Lee JK, Kibler KK, Easley RB, Koehler RC, Shaffner DH. Continuous measurement of autoregulation by spontaneous fluctuations in cerebral perfusion pressure: comparison of 3 methods. *Stroke* 2008; **39**: 2531–7.

15 Aries MJH, Czosnyka M, Budohoski KP, *et al.* Continuous monitoring of cerebrovascular reactivity using pulse waveform of intracranial pressure. *Neurocrit Care* 2012; **17**: 67–76.

16 Dengl M, Jaeger M, Renner C, Meixensberger J. Comparing brain tissue oxygen measurements and derived autoregulation parameters from different probes (Licox vs. Raumedic). *Acta Neurochir Suppl* 2012; **114**: 165–8.

17 Jaeger M, Soehle M, Schuhmann MU, Meixensberger J. Clinical significance of impaired cerebrovascular autoregulation after severe aneurysmal subarachnoid hemorrhage. *Stroke* 2012; **43**: 2097–101.

18 Jaeger M, Dengl M, Meixensberger J, Schuhmann MU. Effects of cerebrovascular pressure reactivity-guided optimization of cerebral perfusion pressure on brain tissue oxygenation after traumatic brain injury. *Crit Care Med* 2010; **38**: 1343–7.

19 Zweifel C, Castellani G, Czosnyka M, *et al.* Continuous assessment of cerebral autoregulation with near-infrared spectroscopy in adults after subarachnoid hemorrhage. *Stroke* 2010; **41**: 1963–8.

20 Zweifel C, Castellani G, Czosnyka M, *et al.* Noninvasive monitoring of cerebrovascular reactivity with near infrared spectroscopy in head-injured patients. *J Neurotrauma* 2010; **27**: 1951–8.

21 Zeiler FA, Donnelly J, Menon D, Smieleweski P, Hutchinson PJ, Czosnyka M. A Description of a New Continuous Physiologic Index in TBI using the Correlation Between Pulse Amplitude of ICP and Cerebral Perfusion Pressure. *J Neurotrauma* 2017; published online Dec 6. DOI:10.1089/neu.2017.5241.

22 Timofeev I, Czosnyka M, Nortje J, *et al.* Effect of decompressive craniectomy on intracranial pressure and cerebrospinal compensation following traumatic brain injury. *J Neurosurg* 2008; **108**: 66–73.

23 Winn H. Youmans Neurological Surgery, 6th edn. Saunders, 2011.

24 Hundley WG, Renaldo GJ, Levasseur JE, Kontos HA. Vasomotion in cerebral microcirculation of awake rabbits. *Am J Physiol* 1988; **254**: H67-71.

25 Halpern W, Osol G. Influence of transmural pressure of myogenic responses of isolated cerebral arteries of the rat. *Ann Biomed Eng* 1985; **13**: 287–93.

26 Auer LM, Ishiyama N, Pucher R. Cerebrovascular response to intracranial hypertension. *Acta Neurochir (Wien)* 1987; **84**: 124–8.

27 Howells T, Johnson U, McKelvey T, Enblad P. An optimal frequency range for assessing the pressure reactivity index in patients with traumatic brain injury. *J Clin Monit Comput* 2015; **29**: 97–105.

28 Zeiler FA, Thelin EP, Donnelly J, *et al.* Genetic drivers of cerebral blood flow dysfunction in traumatic brain injury: a speculative synthesis. *Nat Rev Neurol* 2018; **In Press**.

29 Zeiler FA, Thelin EP, Czosnyka M, Hutchinson PJ, Menon DK, Helmy A. Cerebrospinal Fluid and Microdialysis Cytokines in Severe Traumatic Brain Injury: A Scoping Systematic Review. *Front Neurol* 2017; **8**: 331.

30 Wu W, Guan Y, Zhao G, *et al.* Elevated IL-6 and TNF-α Levels in Cerebrospinal Fluid of Subarachnoid Hemorrhage Patients. *Mol Neurobiol* 2016; **53**: 3277–85.

31 Zeiler FA, Thelin EP, Czosnyka M, Hutchinson PJ, Menon DK, Helmy A. Cerebrospinal Fluid and Microdialysis Cytokines in Aneurysmal Subarachnoid Hemorrhage: A Scoping Systematic Review. *Front Neurol* 2017; **8**: 379.

32 Lavinio A, Ene-Iordache B, Nodari I, *et al.* Cerebrovascular reactivity and autonomic drive following traumatic brain injury. *Acta Neurochir Suppl* 2008; **102**: 3–7.

33 Brennan KC, Beltrán-Parrazal L, López-Valdés HE, Theriot J, Toga AW, Charles AC. Distinct vascular conduction with cortical spreading depression. *J Neurophysiol* 2007; **97**: 4143–51.

34 Hoffmann U, Ayata C. Neurovascular coupling during spreading depolarizations. *Acta Neurochir Suppl* 2013; **115**: 161–5.

35 Guiou M, Sheth S, Nemoto M, *et al.* Cortical spreading depression produces long-term disruption of activity-related changes in cerebral blood volume and neurovascular coupling. *J Biomed Opt* 2005; **10**: 11004.

36 Shibata M, Leffler CW, Busija DW. Cerebral hemodynamics during cortical spreading depression in rabbits. *Brain Res* 1990; **530**: 267–74.

37 Toth P, Szarka N, Farkas E, *et al.* Traumatic brain injury-induced autoregulatory dysfunction and spreading depression-related neurovascular uncoupling: Pathomechanisms, perspectives, and therapeutic implications. *Am J Physiol Heart Circ Physiol* 2016; **311**: H1118–31.

38 Hinzman JM, Andaluz N, Shutter LA, *et al.* Inverse neurovascular coupling to cortical spreading depolarizations in severe brain trauma. *Brain J Neurol* 2014; **137**: 2960–72.

39 Hartings JA, Wilson JA, Hinzman JM, *et al.* Spreading depression in continuous electroencephalography of brain trauma. *Ann Neurol* 2014; **76**: 681–94.

40 Hinzman JM, Wilson JA, Mazzeo AT, Bullock MR, Hartings JA. Excitotoxicity and Metabolic Crisis Are Associated with Spreading Depolarizations in Severe Traumatic Brain Injury Patients. *J Neurotrauma* 2016; **33**: 1775–83.

41 Higgins J, Green S. Cochrane Handbook for Systematic Review of Interventions, 1st edn. Wiley-Blackwell, 2008.

42 Zeiler FA, Thelin EP, Helmy A, Czosnyka M, Hutchinson PJA, Menon DK. A systematic review of cerebral microdialysis and outcomes in TBI: relationships to patient functional outcome, neurophysiologic measures, and tissue outcome. *Acta Neurochir (Wien)* 2017; **159**: 2245–73.

43 Bouma G, Muizelaar J, Bandoh K, Marmarou A. Blood pressure and intracranial pressure-volume dynamics in severe head injury: relationship with cerebral blood flow. *J Neurosurg* 1992; **77**: 15–7.

44 Chieregato A, Fainardi E, Tanfani A, *et al.* Induced acute arterial hypertension and regional cerebral flow in intracontusional low density area. *Acta Neurochir Suppl* 2003; **86**: 361–5.

45 Chieregato A, Tanfani A, Compagnone C, *et al.* Global cerebral blood flow and CPP after severe head injury: a xenon-CT study. *Intensive Care Med* 2007; **33**: 856–62.

46 Cold GE, Jensen FT. Cerebral autoregulation in unconscious patients with brain injury. *Acta Anaesthesiol Scand* 1978; **22**: 270–80.

47 Peterson E, Chesnut RM. Static autoregulation is intact in majority of patients with severe traumatic brain injury. *J Trauma* 2009; **67**: 944–9.

48 Peterson E, Tozer K, Cohen W, Lam A, Chesnut R. Rethinking autoregulation in traumatic brain injury: a majority of patients with disruptive dynamic autoregulation do not respond to an elevated cerebral perfusion pressure. *Neurosurgery* 2012; **71**: E560.

49 Mascia L, Andrews PJ, McKeating EG, Souter MJ, Merrick MV, Piper IR. Cerebral blood flow and metabolism in severe brain injury: the role of pressure autoregulation during cerebral perfusion pressure management. *Intensive Care Med* 2000; **26**: 202–5.

50 Ng SCP, Poon WS, Chan MTV, Lam JMK, Lam WWM. Is transcranial Doppler ultrasonography (TCD) good enough in determining CO2 reactivity and pressure autoregulation in head-injured patients? *Acta Neurochir Suppl* 2002; **81**: 125–7.

51 Wintermark M, Chiolero R, Van Melle G, *et al.* Cerebral vascular autoregulation assessed by perfusion-CT in severe head trauma patients. *J Neuroradiol J Neuroradiol* 2006; **33**: 27–37.

52 Wintermark M, Chioléro R, van Melle G, *et al.* Relationship between brain perfusion computed tomography variables and cerebral perfusion pressure in severe head trauma patients. *Crit Care Med* 2004; **32**: 1579–87.

53 Coles JP, Steiner LA, Johnston AJ, *et al.* Does induced hypertension reduce cerebral ischaemia within the traumatized human brain? *Brain J Neurol* 2004; **127**: 2479–90.

54 Czosnyka M, Timofeev I, Smielewski P, *et al.* Pressure and flow regulation within the brain – facts, myths and missing links. *J Cereb Blood Flow Metab* 2007; **27**: B001-009.

55 Steiner LA, Coles JP, Czosnyka M, *et al.* Cerebrovascular pressure reactivity is related to global cerebral oxygen metabolism after head injury. *J Neurol Neurosurg Psychiatry* 2003; **74**: 765–70.

56 Steiner LA, Coles JP, Johnston AJ, *et al.* Assessment of cerebrovascular autoregulation in head-injured patients: a validation study. *Stroke* 2003; **34**: 2404–9.

57 Steiner LA, Coles JP, Johnston AJ, *et al.* Responses of posttraumatic pericontusional cerebral blood flow and blood volume to an increase in cerebral perfusion pressure. *J Cereb Blood Flow Metab Off J Int Soc Cereb Blood Flow Metab* 2003; **23**: 1371–7.

58 Zweifel C, Lavinio A, Steiner LA, *et al.* Continuous monitoring of cerebrovascular pressure reactivity in patients with head injury. *Neurosurg Focus* 2008; **25**: E2.

59 Berre J, Moraine J, Melot C. Cerebral pressure autoregulation in comatose patients with brain injury. *Anesthesiology* 2002; **2000**: A350.

60 de Nadal M, Munar F, Poca MA, Sahuquillo J, Garnacho A, Rosselló J. Cerebral hemodynamic effects of morphine and fentanyl in patients with severe head injury: absence of correlation to cerebral autoregulation. *Anesthesiology* 2000; **92**: 11–9.

61 Munar F, Ferrer AM, de Nadal M, *et al.* Cerebral hemodynamic effects of 7.2% hypertonic saline in patients with head injury and raised intracranial pressure. *J Neurotrauma* 2000; **17**: 41–51.

62 Puppo C, Lopez L, Farina G, *et al.* Indomethacin and cerebral autoregulation in severe head injured patients: a transcranial Doppler study. *Acta Neurochir (Wien)* 2007; **149**: 139–49; discussion 149.

63 Puppo C, López L, Panzardo H, Caragna E, Mesa P, Biestro A. Comparison between two static autoregulation evaluation methods. *Acta Neurochir Suppl* 2002; **81**: 129–32.

64 Rosenthal G, Hemphill JC, Sorani M, *et al.* Brain tissue oxygen tension is more indicative of oxygen diffusion than oxygen delivery and metabolism in patients with traumatic brain injury. *Crit Care Med* 2008; **36**: 1917–24.

65 Sahuquillo J, Amoros S, Santos A, *et al.* False autoregulation (pseudoautoregulation) in patients with severe head injury. Its importance in CPP management. *Acta Neurochir Suppl* 2000; **76**: 485–90.

66 Sahuquillo J, Munar F, Baguena M, Poca MA, Pedraza S, Rodríguez-Baeza A. Evaluation of cerebrovascular CO2-reactivity and autoregulation in patients with post-traumatic diffuse brain swelling (diffuse injury III). *Acta Neurochir Suppl* 1998; **71**: 233–6.

67 Sahuquillo J, Poca MA, Ausina A, Báguena M, Gracia RM, Rubio E. Arterio-jugular differences of oxygen (AVDO2) for bedside assessment of CO2-reactivity and autoregulation in the acute phase of severe head injury. *Acta Neurochir (Wien)* 1996; **138**: 435–44.

68 Aaslid R, Blaha M, Sviri G, Douville CM, Newell DW. Asymmetric dynamic cerebral autoregulatory response to cyclic stimuli. *Stroke* 2007; **38**: 1465–9.

69 Christ M, Noack F, Schroeder T, *et al.* Continuous cerebral autoregulation monitoring by improved cross-correlation analysis: comparison with the cuff deflation test. *Intensive Care Med* 2007; **33**: 246–54.

70 Hlatky R, Furuya Y, Valadka AB, *et al.* Dynamic autoregulatory response after severe head injury. *J Neurosurg* 2002; **97**: 1054–61.

71 Hlatky R, Valadka AB, Robertson CS. Analysis of dynamic autoregulation assessed by the cuff deflation method. *Neurocrit Care* 2006; **4**: 127–32.

72 Jünger EC, Newell DW, Grant GA, *et al.* Cerebral autoregulation following minor head injury. *J Neurosurg* 1997; **86**: 425–32.

73 Rangel-Castilla L, Ahmed O, Goodman JC, Gopinath S, Valadka A, Robertson C. L-arginine reactivity in cerebral vessels after severe traumatic brain injury. *Neurol Res* 2010; **32**: 1033–40.

74 Schramm P, Klein KU, Pape M, *et al.* Serial measurement of static and dynamic cerebrovascular autoregulation after brain injury. *J Neurosurg Anesthesiol* 2011; **23**: 41–4.

75 Sviri GE, Aaslid R, Douville CM, Moore A, Newell DW. Time course for autoregulation recovery following severe traumatic brain injury. *J Neurosurg* 2009; **111**: 695–700.

76 Giller CA. A bedside test for cerebral autoregulation using transcranial Doppler ultrasound. *Acta Neurochir (Wien)* 1991; **108**: 7–14.

77 Ng SC, Poon WS, Chan MT, Lam JM, Lam W, Metreweli C. Transcranial Doppler ultrasonography (TCD) in ventilated head injured patients: correlation with stable xenon-enhanced CT. *Acta Neurochir Suppl* 2000; **76**: 479–82.

78 Smielewski P, Czosnyka M, Kirkpatrick P, Pickard JD. Evaluation of the transient hyperemic response test in head-injured patients. *J Neurosurg* 1997; **86**: 773–8.

79 Steinmeier R, Hofmann RP, Bauhuf C, Hübner U, Fahlbusch R. Continuous cerebral autoregulation monitoring by cross-correlation analysis. *J Neurotrauma* 2002; **19**: 1127–38.

80 Vajramani GV, Chandramouli BA, Jayakumar PN, Kolluri S. Evaluation of posttraumatic vasospasm, hyperaemia, and autoregulation by transcranial colour-coded duplex sonography. *Br J Neurosurg* 1999; **13**: 468–73.

81 McNair N, Woo M, Rinsky B. Baroreflex sensitivity as a marker for cerebrovascular autoregulation status in patients with traumatic brain injury. *Brain Inj* 2012; **26**: 558.

82 Riberholt CG, Olesen ND, Thing M, Juhl CB, Mehlsen J, Petersen TH. Impaired Cerebral Autoregulation during Head Up Tilt in Patients with Severe Brain Injury. *PloS One* 2016; **11**: e0154831.

83 Budohoski KP, Czosnyka M, de Riva N, *et al.* The relationship between cerebral blood flow autoregulation and cerebrovascular pressure reactivity after traumatic brain injury. *Neurosurgery* 2012; **71**: 652–60; discussion 660-661.

84 Budohoski KP, Reinhard M, Aries MJH, *et al.* Monitoring cerebral autoregulation after head injury. Which component of transcranial Doppler flow velocity is optimal? *Neurocrit Care* 2012; **17**: 211–8.

85 Czosnyka M, Smielewski P, Piechnik S, Pickard JD. Clinical significance of cerebral autoregulation. *Acta Neurochir Suppl* 2002; **81**: 117–9.

86 Czosnyka M, Balestreri M, Steiner L, *et al.* Age, intracranial pressure, autoregulation, and outcome after brain trauma. *J Neurosurg* 2005; **102**: 450–4.

87 Czosnyka M, Smielewski P, Czosnyka Z, *et al.* Continuous assessment of cerebral autoregulation: clinical and laboratory experience. *Acta Neurochir Suppl* 2003; **86**: 581–5.

88 Czosnyka M, Smielewski P, Piechnik S, *et al.* Critical closing pressure in cerebrovascular circulation. *J Neurol Neurosurg Psychiatry* 1999; **66**: 606–11.

89 Czosnyka M, Smielewski P, Piechnik S, *et al.* Continuous assessment of cerebral autoregulation--clinical verification of the method in head injured patients. *Acta Neurochir Suppl* 2000; **76**: 483–4.

90 Czosnyka M, Smielewski P, Piechnik S, Steiner LA, Pickard JD. Cerebral autoregulation following head injury. *J Neurosurg* 2001; **95**: 756–63.

91 Eide PK, Czosnyka M, Sorteberg W, Pickard JD, Smielewski P. Association between intracranial, arterial pulse pressure amplitudes and cerebral autoregulation in head injury patients. *Neurol Res* 2007; **29**: 578–82.

92 Lewis PM, Smielewski P, Pickard JD, Czosnyka M. Dynamic cerebral autoregulation: should intracranial pressure be taken into account? *Acta Neurochir (Wien)* 2007; **149**: 549–55; discussion 555.

93 Lewis PM, Smielewski P, Rosenfeld JV, Pickard JD, Czosnyka M. Monitoring of the association between cerebral blood flow velocity and intracranial pressure. *Acta Neurochir Suppl* 2012; **114**: 147–51.

94 Liu X, Czosnyka M, Donnelly J, *et al.* Comparison of frequency and time domain methods of assessment of cerebral autoregulation in traumatic brain injury. *J Cereb Blood Flow Metab Off J Int Soc Cereb Blood Flow Metab* 2015; **35**: 248–56.

95 Radolovich DK, Aries MJH, Castellani G, *et al.* Pulsatile intracranial pressure and cerebral autoregulation after traumatic brain injury. *Neurocrit Care* 2011; **15**: 379–86.

96 Schmidt EA, Czosnyka M, Steiner LA, *et al.* Asymmetry of pressure autoregulation after traumatic brain injury. *J Neurosurg* 2003; **99**: 991–8.

97 Czosnyka M, Smielewski P, Lavinio A, Pickard JD, Panerai R. An assessment of dynamic autoregulation from spontaneous fluctuations of cerebral blood flow velocity: a comparison of two models, index of autoregulation and mean flow index. *Anesth Analg* 2008; **106**: 234–9, table of contents.

98 Liu X, Czosnyka M, Pickard JD, Varsos GV, Nasr N, Smielewski P. Derangement of Cerebral Blood Flow Autoregulation During Intracranial Pressure Plateau Waves as Detected by Time and Frequency-Based Methods. *Acta Neurochir Suppl* 2016; **122**: 233–8.

99 Panerai RB, Kerins V, Fan L, Yeoman PM, Hope T, Evans DH. Association between dynamic cerebral autoregulation and mortality in severe head injury. *Br J Neurosurg* 2004; **18**: 471–9.

100 Varsos GV, Budohoski KP, Kolias AG, *et al.* Relationship of vascular wall tension and autoregulation following traumatic brain injury. *Neurocrit Care* 2014; **21**: 266–74.

101 Zhang Y, Liu X, Steiner L, *et al.* Correlation Between Cerebral Autoregulation and Carbon Dioxide Reactivity in Patients with Traumatic Brain Injury. *Acta Neurochir Suppl* 2016; **122**: 205–9.

102 Donnelly J, Aries MJ, Czosnyka M. Further understanding of cerebral autoregulation at the bedside: possible implications for future therapy. *Expert Rev Neurother* 2015; **15**: 169–85.

103 Sánchez-Porras R, Santos E, Czosnyka M, Zheng Z, Unterberg AW, Sakowitz OW. 'Long' pressure reactivity index (L-PRx) as a measure of autoregulation correlates with outcome in traumatic brain injury patients. *Acta Neurochir (Wien)* 2012; **154**: 1575–81.

104 Adams H, Donelly J, Kolias A, *et al.* Characterising the temporal evolution of ICP and cerebrovascular reactivity after severe traumatic brain injury: best international abstract award. *J Neurosurg* 2016; **124**: A1195–6.

105 Balestreri M, Czosnyka M, Steiner LA, *et al.* Intracranial hypertension: what additional information can be derived from ICP waveform after head injury? *Acta Neurochir (Wien)* 2004; **146**: 131–41.

106 Gao L, Smielewski P, Czosnyka M, Ercole A. Cerebrovascular Signal Complexity Six Hours after Intensive Care Unit Admission Correlates with Outcome after Severe Traumatic Brain Injury. *J Neurotrauma* 2016; **33**: 2011–8.

107 Hiler M, Czosnyka M, Hutchinson P, *et al.* Predictive value of initial computerized tomography scan, intracranial pressure, and state of autoregulation in patients with traumatic brain injury. *J Neurosurg* 2006; **104**: 731–7.

108 Johnson U, Lewén A, Ronne-Engström E, Howells T, Enblad P. Should the neurointensive care management of traumatic brain injury patients be individualized according to autoregulation status and injury subtype? *Neurocrit Care* 2014; **21**: 259–65.

109 Lang EW, Kasprowicz M, Smielewski P, Santos E, Pickard J, Czosnyka M. Short pressure reactivity index versus long pressure reactivity index in the management of traumatic brain injury. *J Neurosurg* 2015; **122**: 588–94.

110 Lazaridis C, DeSantis SM, Smielewski P, *et al.* Patient-specific thresholds of intracranial pressure in severe traumatic brain injury. *J Neurosurg* 2014; **120**: 893–900.

111 Steiner LA, Czosnyka M, Piechnik SK, *et al.* Continuous monitoring of cerebrovascular pressure reactivity allows determination of optimal cerebral perfusion pressure in patients with traumatic brain injury. *Crit Care Med* 2002; **30**: 733–8.

112 Sykora M, Czosnyka M, Liu X, *et al.* Autonomic Impairment in Severe Traumatic Brain Injury: A Multimodal Neuromonitoring Study. *Crit Care Med* 2016; **44**: 1173–81.

113 Timofeev I, Carpenter KLH, Nortje J, *et al.* Cerebral extracellular chemistry and outcome following traumatic brain injury: a microdialysis study of 223 patients. *Brain J Neurol* 2011; **134**: 484–94.

114 Czosnyka M, Aries M, Weersink C, *et al.* 'Solid Red Line': An Observational Study on Death from Refractory Intracranial Hypertension. *Acta Neurochir Suppl* 2016; **122**: 113–6.

115 De La Cerda G, Verma V, Thavosothy M, Healy M. Secondary intracranial pressure (ICP) indices correlate with marshall classification an outcome in traumatic brain injury (TBI). *Intensive Care Med* 2009; **35**: S72.

116 Jaeger M, Schuhmann MU, Soehle M, Meixensberger J. Continuous assessment of cerebrovascular autoregulation after traumatic brain injury using brain tissue oxygen pressure reactivity. *Crit Care Med* 2006; **34**: 1783–8.

117 Kirkness CJ, Mitchell PH, Burr RL, Newell DW. Cerebral autoregulation and outcome in acute brain injury. *Biol Res Nurs* 2001; **2**: 175–85.

118 Nikouei A, Saied S, Afsoun S, Shahram A, Amir N, Shoeib N. A clinical trial on efficacy of intravenous erythropoietin on improvement of cerebral autoregulation and outcome in traumatic brain injury patients. *Arch Phys Med Rehabil* 2016; **97**: e52.

119 Oshorov A, Savin I, Popugaev K, Goriachev A, Polupan A. Comparison of the outcomes in two similar groups of TBI patients treated on the base ICP/CPP protocol versus patients treated on the base of autoregulation protocol with the support of evaluation of vascular autoregulation using PRx index. *Intensive Care Med* 2011; **36**: S46.

120 Schmidt B, Lezaic V, Weinhold M, Plontke R, Schwarze J, Klingelhöfer J. Is Impaired Autoregulation Associated with Mortality in Patients with Severe Cerebral Diseases? *Acta Neurochir Suppl* 2016; **122**: 181–5.

121 Schmidt B, Reinhard M, Lezaic V, *et al.* Autoregulation monitoring and outcome prediction in neurocritical care patients: Does one index fit all? *J Clin Monit Comput* 2016; **30**: 367–75.

122 Kirkpatrick PJ, Smielewski P, Czosnyka M, Pickard JD. Continuous monitoring of cortical perfusion by laser Doppler flowmetry in ventilated patients with head injury. *J Neurol Neurosurg Psychiatry* 1994; **57**: 1382–8.

123 Lam JM, Hsiang JN, Poon WS. Monitoring of autoregulation using laser Doppler flowmetry in patients with head injury. *J Neurosurg* 1997; **86**: 438–45.

124 Lang EW, Diehl RR, Timmermann L, *et al.* Spontaneous oscillations of arterial blood pressure, cerebral and peripheral blood flow in healthy and comatose subjects. *Neurol Res* 1999; **21**: 665–9.

125 Zweifel C, Czosnyka M, Lavinio A, *et al.* A comparison study of cerebral autoregulation assessed with transcranial Doppler and cortical laser Doppler flowmetry. *Neurol Res* 2010; **32**: 425–8.

126 Bindra J, Pham P, Aneman A, Chuan A, Jaeger M. Non-invasive Monitoring of Dynamic Cerebrovascular Autoregulation Using Near Infrared Spectroscopy and the Finometer Photoplethysmograph. *Neurocrit Care* 2016; **24**: 442–7.

127 Dias C, Maia I, Cerejo A, *et al.* Pressures, flow, and brain oxygenation during plateau waves of intracranial pressure. *Neurocrit Care* 2014; **21**: 124–32.

128 Dias C, Silva MJ, Pereira E, *et al.* Optimal Cerebral Perfusion Pressure Management at Bedside: A Single-Center Pilot Study. *Neurocrit Care* 2015; **23**: 92–102.

129 Diedler J, Zweifel C, Budohoski KP, *et al.* The limitations of near-infrared spectroscopy to assess cerebrovascular reactivity: the role of slow frequency oscillations. *Anesth Analg* 2011; **113**: 849–57.

130 Highton D, Ghosh A, Tachtsidis I, Kolyva C, Panovska J, Elwell D. Deoxyhaemoglobin as a biomarker of cerebral autoregulation. *M* 2012; **16**: S106–7.

131 Highton D, Ghosh A, Tachtsidis I, Panovska-Griffiths J, Elwell CE, Smith M. Monitoring cerebral autoregulation after brain injury: multimodal assessment of cerebral slow-wave oscillations using near-infrared spectroscopy. *Anesth Analg* 2015; **121**: 198–205.

132 Highton D, Ghosh A, Tachtsidis I, Kolyva C, Elwell C, Smith M. A comparison between pressure reactivity index, mean velocity index, and near infrared spectroscopy in brain injury. *Anesthesiology* 2010; **22**: 419–20.

133 Smielewski P, Czosnyka M, Zweifel C, *et al.* Multicentre experience of using ICM+ for investigations of cerebrovascular dynamics with near infrared spectroscopy. *J Neurotrauma* 2009; **26**: A47.

134 Dengler J, Frenzel C, Vajkoczy P, Horn P, Wolf S. The oxygen reactivity index and its relation to sensor technology in patients with severe brain lesions. *Neurocrit Care* 2013; **19**: 74–8.

135 Dias C, Maia I, Cerejo A, Smielewski P, Paiva J-A, Czosnyka M. Plateau Waves of Intracranial Pressure and Multimodal Brain Monitoring. *Acta Neurochir Suppl* 2016; **122**: 143–6.

136 Lang EW, Kasprowicz M, Smielewski P, Pickard J, Czosnyka M. Changes in Cerebral Partial Oxygen Pressure and Cerebrovascular Reactivity During Intracranial Pressure Plateau Waves. *Neurocrit Care* 2015; **23**: 85–91.

137 Menzel M, Soukup J, Henze D, *et al.* Brain tissue oxygen monitoring for assessment of autoregulation: preliminary results suggest a new hypothesis. *J Neurosurg Anesthesiol* 2003; **15**: 33–41.

138 Radolovich DK, Czosnyka M, Timofeev I, *et al.* Reactivity of brain tissue oxygen to change in cerebral perfusion pressure in head injured patients. *Neurocrit Care* 2009; **10**: 274–9.

139 Soehle M, Jaeger M, Meixensberger J. Online assessment of brain tissue oxygen autoregulation in traumatic brain injury and subarachnoid hemorrhage. *Neurol Res* 2003; **25**: 411–7.

140 Dias C, Silva MJ, Pereira E, *et al.* Post-traumatic multimodal brain monitoring: response to hypertonic saline. *J Neurotrauma* 2014; **31**: 1872–80.

141 Oshorov A, Savin I, Popugaev K, Potopov A. Influence of hyperthermia on the parameters of MAP, CPP and PRx in patients with severe TBI. *Brain Inj* 2014; **28**: 797.

142 Rosenthal G, Sanchez-Mejia RO, Phan N, Hemphill JC, Martin C, Manley GT. Incorporating a parenchymal thermal diffusion cerebral blood flow probe in bedside assessment of cerebral autoregulation and vasoreactivity in patients with severe traumatic brain injury. *J Neurosurg* 2011; **114**: 62–70.

143 Tackla R, Hinzman JM, Foreman B, Magner M, Andaluz N, Hartings JA. Assessment of Cerebrovascular Autoregulation Using Regional Cerebral Blood Flow in Surgically Managed Brain Trauma Patients. *Neurocrit Care* 2015; **23**: 339–46.

144 Needham E, McFadyen C, Newcombe V, Synnot AJ, Czosnyka M, Menon D. Cerebral Perfusion Pressure Targets Individualized to Pressure-Reactivity Index in Moderate to Severe Traumatic Brain Injury: A Systematic Review. *J Neurotrauma* 2017; **34**: 963–70.

145 Donnelly J, Czosnyka M, Harland S, *et al.* Cerebral haemodynamics during experimental intracranial hypertension. *J Cereb Blood Flow Metab Off J Int Soc Cereb Blood Flow Metab* 2017; **37**: 694–705.

146 Czosnyka M, Richards H, Kirkpatrick P, Pickard J. Assessment of cerebral autoregulation with ultrasound and laser Doppler wave forms--an experimental study in anesthetized rabbits. *Neurosurgery* 1994; **35**: 287–92; discussion 292-293.

147 Lee JK, Yang Z-J, Wang B, *et al.* Noninvasive autoregulation monitoring in a swine model of pediatric cardiac arrest. *Anesth Analg* 2012; **114**: 825–36.

148 Lee JK, Brady KM, Mytar JO, *et al.* Cerebral blood flow and cerebrovascular autoregulation in a swine model of pediatric cardiac arrest and hypothermia. *Crit Care Med* 2011; **39**: 2337–45.

149 Kilkenny C, Browne WJ, Cuthill IC, Emerson M, Altman DG. Improving bioscience research reporting: the ARRIVE guidelines for reporting animal research. *PLoS Biol* 2010; **8**: e1000412.

150 Carney N, Totten AM, O'Reilly C, *et al.* Guidelines for the Management of Severe Traumatic Brain Injury, Fourth Edition. *Neurosurgery* 2017; **80**: 6–15.

151 Donnelly J, Czosnyka M, Adams H, *et al.* Twenty-Five Years of Intracranial Pressure Monitoring After Severe Traumatic Brain Injury: A Retrospective, Single-Center Analysis. *Neurosurgery* 2018; published online Nov 23. DOI:10.1093/neuros/nyy468.

152 Zeiler FA, Donnelly J, Smieleweski P, Menon D, Hutchinson PJ, Czosnyka M. Critical Thresholds of ICP Derived Continuous Cerebrovascular Reactivity Indices for outcome prediction in Non-Craniectomized TBI Patients: PRx, PAx and RAC. *J Neurotrauma* 2018; **35**: 1107–15.

153 Marshall LF, Marshall SB, Klauber MR, *et al.* The diagnosis of head injury requires a classification based on computed axial tomography. *J Neurotrauma* 1992; **9 Suppl 1**: S287-292.

154 Maas AIR, Hukkelhoven CWPM, Marshall LF, Steyerberg EW. Prediction of outcome in traumatic brain injury with computed tomographic characteristics: a comparison between the computed tomographic classification and combinations of computed tomographic predictors. *Neurosurgery* 2005; **57**: 1173–82; discussion 1173-1182.

155 Raj R, Siironen J, Skrifvars MB, Hernesniemi J, Kivisaari R. Predicting outcome in traumatic brain injury: development of a novel computerized tomography classification system (Helsinki computerized tomography score). *Neurosurgery* 2014; **75**: 632–46; discussion 646-647.

156 Nelson DW, Nyström H, MacCallum RM, *et al.* Extended analysis of early computed tomography scans of traumatic brain injured patients and relations to outcome. *J Neurotrauma* 2010; **27**: 51–64.

157 Kothari RU, Brott T, Broderick JP, *et al.* The ABCs of measuring intracerebral hemorrhage volumes. *Stroke* 1996; **27**: 1304–5.

158 UK Health Departments. Governance arrangements for research ethics committees: a harmonised edition. 2011. https://assets.publishing.service.gov.uk/government/uploads/system/uploads/attachment_data/file/213753/dh_133993.pdf. (accessed May 31, 2018).

159 Crawley M. The R Book, 2nd edn. West Sussex, United Kingdom: Wiley-Blackwell, 2012.

160 Pandey M. Biostatistics: Basic and Advanced, 1st edn. New Dehli, India: MV Learning, 2015.

161 Helmy A, Antoniades CA, Guilfoyle MR, Carpenter KLH, Hutchinson PJ. Principal component analysis of the cytokine and chemokine response to human traumatic brain injury. *PloS One* 2012; **7**: e39677.

162 Cardona G, Mir A, Rosselló F, Rotger L, Sánchez D. Cophenetic metrics for phylogenetic trees, after Sokal and Rohlf. *BMC Bioinformatics* 2013; **14**: 3.

163 Chatfield C. The Analysis of Time Series: An Introduction, 6th edn. Boca Raton, Florida, United States: Chapman and Hall/CRC, 2016.

164 Douc R, Moulines E, Stoffer D. Nonlinear Time Series: Theory, Methods and Applications with R Examples, 1st edn. Boca Raton, Florida, United States: Chapman and Hall/CRC, 2014.

165 Faraway J. Extending the Linear Model with R: Generalized Linear, Mixed Effects and Nonparametric Regression Models, 1st edn. Boca Raton, Florida, United States: Chapman and Hall/CRC, 2005.

166 Gelman A, Carlin J, Stern H, Dunson D, Vehtari A, Rubin D. Bayesian Data Analysis, 3rd edn. Boca Raton, Florida, United States: Chapman and Hall/CRC, 2013.

167 Kim D-J, Czosnyka Z, Keong N, *et al.* Index of cerebrospinal compensatory reserve in hydrocephalus. *Neurosurgery* 2009; **64**: 494–501; discussion 501-502.

168 Czosnyka M, Richards HK, Czosnyka Z, Piechnik S, Pickard JD, Chir M. Vascular components of cerebrospinal fluid compensation. *J Neurosurg* 1999; **90**: 752–9.

169 Calviello L, Donnelly J, Cardim D, *et al.* Compensatory-Reserve-Weighted Intracranial Pressure and Its Association with Outcome After Traumatic Brain Injury. *Neurocrit Care* 2017; published online Oct 17. DOI:10.1007/s12028-017-0475-7.

170 Carrera E, Kim D-J, Castellani G, *et al.* What shapes pulse amplitude of intracranial pressure? *J Neurotrauma* 2010; **27**: 317–24.

171 Zeiler FA, Donnelly J, Calviello L, *et al.* Validation of pressure reactivity and pulse amplitude indices against the lower limit of autoregulation, Part I: experimental intra-cranial hypertension. *J Neurotrauma* 2018; **In Press**.

172 Zeiler FA, Donnelly J, Calviello L, *et al.* Validation of Pressure Reactivity and Pulse Amplitude Indices against the Lower Limit of Autoregulation: Part I: Experimental Intracranial Hypertension. *J Neurotrauma* 2018; published online Oct 4. DOI:10.1089/neu.2017.5603.

173 Lee JK, Kibler KK, Benni PB, *et al.* Cerebrovascular reactivity measured by near-infrared spectroscopy. *Stroke* 2009; **40**: 1820–6.

174 Caldwell B, Flores R, Lowery J, Brown AT, Culp WC. Variations in the Circle of Willis in the New Zealand White Rabbit. *J Vasc Interv Radiol JVIR* 2011; **22**: 1188–92.

175 Pesek M, Kibler K, Easley RB, *et al.* The upper limit of cerebral blood flow autoregulation is decreased with elevations in intracranial pressure. *Neurosurgery* 2014; **75**: 163–70; discussion 169-170.

176 Pesek M, Kibler K, Easley RB, *et al.* The Upper Limit of Cerebral Blood Flow Autoregulation Is Decreased with Elevations in Intracranial Pressure. *Acta Neurochir Suppl* 2016; **122**: 229–31.

177 Scheller MS, Todd MM, Drummond JC. Isoflurane, halothane, and regional cerebral blood flow at various levels of PaCO2 in rabbits. *Anesthesiology* 1986; **64**: 598–604.

178 Hansen TD, Warner DS, Todd MM, Vust LJ, Trawick DC. Distribution of cerebral blood flow during halothane versus isoflurane anesthesia in rats. *Anesthesiology* 1988; **69**: 332–7.

179 Brüssel T, Fitch W, Brodner G, Arendt I, Van Aken H. Effects of halothane in low concentrations on cerebral blood flow, cerebral metabolism, and cerebrovascular autoregulation in the baboon. *Anesth Analg* 1991; **73**: 758–64.

180 Zeiler FA, Donnelly J, Menon DK, *et al.* Continuous Autoregulatory Indices Derived from Multi-Modal Monitoring: Each One Is Not Like the Other. *J Neurotrauma* 2017; **34**: 3070–80.

181 Zeiler FA, Donnelly J, Cardim D, Menon DK, Smielewski P, Czosnyka M. ICP Versus Laser Doppler Cerebrovascular Reactivity Indices to Assess Brain Autoregulatory Capacity. *Neurocrit Care* 2017; published online Oct 17. DOI:10.1007/s12028-017-0472-x.

182 Zeiler FA, Cardim D, Donnelly J, Menon DK, Czosnyka M, Smielewski P. Transcranial Doppler Systolic Flow Index and ICP-Derived Cerebrovascular Reactivity Indices in Traumatic Brain Injury. *J Neurotrauma* 2018; **35**: 314–22.

183 Blaine Easley R, Kibler KK, Brady KM, *et al.* Continuous cerebrovascular reactivity monitoring and autoregulation monitoring identify similar lower limits of autoregulation in patients undergoing cardiopulmonary bypass. *Neurol Res* 2013; **35**: 344–54.

184 Zeiler FA, Smieleweski P, Donnelly J, Czosnyka M, Menon D, Ercole A. Estimating Pressure Reactivity Index Using Non-Invasive Doppler Based Systolic Flow Index. *J Neurotrauma* 2018; published online Feb 3. DOI:10.1089/neu.2017.5596.

185 Zeiler FA, Smielewski P. Application of robotic transcranial Doppler for extended duration recording in moderate/severe traumatic brain injury: first experiences. *Crit Ultrasound J* 2018; **10**: 16.

186 Zeiler FA, Czosnyka M, Smielewski P. Optimal cerebral perfusion pressure via transcranial Doppler in TBI: application of robotic technology. *Acta Neurochir (Wien)* 2018; **160**: 2149–57.

187 Zeiler FA, Smielewski P, Stevens A, Czosnyka M, Menon DK, Ercole A. Non-Invasive Pressure Reactivity Index Using Doppler Systolic Flow Parameters: A Pilot Analysis. *J Neurotrauma* 2018; published online Sept 27. DOI:10.1089/neu.2018.5987.

188 Wood S. Generalized Additive Models: An Introduction with R, 2nd edn. Boca Raton, Florida, United States: Chapman and Hall/CRC, 2017.

189 Zeiler FA, Donnelly J, Nourallah B, *et al.* Intra- and Extra-Cranial Injury Burden as Drivers of Impaired Cerebrovascular Reactivity in Traumatic Brain Injury. *J Neurotrauma* 2018; published online Feb 12. DOI:10.1089/neu.2017.5595.

190 Maas AIR, Menon DK, Steyerberg EW, *et al.* Collaborative European NeuroTrauma Effectiveness Research in Traumatic Brain Injury (CENTER-TBI): a prospective longitudinal observational study. *Neurosurgery* 2015; **76**: 67–80.

191 Baker SP, O'Neill B, Haddon W, Long WB. The injury severity score: a method for describing patients with multiple injuries and evaluating emergency care. *J Trauma* 1974; **14**: 187–96.

192 Knaus WA, Draper EA, Wagner DP, Zimmerman JE. APACHE II: a severity of disease classification system. *Crit Care Med* 1985; **13**: 818–29.

193 Zeiler FA, McFadyen C, Newcombe V, *et al.* Genetic Influences on Patient Oriented Outcomes in TBI: A Living Systematic Review of Non-APOE Single Nucleotide Polymorphisms. *J Neurotrauma* 2018; published online May 25. DOI:10.1089/neu.2017.5583.

194 Steyerberg EW, Mushkudiani N, Perel P, *et al.* Predicting outcome after traumatic brain injury: development and international validation of prognostic scores based on admission characteristics. *PLoS Med* 2008; **5**: e165; discussion e165.

195 Robertson CS, Gopinath SP, Valadka AB, Van M, Swank PR, Goodman JC. Variants of the endothelial nitric oxide gene and cerebral blood flow after severe traumatic brain injury. *J Neurotrauma* 2011; **28**: 727–37.

APPENDICES

1. **Appendix A: Section 6.1 - PCA Eigenvalues Table, Scree Plot and Factor Loadings Table**

2. **Appendix B: Section 6.2- Spearman Principal Component Analysis (PCA) – Supplementary Material**

3. **Appendix C: Section 6.3 - Spearman Principal Component Analysis (PCA) – Supplementary Material – Entire TBI TCD Cohort**

4. **Appendix D: Section 7.1 - Patient Example and Full Population ARMA Models Tested (AIC, LL)**

5. **Appendix E: Section 7.3 - ACF/PACF/QQ Plots for Top LME Models and Bland-Altman Plots for Estimated and Predicted PRx Results from LME Models**

6. **Appendix F: Section 8.1 - Sequential Chi-Square Threshold Analysis – 24hr, 72hr, 5d, 7d and 10d Recording Periods**

7. **Appendix G: Chapter 9 - Injury and Lesion Data, Patient Numbers – Grand Mean Data**

8. **Appendix H: Chapter 9 - IC Scoring Systems and Mean Index/%Time Above Threshold Results**

9. **Appendix I: Chapter 9 - Mann U testing for Thresholds of PRx and PAx**

10. **Appendix J: Chapter 9 - Univariate Logistic Regression for CT Injury Characteristics and ICP Indices – Grand Mean Data**

Appendix A – Section 6.1 - PCA Eigenvalues Table, Scree Plot and Factor Loadings Table

*** PCA = principal component analysis, F = factor, PC = principal component, F1 = PC1 = principal component #1, F2 = PC2 = principal component #2. PC1 and PC2 are the two components which contribute the largest amount of variance to the entire data set.**

***Biplots of PC1 vs. PC2 display which variables contribute variance to PC1 and PC2. The longer the arm connecting (0,0) to the variable (such as PRx), the larger the contribution of that variable. Similarly, the quadrant on the biplot in which the variable fallscorrelates to its contribution to a particular PC. The upper left quadrant is primarily PC2; lower left quadrant is neither PC1 or PC2; the upper right quadrant is PC1 and PC2; the lower right quadrant is primarily PC1.**

***Eigenvalue tables display the eigenvalue for each principal component (PC) (also denoted F), with the % variability and cumulative variability for each factor/principal component.**

***Scree plot displays the same information form the eigenvalue table in a histogram format, with each F (or PC) along the x-axis, the eigenvalue along the left side y-axis and the % variability along the right y-axis. Furthermore, the red line on the graph displays the cumulative variability with the addition of each F (or PC) moving from F1 to F18.**

***Factor loading tables display the loading of each variable (ie. PRx, etc.) for each principal component. Loading varies from -1 to +1, with negative values indicating that particular variable is less likely to contribute to the variance in that particular factor (F). Similarly, positive loadings indicate that particular variable likely contribute to the variance in that corresponding factor (F).**

***Contribution % of Variables tables displays the % contribution to the variance of each individual variable for each individual factor (F).**

Summary of 30-minute mean and Minute-by-minute Data - PCA

Using the 30-minute mean data sheet, PCA analysis displayed similar results for the PC's and biplot, supporting our results described for the minute-by-minute analysis. Finally, using the grand mean data sheet, similar PCA results were displayed with the exception of the PbtO2 based indices (ORx-5, ORx-30 and ORx-60). Within the grand mean PCA, ORx-5/ORx-30/ORx-60 contributed more to the variance of the data set, with positive loadings towards PC1 and PC2. The PbtO2 indices still displayed a lack of association with other indices in the minute-by-minute data sheet. These can be seen in Appendix B of the supplementary materials.

1. ***Minute-by-Minute Data Set:***

Eigenvalues Table

	F1	F2	F3	F4	F5	F6	F7	F8	F9	F10	F11	F12	F13	F14	F15	F16
Eigenvalue	4.293	2.945	2.055	1.803	1.386	0.863	0.805	0.520	0.360	0.252	0.194	0.180	0.155	0.097	0.077	0.016
Variability	26.833	18.408	12.842	11.269	8.664	5.393	5.032	3.250	2.251	1.578	1.209	1.124	0.966	0.603	0.478	0.099
Cumulative	26.833	45.241	58.083	69.352	78.016	83.409	88.441	91.691	93.942	95.520	96.730	97.854	98.819	99.423	99.901	100.000

Scree Plot

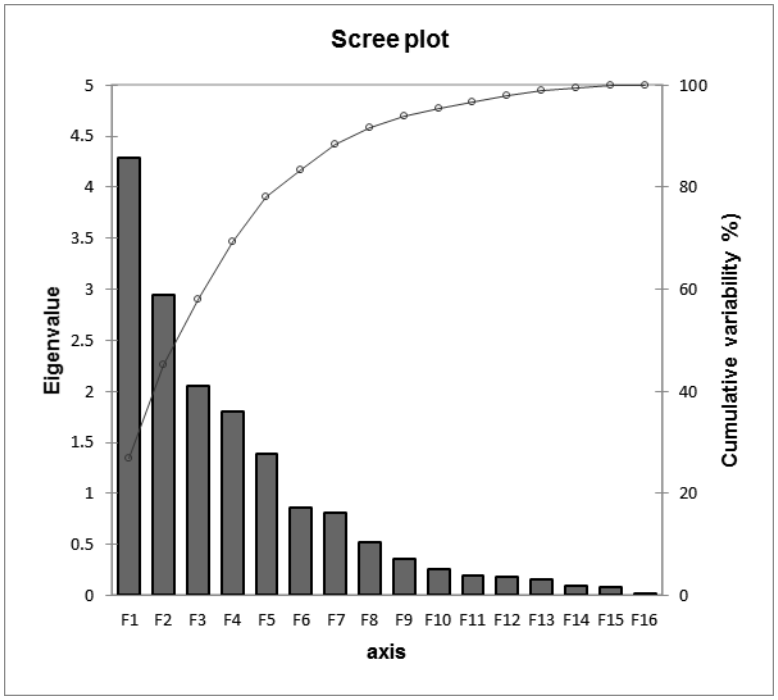

Factor Loading Table

	F1	F2	F3	F4	F5	F6	F7	F8
PRx	0.493	0.660	-0.163	0.040	-0.129	0.112	-0.262	-0.199
PAx	0.438	0.730	-0.234	0.107	-0.156	0.098	-0.276	-0.026
RAC	0.443	0.636	-0.080	0.071	-0.278	0.099	-0.148	0.417
Mx	0.783	-0.492	-0.083	-0.060	-0.033	-0.004	0.025	0.213
Mx_a	0.781	-0.404	-0.123	-0.157	-0.047	0.024	-0.186	-0.220
Sx	0.698	0.143	-0.372	0.163	0.036	-0.156	0.489	0.142
Sx_a	0.641	0.269	-0.443	0.142	0.053	-0.148	0.373	-0.296
Dx	0.668	-0.648	0.018	-0.065	-0.071	-0.003	-0.065	0.211
Dx_a	0.657	-0.593	-0.007	-0.151	-0.102	0.023	-0.270	-0.155
TOx	0.499	0.233	0.447	0.105	0.623	-0.120	-0.082	0.073
TOx_a	0.429	0.258	0.481	0.073	0.646	-0.123	-0.089	-0.019
THx	0.336	0.191	0.737	-0.164	-0.403	0.042	0.229	0.020
THx_a	0.311	0.175	0.755	-0.199	-0.374	0.027	0.180	-0.162
ORx_5	0.142	-0.178	0.059	0.411	0.218	0.831	0.184	-0.036
ORx_30	0.006	-0.190	0.178	0.869	-0.155	-0.105	-0.102	-0.015
ORx_60	-0.027	-0.214	0.179	0.822	-0.255	-0.225	-0.065	-0.046

F9	F10	F11	F12	F13	F14	F15	F16
0.320	-0.047	0.109	0.129	-0.144	0.001	-0.029	-0.001
0.036	-0.068	-0.131	-0.188	0.178	0.029	0.086	-0.002
-0.293	0.075	0.040	0.039	-0.073	-0.025	-0.070	0.002
0.160	-0.088	-0.187	0.101	0.036	0.027	-0.042	0.069
-0.197	0.029	-0.131	0.194	0.036	-0.042	0.034	-0.055
0.066	0.013	0.029	-0.008	-0.086	-0.081	0.149	-0.012
-0.122	0.041	0.037	-0.051	0.063	0.074	-0.137	0.011
0.168	-0.041	0.075	-0.161	-0.008	0.056	-0.073	-0.068
-0.131	0.083	0.191	-0.124	-0.048	-0.020	0.068	0.055
0.050	-0.004	0.130	0.048	0.178	-0.132	-0.034	0.002
-0.095	-0.012	-0.109	-0.052	-0.174	0.131	0.032	-0.001
0.009	0.033	0.112	0.113	0.110	0.147	0.065	-0.002
0.017	-0.018	-0.131	-0.126	-0.080	-0.144	-0.055	0.002
-0.037	-0.038	0.012	-0.008	-0.003	-0.004	0.001	0.000
0.117	0.335	-0.071	0.003	0.009	0.003	-0.004	-0.001
-0.121	-0.325	0.051	0.025	-0.017	-0.005	0.005	0.000

% Contribution of Variables

	F1	F2	F3	F4	F5	F6	F7	F8
PRx	5.666	14.805	1.291	0.090	1.202	1.445	8.535	7.626
PAx	4.462	18.109	2.666	0.641	1.748	1.120	9.440	0.135
RAC	4.568	13.735	0.310	0.280	5.579	1.131	2.738	33.378
Mx	14.272	8.226	0.335	0.198	0.078	0.002	0.075	8.766
Mx_a	14.194	5.555	0.732	1.363	0.162	0.064	4.292	9.284
Sx	11.362	0.690	6.748	1.478	0.093	2.805	29.712	3.885
Sx_a	9.573	2.462	9.532	1.126	0.205	2.549	17.289	16.820
Dx	10.402	14.269	0.015	0.238	0.362	0.001	0.519	8.583
Dx_a	10.056	11.927	0.003	1.257	0.758	0.064	9.043	4.607
TOx	5.797	1.840	9.733	0.616	27.971	1.678	0.837	1.019
TOx_a	4.279	2.259	11.241	0.297	30.143	1.746	0.973	0.067
THx	2.624	1.233	26.412	1.498	11.714	0.203	6.523	0.074
THx_a	2.254	1.042	27.709	2.201	10.113	0.084	4.029	5.049
ORx_5	0.472	1.077	0.169	9.361	3.440	79.974	4.191	0.247
ORx_30	0.001	1.224	1.541	41.886	1.742	1.286	1.280	0.045
ORx_60	0.017	1.548	1.563	37.470	4.693	5.847	0.523	0.416

F9	F10	F11	F12	F13	F14	F15	F16
28.501	0.879	6.138	9.267	13.456	0.001	1.085	0.013
0.352	1.824	8.824	19.693	20.416	0.850	9.691	0.029
23.756	2.201	0.837	0.849	3.477	0.644	6.482	0.034
7.105	3.064	18.132	5.705	0.826	0.764	2.310	30.141
10.807	0.332	8.849	20.883	0.834	1.869	1.553	19.227
1.202	0.063	0.445	0.033	4.776	6.796	28.947	0.964
4.133	0.656	0.703	1.465	2.577	5.624	24.522	0.764
7.797	0.668	2.914	14.468	0.043	3.280	7.054	29.386
4.760	2.755	18.909	8.539	1.478	0.400	6.087	19.358
0.686	0.008	8.679	1.279	20.397	17.957	1.478	0.025
2.515	0.054	6.194	1.506	19.529	17.811	1.375	0.010
0.023	0.439	6.465	7.049	7.835	22.434	5.453	0.023
0.079	0.124	8.876	8.878	4.112	21.515	3.910	0.023
0.380	0.558	0.073	0.033	0.008	0.015	0.002	0.000
3.823	44.475	2.602	0.005	0.058	0.010	0.018	0.002
4.082	41.898	1.359	0.347	0.177	0.029	0.031	0.001

2. <u>30 Minute Mean Data Set:</u>

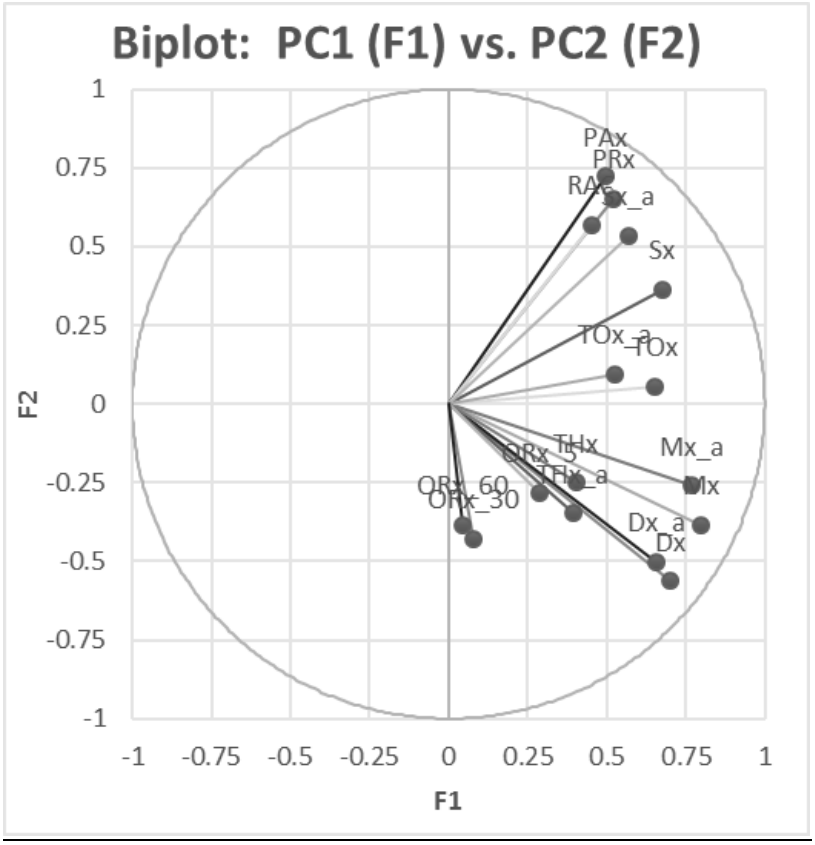

Eigenvalue Table

	F1	F2	F3	F4	F5	F6	F7	F8	F9	F10	F11	F12	F13	F14	F15	F16
Eigenvalue	4.765	3.083	2.144	1.901	1.294	0.815	0.572	0.457	0.288	0.173	0.145	0.128	0.116	0.064	0.047	0.009
Variability	29.780	19.268	13.402	11.883	8.086	5.093	3.576	2.854	1.798	1.083	0.903	0.800	0.722	0.403	0.295	0.055
Cumulative	29.780	49.048	62.449	74.332	82.418	87.511	91.087	93.941	95.739	96.822	97.726	98.525	99.248	99.651	99.945	100.000

Scree Plot

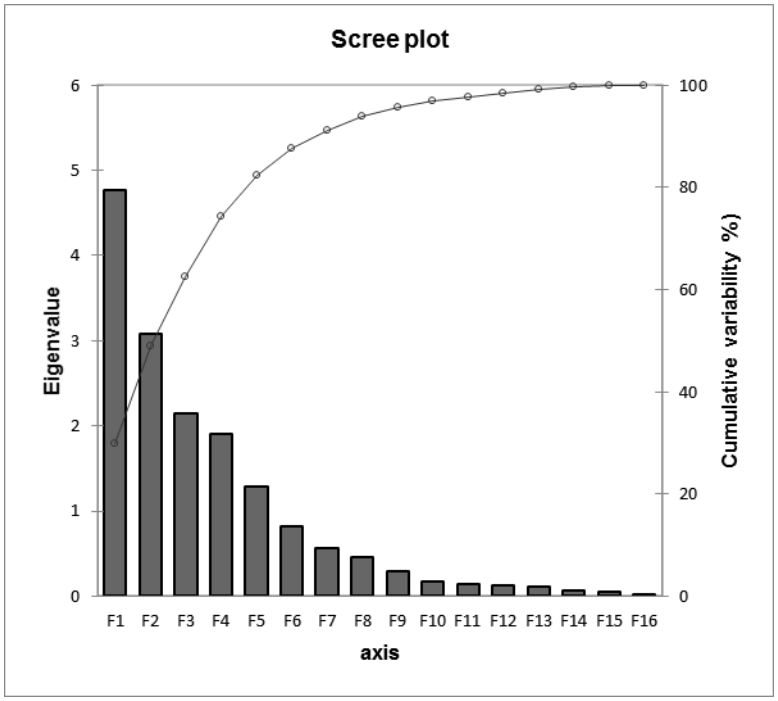
Scree plot
Eigenvalue
Cumulative variability %)
axis
F1 F2 F3 F4 F5 F6 F7 F8 F9 F10 F11 F12 F13 F14 F15 F16
0 1 2 3 4 5 6
0 20 40 60 80 100

Factor Loading

	F1	F2	F3	F4	F5	F6	F7	F8
PRx	0.522	0.653	0.001	0.112	-0.116	-0.331	0.085	-0.127
PAx	0.496	0.724	0.130	0.128	-0.165	-0.268	0.039	-0.037
RAC	0.451	0.570	0.013	0.286	-0.440	0.143	0.061	-0.262
Mx	0.796	-0.383	-0.072	-0.287	-0.108	0.203	-0.010	-0.182
Mx_a	0.767	-0.259	-0.044	-0.377	-0.010	-0.334	0.053	0.084
Sx	0.679	0.365	0.246	-0.214	-0.057	0.477	-0.158	0.093
Sx_a	0.569	0.536	0.324	-0.253	0.059	0.039	-0.189	0.396
Dx	0.702	-0.562	-0.084	-0.280	-0.077	0.171	-0.047	-0.176
Dx_a	0.655	-0.502	-0.054	-0.349	-0.046	-0.357	0.008	0.027
TOx	0.651	0.057	-0.059	0.347	0.598	0.104	0.006	-0.144
TOx_a	0.526	0.095	-0.131	0.370	0.704	-0.037	-0.011	0.002
THx	0.406	-0.249	-0.481	0.574	-0.350	0.111	-0.030	0.167
THx_a	0.394	-0.347	-0.515	0.575	-0.189	-0.045	-0.035	0.216
ORx_5	0.288	-0.282	0.631	0.184	-0.039	0.145	0.590	0.168
ORx_30	0.076	-0.428	0.747	0.390	-0.021	-0.091	-0.078	-0.095
ORx_60	0.045	-0.384	0.687	0.390	-0.135	-0.137	-0.371	-0.027

F9	F10	F11	F12	F13	F14	F15	F16
-0.339	-0.085	-0.076	-0.067	-0.099	0.002	-0.015	0.003
0.057	0.263	0.093	0.056	0.069	0.007	0.072	0.001
0.284	-0.131	0.001	0.032	-0.022	-0.024	-0.060	0.001
-0.047	0.140	-0.091	-0.090	0.043	-0.038	-0.032	-0.054
0.160	-0.064	-0.109	-0.132	0.127	0.037	0.007	0.033
-0.023	-0.053	0.046	-0.076	-0.059	0.119	0.079	0.003
-0.024	-0.013	0.013	0.058	0.027	-0.093	-0.090	-0.004
-0.093	0.076	0.057	0.084	-0.071	-0.072	-0.008	0.057
0.054	-0.123	0.129	0.133	-0.087	0.033	0.029	-0.036
-0.086	-0.050	-0.020	0.142	0.145	0.080	-0.036	0.000
0.160	0.010	0.000	-0.097	-0.130	-0.088	0.045	-0.003
-0.098	-0.107	-0.003	0.015	0.105	-0.086	0.091	-0.005
0.023	0.121	0.029	-0.039	-0.086	0.100	-0.090	0.005
-0.002	0.021	-0.061	0.043	-0.038	-0.001	0.009	0.000
-0.062	-0.042	0.211	-0.141	0.071	-0.015	-0.034	0.000
0.043	0.028	-0.195	0.080	-0.053	0.014	0.031	0.000

% Contribution of Variables

	F1	F2	F3	F4	F5	F6	F7	F8
PRx	5.725	13.833	0.000	0.660	1.048	13.413	1.253	3.528
PAx	5.170	17.008	0.787	0.868	2.113	8.783	0.262	0.292
RAC	4.272	10.523	0.007	4.299	14.954	2.506	0.652	15.061
Mx	13.296	4.769	0.244	4.340	0.905	5.047	0.017	7.253
Mx_a	12.360	2.184	0.090	7.490	0.008	13.723	0.483	1.532
Sx	9.669	4.315	2.817	2.403	0.253	27.971	4.362	1.910
Sx_a	6.802	9.319	4.907	3.358	0.265	0.184	6.264	34.361
Dx	10.331	10.254	0.328	4.120	0.453	3.572	0.383	6.761
Dx_a	9.015	8.176	0.136	6.414	0.161	15.617	0.012	0.163
TOx	8.903	0.104	0.162	6.338	27.651	1.331	0.005	4.546
TOx_a	5.817	0.292	0.805	7.212	38.356	0.171	0.023	0.001
THx	3.468	2.006	10.799	17.325	9.491	1.515	0.158	6.079
THx_a	3.264	3.915	12.353	17.367	2.773	0.254	0.216	10.182
ORx_5	1.744	2.575	18.539	1.774	0.117	2.591	60.789	6.205
ORx_30	0.123	5.938	26.043	8.019	0.035	1.012	1.066	1.968
ORx_60	0.042	4.788	21.982	8.013	1.416	2.309	24.056	0.159

F9	F10	F11	F12	F13	F14	F15	F16
39.827	4.149	4.009	3.466	8.500	0.006	0.471	0.112
1.117	39.980	5.927	2.478	4.112	0.083	10.998	0.022
28.100	9.968	0.001	0.819	0.414	0.879	7.535	0.010
0.779	11.334	5.778	6.364	1.626	2.252	2.122	33.875
8.859	2.382	8.287	13.644	14.000	2.086	0.094	12.779
0.179	1.613	1.483	4.530	3.058	22.031	13.276	0.127
0.196	0.097	0.114	2.661	0.644	13.420	17.233	0.175
2.982	3.371	2.254	5.513	4.338	8.040	0.126	37.173
1.027	8.777	11.472	13.923	6.555	1.721	1.806	15.026
2.550	1.420	0.289	15.837	18.225	9.854	2.780	0.002
8.870	0.058	0.000	7.356	14.643	12.032	4.236	0.128
3.354	6.642	0.007	0.172	9.517	11.560	17.632	0.275
0.179	8.487	0.579	1.186	6.432	15.364	17.155	0.293
0.002	0.246	2.578	1.442	1.228	0.000	0.169	0.001
1.337	1.016	30.807	15.565	4.306	0.370	2.395	0.000
0.641	0.457	26.416	5.045	2.402	0.300	1.973	0.001

3. ***Grand Mean Data Set:***

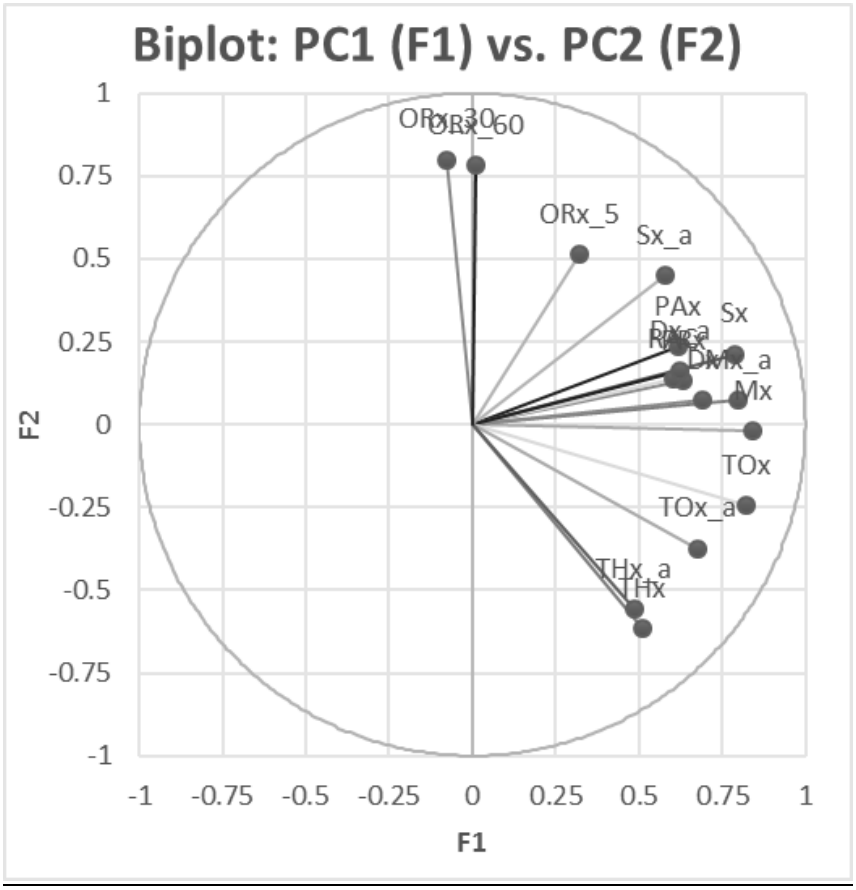

Eigenvalue Table

	F1	F2	F3	F4	F5	F6	F7	F8	F9	F10	F11	F12	F13	F14	F15	F16
Eigenvalue	6.062	2.779	2.542	1.294	0.844	0.672	0.561	0.395	0.263	0.180	0.133	0.107	0.088	0.037	0.028	0.015
Variability	37.889	17.366	15.887	8.088	5.277	4.201	3.507	2.468	1.644	1.123	0.833	0.666	0.551	0.232	0.174	0.094
Cumulative	37.889	55.255	71.142	79.230	84.507	88.708	92.215	94.683	96.327	97.450	98.283	98.949	99.500	99.732	99.906	100.000

Scree Plot

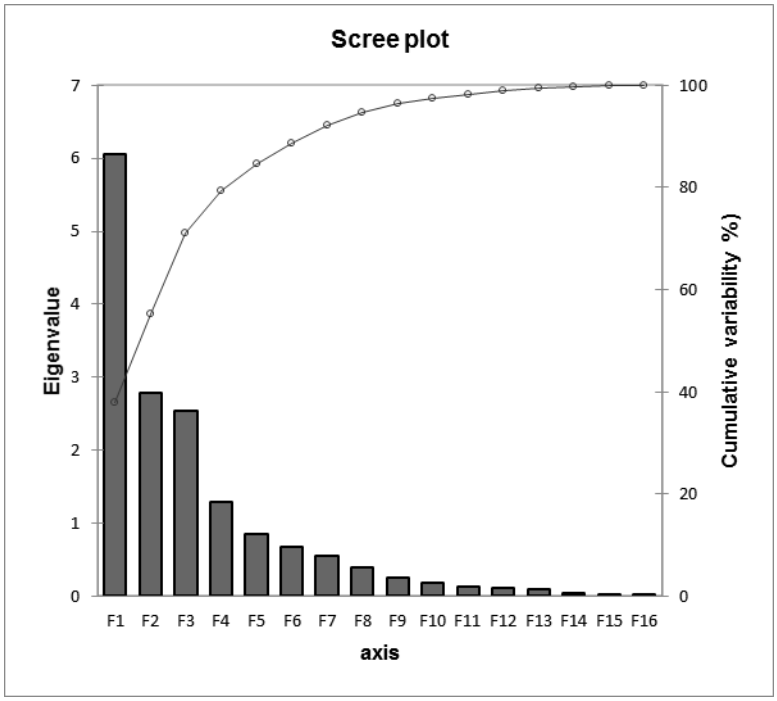

Factor Loadings

	F1	F2	F3	F4	F5	F6	F7	F8
PRx	0.631	0.131	0.628	0.181	0.050	-0.080	-0.140	0.059
PAx	0.620	0.233	0.636	0.215	0.063	-0.123	0.014	-0.126
RAC	0.602	0.136	0.552	0.388	-0.167	-0.013	-0.008	-0.259
Mx	0.843	-0.020	-0.285	-0.212	-0.257	-0.059	0.144	-0.206
Mx_a	0.798	0.072	-0.079	-0.234	0.406	-0.205	0.029	-0.135
Sx	0.790	0.211	0.165	-0.226	-0.396	0.193	0.032	0.185
Sx_a	0.581	0.451	0.430	-0.323	0.062	0.025	-0.079	0.347
Dx	0.691	0.072	-0.492	-0.260	-0.406	-0.026	0.018	-0.095
Dx_a	0.623	0.161	-0.471	-0.235	0.245	-0.377	-0.202	0.037
TOx	0.821	-0.246	-0.122	0.052	0.221	0.346	0.022	0.003
TOx_a	0.677	-0.373	-0.179	0.004	0.298	0.478	-0.041	-0.055
THx	0.511	-0.615	-0.161	0.438	-0.164	-0.140	-0.056	0.212
THx_a	0.489	-0.558	-0.380	0.422	-0.053	-0.148	-0.157	0.105
ORx_5	0.323	0.514	-0.326	0.380	0.156	-0.068	0.570	0.149
ORx_30	-0.078	0.798	-0.439	0.312	-0.042	0.119	-0.124	-0.013
ORx_60	0.013	0.783	-0.399	0.270	0.001	0.128	-0.319	-0.038

F9	F10	F11	F12	F13	F14	F15	F16
0.299	0.123	0.057	-0.020	-0.130	-0.020	-0.027	-0.013
-0.055	-0.070	0.196	0.093	0.135	-0.021	0.027	-0.001
-0.093	-0.141	-0.179	-0.072	-0.043	0.038	-0.009	0.004
-0.043	0.127	0.043	-0.013	-0.043	-0.050	-0.005	0.076
-0.118	0.219	-0.067	-0.005	0.026	0.054	0.011	-0.039
-0.022	0.028	-0.067	0.086	-0.031	-0.005	0.096	-0.027
-0.171	-0.036	0.003	-0.045	0.019	0.027	-0.067	0.033
0.088	-0.080	0.081	-0.036	0.042	0.033	-0.069	-0.055
0.116	-0.213	-0.036	-0.015	-0.026	-0.020	0.049	0.017
0.180	-0.012	-0.142	0.085	0.125	-0.038	-0.037	0.014
-0.076	-0.080	0.140	-0.084	-0.089	0.026	0.027	-0.003
0.012	0.078	0.007	-0.170	0.108	0.008	0.033	0.006
-0.158	-0.003	0.009	0.183	-0.083	0.014	-0.038	-0.002
0.001	-0.045	0.006	-0.015	-0.045	-0.023	-0.007	-0.013
0.115	0.058	0.029	0.041	0.027	0.117	0.019	0.037
-0.136	0.060	-0.012	-0.052	0.009	-0.104	-0.009	-0.025

% Contribution of Variables

	F1	F2	F3	F4	F5	F6	F7	F8
PRx	6.569	0.616	15.491	2.523	0.298	0.961	3.499	0.871
PAx	6.347	1.960	15.931	3.562	0.477	2.249	0.035	3.993
RAC	5.984	0.661	11.966	11.624	3.308	0.026	0.011	17.016
Mx	11.716	0.014	3.197	3.478	7.849	0.522	3.678	10.778
Mx_a	10.503	0.187	0.246	4.214	19.515	6.231	0.151	4.598
Sx	10.287	1.609	1.067	3.940	18.575	5.552	0.177	8.689
Sx_a	5.565	7.314	7.265	8.063	0.453	0.090	1.100	30.498
Dx	7.869	0.188	9.538	5.237	19.505	0.103	0.059	2.284
Dx_a	6.406	0.930	8.744	4.278	7.102	21.096	7.283	0.341
TOx	11.122	2.172	0.590	0.207	5.782	17.818	0.085	0.002
TOx_a	7.567	5.020	1.257	0.001	10.511	33.954	0.295	0.769
THx	4.301	13.632	1.016	14.848	3.187	2.900	0.562	11.355
THx_a	3.942	11.208	5.669	13.732	0.335	3.272	4.416	2.806
ORx_5	1.718	9.515	4.193	11.140	2.894	0.694	57.808	5.601
ORx_30	0.101	22.936	7.579	7.520	0.208	2.113	2.731	0.041
ORx_60	0.003	22.037	6.251	5.631	0.000	2.420	18.109	0.357

F9	F10	F11	F12	F13	F14	F15	F16
33.964	8.376	2.399	0.391	19.145	1.075	2.711	1.110
1.166	2.735	28.923	8.110	20.704	1.138	2.657	0.013
3.275	11.020	23.920	4.924	2.096	3.796	0.288	0.083
0.689	8.995	1.387	0.167	2.071	6.613	0.081	38.766
5.253	26.756	3.404	0.028	0.753	7.721	0.430	10.011
0.188	0.440	3.400	6.919	1.088	0.062	33.100	4.905
11.147	0.737	0.005	1.877	0.429	1.999	16.348	7.112
2.940	3.599	4.930	1.200	2.020	2.930	17.287	20.310
5.158	25.270	0.980	0.201	0.788	1.033	8.555	1.835
12.384	0.083	15.149	6.720	17.631	3.980	5.022	1.252
2.215	3.544	14.614	6.655	9.070	1.825	2.629	0.076
0.058	3.422	0.041	27.085	13.233	0.160	3.930	0.269
9.502	0.007	0.067	31.417	7.761	0.552	5.286	0.027
0.000	1.132	0.028	0.211	2.318	1.413	0.162	1.173
5.048	1.863	0.638	1.591	0.801	36.612	1.250	8.969
7.014	2.022	0.115	2.502	0.094	29.091	0.265	4.091

Appendix B: Section 6.2 - Spearman Principal Component Analysis (PCA) – Supplementary Material

*** PCA = principal component analysis, F = factor, PC = principal component, F1 = PC1 = principal component #1, F2 = PC2 = principal component #2. PC1 and PC2 are the two components which contribute the largest amount of variance to the entire data set.**

***Biplots of PC1 vs. PC2 display which variables contribute variance to PC1 and PC2. The longer the arm connecting (0,0) to the variable (such as PRx), the larger the contribution of that variable. Similarly, the quadrant on the biplot in which the variable falls correlates to its contribution to a particular PC. The upper left quadrant is primarily PC2; lower left quadrant is neither PC1 or PC2; the upper right quadrant is PC1 and PC2; the lower right quadrant is primarily PC1.**

***Eigenvalue tables display the eigenvalue for each principal component (PC) (also denoted F), with the % variability and cumulative variability for each factor/principal component.**

***Scree plot displays the same information form the eigenvalue table in a histogram format, with each F (or PC) along the x-axis, the eigenvalue along the left side y-axis and the % variability along the right y-axis. Furthermore, the red line on the graph displays the cumulative variability with the addition of each F (or PC) moving from F1 to F18.**

***Factor loading tables display the loading of each variable (ie. PRx, etc.) for each principal component. Loading varies from -1 to +1, with negative values indicating that particular variable is less likely to contribute to the variance in that particular factor (F). Similarly, positive loadings indicate that particular variable likely contribute to the variance in that corresponding factor (F).**

***Contribution % of Variables tables displays the % contribution to the variance of each individual variable for each individual factor (F).**

***Correlation between variables and factor table – denotes the strength of association between various autoregulatory indices and the individual factors**

1. Grand Mean Data Set

Loading Biplot: PC1 vs. PC2

Spearman Type Principal Component Analysis of Autoregulatory Indices – Biplot of PC1 vs. PC2 (Grand Mean Data)

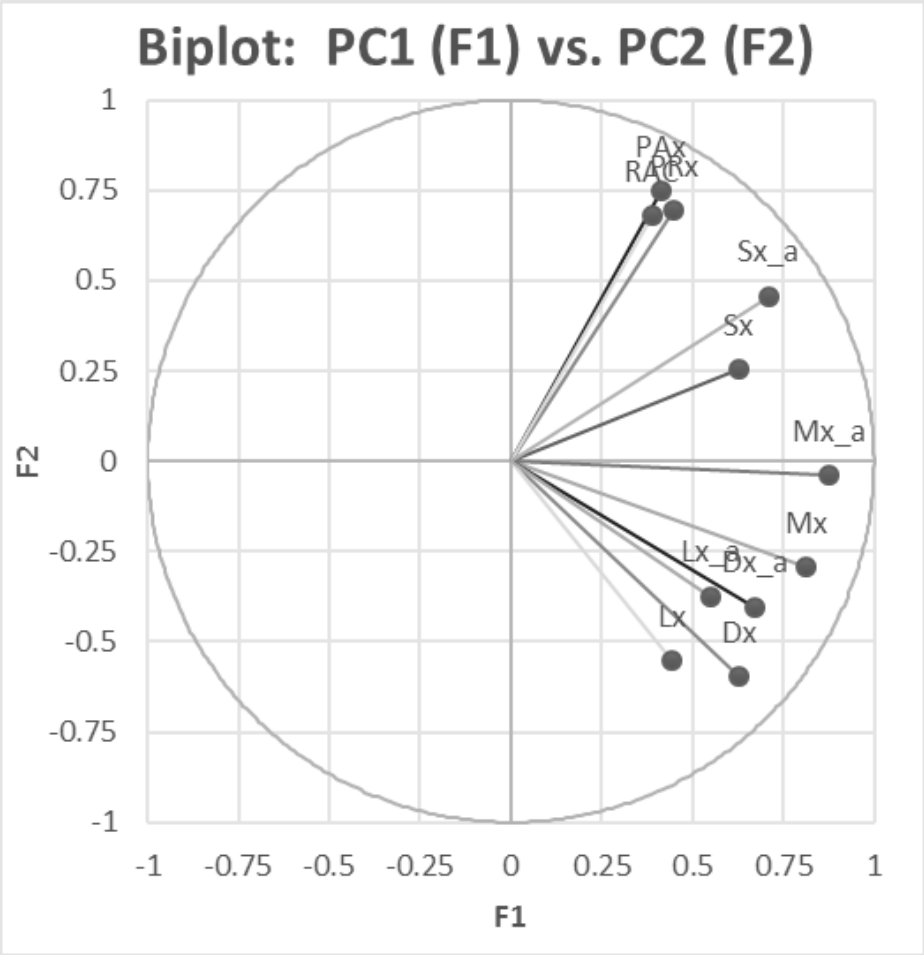

PCA = principal component analysis, F = factor, PC = principal component, F1 = PC1 = principal component #1, F2 = PC2 = principal component #2. PC1 and PC2 are the two components which contribute the largest amount of variance to the entire data set. The above biplot of PC1 vs. PC2 displays which variables contribute variance to PC1 and PC2. The longer the arm connecting (0,0) to the variable (such as PRx), the larger the contribution of that variable. Similarly, the quadrant on the biplot in which the variable falls correlates to its contribution to a particular PC. The upper left quadrant is primarily PC2; lower left quadrant is neither PC1 or PC2; the upper right quadrant is PC1 and PC2; the lower right quadrant is primarily PC1.

Spearman Correlation Matrix

Variables	PRx	PAx	RAC	Mx	Mx_a	Sx	Sx_a	Dx	Dx_a	Lx	Lx_a
PRx	**1**	**0.639**	**0.595**	0.192	**0.384**	**0.334**	**0.504**	-0.145	0.008	-0.143	0.052
PAx	**0.639**	**1**	**0.706**	0.026	**0.311**	**0.264**	**0.573**	-0.186	0.018	-0.139	0.124
RAC	**0.595**	**0.706**	**1**	0.104	0.237	**0.310**	**0.401**	-0.119	-0.023	-0.026	0.037
Mx	0.192	0.026	0.104	**1**	**0.676**	**0.610**	**0.360**	**0.746**	**0.494**	**0.464**	**0.408**
Mx_a	**0.384**	**0.311**	0.237	**0.676**	**1**	**0.376**	**0.629**	**0.501**	**0.742**	**0.279**	**0.433**
Sx	**0.334**	**0.264**	**0.310**	**0.610**	**0.376**	**1**	**0.668**	**0.271**	0.084	0.113	0.083
Sx_a	**0.504**	**0.573**	**0.401**	**0.360**	**0.629**	**0.668**	**1**	0.140	**0.338**	-0.030	0.145
Dx	-0.145	-0.186	-0.119	**0.746**	**0.501**	**0.271**	0.140	**1**	**0.778**	**0.416**	**0.322**
Dx_a	0.008	0.018	-0.023	**0.494**	**0.742**	0.084	**0.338**	**0.778**	**1**	0.257	**0.360**
Lx	-0.143	-0.139	-0.026	**0.464**	**0.279**	0.113	-0.030	**0.416**	0.257	**1**	**0.814**
Lx_a	0.052	0.124	0.037	**0.408**	**0.433**	0.083	0.145	**0.322**	**0.360**	**0.814**	**1**

Eigenvalue Table

	F1	F2	F3	F4	F5	F6	F7	F8	F9	F10	F11
Eigenvalue	4.197	2.827	1.291	0.972	0.584	0.457	0.255	0.206	0.115	0.078	0.019
Variability	38.152	25.699	11.735	8.835	5.310	4.154	2.320	1.877	1.044	0.705	0.169
Cumulative	38.152	63.852	75.587	84.422	89.733	93.886	96.206	98.082	99.126	99.831	100.000

Scree Plot

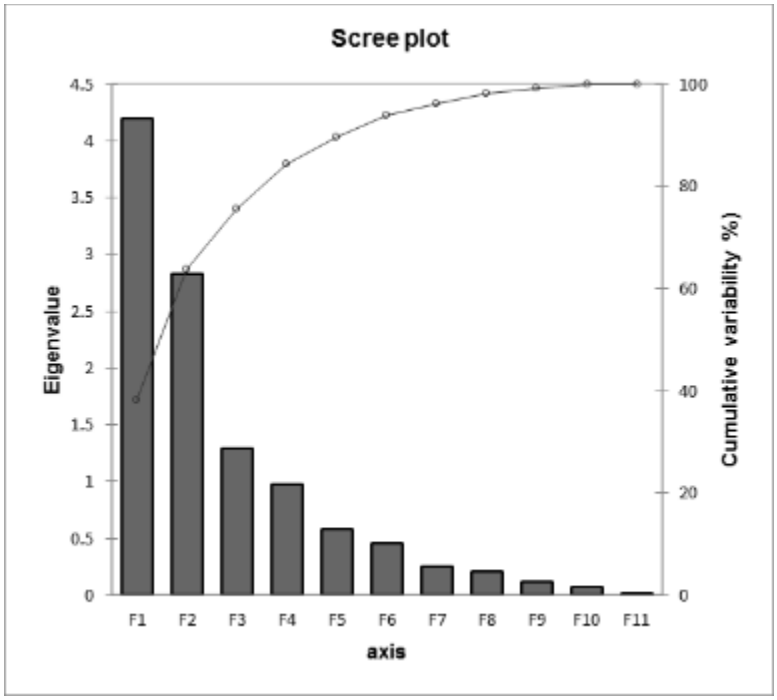

Factor Loading Table

	F1	F2	F3	F4	F5	F6	F7	F8	F9	F10	F11
PRx	0.449	0.694	0.101	-0.078	0.112	0.493	0.053	-0.201	-0.020	-0.016	0.001
PAx	0.416	0.748	0.237	-0.215	-0.003	-0.198	0.312	0.144	-0.057	-0.075	-0.007
RAC	0.391	0.681	0.256	-0.045	0.442	-0.244	-0.235	-0.016	0.053	0.055	0.003
Mx	0.813	-0.294	-0.150	0.307	0.215	0.174	0.062	0.208	-0.025	0.091	-0.063
Mx_a	0.876	-0.039	-0.116	-0.278	-0.144	0.156	-0.198	0.220	-0.004	-0.063	0.061
Sx	0.626	0.253	-0.252	0.654	-0.084	-0.101	0.005	-0.063	0.124	-0.126	0.007
Sx_a	0.708	0.456	-0.206	0.047	-0.419	-0.157	-0.055	-0.106	-0.114	0.135	-0.006
Dx	0.629	-0.597	-0.299	-0.049	0.294	-0.110	0.184	-0.124	-0.046	0.043	0.073
Dx_a	0.672	-0.403	-0.271	-0.518	-0.001	-0.103	-0.037	-0.130	0.069	-0.077	-0.071
Lx	0.445	-0.552	0.626	0.209	0.012	-0.047	-0.098	-0.076	-0.190	-0.090	-0.012
Lx_a	0.551	-0.374	0.680	-0.039	-0.199	0.021	0.093	-0.022	0.191	0.082	0.013

% Contribution

	F1	F2	F3	F4	F5	F6	F7	F8	F9	F10	F11
PRx	4.812	17.052	0.793	0.620	2.154	53.259	1.112	19.525	0.335	0.333	0.004
PAx	4.114	19.775	4.352	4.757	0.002	8.545	38.122	10.035	2.836	7.208	0.255
RAC	3.641	16.384	5.061	0.205	33.495	13.044	21.724	0.121	2.430	3.844	0.052
Mx	15.744	3.058	1.735	9.697	7.884	6.597	1.483	20.993	0.536	10.582	21.691
Mx_a	18.284	0.053	1.047	7.928	3.555	5.360	15.441	23.412	0.012	5.051	19.857
Sx	9.337	2.265	4.933	44.040	1.203	2.221	0.009	1.940	13.423	20.328	0.302
Sx_a	11.953	7.352	3.280	0.230	30.103	5.397	1.187	5.393	11.241	23.638	0.226
Dx	9.417	12.593	6.931	0.247	14.787	2.655	13.293	7.408	1.826	2.350	28.493
Dx_a	10.752	5.745	5.673	27.633	0.000	2.342	0.541	8.127	4.139	7.571	27.477
Lx	4.713	10.786	30.346	4.483	0.023	0.484	3.732	2.806	31.508	10.362	0.758
Lx_a	7.233	4.938	35.850	0.159	6.794	0.096	3.357	0.240	31.714	8.734	0.885

Correlation Between Variables and Factors

	F1	F2	F3	F4	F5	F6	F7	F8	F9	F10	F11
PRx	0.449	0.694	0.101	-0.078	0.112	0.493	0.053	-0.201	-0.020	-0.016	0.001
PAx	0.416	0.748	0.237	-0.215	-0.003	-0.198	0.312	0.144	-0.057	-0.075	-0.007
RAC	0.391	0.681	0.256	-0.045	0.442	-0.244	-0.235	-0.016	0.053	0.055	0.003
Mx	0.813	-0.294	-0.150	0.307	0.215	0.174	0.062	0.208	-0.025	0.091	-0.063
Mx_a	0.876	-0.039	-0.116	-0.278	-0.144	0.156	-0.198	0.220	-0.004	-0.063	0.061
Sx	0.626	0.253	-0.252	0.654	-0.084	-0.101	0.005	-0.063	0.124	-0.126	0.007
Sx_a	0.708	0.456	-0.206	0.047	-0.419	-0.157	-0.055	-0.106	-0.114	0.135	-0.006
Dx	0.629	-0.597	-0.299	-0.049	0.294	-0.110	0.184	-0.124	-0.046	0.043	0.073
Dx_a	0.672	-0.403	-0.271	-0.518	-0.001	-0.103	-0.037	-0.130	0.069	-0.077	-0.071
Lx	0.445	-0.552	0.626	0.209	0.012	-0.047	-0.098	-0.076	-0.190	-0.090	-0.012
Lx_a	0.551	-0.374	0.680	-0.039	-0.199	0.021	0.093	-0.022	0.191	0.082	0.013

2. <u>10 Second by 10 Second Data</u>

Loading Biplot: PC1 vs. PC2

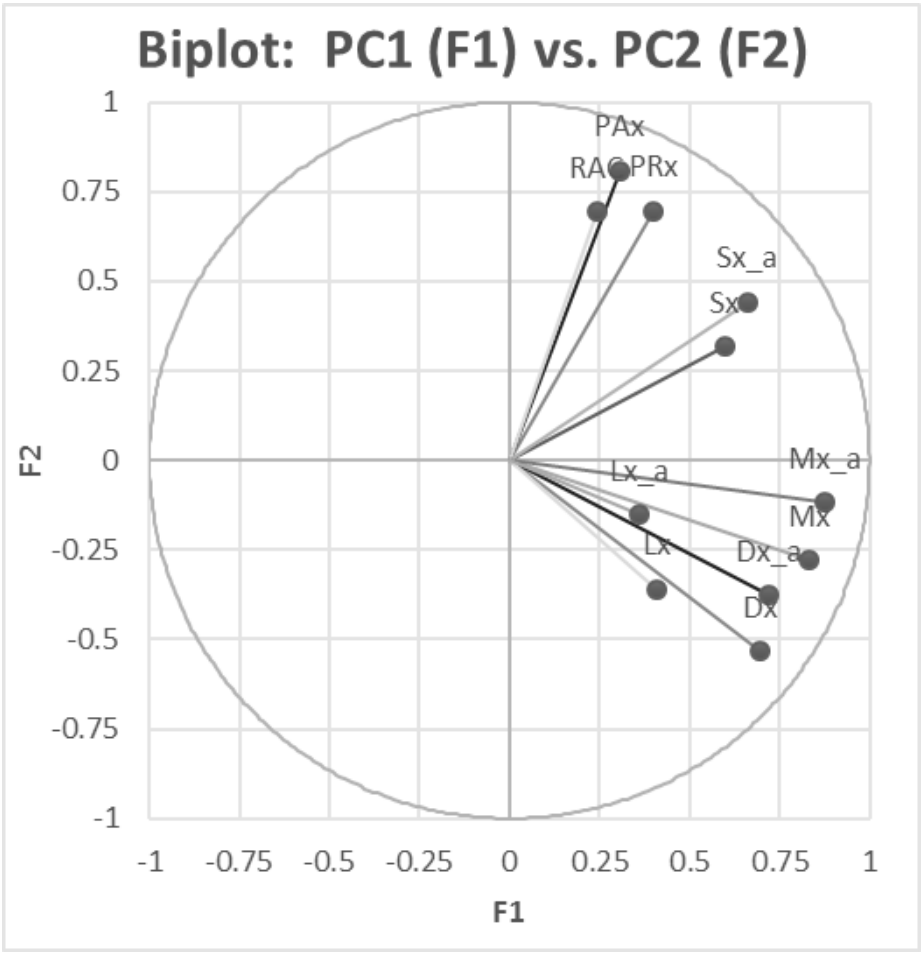

Spearman Correlation Matrix

Variables	PRx	PAx	RAC	Mx	Mx_a	Sx	Sx_a	Dx	Dx_a	Lx	Lx_a
PRx	**1**	**0.704**	**0.481**	**0.144**	**0.286**	**0.248**	**0.416**	**-0.089**	**0.036**	-0.011	**0.154**
PAx	**0.704**	**1**	**0.565**	0.002	**0.168**	**0.234**	**0.497**	**-0.153**	-0.002	**-0.143**	**0.049**
RAC	**0.481**	**0.565**	**1**	**0.044**	**0.071**	**0.369**	**0.248**	**-0.152**	**-0.112**	**0.034**	**0.063**
Mx	**0.144**	0.002	**0.044**	**1**	**0.705**	**0.536**	**0.310**	**0.815**	**0.535**	**0.380**	**0.175**
Mx_a	**0.286**	**0.168**	**0.071**	**0.705**	**1**	**0.332**	**0.565**	**0.561**	**0.796**	**0.244**	**0.286**
Sx	**0.248**	**0.234**	**0.369**	**0.536**	**0.332**	**1**	**0.650**	**0.266**	**0.097**	**0.101**	0.002
Sx_a	**0.416**	**0.497**	**0.248**	**0.310**	**0.565**	**0.650**	**1**	**0.147**	**0.351**	-0.016	**0.071**
Dx	**-0.089**	**-0.153**	**-0.152**	**0.815**	**0.561**	**0.266**	**0.147**	**1**	**0.733**	**0.338**	**0.088**
Dx_a	**0.036**	-0.002	**-0.112**	**0.535**	**0.796**	**0.097**	**0.351**	**0.733**	**1**	**0.183**	**0.188**
Lx	-0.011	**-0.143**	**0.034**	**0.380**	**0.244**	**0.101**	-0.016	**0.338**	**0.183**	**1**	**0.737**
Lx_a	**0.154**	**0.049**	**0.063**	**0.175**	**0.286**	0.002	**0.071**	**0.088**	**0.188**	**0.737**	**1**

Eigenvalue Table

	F1	F2	F3	F4	F5	F6	F7	F8	F9	F10	F11
Eigenvalue	3.870	2.586	1.559	0.993	0.709	0.472	0.321	0.203	0.183	0.086	0.018
Variability	35.184	23.513	14.174	9.027	6.441	4.292	2.915	1.847	1.665	0.778	0.164
Cumulative	35.184	58.697	72.871	81.898	88.339	92.632	95.546	97.394	99.058	99.836	100.000

Scree Plot

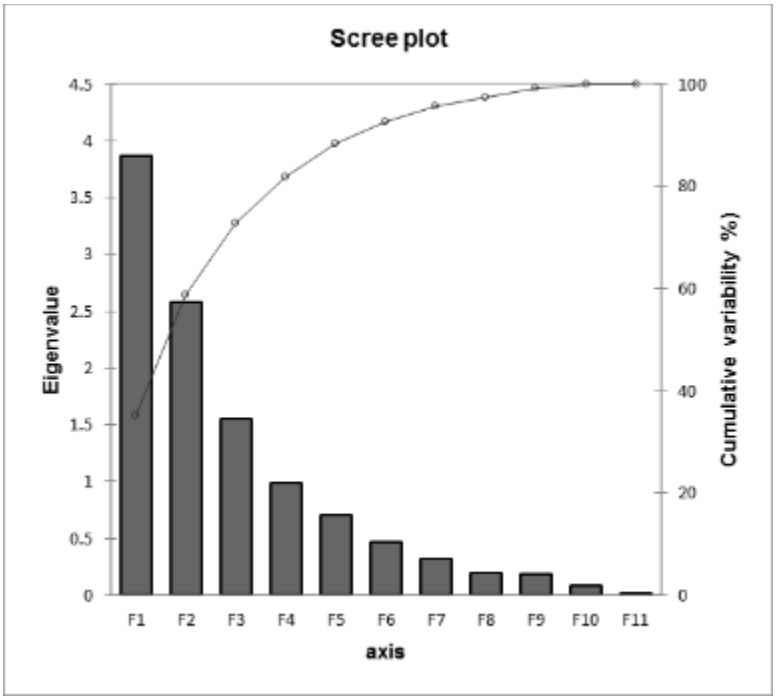

Factor Loading Table

	F1	F2	F3	F4	F5	F6	F7	F8	F9	F10	F11
PRx	0.398	0.698	0.170	-0.268	-0.169	-0.382	-0.189	0.204	0.052	0.005	0.000
PAx	0.309	0.809	0.063	-0.262	-0.107	-0.062	0.350	-0.182	-0.033	-0.081	-0.004
RAC	0.244	0.693	0.210	0.212	-0.398	0.444	-0.096	0.028	-0.010	0.065	0.003
Mx	0.831	-0.278	-0.116	0.253	-0.236	-0.215	-0.075	-0.189	-0.054	0.055	0.073
Mx_a	0.875	-0.118	-0.106	-0.280	0.097	0.091	-0.264	-0.141	-0.136	-0.049	-0.065
Sx	0.600	0.316	-0.187	0.651	0.193	-0.025	-0.023	0.027	0.151	-0.137	-0.017
Sx_a	0.661	0.442	-0.218	0.014	0.516	0.057	0.105	0.089	-0.095	0.150	0.016
Dx	0.698	-0.533	-0.216	0.053	-0.309	-0.061	0.227	0.088	0.088	0.095	-0.066
Dx_a	0.722	-0.376	-0.214	-0.430	-0.013	0.250	0.041	0.135	0.105	-0.100	0.059
Lx	0.408	-0.360	0.754	0.205	0.000	-0.020	0.114	0.148	-0.230	-0.072	0.003
Lx_a	0.360	-0.153	0.845	-0.110	0.214	0.028	-0.019	-0.125	0.233	0.062	-0.003

% Contribution

	F1	F2	F3	F4	F5	F6	F7	F8	F9	F10	F11
PRx	4.098	18.813	1.849	7.224	4.018	30.839	11.181	20.482	1.461	0.034	0.001
PAx	2.471	25.277	0.258	6.890	1.610	0.824	38.117	16.271	0.582	7.599	0.102
RAC	1.537	18.591	2.841	4.531	22.397	41.785	2.897	0.389	0.057	4.929	0.046
Mx	17.838	2.999	0.865	6.429	7.887	9.748	1.757	17.645	1.617	3.555	29.660
Mx_a	19.761	0.536	0.715	7.871	1.337	1.735	21.667	9.775	10.061	2.750	23.792
Sx	9.315	3.873	2.246	42.647	5.237	0.130	0.161	0.352	12.408	22.054	1.578
Sx_a	11.287	7.564	3.045	0.020	37.566	0.699	3.416	3.862	4.885	26.158	1.500
Dx	12.585	10.978	2.990	0.283	13.448	0.796	16.074	3.808	4.270	10.616	24.153
Dx_a	13.459	5.463	2.937	18.649	0.025	13.195	0.534	8.914	6.058	11.679	19.088
Lx	4.304	5.007	36.451	4.233	0.000	0.088	4.083	10.821	28.845	6.123	0.046
Lx_a	3.344	0.901	45.805	1.224	6.474	0.161	0.113	7.681	29.757	4.503	0.035

Correlation Between Variables and Factors

	F1	F2	F3	F4	F5	F6	F7	F8	F9	F10	F11
PRx	0.398	0.698	0.170	-0.268	-0.169	-0.382	-0.189	0.204	0.052	0.005	0.000
PAx	0.309	0.809	0.063	-0.262	-0.107	-0.062	0.350	-0.182	-0.033	-0.081	-0.004
RAC	0.244	0.693	0.210	0.212	-0.398	0.444	-0.096	0.028	-0.010	0.065	0.003
Mx	0.831	-0.278	-0.116	0.253	-0.236	-0.215	-0.075	-0.189	-0.054	0.055	0.073
Mx_a	0.875	-0.118	-0.106	-0.280	0.097	0.091	-0.264	-0.141	-0.136	-0.049	-0.065
Sx	0.600	0.316	-0.187	0.651	0.193	-0.025	-0.023	0.027	0.151	-0.137	-0.017
Sx_a	0.661	0.442	-0.218	0.014	0.516	0.057	0.105	0.089	-0.095	0.150	0.016
Dx	0.698	-0.533	-0.216	0.053	-0.309	-0.061	0.227	0.088	0.088	0.095	-0.066
Dx_a	0.722	-0.376	-0.214	-0.430	-0.013	0.250	0.041	0.135	0.105	-0.100	0.059
Lx	0.408	-0.360	0.754	0.205	0.000	-0.020	0.114	0.148	-0.230	-0.072	0.003
Lx_a	0.360	-0.153	0.845	-0.110	0.214	0.028	-0.019	-0.125	0.233	0.062	-0.003

Appendix C: Section 6.3 - Spearman Principal Component Analysis (PCA) – Supplementary Material – Entire TBI TCD Cohort

*** PCA = principal component analysis, F = factor, PC = principal component, F1 = PC1 = principal component #1, F2 = PC2 = principal component #2. PC1 and PC2 are the two components which contribute the largest amount of variance to the entire data set.**

***Biplots of PC1 vs. PC2 display which variables contribute variance to PC1 and PC2. The longer the arm connecting (0,0) to the variable (such as PRx), the larger the contribution of that variable. Similarly, the quadrant on the biplot in which the variable fallscorrelates to its contribution to a particular PC. The upper left quadrant is primarily PC2; lower left quadrant is neither PC1 or PC2; the upper right quadrant is PC1 and PC2; the lower right quadrant is primarily PC1.**

***Eigenvalue tables display the eigenvalue for each principal component (PC) (also denoted F), with the % variability and cumulative variability for each factor/principal component.**

***Scree plot displays the same information form the eigenvalue table in a histogram format, with each F (or PC) along the x-axis, the eigenvalue along the left side y-axis and the % variability along the right y-axis. Furthermore, the red line on the graph displays the cumulative variability with the addition of each F (or PC) moving from F1 to F18.**

***Factor loading tables display the loading of each variable (ie. PRx, etc.) for each principal component. Loading varies from -1 to +1, with negative values indicating that particular variable is less likely to contribute to the variance in that particular factor (F). Similarly, positive loadings indicate that particular variable likely contribute to the variance in that corresponding factor (F).**

***Contribution % of Variables tables displays the % contribution to the variance of each individual variable for each individual factor (F).**

***Correlation between variables and factor table – denotes the strength of association between various autoregulatory indices and the individual factors**

1. Grand Mean Data Set

Loading Biplot

Spearman Type Principal Component Analysis of Autoregulatory/Cerebrovascular Reactivity Indices – Biplot of PC1 vs. PC2 (Entire TBI TCD Cohort - Grand Mean Data)

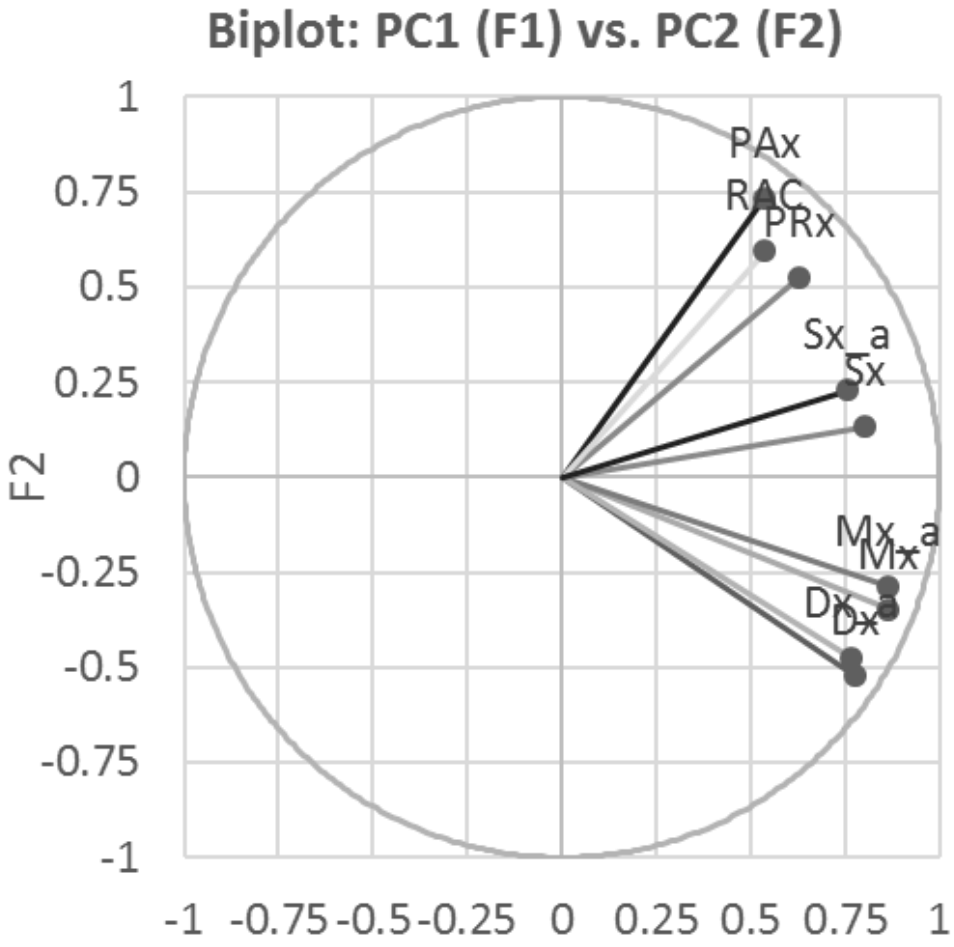

PCA = principal component analysis, F = factor, PC = principal component, F1 = PC1 = principal component #1, F2 = PC2 = principal component #2. PC1 and PC2 are the two components which contribute the largest amount of variance to the entire data set. The above biplot of PC1 vs. PC2 displays which variables contribute variance to PC1 and PC2. The longer the arm connecting (0,0) to the variable (such as PRx), the larger the contribution of that variable. Similarly, the quadrant on the biplot in which the variable falls correlates to its contribution to a particular PC. The upper left quadrant is primarily PC2; lower left quadrant is neither PC1 or PC2; the upper right quadrant is PC1 and PC2; the lower right quadrant is primarily PC1.

Spearman Correlation Matrix

Variables	PRx	PAx	RAC	Mx	Mx_a	Dx	Dx_a	Sx	Sx_a
PRx	**1**	**0.715**	**0.507**	**0.338**	**0.409**	**0.232**	**0.304**	**0.430**	**0.495**
PAx	**0.715**	**1**	**0.651**	**0.191**	**0.305**	0.047	**0.141**	**0.363**	**0.526**
RAC	**0.507**	**0.651**	**1**	**0.340**	**0.224**	**0.191**	**0.109**	**0.545**	**0.339**
Mx	**0.338**	**0.191**	**0.340**	**1**	**0.755**	**0.934**	**0.715**	**0.716**	**0.458**
Mx_a	**0.409**	**0.305**	**0.224**	**0.755**	**1**	**0.713**	**0.886**	**0.508**	**0.654**
Dx	**0.232**	0.047	**0.191**	**0.934**	**0.713**	**1**	**0.801**	**0.561**	**0.327**
Dx_a	**0.304**	**0.141**	**0.109**	**0.715**	**0.886**	**0.801**	**1**	**0.361**	**0.444**
Sx	**0.430**	**0.363**	**0.545**	**0.716**	**0.508**	**0.561**	**0.361**	**1**	**0.743**
Sx_a	**0.495**	**0.526**	**0.339**	**0.458**	**0.654**	**0.327**	**0.444**	**0.743**	**1**

Eigenvalue Table

	F1	F2	F3	F4	F5	F6	F7	F8	F9
Eigenvalue	4.862	1.938	0.788	0.678	0.368	0.202	0.100	0.048	0.016
Variability (%)	54.027	21.533	8.752	7.529	4.084	2.246	1.116	0.531	0.182
Cumulative %	54.027	75.560	84.311	91.841	95.925	98.171	99.287	99.818	100.000

Scree Plot

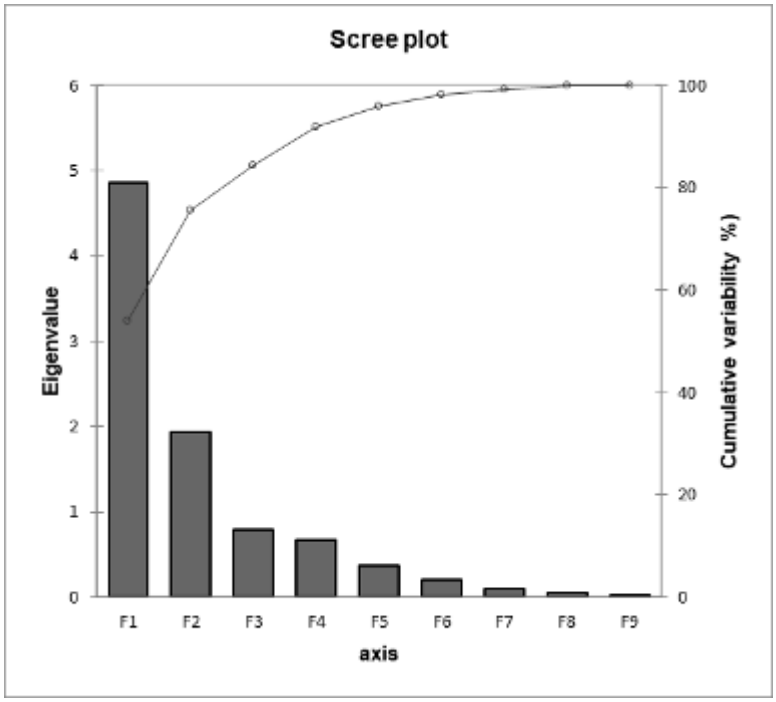

Factor Loading Table

	F1	F2	F3	F4	F5	F6	F7	F8	F9
PRx	0.629	0.525	-0.296	-0.200	-0.418	-0.159	0.013	-0.015	0.000
PAx	0.534	0.731	-0.224	-0.130	0.110	0.314	-0.030	0.047	-0.006
RAC	0.538	0.594	0.379	-0.308	0.293	-0.176	0.000	-0.048	0.002
Mx	0.865	-0.349	0.250	-0.128	-0.106	0.129	0.130	-0.018	0.080
Mx_a	0.861	-0.287	-0.305	0.052	0.180	-0.069	0.199	0.032	-0.050
Dx	0.778	-0.524	0.167	-0.217	-0.101	0.115	-0.100	-0.086	-0.068
Dx_a	0.765	-0.475	-0.319	-0.134	0.150	-0.107	-0.171	0.064	0.043
Sx	0.800	0.133	0.451	0.322	-0.124	-0.038	-0.042	0.130	-0.023
Sx_a	0.757	0.229	-0.130	0.582	0.061	-0.004	-0.045	-0.116	0.019

% Contribution

	F1	F2	F3	F4	F5	F6	F7	F8	F9
PRx	8.148	14.237	11.151	5.906	47.458	12.469	0.170	0.459	0.002
PAx	5.858	27.569	6.389	2.496	3.315	48.627	0.921	4.620	0.205
RAC	5.956	18.223	18.228	13.956	23.295	15.399	0.000	4.909	0.035
Mx	15.380	6.275	7.964	2.409	3.067	8.263	16.740	0.665	39.238
Mx_a	15.256	4.254	11.791	0.406	8.774	2.324	39.431	2.193	15.570
Dx	12.444	14.165	3.542	6.948	2.781	6.569	9.860	15.417	28.274
Dx_a	12.033	11.659	12.940	2.653	6.121	5.640	29.126	8.498	11.331
Sx	13.154	0.908	25.849	15.266	4.161	0.701	1.718	35.107	3.135
Sx_a	11.772	2.710	2.146	49.960	1.027	0.008	2.035	28.132	2.211

Correlation Between Variables and Factors

	F1	F2	F3	F4	F5	F6	F7	F8	F9
PRx	0.629	0.525	-0.296	-0.200	-0.418	-0.159	0.013	-0.015	0.000
PAx	0.534	0.731	-0.224	-0.130	0.110	0.314	-0.030	0.047	-0.006
RAC	0.538	0.594	0.379	-0.308	0.293	-0.176	0.000	-0.048	0.002
Mx	0.865	-0.349	0.250	-0.128	-0.106	0.129	0.130	-0.018	0.080
Mx_a	0.861	-0.287	-0.305	0.052	0.180	-0.069	0.199	0.032	-0.050
Dx	0.778	-0.524	0.167	-0.217	-0.101	0.115	-0.100	-0.086	-0.068
Dx_a	0.765	-0.475	-0.319	-0.134	0.150	-0.107	-0.171	0.064	0.043
Sx	0.800	0.133	0.451	0.322	-0.124	-0.038	-0.042	0.130	-0.023
Sx_a	0.757	0.229	-0.130	0.582	0.061	-0.004	-0.045	-0.116	0.019

2. ***30 Minute Mean Data***

Loading Biplot: PC1 vs. PC2

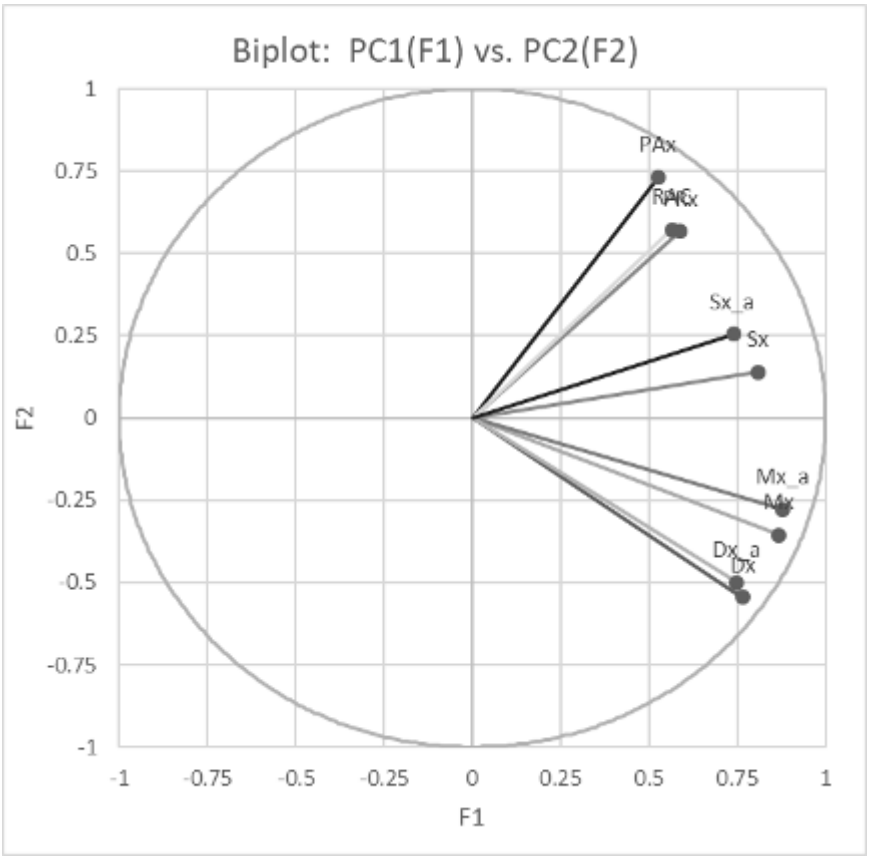

Spearman Correlation Matrix

Variables	PRx	PAx	RAC	Mx	Mx_a	Dx	Dx_a	Sx	Sx_a
PRx	**1**	**0.721**	**0.508**	**0.290**	**0.381**	**0.171**	**0.235**	**0.404**	**0.473**
PAx	**0.721**	**1**	**0.671**	**0.187**	**0.297**	0.040	**0.110**	**0.371**	**0.500**
RAC	**0.508**	**0.671**	**1**	**0.357**	**0.280**	**0.187**	**0.114**	**0.556**	**0.356**
Mx	**0.290**	**0.187**	**0.357**	**1**	**0.796**	**0.919**	**0.715**	**0.707**	**0.442**
Mx_a	**0.381**	**0.297**	**0.280**	**0.796**	**1**	**0.726**	**0.868**	**0.551**	**0.623**
Dx	**0.171**	0.040	**0.187**	**0.919**	**0.726**	**1**	**0.813**	**0.530**	**0.290**
Dx_a	**0.235**	**0.110**	**0.114**	**0.715**	**0.868**	**0.813**	**1**	**0.358**	**0.396**
Sx	**0.404**	**0.371**	**0.556**	**0.707**	**0.551**	**0.530**	**0.358**	**1**	**0.765**
Sx_a	**0.473**	**0.500**	**0.356**	**0.442**	**0.623**	**0.290**	**0.396**	**0.765**	**1**

Eigenvalue Table

	F1	F2	F3	F4	F5	F6	F7	F8	F9
Eigenvalue	4.807	2.018	0.745	0.688	0.356	0.200	0.121	0.050	0.015
Variability (%)	53.407	22.424	8.279	7.649	3.954	2.219	1.345	0.557	0.166
Cumulative %	53.407	75.831	84.110	91.759	95.714	97.933	99.277	99.834	100.000

Scree Plot

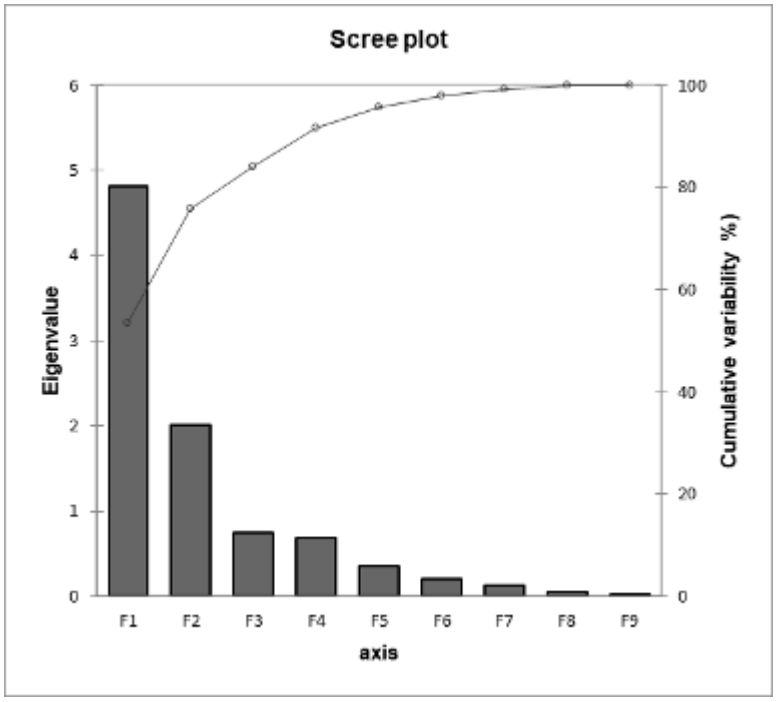

Factor Loading Table

	F1	F2	F3	F4	F5	F6	F7	F8	F9
PRx	0.587	0.566	-0.381	0.101	-0.394	-0.155	-0.003	-0.012	0.000
PAx	0.527	0.732	-0.260	0.000	0.135	0.312	-0.008	0.047	-0.003
RAC	0.564	0.573	0.076	-0.499	0.247	-0.184	-0.022	-0.053	0.001
Mx	0.868	-0.355	0.082	-0.237	-0.133	0.102	0.152	-0.023	0.076
Mx_a	0.877	-0.278	-0.161	0.195	0.178	-0.089	0.215	0.026	-0.053
Dx	0.765	-0.544	-0.057	-0.240	-0.129	0.129	-0.119	-0.084	-0.062
Dx_a	0.748	-0.500	-0.319	0.116	0.173	-0.093	-0.178	0.068	0.043
Sx	0.809	0.139	0.533	-0.030	-0.137	-0.023	-0.049	0.136	-0.020
Sx_a	0.738	0.254	0.324	0.513	0.081	0.012	-0.051	-0.117	0.017

% Contribution

	F1	F2	F3	F4	F5	F6	F7	F8	F9
PRx	7.168	15.871	19.502	1.481	43.714	11.984	0.007	0.274	0.000
PAx	5.781	26.572	9.082	0.000	5.143	48.881	0.055	4.435	0.052
RAC	6.623	16.288	0.779	36.184	17.077	17.008	0.402	5.625	0.014
Mx	15.677	6.261	0.895	8.158	4.945	5.184	18.989	1.099	38.791
Mx_a	16.008	3.830	3.475	5.507	8.919	3.926	38.361	1.300	18.674
Dx	12.169	14.657	0.440	8.371	4.655	8.356	11.751	14.160	25.440
Dx_a	11.625	12.364	13.634	1.943	8.406	4.325	26.257	9.131	12.314
Sx	13.628	0.961	38.124	0.128	5.279	0.266	2.019	36.804	2.793
Sx_a	11.322	3.197	14.069	38.229	1.863	0.071	2.159	27.171	1.921

Correlation Between Variables and Factors

	F1	F2	F3	F4	F5	F6	F7	F8	F9
PRx	0.587	0.566	-0.381	0.101	-0.394	-0.155	-0.003	-0.012	0.000
PAx	0.527	0.732	-0.260	0.000	0.135	0.312	-0.008	0.047	-0.003
RAC	0.564	0.573	0.076	-0.499	0.247	-0.184	-0.022	-0.053	0.001
Mx	0.868	-0.355	0.082	-0.237	-0.133	0.102	0.152	-0.023	0.076
Mx_a	0.877	-0.278	-0.161	0.195	0.178	-0.089	0.215	0.026	-0.053
Dx	0.765	-0.544	-0.057	-0.240	-0.129	0.129	-0.119	-0.084	-0.062
Dx_a	0.748	-0.500	-0.319	0.116	0.173	-0.093	-0.178	0.068	0.043
Sx	0.809	0.139	0.533	-0.030	-0.137	-0.023	-0.049	0.136	-0.020
Sx_a	0.738	0.254	0.324	0.513	0.081	0.012	-0.051	-0.117	0.017

3. Minute-by-Minute Data

Loading Biplot: PC1 vs. PC2

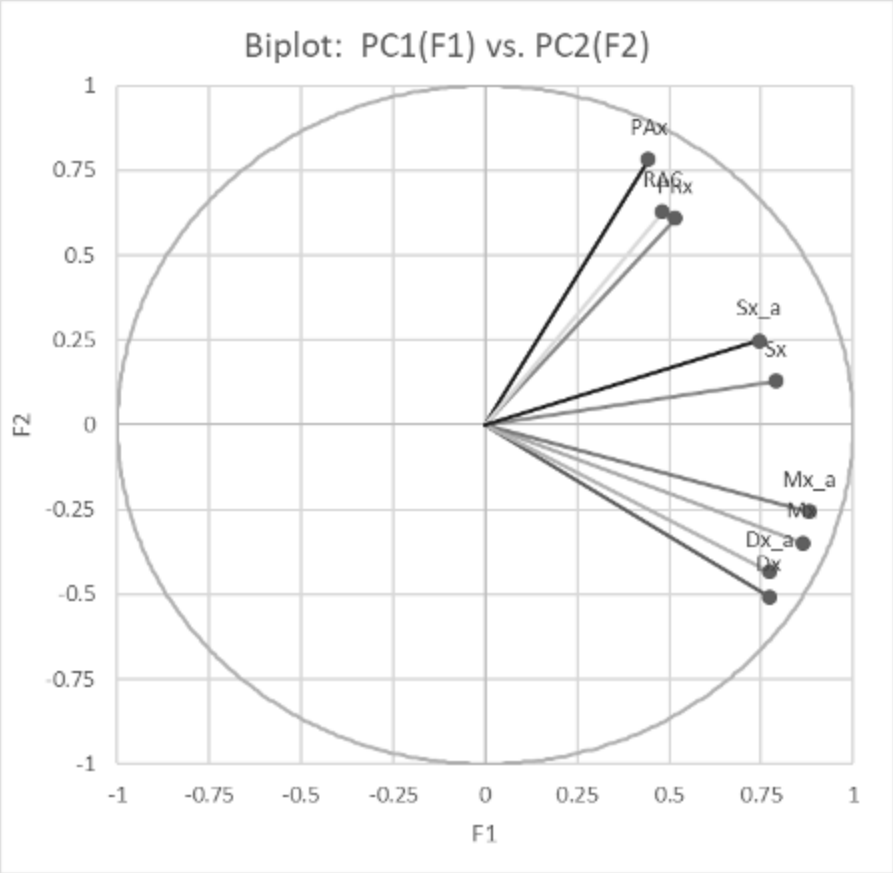

Spearman Correlation Matrix

Variables	PRx	PAx	RAC	Mx	Mx_a	Dx	Dx_a	Sx	Sx_a
PRx	**1**	**0.671**	**0.462**	**0.218**	**0.320**	**0.121**	**0.206**	**0.345**	**0.450**
PAx	**0.671**	**1**	**0.670**	**0.111**	**0.224**	-0.005	**0.082**	**0.300**	**0.446**
RAC	**0.462**	**0.670**	**1**	**0.266**	**0.217**	**0.132**	**0.099**	**0.461**	**0.308**
Mx	**0.218**	**0.111**	**0.266**	**1**	**0.792**	**0.902**	**0.701**	**0.680**	**0.445**
Mx_a	**0.320**	**0.224**	**0.217**	**0.792**	**1**	**0.712**	**0.864**	**0.535**	**0.626**
Dx	**0.121**	-0.005	**0.132**	**0.902**	**0.712**	**1**	**0.803**	**0.501**	**0.296**
Dx_a	**0.206**	**0.082**	**0.099**	**0.701**	**0.864**	**0.803**	**1**	**0.362**	**0.417**
Sx	**0.345**	**0.300**	**0.461**	**0.680**	**0.535**	**0.501**	**0.362**	**1**	**0.767**
Sx_a	**0.450**	**0.446**	**0.308**	**0.445**	**0.626**	**0.296**	**0.417**	**0.767**	**1**

Eigenvalue Table

	F1	F2	F3	F4	F5	F6	F7	F8	F9
Eigenvalue	4.586	2.088	0.778	0.693	0.399	0.223	0.147	0.067	0.020
Variability (%)	50.953	23.198	8.648	7.698	4.434	2.477	1.633	0.742	0.218
Cumulative %	50.953	74.151	82.799	90.497	94.931	97.408	99.041	99.782	100.000

Scree Plot

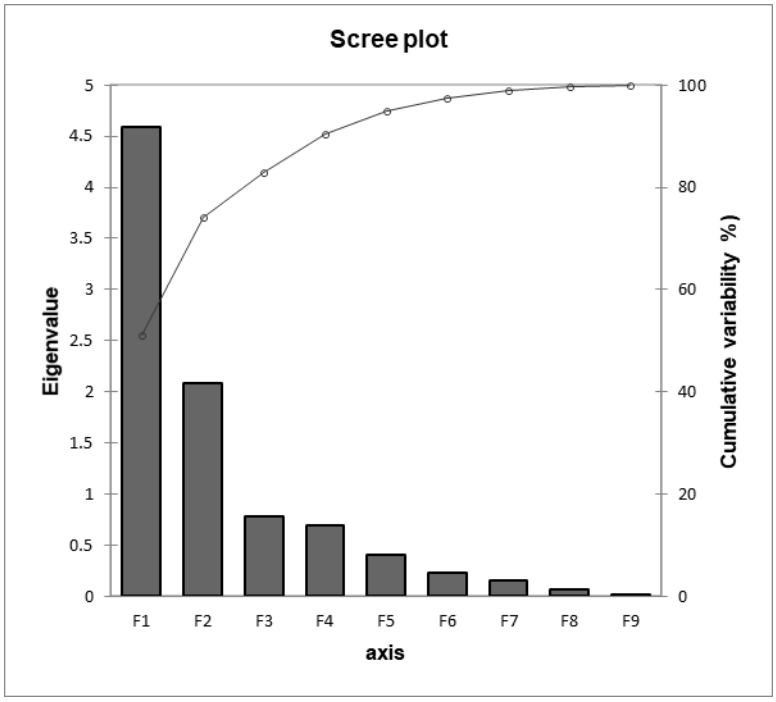

Factor Loading Table

	F1	F2	F3	F4	F5	F6	F7	F8	F9
PRx	0.516	0.609	-0.275	-0.297	0.421	-0.144	0.001	-0.009	0.000
PAx	0.444	0.782	-0.235	-0.041	-0.150	0.329	-0.012	0.055	-0.003
RAC	0.482	0.628	-0.127	0.520	-0.194	-0.212	-0.006	-0.059	0.003
Mx	0.863	-0.348	-0.005	0.239	0.165	0.111	0.176	-0.019	0.084
Mx_a	0.881	-0.256	-0.102	-0.214	-0.194	-0.082	0.230	0.029	-0.066
Dx	0.771	-0.508	-0.176	0.205	0.149	0.129	-0.145	-0.100	-0.066
Dx_a	0.773	-0.433	-0.298	-0.185	-0.191	-0.108	-0.186	0.081	0.052
Sx	0.789	0.130	0.529	0.185	0.136	-0.025	-0.067	0.150	-0.026
Sx_a	0.745	0.248	0.470	-0.346	-0.139	0.014	-0.052	-0.141	0.023

% Contribution

	F1	F2	F3	F4	F5	F6	F7	F8	F9
PRx	5.809	17.781	9.744	12.721	44.481	9.349	0.001	0.113	0.001
PAx	4.297	29.303	7.104	0.238	5.627	48.686	0.100	4.598	0.046
RAC	5.066	18.917	2.060	39.036	9.425	20.250	0.024	5.186	0.035
Mx	16.223	5.799	0.003	8.219	6.860	5.539	21.060	0.522	35.774
Mx_a	16.916	3.143	1.340	6.582	9.431	3.008	36.096	1.303	22.181
Dx	12.978	12.338	3.969	6.042	5.573	7.521	14.389	15.020	22.171
Dx_a	13.036	8.963	11.392	4.934	9.185	5.275	23.474	9.881	13.860
Sx	13.580	0.804	35.961	4.927	4.601	0.280	3.026	33.499	3.322
Sx_a	12.096	2.952	28.426	17.301	4.816	0.091	1.829	29.877	2.611

Correlation Between Variables and Factors

	F1	F2	F3	F4	F5	F6	F7	F8	F9
PRx	0.516	0.609	-0.275	-0.297	0.421	-0.144	0.001	-0.009	0.000
PAx	0.444	0.782	-0.235	-0.041	-0.150	0.329	-0.012	0.055	-0.003
RAC	0.482	0.628	-0.127	0.520	-0.194	-0.212	-0.006	-0.059	0.003
Mx	0.863	-0.348	-0.005	0.239	0.165	0.111	0.176	-0.019	0.084
Mx_a	0.881	-0.256	-0.102	-0.214	-0.194	-0.082	0.230	0.029	-0.066
Dx	0.771	-0.508	-0.176	0.205	0.149	0.129	-0.145	-0.100	-0.066
Dx_a	0.773	-0.433	-0.298	-0.185	-0.191	-0.108	-0.186	0.081	0.052
Sx	0.789	0.130	0.529	0.185	0.136	-0.025	-0.067	0.150	-0.026
Sx_a	0.745	0.248	0.470	-0.346	-0.139	0.014	-0.052	-0.141	0.023

Appendix D: Section 7.1 - Patient Example and Full Population ARMA Models Tested (AIC, LL)

Patient Example – ARIMA Modeling

ARIMA Model Parameters		AIC	LL
p	q		
2	**2**	**-69.3**	**39.65**
2	0	-53.06	30.53
1	0	-40.16	23.08
3	0	-61.58	35.79
0	0	153.81	-74.91
0	1	22.0	-8.0
0	2	-42.03	25.01
0	3	-67.76	38.88
1	1	-47.19	27.59
1	2	-65.5	37.75
1	3	-67.66	39.83
2	1	-55.42	32.71
2	3	-66.11	40.05
3	1	-61.12	36.56
3	2	-66.11	40.06
3	3	-64.16	40.08

*AIC = Akaike Information Criterion, ARIMA = auto-regressive integrative moving average, LL = log likelihood, p = auto-regression parameter for ARIMA model, q = moving average parameter for ARIMA model.*Note: bolded value represents the most appropriate ARIMA structure for the patient example. This was the case for the 10 representative patient examples tested. There was no integrative parameter (ie. "d" parameter) included within the ARIMA models, given stationarity testing and auto.arima testing displayed stationary signals within the short recordings tested, hence no differencing of the signal was required.*

LME Modelling with Embedded PRx ARIMA Structure – Full Population Assessing Best ARIMA Structure

LME Model		PRx ARIMA Structure		AIC	BIC	LL
Fixed Effects	Random	p	q			
PRx ~ Sx_a	**intercept**	**2**	**2**	**-9797.294**	**-9735.699**	**4906.647**
PRx ~ Sx_a	intercept	3	0	-9795.848	-9741.953	4904.924
PRx ~ Sx_a	intercept	3	1	-9797.767	-9736.172	4906.883
PRx ~ Sx_a	intercept	3	2	-9795.767	-9726.473	4906.884
PRx ~ Sx_a	intercept	3	3	FTC	FTC	FTC
PRx ~ Sx_a	intercept	2	0	-9795.465	-9749.269	4903.732
PRx ~ Sx_a	intercept	2	1	-9795.409	-9741.514	4904.705
PRx ~ Sx_a	intercept	2	3	-9794.578	-9725.284	4906.289
PRx ~ Sx_a	intercept	1	0	09271.307	-9232.810	4640.653
PRx ~ Sx_a	intercept	1	1	-9752.712	-9706.515	4882.356
PRx ~ Sx_a	intercept	1	2	-9707.924	-9744.029	4905.962
PRx ~ Sx_a	intercept	1	3	FTC	FTC	FTC
PRx ~ Sx_a	intercept	0	0	FTC	FTC	FTC
PRx ~ Sx_a	intercept	0	1	-4955.052	-4916.55	2482.526
PRx ~ Sx_a	intercept	0	2	-8254.316	-8208.199	4133.158
PRx ~ Sx_a	intercept	0	3	-9263.106	-9209.210	4638.553

*AIC = Akaike Information Criterion, ARIMA = auto-regressive integrative moving average, BIC = Bayesian Information Criterion, Dx_a = diastolic flow velocity (correlation between TCD based FVd and MAP), FTC = "failure to converge" for the model, FVd = TCD based diastolic flow velocity, FVm = mean TCD flow velocity, FVs = TCD based systolic flow velocity, ICP = intra-cranial pressure, LL = log likelihood, LME = linear mixed effects model, p = auto-regression parameter for ARIMA model, MAP = mean arterial pressure, PRx = pressure reactivity index (correlation between ICP and MAP), q = moving average parameter for ARIMA model, Sx_a = systolic flow index (correlation between TCD based FVs and MAP), TCD = transcranial Doppler. *Note: bolded value represents the most appropriate ARIMA structure for the patient population tested, based on principal of parsimony, lowest AIC and BIC. There was no integrative parameter (ie. "d" parameter) included within the ARIMA models, given stationarity testing during patient examples (see appendix A and Methodology section of manuscript).*

Appendix E: Section 7.3 – ACF/PACF/QQ Plots for Top LME Models and Bland-Altman Plots for Estimated and Predicted PRx Results from LME Models

A. QQ, Residual Density, ACF and PACF Plots for Top Two LME Models

1. PRx ~ Sx_a LME Model (with random effects by patient in intercept and coefficients)

QQ Plot

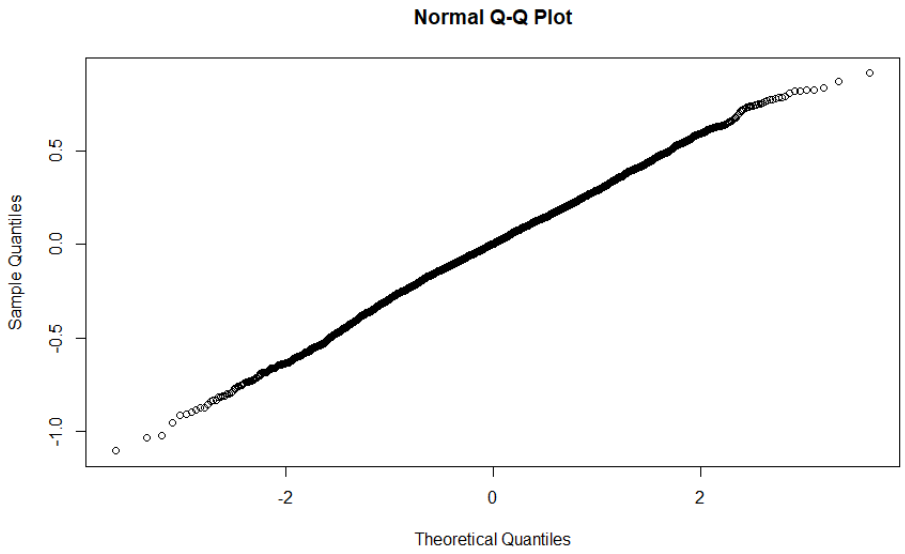

Residual Density Plot

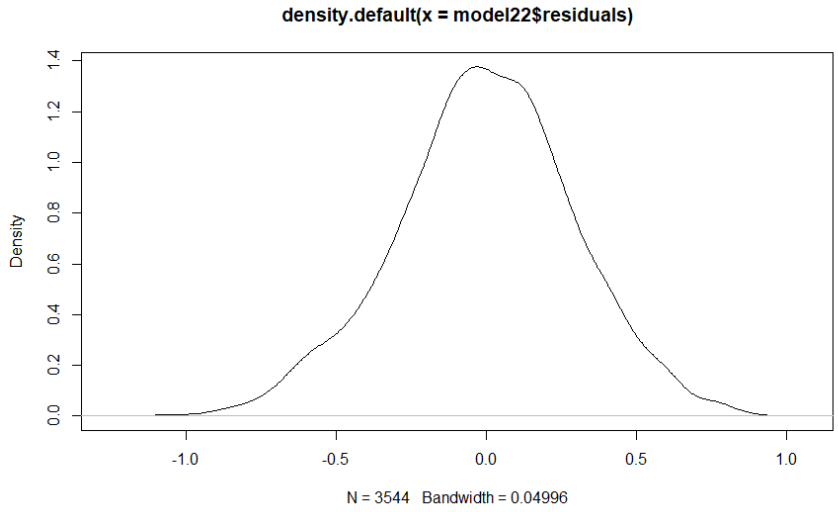

ACF Plot

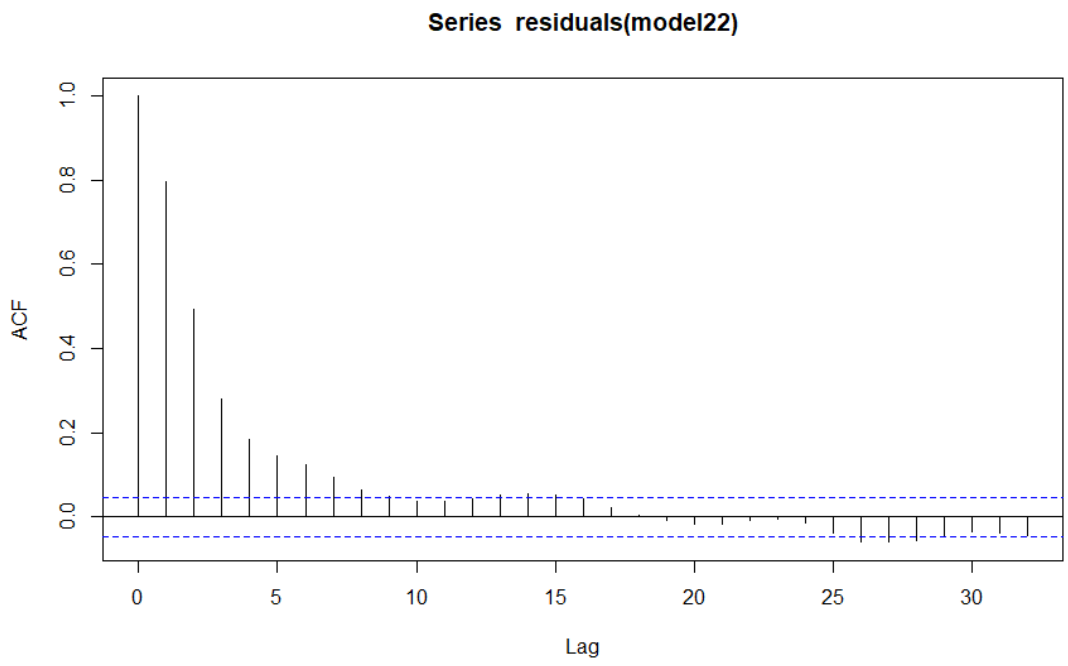

PACF Plot

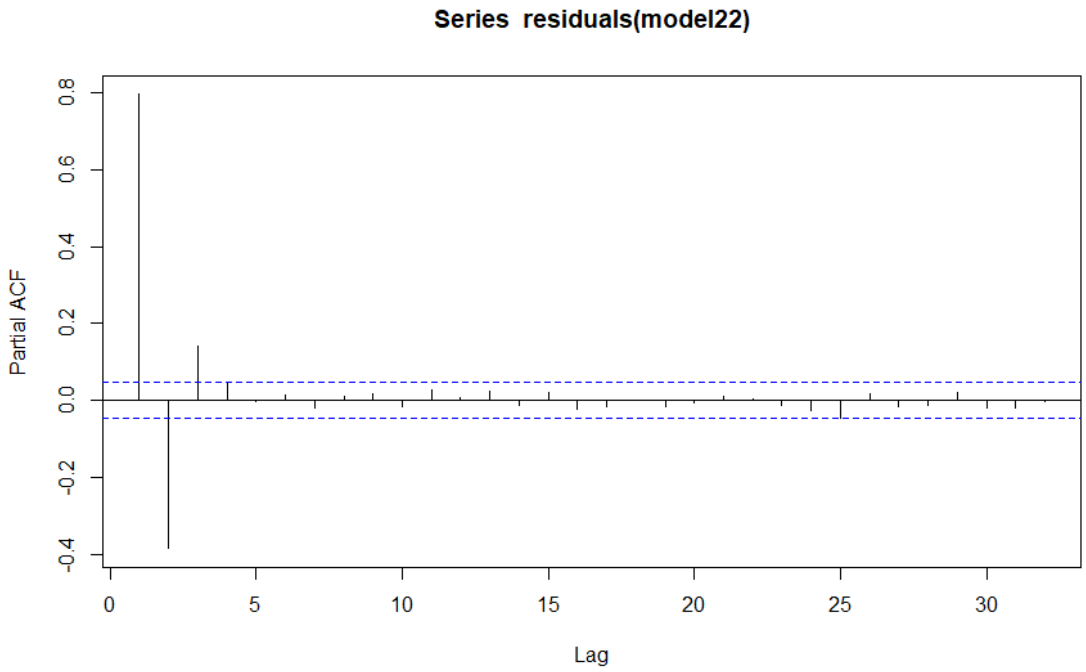

---

2. PRx ~ Sx_a + Mx_a LME Model (with random effects by patient in intercept and coefficients)

QQ Plot

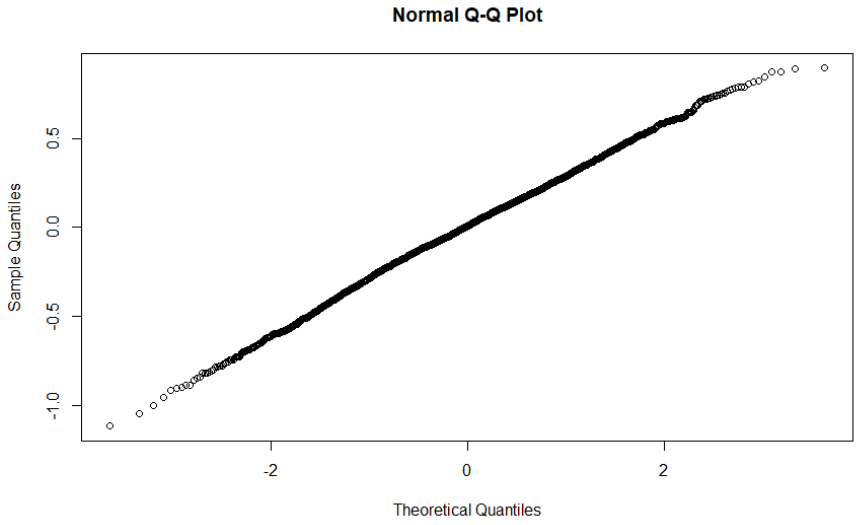

Residual Density Plot

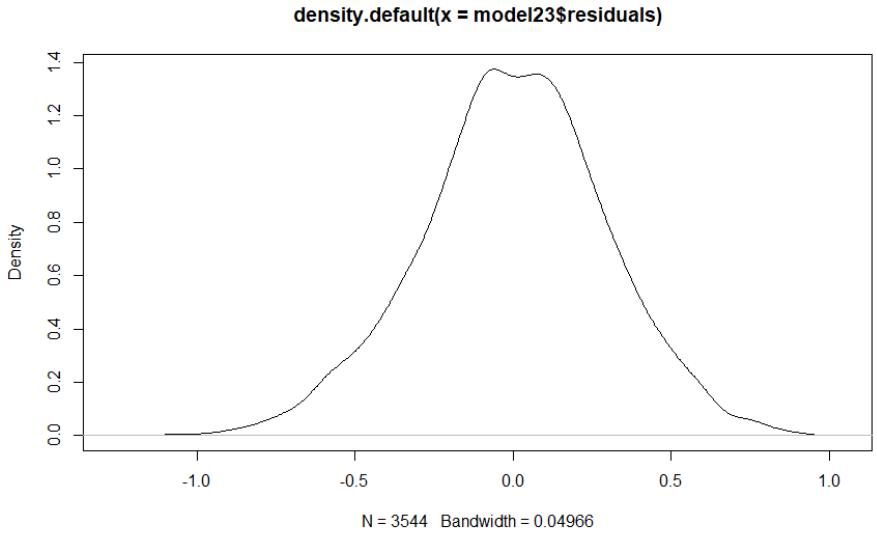

ACF Plot

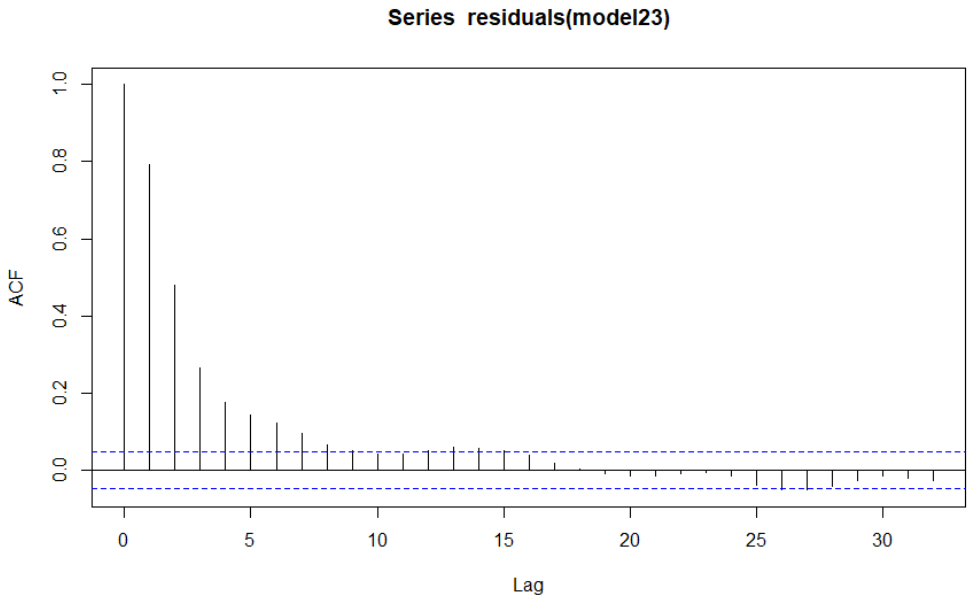

PACF Plot

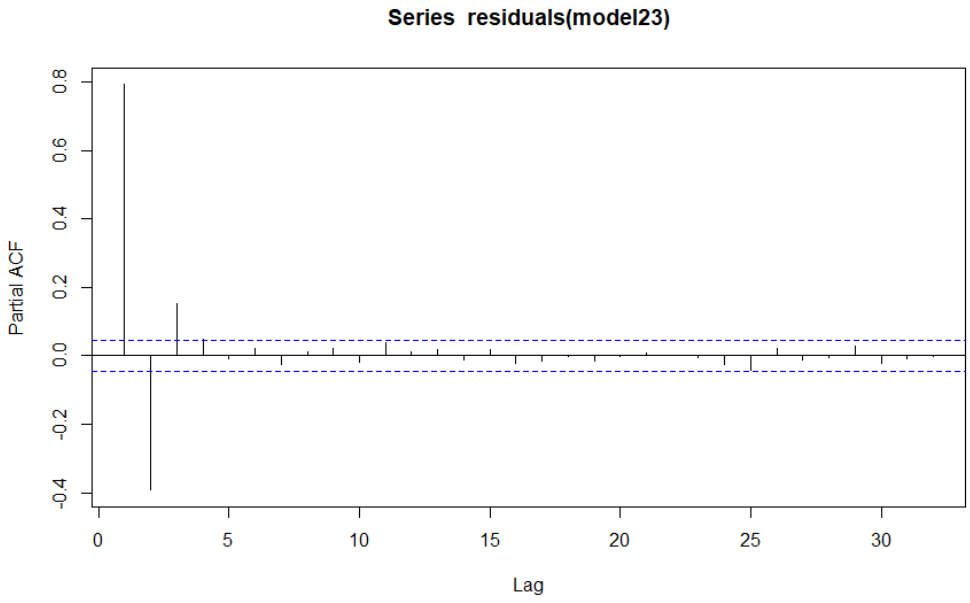

B. – Bland Altman Analysis for Estimated vs. Observed PRx for Top Two LME Models

***Grand mean Fisher transformed data utilized for Bland-Altman analysis**

1. PRx ~ Sx_a (with random effects introduced into intercept and coefficient)

```
$lower.limit
[1] -0.0628747

$mean.diffs
[1] -0.003253664

$upper.limit
[1] 0.05636738

$lines
 lower.limit   mean.diffs  upper.limit
-0.062874705 -0.003253664  0.056367377

$CI.lines
lower.limit.ci.lower lower.limit.ci.upper   mean.diff.ci.lower   mean.diff.ci
.upper upper.limit.ci.lower
         -0.10056477          -0.02518464          -0.02501403           0.01
850671           0.01867731
upper.limit.ci.upper
```

```
          0.09405744

$critical.diff
[1] 0.05962104
```

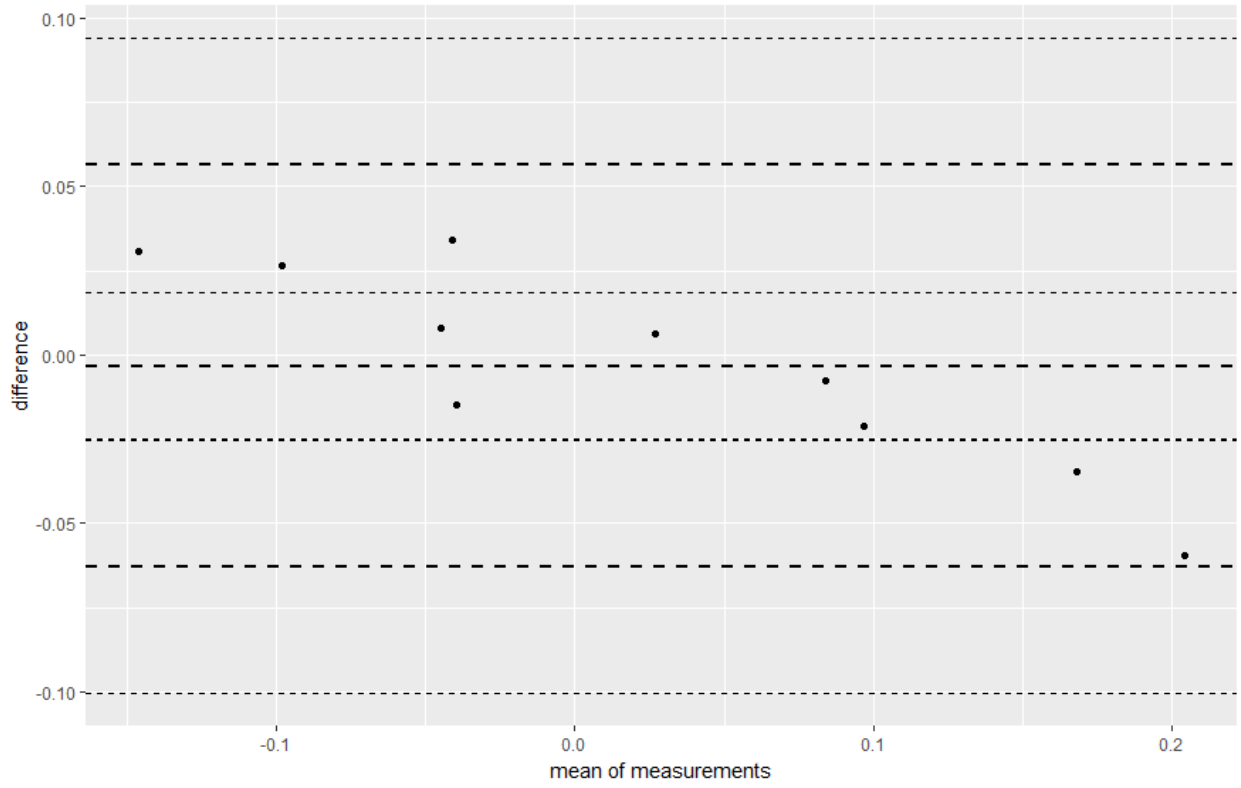

2. PRx ~ Sx_a + Mx_a (with random effects introduced into intercept and coefficient)

```
$lower.limit
[1] -0.0664208

$mean.diffs
[1] -0.003062638

$upper.limit
[1] 0.06029553

$lines
 lower.limit   mean.diffs  upper.limit
-0.066420801 -0.003062638  0.060295526

$CI.lines
lower.limit.ci.lower lower.limit.ci.upper   mean.diff.ci.lower   mean.diff.ci
.upper upper.limit.ci.lower
         -0.10647333          -0.02636828          -0.02618697           0.02
006170           0.02024300
upper.limit.ci.upper
          0.10034805
```

```
$critical.diff
[1] 0.06335816
```

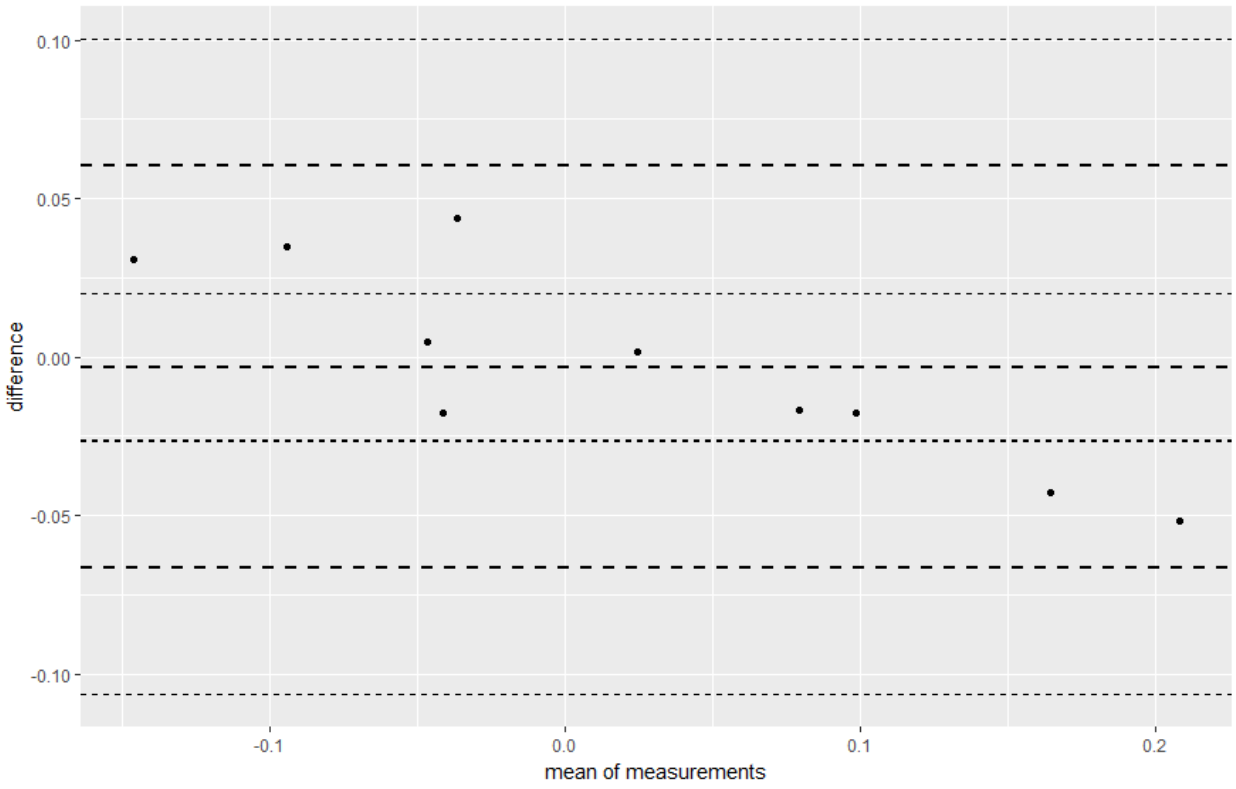

C. – Bland Altman Analysis for Predicted vs. Observed PRx for Top Two LME Models

***Grand mean Fisher transformed data utilized for Bland-Altman analysis**

1. PRx ~ Sx_a (with random effects introduced into intercept and coefficient)

```
$lower.limit
[1] -0.2826737

$mean.diffs
[1] -0.05195699

$upper.limit
```

```
[1] 0.1787597

$lines
lower.limit  mean.diffs upper.limit
-0.28267367 -0.05195699  0.17875969

$CI.lines
lower.limit.ci.lower lower.limit.ci.upper   mean.diff.ci.lower   mean.diff.ci
.upper upper.limit.ci.lower
         -0.42852364          -0.13682371          -0.13616351           0.03
224952           0.03290972
upper.limit.ci.upper
          0.32460965


$critical.diff
[1] 0.2307167
```

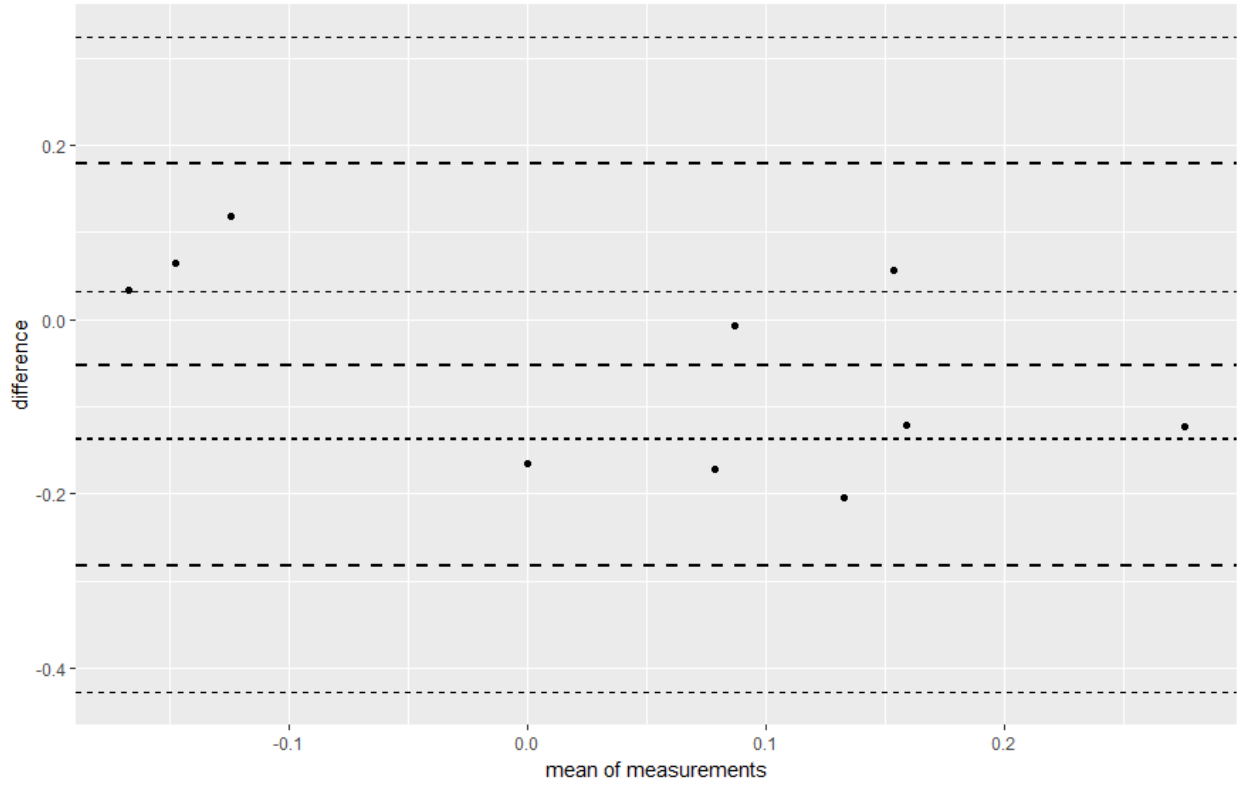

2. PRx ~ Sx_a + Mx_a (with random effects introduced into intercept and coefficient)

```
$lower.limit
[1] -0.2932762

$mean.diffs
[1] -0.04899657

$upper.limit
[1] 0.195283
```

```
$lines
lower.limit  mean.diffs upper.limit
-0.29327618 -0.04899657  0.19528303

$CI.lines
lower.limit.ci.lower lower.limit.ci.upper   mean.diff.ci.lower   mean.diff.ci
.upper upper.limit.ci.lower
         -0.44770008          -0.13885227          -0.13815326           0.04
016011           0.04085912
upper.limit.ci.upper
          0.34970694


$critical.diff
[1] 0.2442796
```

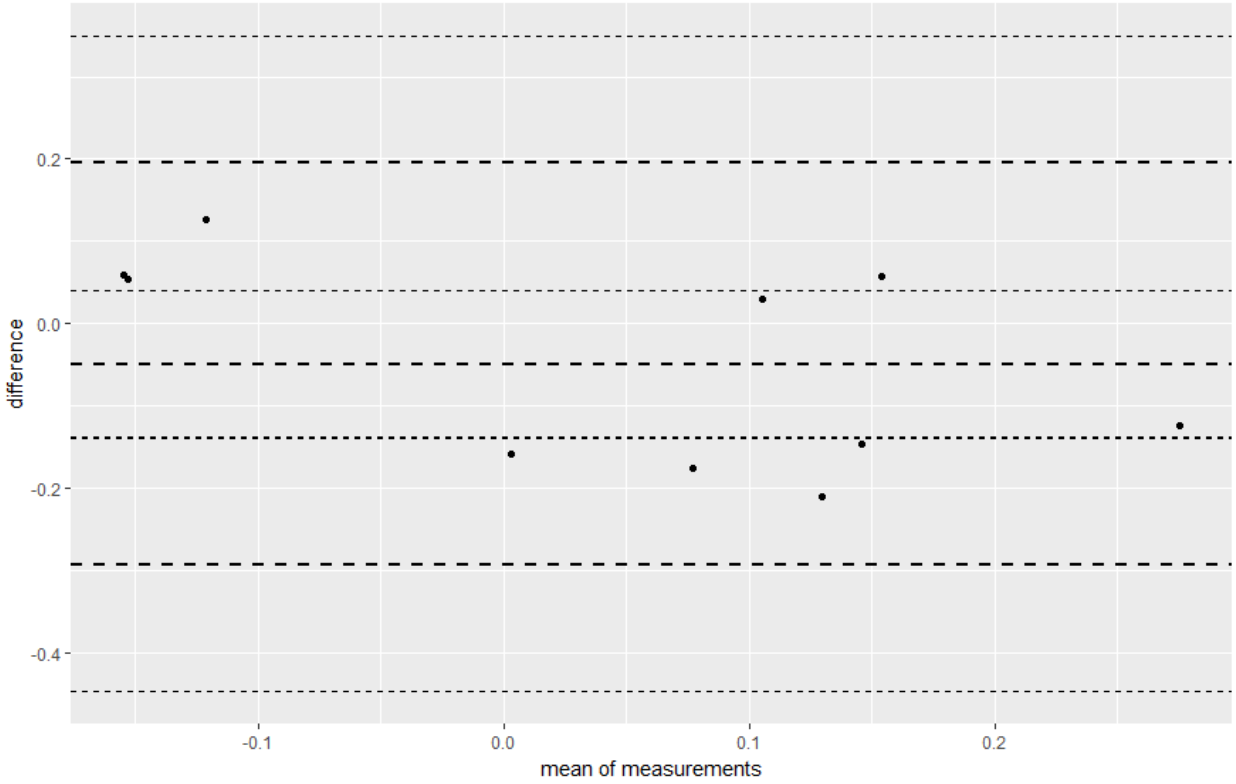

Appendix F: Section 8.1 - Sequential Chi-Square Threshold Analysis – 24hr, 72hr, 5d, 7d and 10d Recording Periods

1. **1st 24hr of Recording**

PRx

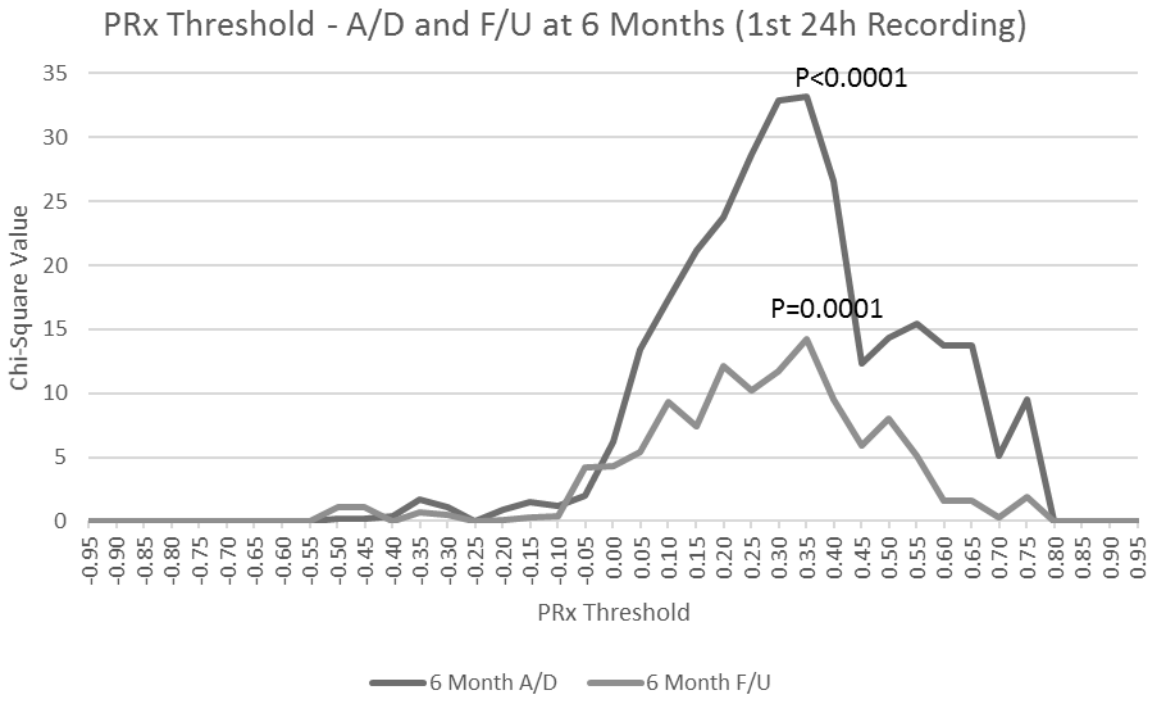

PAx

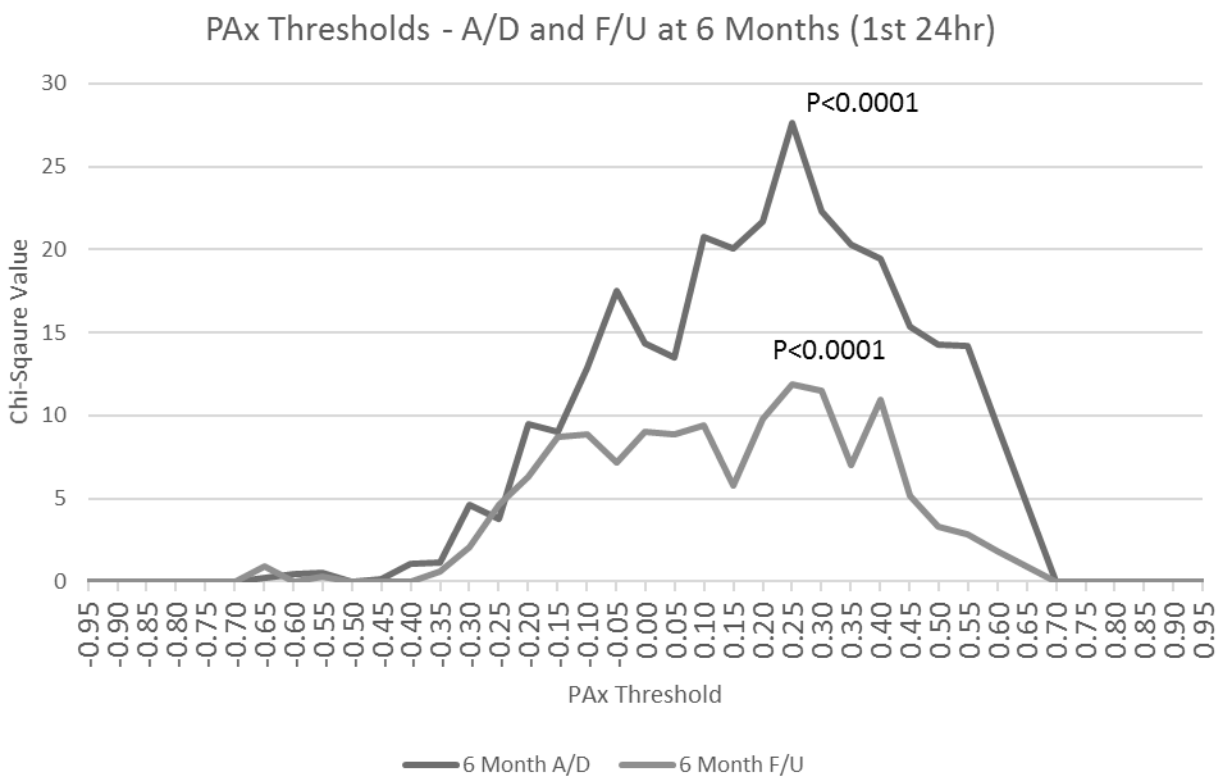
PAx Thresholds - A/D and F/U at 6 Months (1st 24hr)
Chi-Sqaure Value
30
25
20
15
10
5
0
P<0.0001
P<0.0001
-0.95 -0.90 -0.85 -0.80 -0.75 -0.70 -0.65 -0.60 -0.55 -0.50 -0.45 -0.40 -0.35 -0.30 -0.25 -0.20 -0.15 -0.10 -0.05 0.00 0.05 0.10 0.15 0.20 0.25 0.30 0.35 0.40 0.45 0.50 0.55 0.60 0.65 0.70 0.75 0.80 0.85 0.90 0.95
PAx Threshold
6 Month A/D
6 Month F/U

RAC

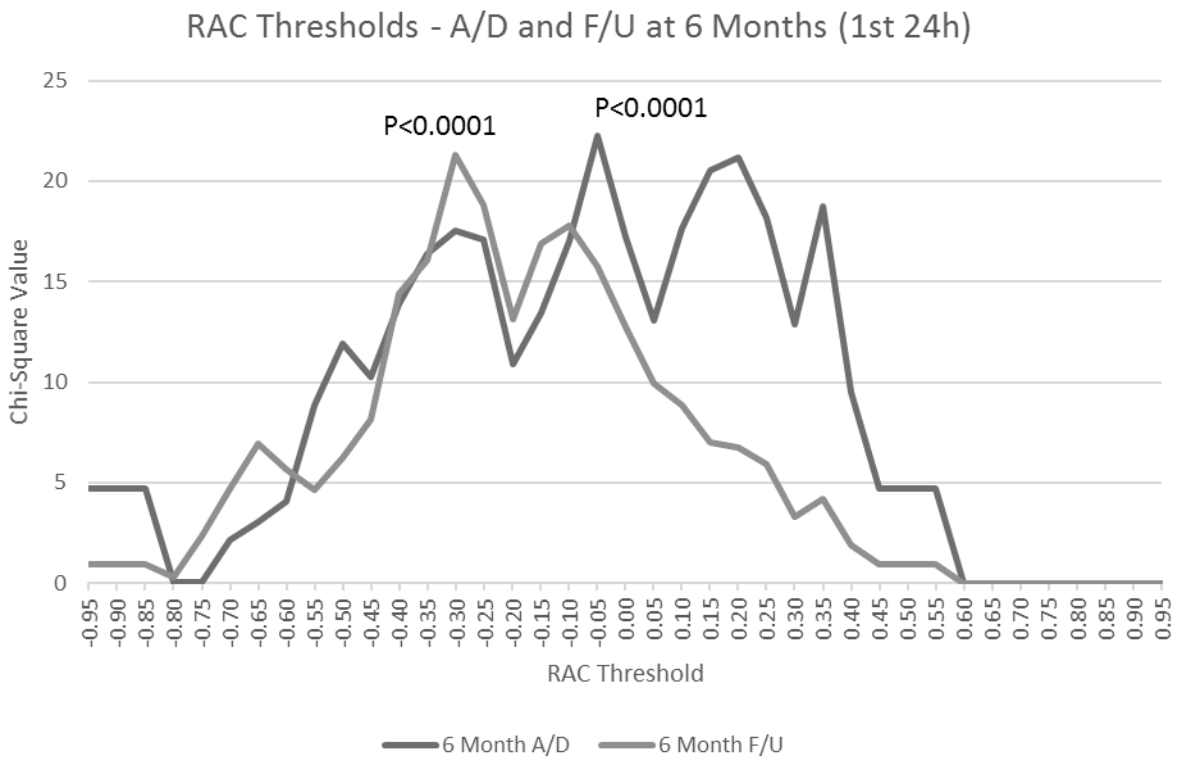
RAC Thresholds - A/D and F/U at 6 Months (1st 24h)
P<0.0001
P<0.0001
Chi-Square Value
25
20
15
10
5
0
-0.95 -0.90 -0.85 -0.80 -0.75 -0.70 -0.65 -0.60 -0.55 -0.50 -0.45 -0.40 -0.35 -0.30 -0.25 -0.20 -0.15 -0.10 -0.05 0.00 0.05 0.10 0.15 0.20 0.25 0.30 0.35 0.40 0.45 0.50 0.55 0.60 0.65 0.70 0.75 0.80 0.85 0.90 0.95
RAC Threshold
6 Month A/D
6 Month F/U

2. 1st 72hr of Recording

PRx

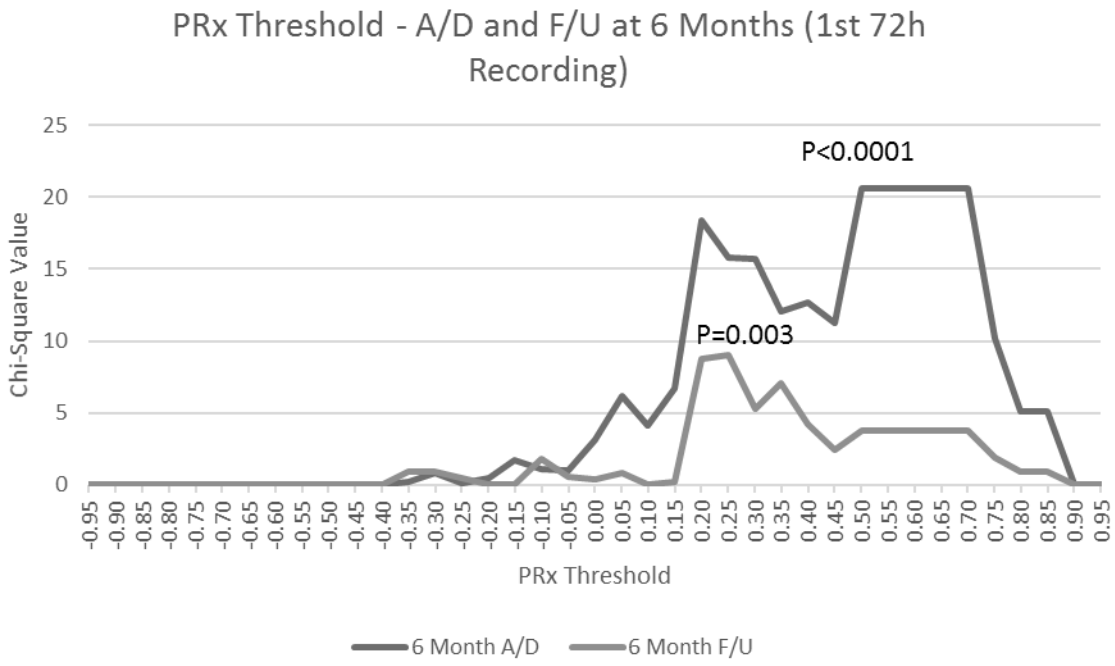

PAx

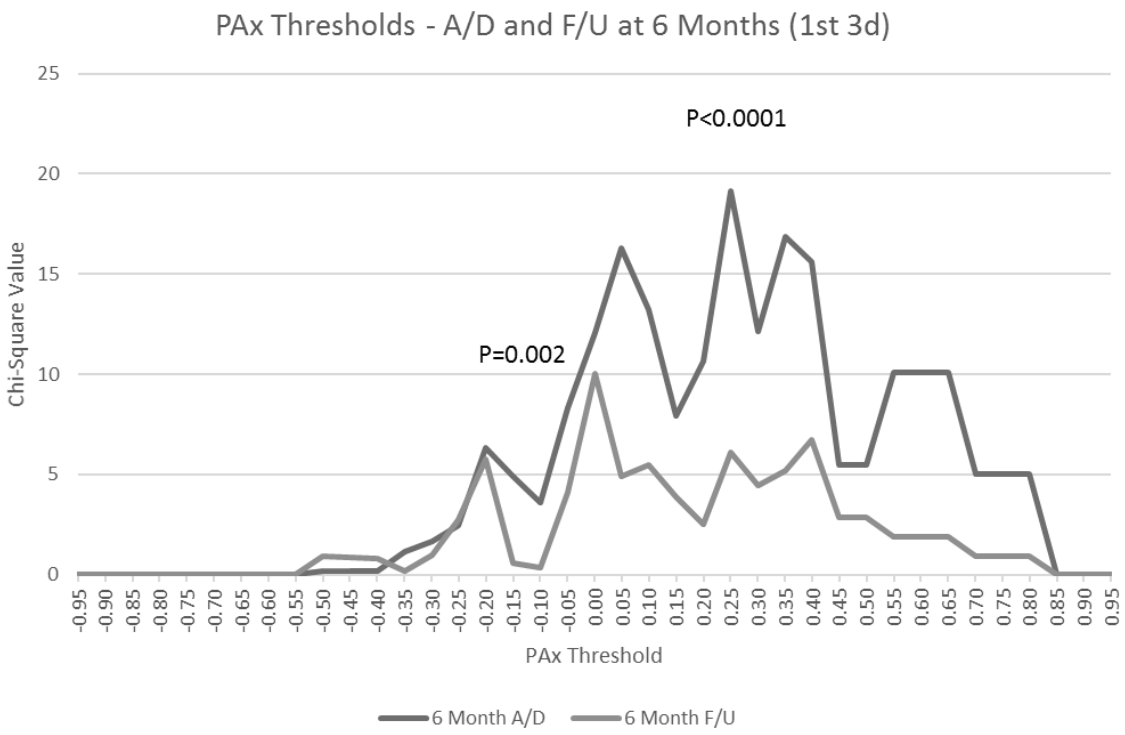
PAx Thresholds - A/D and F/U at 6 Months (1st 3d)
P<0.0001
P=0.002
Chi-Square Value
PAx Threshold
6 Month A/D
6 Month F/U

RAC

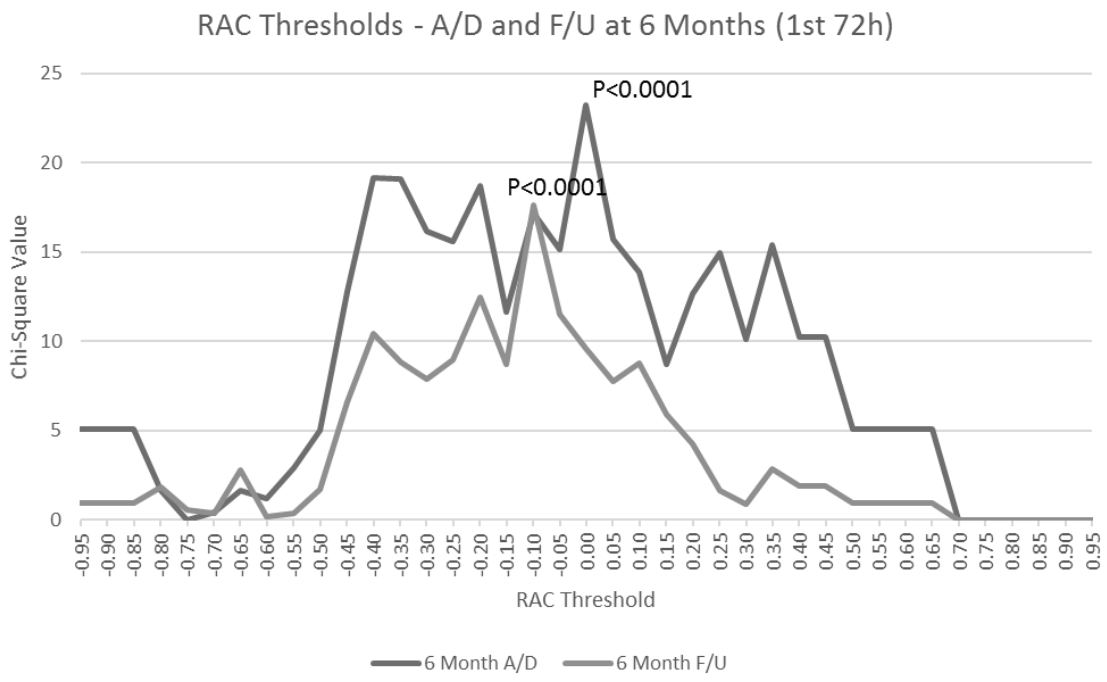
RAC Thresholds - A/D and F/U at 6 Months (1st 72h)
P<0.0001
P<0.0001
Chi-Square Value
RAC Threshold
6 Month A/D
6 Month F/U

3. <u>1st 5d of Recording</u>

PRx

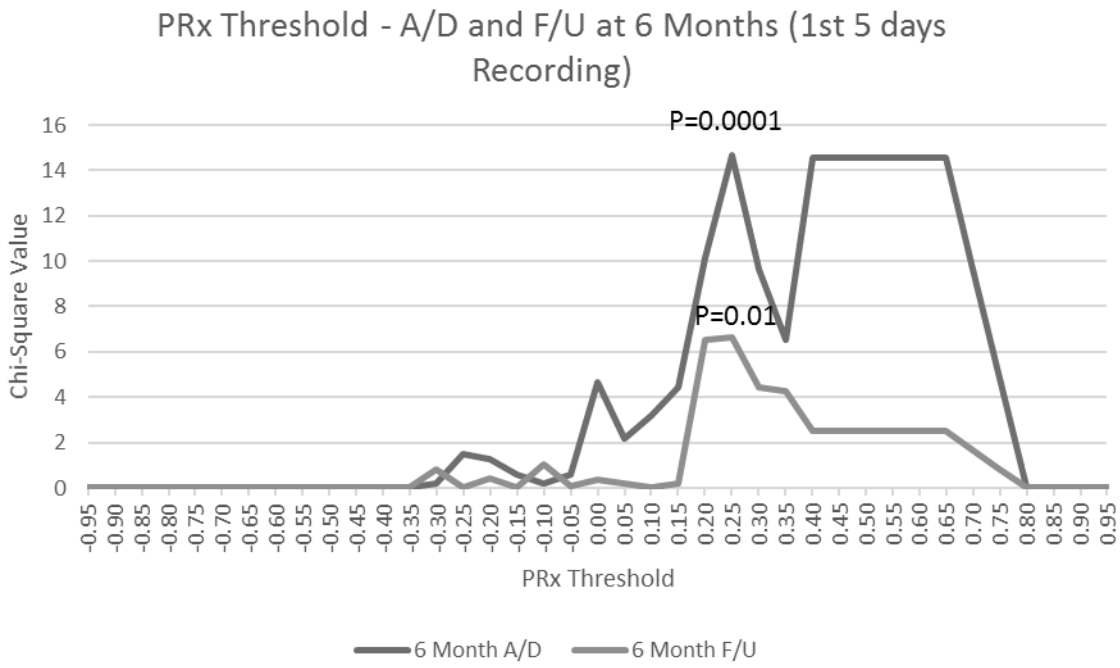

PAx

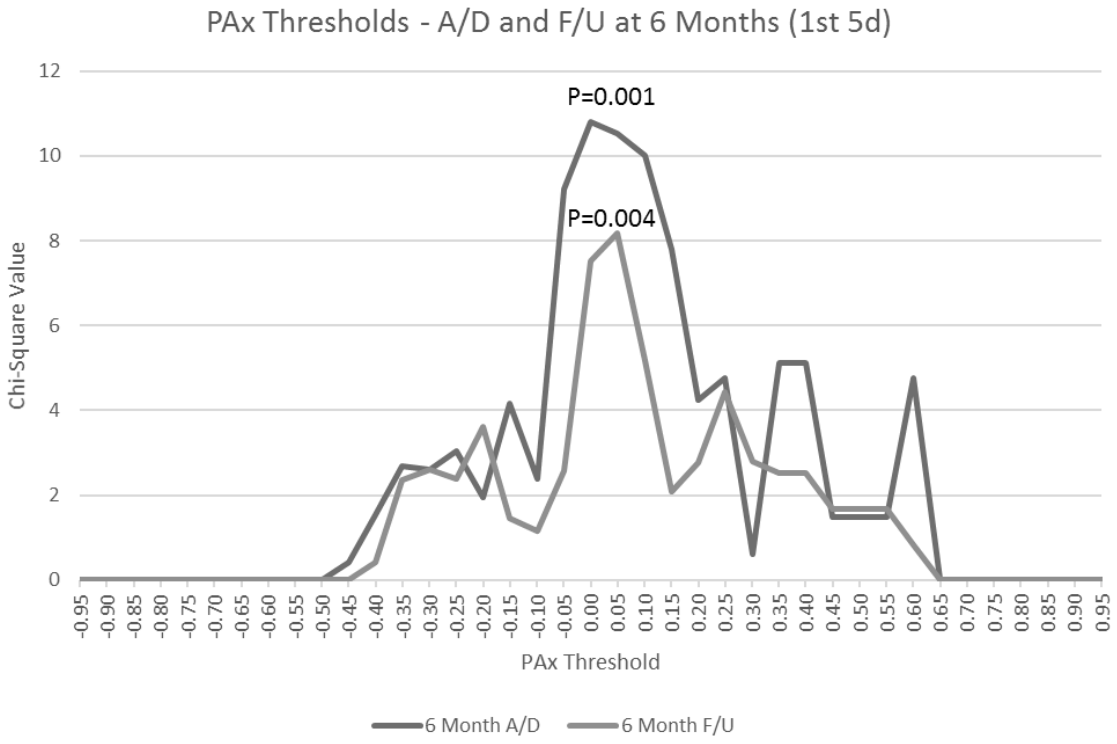
PAx Thresholds - A/D and F/U at 6 Months (1st 5d)
P=0.001
P=0.004
Chi-Square Value
PAx Threshold
6 Month A/D
6 Month F/U

RAC

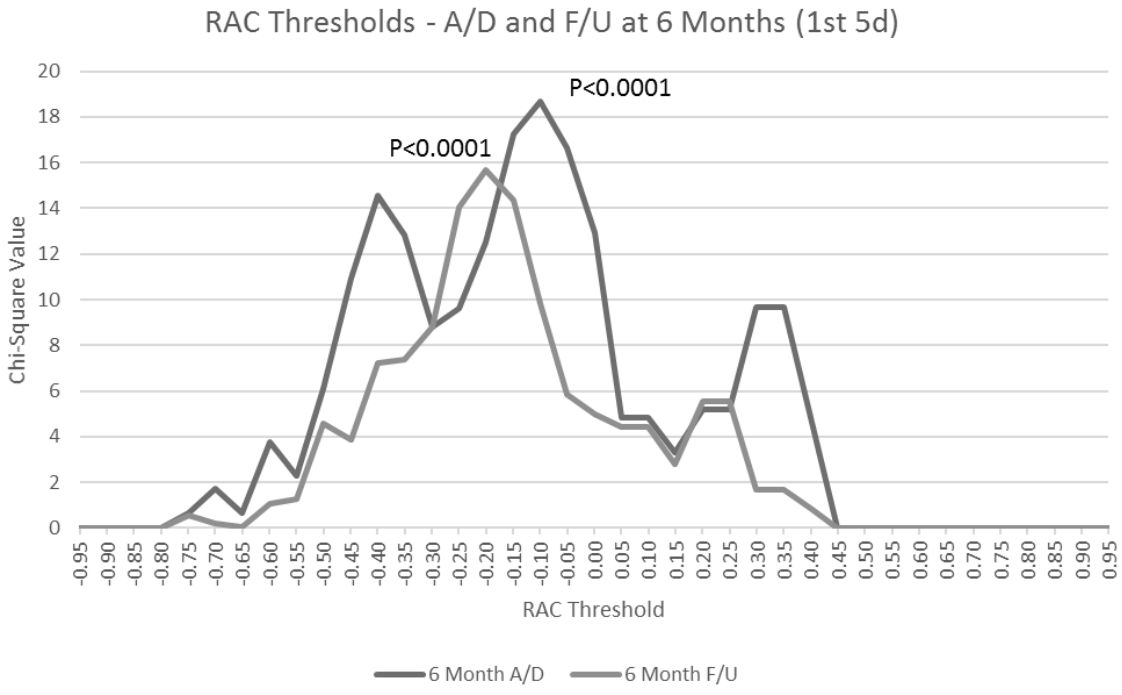
RAC Thresholds - A/D and F/U at 6 Months (1st 5d)
P<0.0001
P<0.0001
Chi-Square Value
RAC Threshold
6 Month A/D
6 Month F/U

4. 1st 7d of Recording

PRx

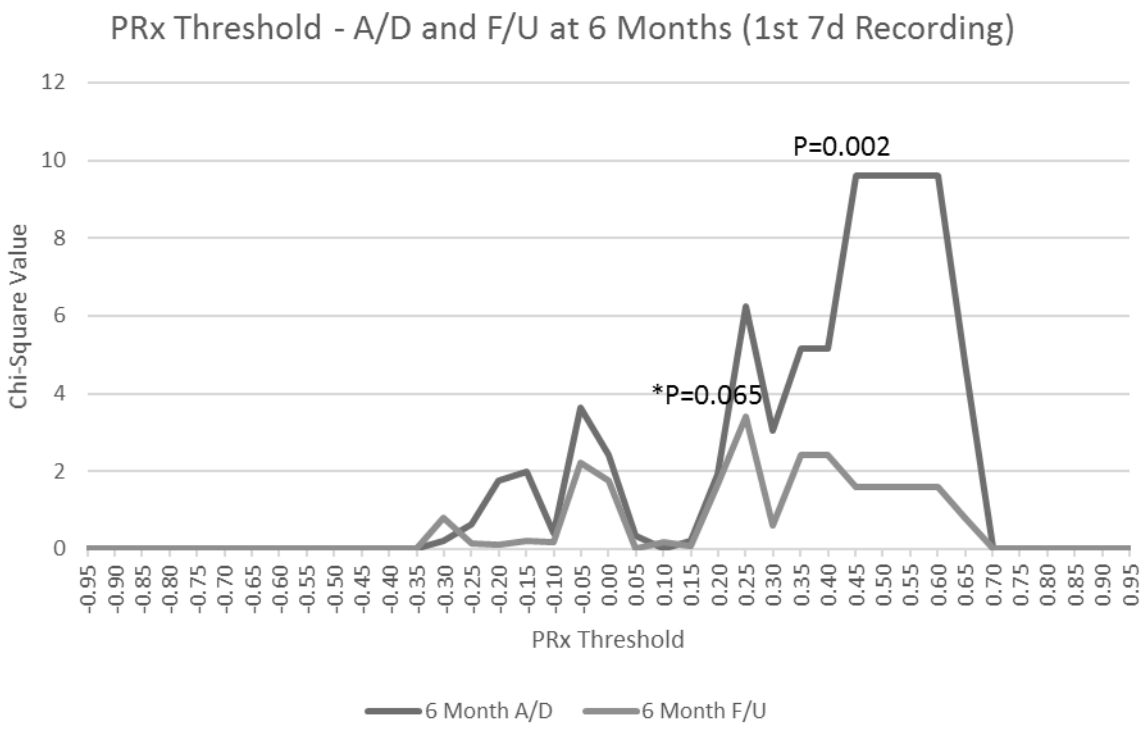

PAx

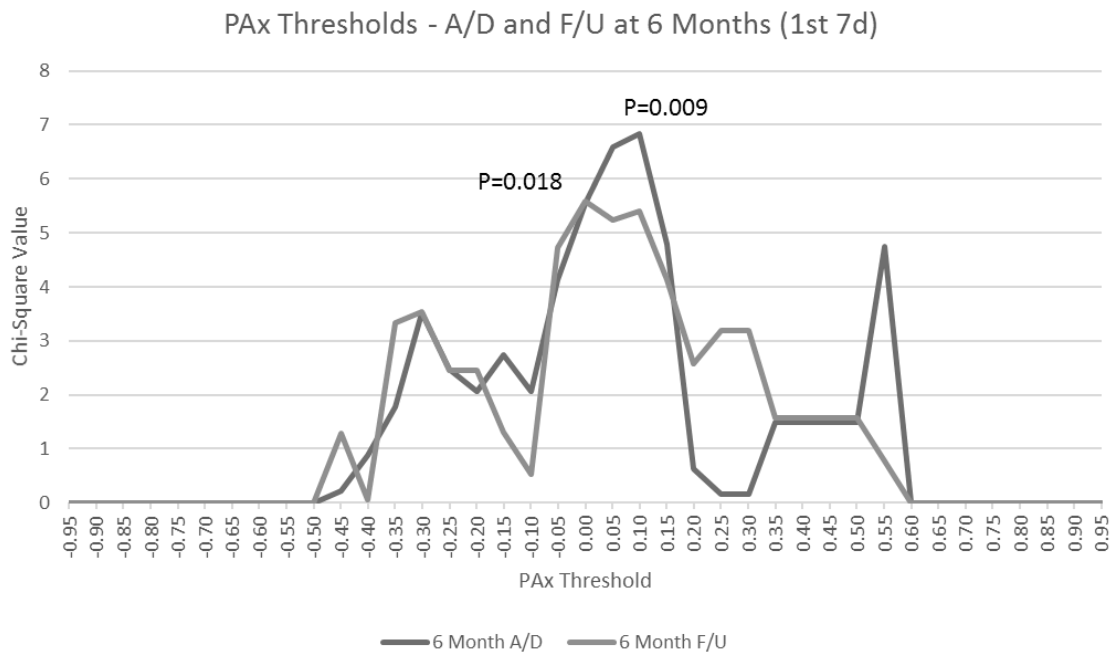
PAx Thresholds - A/D and F/U at 6 Months (1st 7d)
P=0.009
P=0.018
Chi-Square Value
PAx Threshold
6 Month A/D
6 Month F/U

RAC

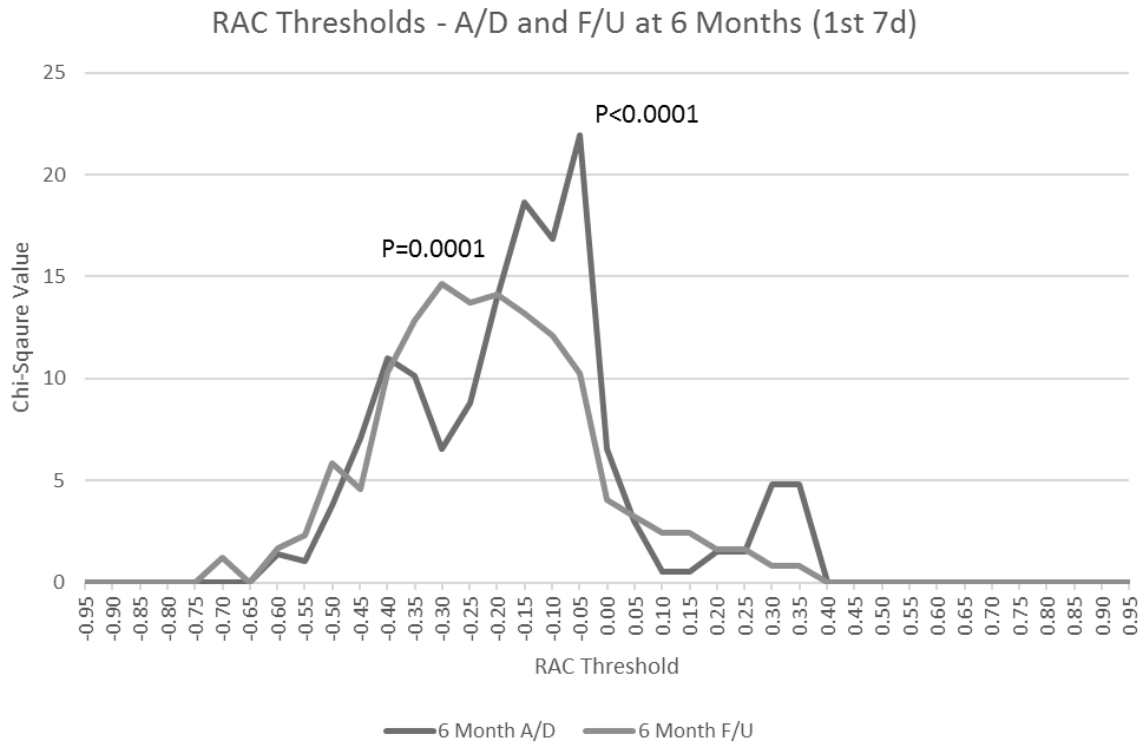
RAC Thresholds - A/D and F/U at 6 Months (1st 7d)
P<0.0001
P=0.0001
Chi-Sqaure Value
RAC Threshold
6 Month A/D
6 Month F/U

5. 1st 10d of Recording

PRx

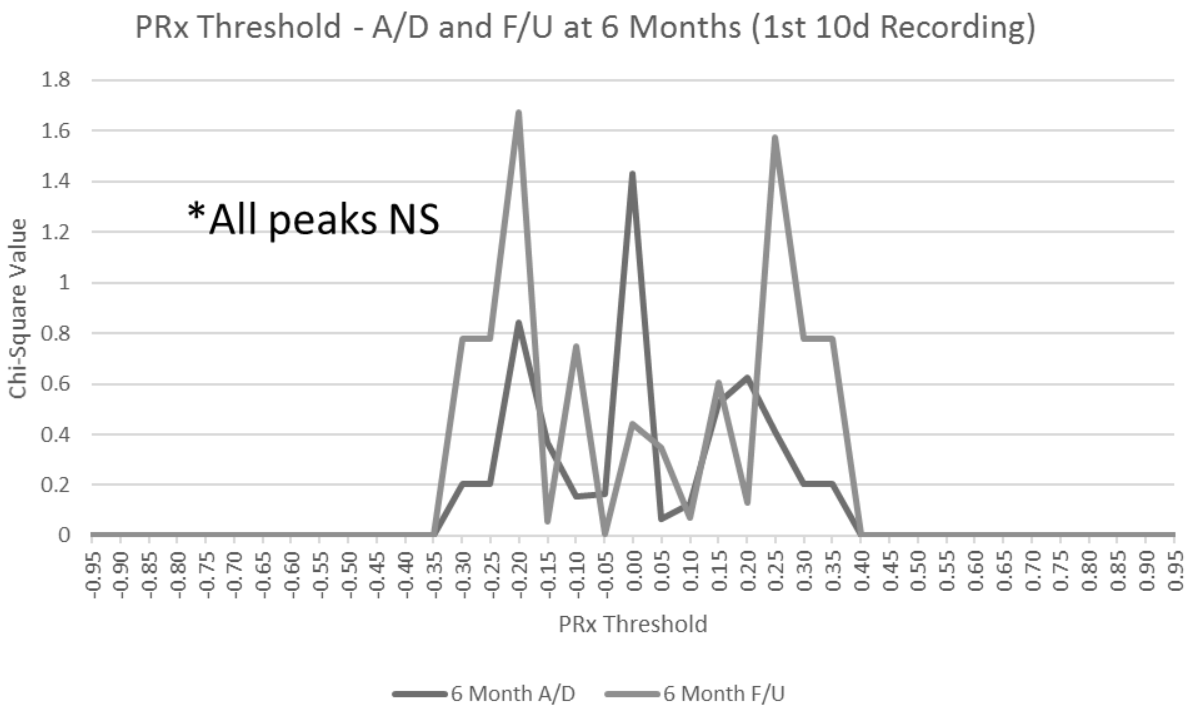

PAx

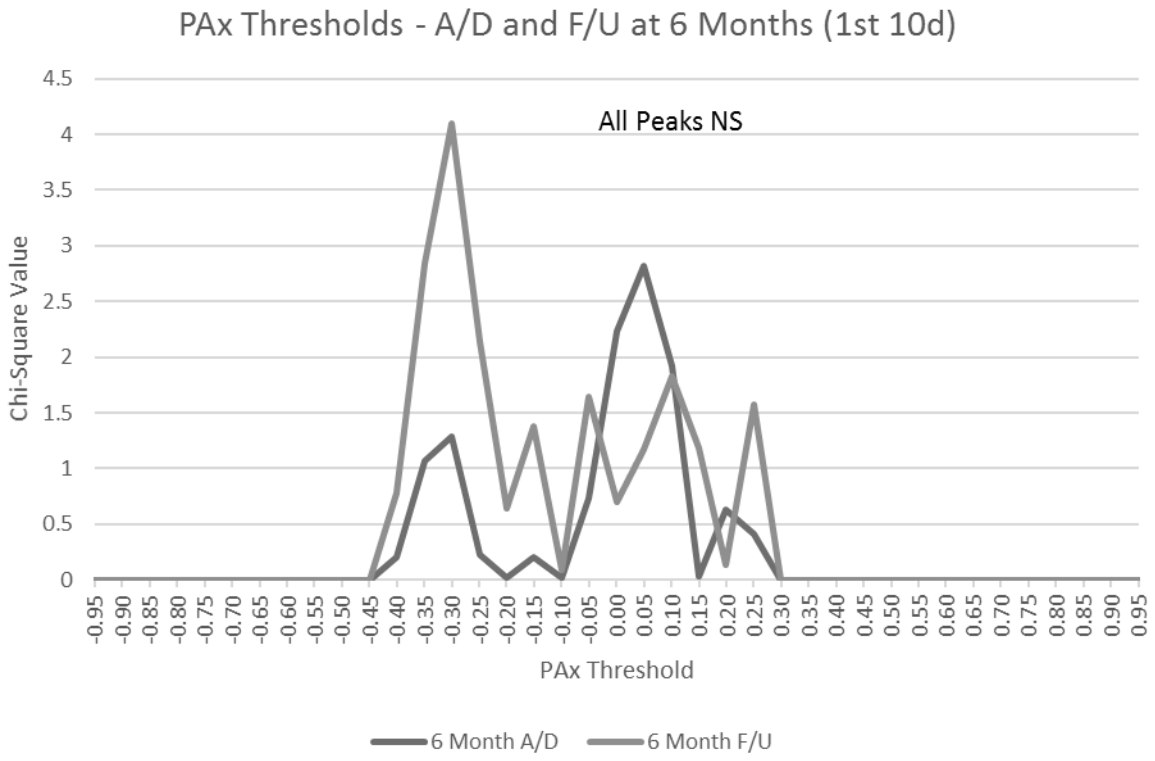
PAx Thresholds - A/D and F/U at 6 Months (1st 10d)
All Peaks NS
Chi-Square Value
4.5
4
3.5
3
2.5
2
1.5
1
0.5
0
-0.95 -0.90 -0.85 -0.80 -0.75 -0.70 -0.65 -0.60 -0.55 -0.50 -0.45 -0.40 -0.35 -0.30 -0.25 -0.20 -0.15 -0.10 -0.05 0.00 0.05 0.10 0.15 0.20 0.25 0.30 0.35 0.40 0.45 0.50 0.55 0.60 0.65 0.70 0.75 0.80 0.85 0.90 0.95
PAx Threshold
6 Month A/D
6 Month F/U

RAC

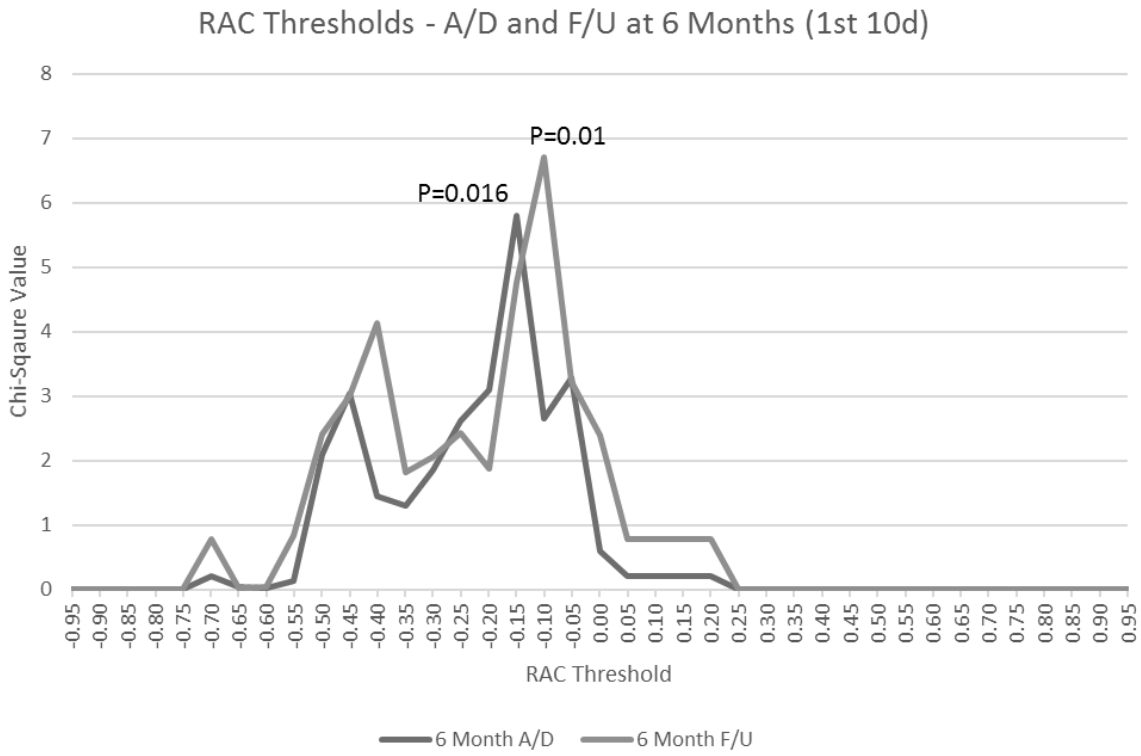
RAC Thresholds - A/D and F/U at 6 Months (1st 10d)
P=0.01
P=0.016
Chi-Sqaure Value
RAC Threshold
6 Month A/D
6 Month F/U

Appendix G: Chapter 9 - Injury and Lesion Data, Patient Numbers – Grand Mean Data

Patient Demographics and Injury Characteristics

Variable\Statistic	Sum of weights	Categories	Frequency per category
Gender	358	F	86.00
		M	272.00
Side of Shift (L = R to L; R = L to R)	358	L	40.00
		NA	259.00
		R	59.00
Basal Cisterns (Normal = 0/Compressed = 1/Absent = 2)	358	0	218.00
		1	81.00
		2	59.00
Lateral Ventricles (Normal = 0/mild compression = 1/compressed-absent = 2)	358	0	165.00
		1	127.00
		2	66.00
4th Ventricle (Normal = 0/mild compression = 1/compressed-absent = 2)	358	0	329.00
		1	21.00
		2	8.00
4th Vent Shift (mm)	358	0	358.00
Direction of 4th Shift (L = R to L; R = L to R)	358	NA	358.00
Convexity Gyri (Normal = 0/mild compression = 1/compressed-absent = 2)	358	0	89.00
		1	149.00
		2	120.00

Tonsillor Descent (N = 0/Y = 1)	358	0	342.00
		1	15.00
		2	1.00
Largest Lesion Type	358	0	4.00
		Contusion	67.00
		DAI	76.00
		EDH	25.00
		Falcine	
		SDH	1.00
		NA	82.00
		Post Fossa	
		EDH	2.00
		SDH	101.00
Lesion <25 mL (N = 0/Y = 1)	358	0	142.00
		1	216.00
Lesion >25 mL (N = 0/Y = 1)	358	0	301.00
		1	57.00
Evacuated Lesion (Y/N)	358	N	313.00
		Y	45.00
Non-Evacuated Mass (>25 mL) (N = 0/Y = 1)	358	0	337.00
		1	20.00
		NA	1.00
DC (y/n)	358	N	358.00
Convexity Subdural hematoma (Present = 1, Absent = 0)	358	0	235.00
		1	123.00
SDH Side (L or R)	358	L	66.00
		NA	250.00
		R	42.00

Tentorial SDH (Absent = 0/Present = 1)	358	0	349.00
		1	9.00
Falcine SDH (Absent = 0/Present = 1)	358	0	345.00
		1	13.00
Bilat SDH (Absent = 0/Present = 1)	358	0	338.0
		1	20.00
Epidural Mass Lesion (Present = 1/Absent = 0)	358	0	332.00
		1	26.00
EDH Side (L or R)	358	L	9.00
		NA	334.00
		R	15.00
Bilat EDH (Absent = 0/Present = 1)	358	0	356.00
		1	2.00
ICH-contusion (Present = 1/ Absent = 0)	358	0	263.00
		1	95.00
ICH-contusion Side (L or R)	358	L	29.00
		NA	297.00
		R	32.00
Bilat ICH-contusion (Absent = 0/Present = 1)	358	0	323.00
		1	34.00
		2	1.00
IVH (Absent = 0/Present = 1)	358	0	271.00
		1	87.00
tSAH-conv (Extensive bilat (>90% convexity) = 2/visible in gyri = 1/ Absent = 0)	358	0	85.00
		1	259.00
		2	14.00

tSAH-conv thickness (>5mm = 2/1-5mm = 1/no blood = 0; *Note: visible blood is at least 1mm)	358	0	84.00
		1	218.00
		2	56.00
tSAH-cist (Filled cisterns = 2/visible blood = 1/Absent = 0)	358	0	255.00
		1	95.00
		2	8.00
DAI-SC (Present = 1/Absent = 0)	358	0	276.00
		1	82.00
DAI-CC (Present = 1/Absent = 0)	358	0	337.00
		1	21.00
DAI-BG (Present =1/Absent = 0)	358	0	335.00
		1	23.00
DAI-BS (Present = 1/Absent = 0)	358	0	346.00
		1	12.00
Post Fossa EDH (Present = 1/Absent = 0)	358	0	355.00
		1	3.00
Post Fossa SDH (Present = 1/Absent = 0)	358	0	358.00
Post Fossa ICH-contusion (Present = 1/Absent = 0)	358	0	354.00
		1	4.00

BG = basal ganglia, Bilat = bilateral, BS = brain stem, CC = corpus callosum, cist = cistern, DAI = diffuse axonal injury, DC = decompressive craniectomy, EDH = epidural hematoma, F = female, ICH = intra-cerebral hemorrhage, IVH = intra-ventricular hemorrhage, L = left, M = male, mm = millimeter, mL = milliliters, N = No, NA = not applicable, R = right, SC = sub-cortical, SDH = subdural hematoma, tSAH = traumatic subarachnoid hemorrhage, Y = yes.

Appendix H – Chapter 9: IC Scoring Systems and Mean Index/%Time Above Threshold Results

Intra-Cranial Ordinal CT Scoring Systems – KW and JT Testing

	Marshall CT Grade						p-value	Rotterdam CT Score						p-value
	I	**II**	**III**	**IV**	**V**	**VI**		**1**	**2**	**3**	**4**	**5**	**6**	
Mean PRx	NA	0.028 (+/- 0.165)	0.058 (+/- 0.176)	0.088 (+/- 0.256)	0.085 (+/- 0.143)	0.053 (+/- 0.225)	0.096	0.043 (+/- 0.167)	0.031 (+/- 0.163)	0.041 (+/- 0.154)	0.058 (+/- 0.210)	0.164 (+/- 0.214)	-0.055 (+/- 0.076)	**0.001**
Mean PAx	NA	-0.078 (+/- 0.196)	-0.046 (+/- 0.169)	0.003 (+/- 0.260)	-0.028 (+/- 0.195)	-0.015 (+/- 0.233)	0.354	-0.81 (+/- 0.208)	-0.071 (+/- 0.192)	-0.050 (+/- 0.165)	-0.028 (+/- 0.228)	0.016 (+/- 0.208)	-0.105 (+/- 0.225)	**0.001**
Mean RAC	NA	-0.383 (+/- 0.251)	-0.337 (+/- 0.224)	-0.275 (+/- 0.310)	-0.281 (+/- 0.259)	-0.316 (+/- 0.315)	0.054	-0.354 (+/- 0.288)	-0.385 (+/- 0.237)	-0.363 (+/- 0.230)	-0.267 (+/- 0.265)	-0.224 (+/- 0.289)	-0.394 (+/- 0.348)	**0.001**
% Time Above PRx of 0	NA	49.7 +/-16.8	52.6 +/- 17.1	54.8 +/- 20.2	57.8 +/- 15.1	52.2 +/- 17.6	**0.037**	51.7 +/- 18.0	50.4 +/- 16.6	51.8 +/- 16.2	52.3 +/- 17.2	62.6 +/- 17.5	39.9 +/-7.8	0.074
% Time Above PRx of +0.25	NA	28.9 +/- 15.5	32.6 +/- 17.4	34.2 +/- 22.3	34.5 +/- 15.6	31.5 +/- 18.8	0.076	30.0 +/- 15.7	29.6 +/- 15.4	30.3 +/- 15.7	32.3 +/- 18.9	41.6 +/- 20.9	21.5 +/- 7.1	0.052
% Time Above PRx of +0.35	NA	22.3 +/- 14.4	26.1 +/- 16.5	27.8 +/- 22.4	26.3 +/- 14.4	24.8 +/- 18.9	0.130	23.2 +-/- 14.8	22.8 +/- 14.2	22.5 +/- 14.3	26.0 +/- 19.0	34.0 +/- 21.1	16.4 +/- 5.8	**0.04**
% Time Above PAx of 0	NA	40.4 +/- 19.6	43.8 +/- 17.3	49.1 +/- 26.6	45.9 +/- 19.4	44.8 +/- 19.0	0.268	39.8 +/- 21.2	41.3 +/- 19.1	43.0 +/- 17.3	45.4 +/- 21.1	50.4 +/- 21.3	36.4 +/- 22.3	**0.022**

% Time Above PAx of +0.25	NA	21.0 +/- 15.9	23.2 +/- 14.2	28.3 +/- 23.3	24.5 +/- 19.0	24.45 +/- 20.4	0.310	20/8 +/- 15.4	21.5 +/- 15.7	22.1 +/- 15.0	25.0 +/- 19.1	29.0 +/- 19.6	18.6 +/- 19.2	**0.016**
% Time Above RAC of -0.05	NA	22.0 +/- 19.3	25.4 +/- 17.8	28.8 +/- 26.8	28.6 +/- 22.6	26.2 +/- 22.4	0.119	24.7 +/- 22.1	21.7 +/- 18.3	23.0 +/- 18.8	30.1 +/- 20.8	33.8 +/- 25.1	21.9 +/- 26.2	**0.005**
% Time Above PRx of -0.10	NA	24.6 +/- 20.4	28.3 +/- 19.0	31.4 +/- 27.2	23.2 +/- 23.2	29.1 +/- 23.0	0.117	27.5 +/- 23.2	24.3 +/- 19.2	25.8 +/- 19.9	33.2 +/- 21.6	37.0 +/- 25.8	23.9 +/- 27.7	**0.013**

	Helsinki CT Score	**p-value**	**Stockholm CT Score – "Range"**						**p-value**
	-3 to +14		**0 – 1**	**1.1 – 2**	**2.1 – 3**	**3.1 – 4**	**4.1 – 5**	**5.1 - 6**	
Mean PRx	*Please refer to figure for box plot of PRx, PAx and RAC across each category of the Helsinki Score.	**0.001**	0.034 (+/- 0.152)	0.024 (+/- 0.165)	0.065 (+/- 0.194)	0.058 (+/- 0.183)	0.032 (+/- 0.097)	0.301	0.173
Mean PAx		**0.001**	-0.082 (+/- 0.186)	-0.076 (+/- 0.185)	-0.026 (+/- 0.203)	-0.031 (+/- 0.220)	-0.080 (+/- 0.119)	0.268	0.057
Mean RAC		**0.001**	-0.356 (+/- 0.249)	-0.389 (+/- 0.234)	-0.314 (+/- 0.264)	-0.291 (+/- 0.290)	-0.435 (+/- 0.135)	0.194	**0.018**
% Time Above PRx of 0		**0.002**	51.0 +/- 16.7	50.7 +/- 17.3	53.1 +/- 16.5	53.2 +/- 17.9	51.5 +/- 10.7	82.6	0.124
% Time Above PRx of +0.25		**0.001**	29.4 +/- 14.1	29.9 +/- 16.1	32.2 +/- 18.2	32.5 +/- 17.4	28.0 +/- 9.5	62.0	0.104

% Time Above PRx of +0.35		**0.001**	22.7 +/- 12.8	23.2 +/- 14.7	25.5 +/- 18.0	25.8 +/- 16.3	20.5 +/- 7.9	50.5	0.134
% Time Above PAx of 0		**0.001**	40.1 +/- 19.4	40.7 +/- 18.9	45.2 +/- 19.1	45.3 +/- 21.3	40.4 +/- 11.6	80.1	**0.038**
% Time Above PAx of +0.25		**0.001**	20.6 +/- 14.3	21.0 +/- 15.3	24.4 +/- 18.0	25.3 +/- 20.0	18.9 +/- 9.2	56.3	**0.040**
% Time Above RAC of -0.05		**0.001**	23.4 +/- 19.6	21.5 +/- 18.0	26.3 +/- 20.9	30.0 +/- 23.5	15.8 +/- 12.7	76.2	**0.020**
% Time Above PRx of -0.10		**0.001**	26.6 +/- 20.8	24.1 +/- 19.1	29.1 +/- 21.6	32.9 +/- 24.5	18.0 +/- 13.3	80.4	**0.029**

*KW = Kruskal-Wallis Test for variance, JT = Jonckheere-Terpstra test for ordinal variance, NA = not available, CT = computed tomography, PRx = pressure reactivity index (correlation between ICP and MAP), PAx = pulse amplitude index (correlation between pulse amplitude of ICP (AMP) and MAP), RAC = correlation between AMP and CPP. *NOTE: bolded values are those which have reached statistical significance (p<0.05). The mean values for PRx, PAx, RAC and % time above threshold were tested across the Marshall CT grades with the KW test. The mean values for PRx, PAx, RAC and % time above threshold were tested across the ordinal Rotterdam, Helsinki and Stockholm scores using the JT test.*

Appendix I – Chapter 9: Mann U testing for Thresholds of PRx and PAx

Mann U Testing For Continuous Variables Across Index Thresholds – PRx Thresholds of 0, +0.25, and +0.35

Demo (Mean and Medians with Std Dev/IQR)	PRx		p-value	PRx		p-value	PRx		p-value
	<0	≥0		<0.25	≥0.25		<0.35	≥0.35	
N	153	205	-	324	34	-	340	18	-
Age	37.1 (17.4)	43.2 (16.5)	**<0.0001**	39.8 (16.9)	48.2 (18.1)	**0.009**	40.1 (17.0)	49.6 (18.7)	**0.029**
GCS	7 (4-9)	7 (3-10)	0.674	7 (4-9)	5.5 (3-9)	0.434	7 (4-95)	3.5 (3-8)	0.088
Marshall	2 (2-3)	3 (2-4)	**0.002**	2 (2-3)	3 (2-3.75)	0.532	2 (2-3)	3 (2-4)	0.113
Rotterdam	2 (2-3)	2 (2-3)	0.097	2 (2-3)	2.5 (2-4)	0.222	2 (2-3)	3 (2-4)	0.041
Helsinki	2 (0-4)	3 (1-5)	**0.001**	3 (0-5)	4 (2-5)	**0.047**	3 (0-5)	4 (3.25-5)	**0.008**
Stockholm	1.993 (0.849)	2.166 (0.927)	0.114	2.084 (0.893)	2.169 (0.955)	0.834	2.072 (0.901)	2.479 (0.759)	0.034
Stockholm Range	2 (2-3)	2 (2-3)	0.072	2 (2-3)	2 (2-3)	0.612	2 (2-3)	3 (2-3)	**0.033**
ISS	32.732 (11.342)	33.175 (11.379)	0.614	32.451 (11.084)	37.333 (12.866)	0.100	32.800 (11.346)	35.467 (11.351)	0.522
APACHE II	12.272 (5.722)	11.773 (5.382)	0.362	11.849 (5.495)	14.029 (6.028)	**0.030**	11.838 (5.467)	16.167 (6.167)	**0.004**
MLS (mm)	1.4 (3.2)	2.1 (3.9)	**0.044**	1.7 (3.6)	2.4 (4.2)	0.391	1.7 (3.6)	3.1 (4.8)	0.165
Largest Lesion Volume	9.5 (19.3)	15.8 (26.0)	**0.004**	13.1 (24.3)	13.1 (15.4)	0.412	13.1 (24.0)	13.9 (14.8)	0.246
# Contusions	0.31 (0.73)	0.53 (0.92)	**0.008**	0.43 (0.84)	0.56 (0.93)	0.362	0.44 (0.85)	0.50 (0.92)	0.816
# DAI Lesions	1.5 (2.6)	0.74 (2.7)	**<0.0001**	0.35 (1.2)	1.1 (2.8)	**0.018**	1.1 (2.8)	0.44 (1.3)	0.149
Total Contusion Volume	4.3 (14.0)	7.2 (18.0)	**0.003**	6.1 (17.0)	4.5 (9.7)	0.741	6.1 (16.8)	3.3 (7.2)	0.847

*# = number, DAI = diffuse axonal injury, GCS = Glasgow Coma Scale, IQR = inter-quartile range, ISS = injury severity score, mm = millimeters, N = number of patients, Std Dev = standard deviation. *Bolded values are those reaching a p<0.05.*

Mann U Testing For Continuous Variables Across Index Thresholds – PAx Thresholds of 0, and +0.25

Demo (Mean and Medians with Std Dev/IQR)	PAx		p-value	PAx		p-value
	<0	≥0		<0.25	≥0.25	
N	239	119	-	338	20	-
Mean Age	36.3 (16.7)	49.2 (14.9)	**<0.0001**	40.0 (16.6)	58.0 (17.3)	**<0.0001**
Median GCS	6 (3-9)	7 (4-10)	0.120	7 (3-9)	6.5 (3-9.25)	0.855
Marshall	2 (2-3)	3(2-3)	0.173	2 (2-3)	3 (2-5)	**0.035**
Rotterdam	2 (2-3)	2(2-3)	0.077	2 (2-3)	3 (2-4)	0.081
Helsinki	2 (0-4)	4 (1.5-6)	**0.001**	3 (0-5)	4 (2.75-7)	**0.010**
Stockholm	2.0 (0.90)	2.2 (0.89)	0.169	2.1 (0.89)	2.5 (1.0)	**0.041**
Stockholm Range	2 (2-3)	2 (2-3)	0.341	2 (2-3)	3 (2-4)	**0.010**
ISS	33.3 (11.2)	32.1 (11.7)	0.274	32.8 (11.5)	34.6 (9.2)	0.479
APACHE II	11.2 (5.6)	13.8 (5.0)	**<0.0001**	11.8 (5.4)	16.3 (6.3)	**0.004**
MLS (mm)	1.6 (3.4)	2.1 (4.1)	0.310	1.6 (3.5)	4.0 (4.7)	**0.002**
Largest Lesion Volume	11.6 (22.6)	16.2 (25.2)	**0.001**	12.8 (23.9)	19.1 (16.7	**0.007**
# Contusions	0.32 (0.75)	0.68 (0.98)	**<0.0001**	0.43 (0.85)	0.60 (0.94)	0.334
# DAI Lesions	1.4 (3.1)	0.46 (1.5)	**<0.0001**	1.1 (2.8)	0.15 (0.67)	**0.026**
Total Contusion Volume	4.8 (14.7)	8.4 (19.3)	**<0.0001**	6.0 (16.7)	5.2 (11.0)	0.606

*# = number, DAI = diffuse axonal injury, GCS = Glasgow Coma Scale, IQR = inter-quartile range, ISS = injury severity score, mm = millimeters, N = number of patients, Std Dev = standard deviation. *Bolded values are those reaching a p<0.05.*

Appendix J – Chapter 9: Univariate Logistic Regression for CT Injury Characteristics and ICP Indices – Grand Mean Data

Univariate Logistic Regression Analysis for Injury Characteristics and ICP Indices – Grand Mean Data

	PRx >0		PRx >0.25		PRx >0.35		PAx >0		PAx >0.25		RAC >-0.05		RAC>-0.10	
	AUC	P	AUC	P	AUC	P	AUC	P	AUC	P	AUC	P	AUC	P
MLS	0.533	0.084	0.590	0.270	0.629	0.113	0.561	0.204	**0.703**	**0.009**	**0.590**	**0.018**	0.533	0.072
Largest Lesion Volume	**0.590**	**0.015**	**0.549**	**0.001**	**0.586**	**0.022**	0.607	0.088	0.675	0.251	0.590	0.106	0.568	0.192
# of Contusions	**0.565**	**0.019**	0.588	0.388	0.578	0.753	**0.643**	**0.001**	0.613	0.385	0.518	0.955	0.546	0.448
# of DAI Lesions	**0.614**	**0.017**	0.659	0.095	0.667	0.302	**0.648**	**0.003**	0.706	0.125	0.618	0.132	**0.602**	**0.050**
Total Contusion Volume	0.578	0.114	0.531	0.590	0.568	0.493	0.640	0.058	0.526	0.829	0.513	0.401	0.533	0.958
Basal Cistern Compression Grade	0.557	0.053	0.619	0.111	0.683	0.101	0.591	0.057	0.663	0.159	0.576	0.252	0.560	0.241
Basal Cistern Compression – Any	**0.555**	**0.018**	0.610	0.174	0.679	0.057	**0.598**	**0.017**	0.678	0.055	0.576	0.213	0.561	0.130
Basal Cistern Compression – Severe	0.512	0.076	0.635	0.037	0.673	0.056	0.558	0.186	0.626	0.296	0.579	0.108	0.536	0.142
Lat Ventricle Compression Grade	0.538	0.183	0.636	0.074	0.624	0.263	0.570	0.263	0.643	0.155	0.592	0.243	0.556	0.415

Lat Ventricle Compression – Any	0.532	0.165	0.559	0.808	0.602	0.531	0.576	0.124	0.605	0.575	0.553	0.579	0.525	0.729
Lat Ventricle Compression - Severe	0.508	0.089	**0.637**	**0.032**	0.651	0.103	0.563	0.241	0.662	0.057	0.575	0.234	0.534	0.317
4th Ventricle Compression Grade	0.495	0.387	0.629	0.249	0.656	0.118	0.570	0.194	0.644	0.571	0.586	0.471	0.543	0.641
4th Ventricle Compression – Any	0.496	0.188	0.606	0.414	0.655	0.185	0.551	0.577	0.622	0.749	0.562	0.797	0.529	0.775
4th Ventricle Compression – Severe	0.480	0.762	0.612	0.691	0.621	0.972	0.570	0.238	0.654	0.973	0.572	0.560	0.353	0.446
Gyri Compression Grade	0.545	0.166	**0.653**	**0.042**	0.662	0.214	0.567	0.327	0.623	0.476	0.615	0.109	0.592	0.121
Gyri Compression – Any	0.507	0.627	0.620	0.143	0.606	0.769	0.570	0.353	0.596	0.988	0.604	0.133	0.582	0.090
Gyri Compression – Severe	0.529	0.062	0.608	0.172	0.650	0.136	0.572	0.147	0.628	0.267	0.555	0.444	0.516	0.705
Tonsillar Descent	0.507	0.113	0.597	0.887	0.624	0.318	0.551	0.981	0.632	0.648	0.557	0.874	0.522	0.971
Lesion >25 mL	**0.547**	**0.003**	0.588	0.773	0.614	0.929	0.559	0.529	0.690	0.085	0.552	0.662	0.522	0.409
Evacuated Mass – Any Size	**0.528**	**0.010**	0.593	0.693	0.623	0.592	0.558	0.746	0.689	0.094	0.566	0.477	0.524	0.674

Non-Evacuated Mass >25 mL	0.507	0.242	0.617	0.299	0.648	0.562	0.565	0.509	0.614	0.906	0.539	0.749	0.493	0.935
Convexity SDH	**0.538**	**0.032**	**0.641**	**0.019**	**0.706**	**0.006**	**0.631**	**<0.0001**	**0.774**	**0.001**	**0.633**	**0.003**	**0.585**	**0.008**
Tentorial SDH	0.511	0.088	0.590	0.867	0.638	0.970	0.586	0.164	0.642	0.476	0.589	0.068	0.541	0.155
Falcine SDH	0.510	0.061	**0.639**	**0.015**	**0.696**	**0.008**	**0.592**	**0.010**	**0.748**	**0.001**	0.591	0.239	0.544	0.457
Bilateral Convexity SDH	**0.518**	**0.008**	**0.631**	**0.003**	**0.689**	**0.001**	**0.586**	**0.013**	**0.708**	**<0.0001**	0.569	0.084	0.531	0.077
Supra-tentorial EDH	0.498	0.438	0.608	0.745	0.648	0.775	0.585	0.258	0.677	0.397	0.579	0.619	0.532	0.970
Bilateral Supra-tentorial EDH	0.491	0.485	0.598	0.743	0.632	0.497	0.570	0.627	0.641	0.534	0.557	0.858	0.519	0.975
Contusion – Any	**0.559**	**0.011**	0.588	0.421	0.579	0.903	**0.639**	**0.001**	0.618	0.381	0.552	0.630	0.551	0.175
Bilateral Contusions	**0.527**	**0.015**	0.624	0.112	0.632	0.320	**0.613**	**0.001**	0.651	0.124	0.550	0.361	0.523	0.220
IVH	0.529	0.298	0.572	0.596	0.589	0.833	0.552	0.983	0.614	0.645	0.595	0.217	0.575	0.139
tSAH Convexity Grade	0.516	0.406	0.574	0.846	0.639	0.755	**0.583**	**0.026**	0.638	0.640	0.548	0.580	0.540	0.476
tSAH Convexity – Any	0.514	0.357	0.566	0.650	0.612	0.473	**0.578**	**0.031**	0.640	0.351	0.542	0.866	0.537	0.262
tSAH Convexity - >90%	0.491	0.282	0.606	0.760	0.658	0.742	0.571	0.062	0.643	0.797	0.566	0.297	0.525	0.546

tSAH Convexity Thickness Grade	**0.542**	**0.016**	0.595	0.200	**0.662**	**0.032**	**0.609**	**0.001**	**0.679**	**0.015**	0.547	0.643	0.542	0.454
tSAH Convexity Thickness ->5mm	**0.521**	**0.004**	0.633	0.073	**0.698**	**0.009**	**0.598**	**0.001**	**0.700**	**0.004**	0.558	0.350	0.529	0.371
tSAH Cisterns Grade	0.542	0.074	0.607	0.285	0.639	0.072	0.590	0.137	0.617	0.642	0.577	0.104	**0.557**	**0.045**
tSAH Cisterns – Any	**0.540**	**0.034**	0.578	0.756	0.637	0.335	0.591	0.055	0.619	0.528	0.576	0.237	0.553	0.213
tSAH Cisterns – Severe	0.496	0.095	0.601	0.153	**0.639**	**0.023**	0.562	0.318	0.638	0.405	**0.562**	**0.044**	**0.535**	**0.016**
DAI – SC	**0.585**	**<0.0001**	0.647	0.052	0.658	0.236	**0.631**	**0.001**	0.695	0.083	**0.615**	**0.027**	**0.592**	**0.010**
DAI – CC	**0.518**	**0.028**	0.624	0.282	0.654	0.476	**0.602**	**0.032**	0.663	0.491	0.587	0.203	0.553	0.143
DAI – BG	**0.512**	**0.029**	0.604	0.398	0.624	0.878	**0.585**	**0.045**	0.658	0.450	0.565	0.590	0.533	0.352
DAI – BS	0.504	0.101	0.619	0.502	0.650	0.822	0.578	0.231	0.659	0.767	0.578	0.388	0.541	0.294
Post-Fossa EDH	0.484	0.743	0.597	0.871	0.631	0.587	0.561	0.997	0.641	0.630	0.566	1.000	0.528	0.874
Post-Fossa Contusion	0.495	0.769	0.592	0.985	0.626	0.676	0.568	0.483	0.636	0.724	0.564	0.879	0.526	0.750

AUC = area under the receiver operative curve, BG = basal ganglia, BS = basal cistern, CC = corpus callosum, DAI = diffuse axonal injury, EDH = epidural hematoma, IVH = intra-ventricular hemorrhage, Lat = lateral, mL = milliliter, MLS = midline shift, mm = millimeters, p = p-value, PRx = pressure reactivity index (correlation between ICP and MAP), PAx = pulse amplitude index (correlation between pulse amplitude of ICP (AMP) and MAP), RAC = correlation between AMP and CPP, SC = sub-cortical, SDH = subdural hematoma, tSAH = traumatic subarachnoid hemorrhage, .
*NOTE: bolded values are those which have reached statistical significance ($p<0.05$).